Synthesis and Coordination Behavior of Polyphosphorus Complexes with Sterically Demanding Cp Ligands

Dissertation

zur Erlangung des

DOKTORGRADES DER NATURWISSENSCHAFTEN

(DR. RER. NAT.)

der Fakultät Chemie und Pharmazie

der Universität Regensburg

vorgelegt von

Julian Müller

aus Karlsruhe – Durlach

im Jahr 2020

Diese Arbeit wurde angeleitet von Prof. Dr. Manfred Scheer.

Promotionsgesuch eingereicht am:	18. Dezember 2020
Tag der mündlichen Prüfung:	26. Februar 2021

Vorsitzender:	Prof. Dr. Rainer Müller
Prüfungsausschuss:	Prof. Dr. Manfred Scheer
	Prof. Dr. Henri Brunner
	Prof. Dr. Frank-Michael Matysik

Universität Regensburg

Eidesstattliche Erklärung

Ich erkläre hiermit an Eides statt, dass ich die vorliegende Arbeit ohne unzulässige Hilfe Dritter und ohne Benutzung anderer als der angegebenen Hilfsmittel angefertigt habe; die aus anderen Quellen direkt oder indirekt übernommenen Daten und Konzepte sind unter Angabe des Literaturzitats gekennzeichnet.

_____

Julian Müller

This thesis was elaborated within the period from January 2016 until December 2020 in the Institute of Inorganic Chemistry at the University of Regensburg, under the supervision of Prof. Dr. Manfred Scheer.

List of Publications:

J. Müller, S. Heinl, C. Schwarzmaier, G. Balázs, M. Keilwerth, K. Meyer, M. Scheer.
'Rearrangement of a P_4 Butterfly Complex – The Formation of a Homoleptic Phosphorus–Iron Sandwich Complex'
Angew. Chem. Int. Ed. **2017**, *56*, 7312–7317.
Angew. Chem. **2017**, *129*, 7418–7423.

S. Heinl, A. Y. Timoshkin, J. Müller, M. Scheer.
'Unexpected differences in the reactivity between the phosphorus and arsenic derivatives $[(Cp^{BIG}Fe)_2(\mu,\eta^{4:4}\text{-}E_4)]$ (E = P and As)'
Chem. Commun. **2018***, 54,* 2244–2247.

J. Müller, M. Scheer.
'Coordination Behavior of a P_4 -Butterfly Complex towards Transition Metal Lewis Acids: Preservation versus Rearrangement'
Chem. Eur. J. **2021**, *27*, 3675.

J. Müller, G. Balázs, M. Scheer.
'From a P_4 Butterfly Scaffold to *cyclo*- and *catena*-P_4 Units'
Chem. Commun. **2021**, *57*, 2257.

dedicated to Jessi

‘The great tragedy of Science - the slaying of a beautiful hypothesis
by an ugly fact.’

Thomas Henry Huxley

Preface

Some of the presented results have already been published during the preparation of this thesis (vide supra). The corresponding citations and license number are given at the beginning of the respective chapters.

Each chapter includes a list of authors. At the beginning of each chapter the individual contribution of each author is described. Additionally, if some of the presented results have already been partly discussed in other theses, it is stated at the beginning of the respective chapters.

To ensure uniform design of this work, all chapters are subdivided into ‘Introduction’, ‘Results and Discussion’, ‘Conclusion’, ‘References’, and ‘Supporting Information’. Furthermore, all chapters have the same text settings and the numeration of compounds. The depicted molecular structures may differ in their style. A general ‘Introduction’ and the ‘Research Objectives’ are given at the beginning of this thesis. In addition, a comprehensive ‘Conclusion’ of this work is presented at the end of this thesis.

Table of Contents

1. Introduction

1.1. Phosphorus and its Modifications

Phosphorus is an essential element for organic life. This is the reason why astronomers search, inter alia, for phosphorus compounds on exoplanets, to pursue the question of extraterrestrial life.[1] Surprisingly, since September 2020 these investigations have led to a renewed discussion about possible life on our sister planet Venus, as the group of Greaves et al. claimed to have spectroscopically detected phosphine gas (PH_3) in the atmosphere of Venus.[2] In the meantime, however, these results are strongly doubted, since the group may have misinterpreted the data.[3] Nevertheless, PH_3 is considered a well-suited biomarker as the presence of PH_3 in the atmosphere of an exoplanet may be related to biological activity.[4] Although PH_3 being highly oxophilic, it can also be detected in the earth's lower troposphere in a ppq to ppb range since it is steadily produced, inter alia, by bacteria in an anaerobic environment.[5]

Due to the oxophilicity, phosphorus on earth is generally found in inorganic phosphates in the geosphere, where it accounts for about 0.1 mass percent. Of the many mineral phosphates, apatite ($Ca_5X(PO_4)_3$ (X = F, Cl, OH)) is the most important for the industrial synthesis of elemental phosphorus. In following, the three allotropes of elemental phosphorus – white phosphorus, red phosphorus, and black phosphorus – will be discussed (Scheme 1.1).[6]

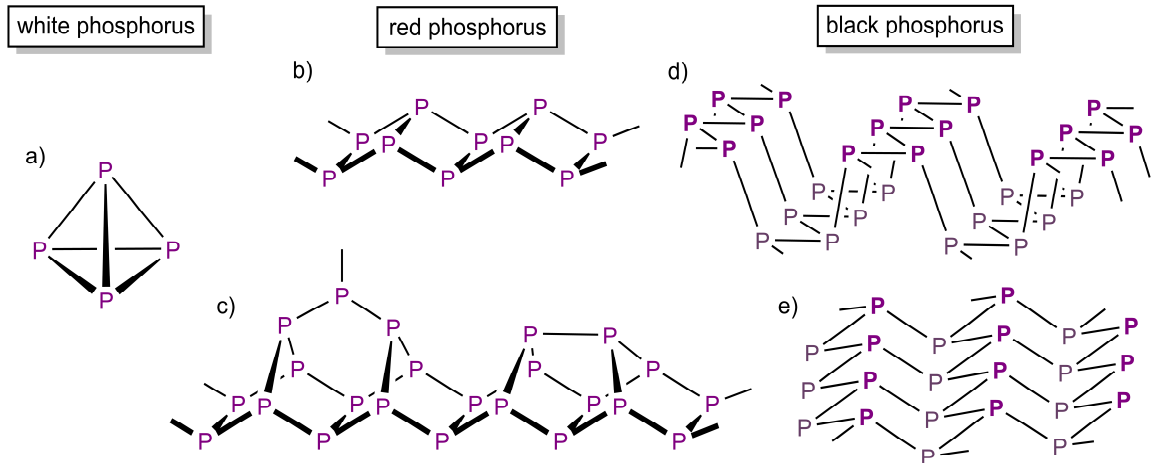

Scheme 1.1. Structures of the three main modifications of phosphorus - white, red, and black phosphorus. a) molecular P_4 tetrahedron of white phosphorus; b) assumed microcrystalline structure of amorphous red phosphorus;[7] c) smallest repeating unit of the crystalline modification (fibrous and violet phosphorus) of red phosphorus; d) structure of orthorhombic black phosphorus; e) structure of hexagonal black phosphorus. The P atoms in bold are above and the grey P atoms are in the paper plane.

The least thermodynamically stable modification is white phosphorus (P_4). However, since all other modifications are obtained starting from P_4, it is the most important one. White phosphorus was firstly discovered by the German alchemist Hennig Brand in 1669.[8] In

his search for the “Philosopher’s stone”, he evaporated urine to dryness and strongly heated the residue in the absence of air to obtain a product which glowed in the dark – white phosphorus. The glow of white phosphorus was also responsible for the naming, because the Greek word phōsphóros means "light bearer". In industry P_4 is synthesized in an electrothermal process via the reduction of calcium phosphate with silicon dioxide and coke:

$$2\ Ca_3(PO_4)_2 + 6\ SiO_2 + 10\ C \longrightarrow P_4 + 6\ CaSiO_3 + 10\ CO$$

After distillation, white phosphorus is obtained as a waxy white solid. P_4 exists in three different crystalline modifications. The α form exists at room temperature and transforms reversible into β-P_4 at −77 C°, while γ-P_4 is the low temperature modification of white phosphorus.[9–11] The four phosphorus atoms in the P_4 molecule form a perfect tetrahedron with P–P single bonds (a) in Scheme 1.1). Since the bond length are not only determined by X-ray analysis (2.199 - 2.212 Å)[9–11] but have also been extensively examined by Raman spectroscopy (2.2228(5) Å),[12] electron diffraction (2.1994(3) Å),[13] as well as quantum chemical calculations (2.194 Å),[14] the approximate value of 2.21 Å is now the standard reference value for P–P single bonds. White phosphorus is the most reactive allotrope of phosphorus due to the high ring tension (PPP angles of 60°) within the P_4 tetrahedron. Furthermore, P_4 is the only modification that is well soluble in organic solvents which is why it is an excellent staring material for several products in industry as well as in academic research.

When white phosphorus is tempered above 200 C° it transforms into the modification of red phosphorus. Red phosphorus is an intermediate modification between white and black phosphorus and can be divided into subgroups I–V that have been examined by the group of Roth extensively.[15] Form I is the commercially available red phosphorus which is mainly described as amorphous solid. Herein, the phosphorus atoms have three neighbors at a distance of 2.29 Å and about six neighbors within 3.48 Å,[16] which is similar to the arrangement in black phosphorus. However, recent studies indicate a microcrystalline structure, which is build up by one-dimensional zig-zag ladders of condensed *cyclo*-P_4 units (b) in Scheme 1.1).[7] With increasing temperature, the phosphorus atoms begin to reorganize, and the crystallinity increases. The structures of the so obtained forms II and III are still unknown. The fourth form or fibrous phosphorus can be obtained above 500 C° and is the first crystalline form of red phosphorus. Fibrous phosphorus is build up by parallel double tubes of alternating P_2, P_9, P_2, P_8 units which are connected via the P_9 units (c) in Scheme 1.1).[17] The fifth form is very similar to the fibrous phosphorus and is obtained by tempering white phosphorus above 550 C° for more than one week. Due to its color this modification is also called violet phosphorus and was first discovered in 1865 by Johann Willhelm Hittorf which is why it is also called the Hittorf’s phosphorus.[18] The structure of violet phosphorus contains the same alternating P_2, P_9, P_2, P_8 units like fibrous phosphorus. However, in contrast to fibrous phosphorus, the connected tubes are not

orientated parallel but angled which leads to a two-dimensional double layer structure.[19] The double layers are hold together by van-der-Waals interactions.

The thermodynamically most stable modification at room temperature is black phosphorus. Black phosphorus has the electric properties of a semi-conductor which is why black phosphorus is the most metallic modification of phosphorus.[20] One way to produce orthorhombic black phosphorus is to treat P_4 at 200 C° while applying 12 kbar.[21] The solid state structure shows strongly corrugated layers, build up by condensed P_6 rings in a chair conformation (d) in Scheme 1.1)[22] The high pressure modification of hexagonal phosphorus is obtained at 110 kbar. The structure is consisting of condensed P_6 rings, similar like in orthorhombic black phosphorus (e) in Scheme 1.1). However, instead of an *endo* conformation, exhibit the P_6 rings in the hexagonal phase an *exo* conformation which leads to more flatten layers.

1.2. Bulky Cyclopentadienyl Ligands

A milestone in organometallic chemistry was the discovery of the ferrocene molecule [$(\eta^5$-$C_5H_5)_2Fe$] in 1951.[23] Due to its remarkable chemical as well as thermal stability,[24] ferrocene derivatives are used in several catalytic[25] and medical[26] applications. In the years after the discovery, the chemistry of cyclopentadienyl (Cp) complexes has rapidly grown and in the meantime, Cp^R complexes (Cp^R = Cp derivative) with all transition metals, lanthanoids, main group metals, and several actinoids have been synthesized. In these complexes the Cp^R ligand does not exclusively bind in an η^5 fashion to the metal, but also

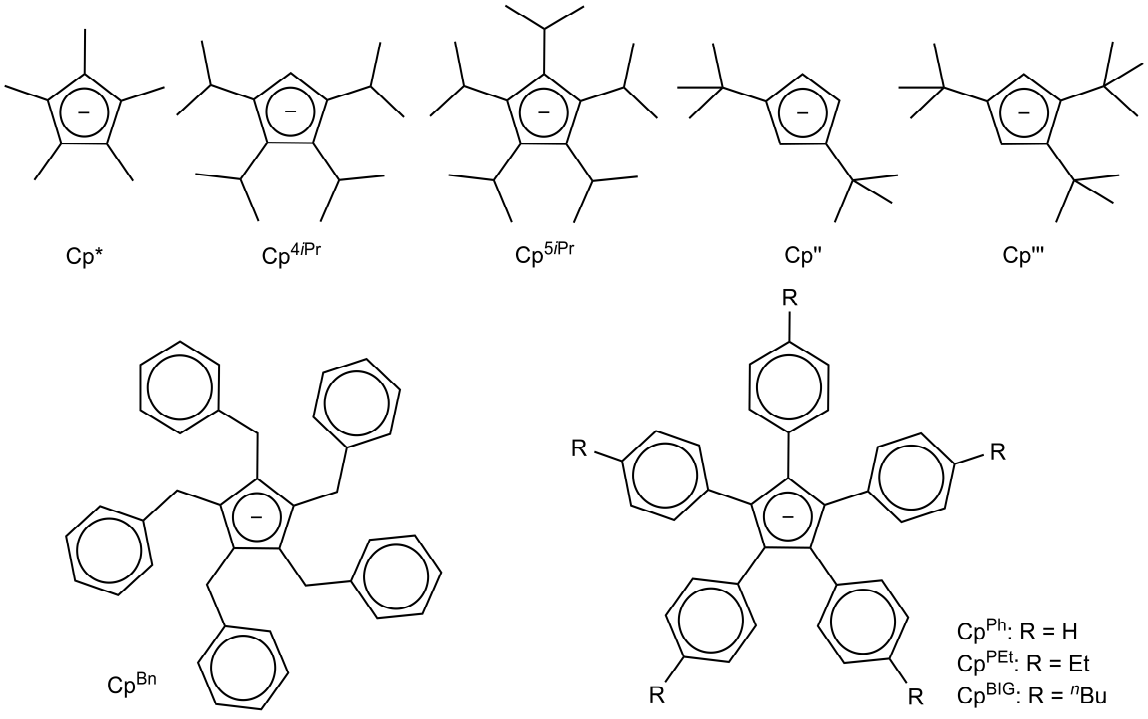

Scheme 1.2. Selected examples of commonly used cyclopentadienyl derivatives, shown as negatively charged 6 π-electron donors.

η^1–η^4 coordination is observed. In 1967, pentamethylcyclopentadiene (Cp*) was introduced which was another turning point in this field,[27] since remarkable differences between complexes stabilized by unsubstituted Cp ligands and complexes stabilized by the sterically more demanding Cp* ligand has been observed.[28] Based on these results, several different substituents have been introduced in the following years which leads to a large variety of cyclopentadienyl derivatives. Some of the most frequently used Cp^R ligands in organometallic chemistry are shown in Scheme 1.2. However, besides the shown Cp^R ligands that exhibit a symmetrical substitution pattern, also unsymmetric Cp^R ligands can be synthesized.[29] In general, the introduction of substituents does not only change the sterical bulk of the ligands but also influences its donor and acceptor properties and alters the solubility of the ligand.

In the last years, a trend towards ever bulkier Cp^R ligands has become apparent. However, the definition of bulky Cp^R ligands is rather unspecific, which is why a new concept of size determination has been developed that is comparable to the procedure used for the phosphines introduced by Tolman.[30] The size estimation of Cp^R ligands is bases on two types of cone angles that can be derived from crystallographic as well as computational data of $[(\eta^7\text{-}C_7H_7)Zr(Cp^R)]$.[31] The first cone angle Θ measures the sterical bulk in the plane spanned out by the C_5 ring, while the second angle Ω indicates the sterical bulk along the Cp–M bond. Using a combination of these two cone angles, the group was able to show that this method is a good indicator of the actual size of a Cp^R ligand, since they derived the size of the Cp^R ligands in the following order: C_5H_5 < Cp'' < Cp* < $C_5H_2{}^i Pr_3$ < $C_5Me_2{}^i Pr_3$ < Cp''' < Cp^{Ph} < $Cp^{4i Pr}$ < C_5Ph_4(p-^{n}BuPh) < $Cp^{5i Pr}$.

According to Janiak et al. the introduction of sterically demanding Cp^R ligands influences mainly the kinetic stabilization of the formed complexes and allows the formation of novel structural motifs.[32] This can be demonstrated at the stannocene molecule since the bend angle along the $Cp_{cent.}$–Sn–$Cp_{cent.}$ axis is strongly related to the sterical bulk of the Cp^R ligand. While in $[Cp^{Ph}{}_2Sn]$ (**1**),[33] $[Cp^{BIG}{}_2Sn]$ (**2**),[34] and $[Cp^{5i Pr}{}_2Sn]$ (**3**) the two ligands are arranged parallel to each other, the bend angel decreases from 180° to 155° in $[Cp^*{}_2Sn]$ (**4**)[35] and finally to 144°/147° (two molecules in the asymmetric unit) in $[Cp_2Sn]$ (**5**).[36] The trend to form more linear metallocene structures with larger Cp^R ligands is also observed for the other group 14 elements[37] as well as for the metallocenes of alkaline earth metals,[37,38] and lanthanoids.[34,38,39]

The kinetic stabilization of bulky Cp^R ligands allows the isolation of alkaline earth (Ca, Sr, Ba) and transition metal (Fe, Ni, Co) half sandwich complexes of the type $[Cp^RM(\mu\text{-}X)(thf)_n]_m$ (n = 0, 1, 2; m = 1, 2, ∞; X = Cl, Br, I).[40] Typically, these complexes tend to dissociate due to the following Schlenk-type rearrangement:

$$2\ [Cp^RMX] \rightleftharpoons [Cp^R{}_2M] + MX_2$$

Furthermore, large Cp^R ligands are also able to stabilize reactive 17 valence electron (VE) radical monomers. In the solid state, these complexes are mainly found as the dimeric complexes $[Cp^RM(CO)_x]_2$ (M = Cr, Mo, x = 3; M = Fe, x = 2; M = Ni, x = 1), in order to fulfil the 18 VE rule.[41] However, by increasing the size of the Cp^R ligand, the amount of radical monomer present in solution can be increased. While for $[Cp^RFe(CO)_2]_2$ (Cp^R = Cp (**6**), Cp* (**7**)) a photolytic activation is needed to produce the highly reactive monomer radicals,[42] the complexes $[Cp^RFe(CO)_2]_2$ (Cp^R = Cp^{Ph} (**8**),[43,44] C_5Ph_4(p-MePh) (**9**),[43,44] Cp^{BIG} (**10**)[45]) already partly dissociate in solution at room temperature. This trend was taken to the limit with $[Cp^{5iPr}Fe(CO)_2]_2$ (**11**), since here, due to the sterically very demanding Cp^{5iPr} ligand, no dimerization could be observed in solution.[46] The corresponding dimeric chromium complexes are stabilized by a rather weak Cr–Cr bond. Therefore, the complexes $[Cp^RCr(CO)_3]_2$ (Cp^R = Cp (**12**), Cp* (**13**)) with rather small Cp^R ligands show a monomer-dimer equilibrium already at room temperature.[47] However, the Cp^{Ph} analogue exists in solution as well as in solid state only in the monomeric form of $[Cp^{Ph}Cr(CO)_3]$ (**14**).[48] In the case of molybdenum, the radical monomer is only detected in solutions of $[Cp^{Ph}Mo(CO)_3]_2$ (**15**).[49]

1.3. The Activation of White Phosphorus by Transition Metals

White phosphorus (P_4) is the starting material for the synthesis of many organophosphorus compounds. Therefore, P_4 is typically first treated with chlorine gas to produce PCl_3. In a second step, PCl_3 is then reacted with either Grignard reagents, organolithium compounds or alcohols to produce the desired phosphorous compounds.[50] Since, in addition to the use of hazardous reagents, a stoichiometric amount of side products is formed, intensive research is being conducted on alternative reaction routes. A suitable route is the activation of P_4 with reactive transition metal complexes[51] or main group compounds[52] which yields in P_n ligand complexes. P_n ligands are P_n units that do not bear any organic substituents and are only stabilized by metal fragments. In the following, some examples of transition metal based P_n ligand complexes will be discussed.

Typically, reactive transition metal fragments are generated under either photolytic or thermolytic conditions. These fragments react readily with P_4 via a successive P–P bond cleavage, until the formed P_n unit is stabilized in the coordination sphere of the transition metal (Scheme 1.3). However, the recombination of smaller units leads to the formation of complexes containing larger P_n units (n = > 4). The first P_n ligand complexes were synthesized by Ginsberg and Lindsell via the reaction of $[L_3RhCl]$ with P_4 and leads to the formation of $[L_2RhCl(\eta^{1:1}\text{-}P_4)]$ (L = PPh_3 (**16**), P(p-MePh)$_3$ (**17**), P(m-MePh)$_3$ (**18**), $AsPh_3$ (**19**); Figure 1.1).[53] In these complexes, the P_4 units are side-on coordinated by the Rh fragments, leading to P–P cleavage in the P_4 tetrahedron and the formation of tetra-phosphabicyclo[1.1.0]butane unit.[54] Since then numerous P_n ligand complexes with up to

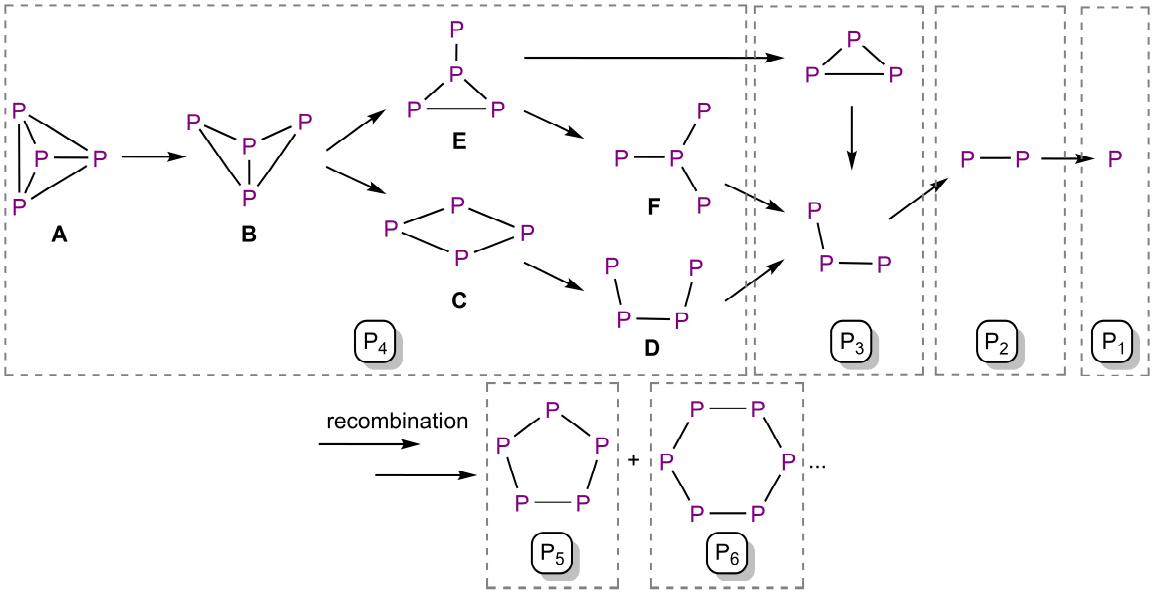

Scheme 1.3. Degradation of P_4 by successive P–P bond cleavage. Recombination of smaller units leads to P_n moieties with n > 4.

24 P atoms have been synthesized.[55] In the following the complexes will be divided into different classes, according to their number of P atoms.

The P_4 unit can be stabilized in six different structural motifs (**A** – **F** in Scheme 1.3). The stabilization of an intact P_4 tetrahedron (**A**) was first reported by Sacconi in 1979 by the synthesis of [(np$_3$)Ni(η^1–P_4)] (**20**, np$_3$ = tris(2-diphenylphosphinoethyl)amine).[56] Besides the terminal bonding, the P_4 tetrahedron can also be side-on coordinated as it could be shown in [M(η^2–P_4)$_2$][A] (M = Cu (**21**),[57] Ag (**22**),[54] A = Al{OC(CF$_3$)$_3$}$_4^-$; M = Au (**23**),[58] A = $GaCl_4^-$). By cleavage of one P–P bond, the tetraphosphabicyclo[1.1.0]butane unit (**B**), or P_4 butterfly unit is obtained which is typically stabilized by either one or two metal fragments. In mononuclear butterfly complexes, the central metal atom is coordinated by the two "wing-tip" P atoms which leads to complexes shown in the upper part of

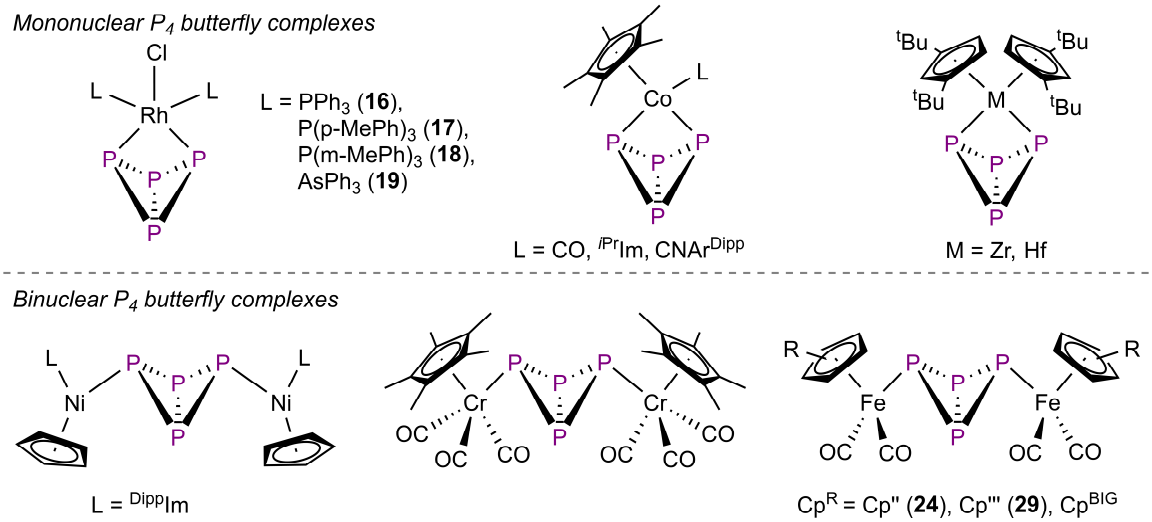

Figure 1.1. Selected examples of mononuclear (top) and binuclear (bottom) P_4 butterfly complexes with ^{iPr}Im = HC(CMeN^{i}Pr)$_2$), ^{Dipp}Im = HC(CMeN(2,6-^{i}Pr$_2$C$_6$H$_3$))$_2$), Ar^{Dipp} = 2,6-(2,6-(^{i}Pr)$_2$C$_6$H$_3$)$_2$C$_6$H$_3$).

Figure 1.1.[53,59–62] the two “wing-tip” P atoms which leads to complexes shown in the upper part of Figure 1.1.[53,59–62] In binuclear P_4 butterfly complexes the “wing-tip” P atoms coordinate to two different metal atoms. A common way to synthesize these binuclear P_4 butterfly complexes is to react P_4 with 17 VE transition metal complexes. Due to the radical character, these complexes are highly reactive which allows the formation of the binuclear P_4 butterfly complexes already under mild conditions (Figure 1.1, bottom).[63,64,65] Remarkable work was done by the Scherer group, since they could observe successive decarbonylation of $[Cp''Fe(CO)_2]_2$ in the presence of P_4 under photolytic conditions.[65] On the one hand this leads to the formation of the butterfly compounds $[\{Cp''Fe(CO)_2\}_2(\mu,\eta^{1:1}\text{-}P_4)]$ (**24**) and $[\{Cp''Fe(CO)_2\}\{Cp''Fe(CO)\}(\mu,\eta^{2:1}\text{-}P_4)]$ (**25**). While, on the other hand the complexes $[\{Cp''Fe(CO)_2\}\{Cp''Fe\}(\mu,\eta^{4:1}\text{-}P_4)]$ (**26**), $[\{Cp''Fe(CO)\}\{Cp''Fe\}(\mu,\eta^{4:2}\text{-}P_4)]$ (**27**), and $[(Cp''Fe)_2(\mu,\eta^{4:4}\text{-}P_4)]$ (**28**) could be isolated. The P_4 unit in **26** is described as a *cyclo*-P_4 unit (**C**), while in **27** an iron-tetraphosphacyclopentadiene-like system is present, which is build up by a *catena*-P_4 unit (**D**). A similar *catena*-P_4 unit is bridging two [Cp’’Fe] fragments in **28**. Comparable complexes were obtained by the thermolytic treatment of $[Cp'''Fe(CO)_2]_2$ since this procedure leads to the formation of the P_4 butterfly complex $[\{Cp'''Fe(CO)_2\}_2(\mu,\eta^{1:1}\text{-}P_4)]$ (**29**), the triple-decker complex $[(Cp'''Fe)_2(\mu,\eta^{4:4}\text{-}P_4)]$ (**30**), and $[Cp'''Fe(\eta^5\text{-}P_5)]$ (**31**).[64] Complex **30** is the analogue Cp’’’ containing complex to **28**, while **31** contains a cyclo-P_5 unit.

Of particular interest are complexes containing a *cyclo*-P_4 end-deck (**C**, Scheme 1.3). The first complexes of this kind were $[(Cp^RM(CO)_2)(\eta^4\text{-}P_4)]$ (M = Nb, Cp^R = Cp* (**32**);[66] M = Ta, Cp^R = Cp’’ (**33**)[67]), while in the last years also complexes of iron[68] and cobalt[69] have been reported. Complexes with P_4 units of type **E** could not be stabilized by a transition metal so far and complexes with P_4 units of type **F** are very rare. The only reported examples are the trinuclear cubanes $[([M])([M'])_2(\mu_3,\eta^{2:2:2}\text{-}P_4)(\mu_3,\eta^{1:1:1}\text{-}P)]$ ([M] = [M’] = Cp*Ni (**34**)[70]; [M] = Cp*Fe, [M’] = Cp’’Ta (**35**)[71]).

Of the two types of P_3 ligands, the *cyclo*-P_3 type is more commonly observed and was first reported by the group of Sacconi.[72] While $[(triphos)Co(\eta^3\text{-}P_3)]$ (**36**, triphos = $CH_3C(CH_2PPh_2)_3$) contains a *cyclo*-P_3 end-deck, the P_3 ligand in $[(triphos)_2Ni(\mu,\eta^3\text{-}P_3)]$ (**37**) acts as a middle deck.

Complexes with biphosphorus ligands can be obtained from the reaction of P_4 with $[CpM(CO)_3]_2$ (M = Cr, Mo) at thermolytic reaction conditions. The obtained complexes $[(CpM(CO)_2)(\mu,\eta^{2:2}\text{-}P_2)]$ (M = Cr (**38**),[73] Mo (**39**)[74]) exhibit a M_2P_2 tetrahedran-like core structure. Under similar conditions, the treatment of P_4 with $[CpCo(CO)_2]$ leads to the triple-decker complexes $[(Cp^RCo)_2(\mu,\eta^{2:2}\text{-}P_2)_2]$ (Cp^R = Cp* (**40**),[75] Cp’’ (**41**),[76] Cp’’’ (**42**)[77]) with bridging side-on coordinated P_2 dumbbells.

Complexes with terminally bound P_1 units are of particular interest due to their formal M≡P triple bond. The first reported complexes of this type were $[(N_3N)M(\eta^1\text{-}P)]$[78] (M = Mo (**43**), W (**44**); N_3N = $(Me_3SiNCH_2CH2)_3N$) and $[Mo(NRAr)_3(\eta^1\text{-}P)]$[79] (**45**, R = $C(CD_3)_2CH_3$, Ar = 3,5-$C_6H_3Me_2$).

P_n units with n > 4 are obtained by aggregation of smaller P_n entities. The most prominent examples are complexes with *cyclo*-P_5 and *cyclo*-P_6 moieties. According to the isolobal concept these units are all-phosphorus analogues of the cyclopentadienyl ligand or benzene, respectively. The pentaphosphaferrocene derivative **31** was already mentioned, however, the first synthesized pentaphosphaferrocene derivative was $[Cp^*Fe(\eta^5\text{-}P_5)]$ (**46**).[80] In 2002, the group of Ellis reported on $[Ti(\eta^5\text{-}P_5)_2]^{2-}$ (**47**), a homoleptic carbon-free sandwich complex.[81] The hexaphosphabenzene unit can only be stabilized as a middle-deck and was first observed in $[(Cp^*Mo)_2(\mu,\eta^{6:6}\text{-}P_6)]$ (**48**).[82]

1.4. Coordination Chemistry of P_n Ligand Complexes

By definition, P_n ligands do not bear any organic substituents. For this reason, P_n ligands typically exhibit stereochemically accessible lone pairs and therefore possess a rich coordination chemistry. The first coordination compound with a P_n ligand complex was presented in 1982 by the group of Sacconi, as they reacted $[(triphos)Co(\eta^3\text{-}P_3)]$ (**36**) with CuBr which yields in $[\{(triphos)Co(\eta^3\text{-}P_3)\}_2(CuBr)_6]$ (**49**).[83] Complex **49** exhibits a central Cu_6Br_6 ring-type structure which bridges two units of **36** (Figure 1.2).

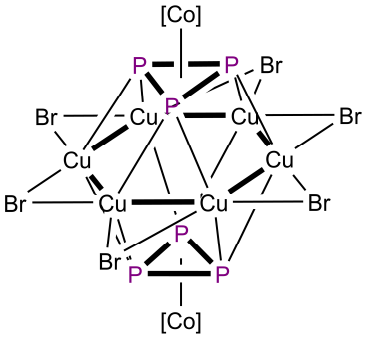

49

Figure 1.2. Structure of $[\{(triphos)Co(\eta^3\text{-}P_3)\}_2(CuBr)_6]$ (**49**) with [Co] = [(triphos)Co].

Especially the pentaphosphaferrocene derivatives show a wide-ranging coordination chemistry, which is extensively investigated by our group. The initial results were obtained by the reaction of $[Cp^*Fe(\eta^5\text{-}P_5)]$ (**46**) with copper halides.[84] The reaction with CuCl yields in the 1D coordination polymer $[\{Cp^*Fe(\eta^{5:1:1}\text{-}P_5)\}CuCl]_n$ (**50**), where two *cyclo*-P_5 units and two Cu cations assemble to form six-membered Cu_2P_4 rings, that are connected via two chlorine atoms (Figure 1.3, left). Surprisingly, the reaction with CuBr a CuI leads to the formation of the 2D polymers $[\{Cp^*Fe(\eta^{5:1:1:1}\text{-}P_5)\}CuX]_n$ (X = Br (**51**), I (**52**)), respectively.

While the *cyclo*-P_5 units in **50** showed a 1,2-coordination pattern, the *cyclo*-P_5 units in **51** and **52** exhibit a 1,2,4-coordination pattern which induces the formation of a 2D network.

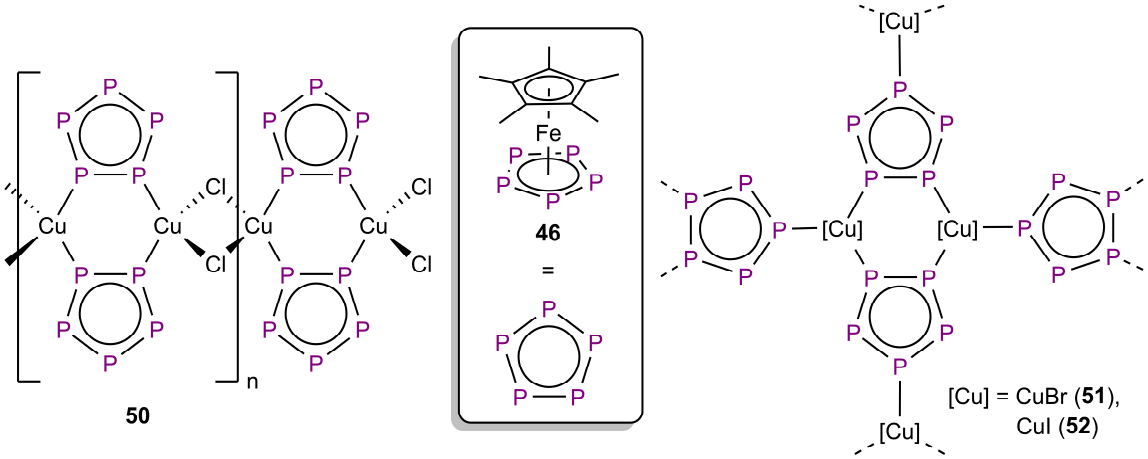

Figure 1.3. 1D and 2D coordination polymers obtained by the reaction of **46** with CuX (X = Cl, Br, I).

By slightly changing the reaction conditions, the reactions of **46** with CuCl and CuBr allow not only the isolation of polymers **50** and **51**, but also the spherical supramolecules $[Cp^*Fe(\eta^5\text{-}P_5)]@[(CuX)_{10}(Cu_2X_3)_5\{Cu(CH_3CN)_2\}_5\{Cp^*Fe(\eta^{5:1:1:1:1:1}\text{-}P_5)\}_{12}]$ (X = Cl (**53**), Br (**54**)).[85] Both aggregates exhibit a similar fullerene-like topology, which is composed of 90 inorganic atoms (Figure 1.4, left). The spheres can be divided in two half-shells that are connected by $[Cu_2X_3]^-$ as well as by $[Cu(CH_3CN)_2]^+$ units. Each half-shell is built up by six *cyclo*-P_5 units and ten Cu_2P_4 rings, which are arranged alternately (Figure 1.4, right). In total, the molecules are composed of twelve units of **46**, with a thirteenth encapsulated inside the sphere. In the following years, several polymers, and supramolecular clusters of different shape could be synthesized.[86,87] However, the most significant progress has

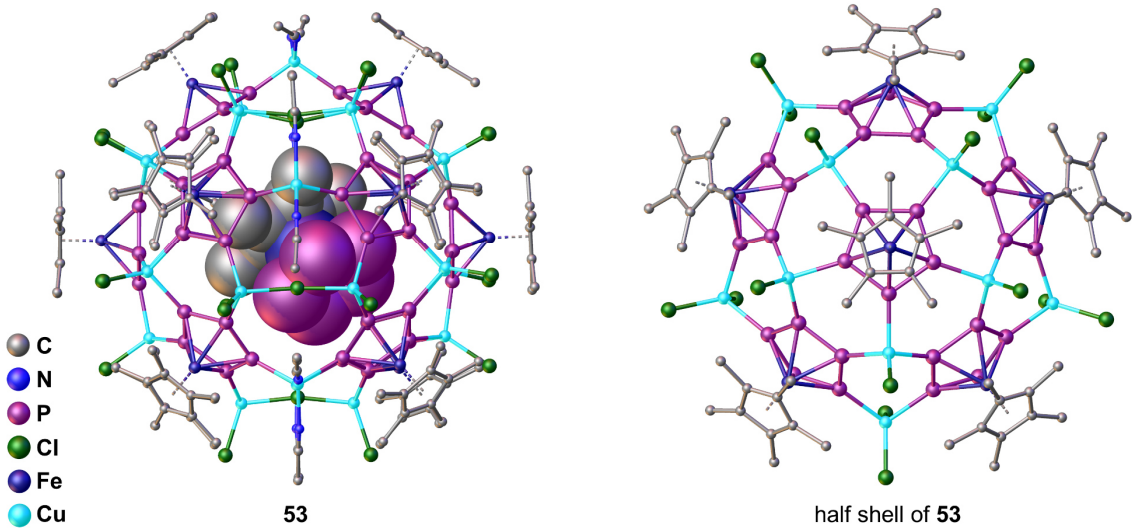

Figure 1.4. Left: Molecular structure of **53** in the crystal. Right: View of a half shell of the molecule of **53**. Hydrogen atoms are omitted for clarity and the encapsulated **46** is depicted in space-filling model.

been made with the use of pentaphosphaferrocene derivatives, which bear larger Cp^R ligands. The introduction of the new building blocks $[Cp^{Bn}Fe(\eta^5\text{-}P_5)]$ (**55**)[88] and $[Cp^{BIG}Fe(\eta^5\text{-}P_5)]$ (**56**)[45] has two advantages. On the one hand, the solubility of the compounds is increased, which allows their characterization in solution. On the other hand, the use of sterically more demanding building blocks leads to the formation of even larger aggregates.[87,89] For example, results the reaction of **56** with CuBr in the formation of the spherical cluster $[\{Cp^{BIG}Fe(\eta^{5:2:1:1:1:1:1}\text{-}P_5)\}_{12}Cu_{70}Br_{83}]$ (**57**).[90] Similar like **53** and **54**, **57** consists also of twelve pentaphosphaferrocene units. However, due to the increased steric bulk of the Cp^{BIG} ligand, the cluster shows topological analogy to the theoretical icosahedral C_{140} fullerene molecule and is build up in several shells.

Furthermore, our group could show that the P_4 butterfly complex $[\{Cp'''Fe(CO)_2\}_2(\mu,\eta^{1:1}\text{-}P_4)]$ (**29**) is a suitable starting material for the synthesis of novel coordination compounds. Due to its geometry and electronic structure, **29** can bind to Lewis acids as a bidentate ligand. The ridged P_4 butterfly scaffold results in small bite angles which is why **29** may be regarded as an inorganic dppm (dppm = $PPh_2CH_2PPh_2$) ligand with larger sterical bulk. An example for this behavior is demonstrated in the reaction of **29** with $[Cu(NCCH_3)_4][BF_4]$.[91] Here, depending on the used stoichiometry, two different coordination compounds were obtained. In a 1:1 reaction the adduct complex $[\{Cp'''Fe(CO)_2\}_2(\mu_3,\eta^{2:1:1}\text{-}P_4)\{Cu(NCCH_3)\}][BF_4]$ (**58**) is formed, where the two “wing-tip” phosphorus atoms of the butterfly unit coordinate the $[Cu(NCCH_3)]^+$ fragment (Figure 1.5). However, by adding an additional equivalent of **29**, the labile acetonitrile ligand is substituted and the

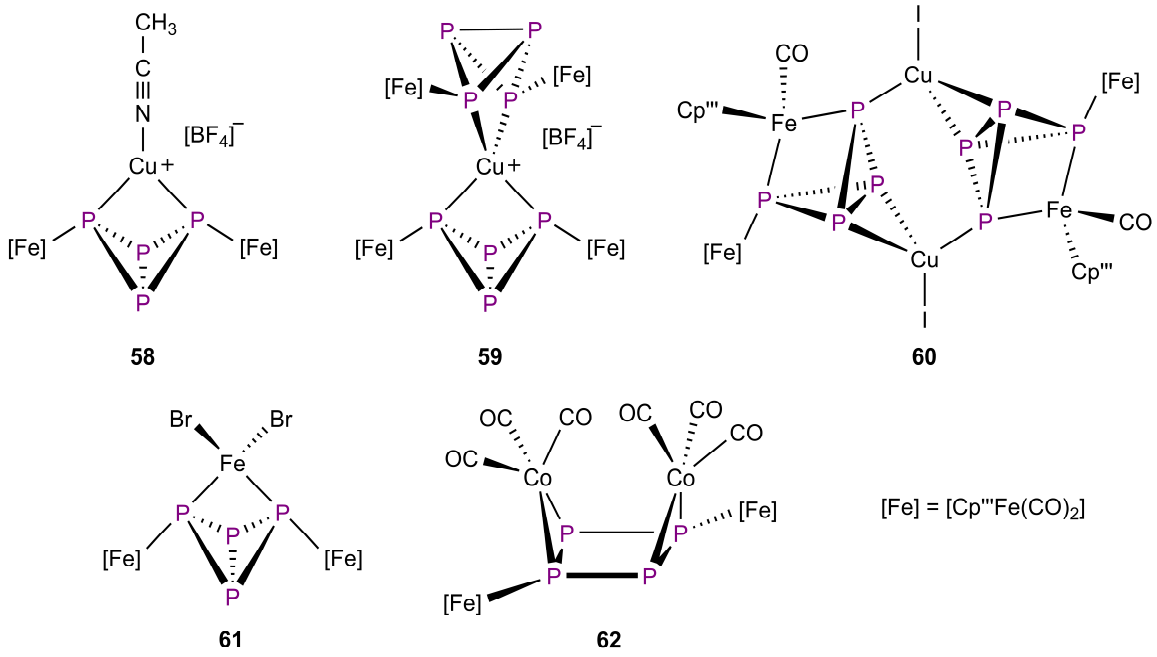

Figure 1.5. Selected examples of coordination compounds derived from $[\{Cp'''Fe(CO)_2\}_2(\mu,\eta^{1:1}\text{-}P_4)]$ (**29**).

spiro-complex [{{Cp'''Fe(CO)$_2$}$_2$(μ_3,$\eta^{2:1:1}$-P$_4$)}$_2$Cu][BF$_4$] (**59**) is formed. Similar reactivity was observed in reactions with monovalent silver and gold salts.[92] Surprisingly, the reaction of **29** with CuI yields in a rearrangement of the butterfly complex and the dimeric complex [{Cp'''Fe(CO)$_2$}{Cp'''Fe(CO)}(μ_4,$\eta^{2:2:1:1}$-P$_4$){CuI}]$_2$ (**60**) is formed after the loss of two CO ligands. This leads to a migration of the [Cp'''Fe(CO)] fragment form an η^1 coordination to an $\eta^{1:1}$ coordination by the two "wing-tip" phosphorus atoms. The two P$_4$units are connected by the coordination of two CuI units via the two "bridge-head" phosphorus atoms and one "wing-tip" phosphorus atom (Figure 1.5). Besides the reactions with coinage metal salts, **29** was also reacted with [FeBr$_2$·dme] (dme = dimethoxyethane) and [Co$_2$(CO)$_8$]. While the reaction with the Fe^{II} compound yields in the adduct complex [{Cp'''Fe(CO)$_2$}$_2$(μ_3,$\eta^{2:1:1}$-P$_4$)(FeBr$_2$)] (**61**),[92] the reaction with [Co$_2$(CO)$_8$] results in {Cp'''Fe(CO)$_2$}$_2$(μ_4,$\eta^{2:2:1:1}$-P$_4$){Co(CO)$_3$}$_2$] (**62**).[93] Complex **62** bears a *cyclo*-P$_4$ unit, which is formed by a P–P bond cleavage and coordinates two [Co(CO)$_3$] fragments in an η^2 coordination mode.

1.5. Reference

[1] N. R. Hinkel, H. E. Hartnett, P. A. Young, *Astrophys. J. Lett.* **2020**, *900*, L38.
[2] J. S. Greaves, A. M. S. Richards, W. Bains, P. B. Rimmer, H. Sagawa, D. L. Clements, S. Seager, J. J. Petkowski, C. Sousa-Silva, S. Ranjan, E. Drabek-Maunder, H. J. Fraser, A. Cartwright, I. Mueller-Wodarg, Z. Zhan, P. Friberg, I. Coulson, E. Lee, J. Hoge, *Nat Astron* **2020**.
[3] a) G. Villanueva, M. Cordiner, P. Irwin, I. de Pater, B. Butler, M. Gurwell, S. Milam, C. Nixon, S. Luszcz-Cook, C. Wilson, V. Kofman, G. Liuzzi, S. Faggi, T. Fauchez, M. Lippi, R. Cosentino, A. Thelen, A. Moullet, P. Hartogh, E. Molter, S. Charnley, G. Arney, A. Mandell, N. Biver, A. Vandaele, K. de Kleer, R. Kopparapu, "No phosphine in the atmosphere of Venus", can be found under https://arxiv.org/pdf/2010.14305, **2020**; b) J. O'Callaghan, *Nature* **2020**, *586*, 182; c) A. Witze, *Nature* **2020**, *587*, 532.
[4] C. Sousa-Silva, S. Seager, S. Ranjan, J. J. Petkowski, Z. Zhan, R. Hu, W. Bains, *Astrobiology* **2020**, *20*, 235.
[5] a) W. Bains, J. J. Petkowski, C. Sousa-Silva, S. Seager, *Sci. Total Environ.* **2019**, *658*, 521; b) R. Jenkins, T.-A. Morris, P. Craig, A. Ritchie, N. Ostah, *Sci. Total Environ.* **2000**, *250*, 73.
[6] a) A. F. Holleman, E. Wiberg, N. Wiberg, *Lehrbuch der anorganischen Chemie*, de Gruyter, Berlin, **2007**; b) H. Diskowski, T. Hofmann in *Ullmann's Encyclopedia of Industrial Chemistry*, Wiley-VCH Verlag GmbH & Co. KGaA, **2000**.
[7] S. Zhang, H.-J. Qian, Z. Liu, H. Ju, Z.-Y. Lu, H. Zhang, L. Chi, S. Cui, *Angew. Chem. Int. Ed.* **2019**, *58*, 1659.
[8] F. Krafft, *Angew. Chem. Int. Ed.* **1969**, *8*, 660.
[9] A. Simon, H. Borrmann, H. Craubner, *Phosphorus Sulfur Silicon Relat. Elem.* **1987**, *30*, 507.
[10] A. Simon, H. Borrmann, J. Horakh, *Chem. Ber.* **1997**, *130*, 1235.
[11] H. Okudera, R. E. Dinnebier, A. Simon, *Z. Kristallogr. Cryst. Mater.* **2005**, *220*.
[12] N. J. Brassington, H. G. M. Edwards, D. A. Long, *J. Raman Spectrosc.* **1981**, *11*, 346.
[13] B. M. Cossairt, C. C. Cummins, A. R. Head, D. L. Lichtenberger, R. J. F. Berger, S. A. Hayes, N. W. Mitzel, G. Wu, *J. Am. Chem. Soc.* **2010**, *132*, 8459.
[14] M. Häser, O. Treutler, *The Journal of Chemical Physics* **1995**, *102*, 3703.
[15] W. L. Roth, T. W. DeWitt, A. J. Smith, *J. Am. Chem. Soc.* **1947**, *69*, 2881.
[16] a) R. Hultgren, N. S. Gingrich, B. E. Warren, *J. Chem. Phys.* **1935**, *3*, 351; b) C. D. Thomas, N. S. Gingrich, *J. Chem. Phys.* **1938**, *6*, 659.
[17] M. Ruck, D. Hoppe, B. Wahl, P. Simon, Y. Wang, G. Seifert, *Angew. Chem. Int. Ed.* **2005**, *44*, 7616.
[18] W. Hittorf, *Ann. Phys. Chem.* **1865**, *202*, 193.
[19] H. Thurn, H. Krebs, *Acta Cryst. B* **1969**, *25*, 125.
[20] a) R. W. Keyes, *Phys. Rev.* **1953**, *92*, 580; b) A. Morita, *Appl. Phys. A* **1986**, *39*, 227.
[21] a) P. W. Bridgman, *J. Am. Chem. Soc.* **1914**, *36*, 1344; b) P. W. Bridgman, *J. Am. Chem. Soc.* **1916**, *38*, 609.
[22] A. Brown, S. Rundqvist, *Acta Cryst.* **1965**, *19*, 684.
[23] T. J. Kealy, P. L. Pauson, *Nat. Chem.* **1951**, *168*, 1039.

[24] a) S. A. Miller, J. A. Tebboth, J. F. Tremaine, *J. Chem. Soc.* **1952**, 632; b) G. Wilkinson, M. Rosenblum, M. C. Whiting, R. B. Woodward, *J. Am. Chem. Soc.* **1952**, *74*, 2125.
[25] a) A.-S. Rodrigues, E. Kirillov, J.-F. Carpentier, *Coord. Chem. Rev.* **2008**, *252*, 2115; b) D. Astruc, C. Ornelas, J. Ruiz, *Acc. Chem. Res.* **2008**, *41*, 841; c) K. Kaleta, A. Hildebrandt, F. Strehler, P. Arndt, H. Jiao, A. Spannenberg, H. Lang, U. Rosenthal, *Angew. Chem. Int. Ed.* **2011**, *50*, 11248; d) J. A. Gladysz, *Chem. Rev.* **2000**, *100*, 1167.
[26] a) G. Gasser, I. Ott, N. Metzler-Nolte, *J. Med. Chem.* **2011**, *54*, 3; b) M. Patra, G. Gasser, *Nat. Rev. Chem.* **2017**, *1*.
[27] R. B. King, M. B. Bisnette, *J. Organomet. Chem.* **1967**, *8*, 287.
[28] a) E. J. Miller, S. J. Landon, T. B. Brill, *Organometallics* **1985**, *4*, 533; b) T. J. Marks, *Science* **1982**, *217*, 989; c) D. C. Calabro, J. L. Hubbard, C. H. Blevins, A. C. Campbell, D. L. Lichtenberger, *J. Am. Chem. Soc.* **1981**, *103*, 6839; d) P. M. Maitlis, *Acc. Chem. Res.* **1978**, *11*, 301; e) R. Bruce King, *Coord. Chem. Rev.* **1976**, *20*, 155.
[29] A. Frei, *Chem. Eur. J.* **2019**, *25*.
[30] a) C. A. Tolman, *Chem. Rev.* **1977**, *77*, 313; b) K. Bunten, *Coord. Chem. Rev.* **2002**, *233-234*, 41.
[31] a) A. Glockner, H. Bauer, M. Maekawa, T. Bannenberg, C. G. Daniliuc, P. G. Jones, Y. Sun, H. Sitzmann, M. Tamm, M. D. Walter, *Dalton Trans.* **2012**, *41*, 6614; b) H. Bauer, A. Glockner, A. C. Tagne Kuate, S. Schafer, Y. Sun, M. Freytag, M. Tamm, M. D. Walter, H. Sitzmann, *Dalton Trans.* **2014**, *43*, 15818.
[32] C. Janiak, H. Schumann, *Adv. Organoment. Chem.* **1991**, *33*, 291.
[33] M. J. Heeg, C. Janiak, J. J. Zuckerman, *J. Am. Chem. Soc.* **1984**, *106*, 4259.
[34] S. Harder, D. Naglav, P. Schwerdtfeger, I. Nowik, R. H. Herber, *Inorg. Chem.* **2014**, *53*, 2188.
[35] P. Jutzi, F. Kohl, P. Hofmann, C. Krüger, Y.-H. Tsay, *Chem. Ber.* **1980**, *113*, 757.
[36] J. L. Atwood, W. E. Hunter, A. H. Cowley, R. A. Jones, C. A. Stewart, *J. Chem. Soc. Chem. Comm.* **1981**, 925.
[37] Y. Schulte, H. Weinert, C. Wölper, S. Schulz, *Organometallics* **2020**, *39*, 206.
[38] G. B. Deacon, C. M. Forsyth, F. Jaroschik, P. C. Junk, D. L. Kay, T. Maschmeyer, A. F. Masters, J. Wang, L. D. Field, *Organometallics* **2008**, *27*, 4772.
[39] H. Sitzmann, T. Dezember, O. Schmitt, F. Weber, G. Wolmershäuser, M. Ruck, *Z. Anorg. Allg. Chem.* **2000**, *626*, 2241.
[40] a) D. J. Burkey, E. K. Alexander, T. P. Hanusa, *Organometallics* **1994**, *13*, 2773; b) M. J. Harvey, T. P. Hanusa, *Organometallics* **2000**, *19*, 1556; c) H. Sitzmann, F. Weber, M. D. Walter, G. Wolmershäuser, *Organometallics* **2003**, *22*, 1931; d) J. J. Schneider, R. Goddard, C. Krüger, *Z. Naturforsch. B* **1995**, *50*, 448; e) F. Baumann, E. Dormann, Y. Ehleiter, W. Kaim, J. Kärcher, M. Kelemen, R. Krammer, D. Saurenz, D. Stalke, C. Wachter, G. Wolmershäuser, H. Sitzmann, *J. Organomet. Chem.* **1999**, *587*, 267; f) M. Wallasch, G. Wolmershäuser, H. Sitzmann, *Angew. Chem. Int. Ed.* **2005**, *44*, 2597; g) D. Weismann, D. Saurenz, R. Boese, D. Bläser, G. Wolmershäuser, Y. Sun, H. Sitzmann, *Organometallics* **2011**, *30*, 6351; h) M. D. Walter, P. S. White, *New J. Chem.* **2011**, *35*, 1842; i) M. Schär, D. Saurenz, F. Zimmer, I. Schädlich, G. Wolmershäuser, S. Demeshko, F. Meyer, H. Sitzmann, O. M. Heigl, F. H. Köhler, *Organometallics* **2013**, *32*, 6298; j) H. Bauer, D. Weismann, G. Wolmershäuser, Y. Sun, H. Sitzmann, *Eur. J. Inorg. Chem.* **2014**, *2014*, 3072; k) U. Chakraborty, M. Modl, B. Mühldorf, M. Bodensteiner, S. Demeshko, van Velzen, Niels J. C., M. Scheer, S. Harder, R. Wolf, *Inorg. Chem.* **2016**, *55*, 3065.
[41] C. Elschenbroich, *Organometallchemie, Vol. 6*, Teubner, Wiesbaden, **2008**.
[42] a) B. D. Moore, M. B. Simpson, M. Poliakoff, J. J. Turner, *J. Chem. Soc. Chem. Comm.* **1984**, 972; b) B. D. Moore, M. Poliakoff, J. J. Turner, *J. Am. Chem. Soc.* **1986**, *108*, 1819; c) A. J. Dixon, M. W. George, C. Hughes, M. Poliakoff, J. J. Turner, *J. Am. Chem. Soc.* **1992**, *114*, 1719.
[43] I. Kuksis, M. C. Baird, *Organometallics* **1994**, *13*, 1551.
[44] I. Kuksis, M. C. Baird, *Organometallics* **1996**, *15*, 4755.
[45] S. Heinl, G. Balázs, M. Scheer, *Phosphorus Sulfur Silicon Relat. Elem.* **2014**, *189*, 924.
[46] H. Sitzmann, T. Dezember, W. Kaim, F. Baumann, D. Stalke, J. Kärcher, E. Dormann, H. Winter, C. Wachter, M. Kelemen, *Angew. Chem. Int. Ed.* **1996**, *35*, 2872.
[47] a) R. D. Adams, F. A. Cotton, *Inorganica Chim. Acta* **1973**, *7*, 153; b) S. J. McLain, *J. Am. Chem. Soc.* **1988**, *110*, 643; c) W. C. Watkins, T. Jaeger, C. E. Kidd, S. Fortier, M. C. Baird, G. Kiss, G. C. Roper, C. D. Hoff, *J. Am. Chem. Soc.* **1992**, *114*, 907.
[48] R. J. Hoobler, M. A. Hutton, M. M. Dillard, M. P. Castellani, A. L. Rheingold, A. L. Rieger, P. H. Rieger, T. C. Richards, W. E. Geiger, *Organometallics* **1993**, *12*, 116.
[49] M. Fei, S. K. Sur, D. R. Tyler, *Organometallics* **1991**, *10*, 419.
[50] D. E. C. Corbridge, *Phosphorus 2000. Chemistry, biochemistry & technology*, Elsevier, Amsterdam, Oxford, **2000**.
[51] a) B. M. Cossairt, N. A. Piro, C. C. Cummins, *Chem. Rev.* **2010**, *110*, 4164; b) M. Caporali, L. Gonsalvi, A. Rossin, M. Peruzzini, *Chem. Rev.* **2010**, *110*, 4178.
[52] M. Scheer, G. Balázs, A. Seitz, *Chem. Rev.* **2010**, *110*, 4236.
[53] A. P. Ginsberg, W. E. Lindsell, *J. Am. Chem. Soc.* **1971**, *93*, 2082.
[54] I. Krossing, L. van Wüllen, *Chem. Eur. J.* **2002**, *8*, 700.
[55] F. Dielmann, M. Sierka, A. V. Virovets, M. Scheer, *Angew. Chem. Int. Ed.* **2010**, *49*, 6860.
[56] P. Dapporto, S. Midollini, L. Sacconi, *Angew. Chem. Int. Ed.* **1979**, *18*, 469.

[57] G. Santiso-Quiñones, A. Reisinger, J. Slattery, I. Krossing, *Chem. Commun.* **2007**, 5046.
[58] L. C. Forfar, T. J. Clark, M. Green, S. M. Mansell, C. A. Russell, R. A. Sanguramath, J. M. Slattery, *Chem. Commun.* **2012**, *48*, 1970.
[59] O. J. Scherer, M. Swarowsky, G. Wolmershaeuser, *Organometallics* **1989**, *8*, 841.
[60] S. Dürr, D. Ertler, U. Radius, *Inorg. Chem.* **2012**, *51*, 3904.
[61] C. C. Mokhtarzadeh, A. L. Rheingold, J. S. Figueroa, *Dalton Trans.* **2016**, *45*, 14561.
[62] O. J. Scherer, M. Swarowsky, H. Swarowsky, G. Wolmershäuser, *Angew. Chem. Int. Ed.* **1988**, *27*, 694.
[63] a) S. Pelties, D. Herrmann, B. de Bruin, F. Hartl, R. Wolf, *Chem. Commun.* **2014**, *50*, 7014; b) D. W. Agnew, C. E. Moore, A. L. Rheingold, J. S. Figueroa, *Angew. Chem. Int. Ed.* **2015**, *54*, 12673; c) S. Heinl, M. Scheer, *Chem. Sci.* **2014**, *5*, 3221; d) C. Schwarzmaier, A. Y. Timoshkin, G. Balázs, M. Scheer, *Angew. Chem. Int. Ed.* **2014**, *53*, 9077; e) L. Weber, U. Sonnenberg, *Chem. Ber.* **1991**, *124*, 725.
[64] O. J. Scherer, T. Hilt, G. Wolmershäuser, *Organometallics* **1998**, *17*, 4110.
[65] O. J. Scherer, G. Schwarz, G. Wolmershäuser, *Z. Anorg. Allg. Chem.* **1996**, *622*, 951.
[66] O. J. Scherer, J. Vondung, G. Wolmershäuser, *Angew. Chem. Int. Ed.* **1989**, *28*, 1355.
[67] O. J. Scherer, R. Winter, G. Wolmershäuser, *Z. Anorg. Allg. Chem.* **1993**, *619*, 827.
[68] a) A. Cavaillé, N. Saffon‐Merceron, N. Nebra, M. Fustier‐Boutignon, N. Mézailles, *Angew. Chem. Int. Ed.* **2018**, *57*, 1874; b) U. Chakraborty, J. Leitl, B. Muhldorf, M. Bodensteiner, S. Pelties, R. Wolf, *Dalton Trans.* **2018**, *47*, 3693.
[69] a) C. M. Hoidn, T. M. Maier, K. Trabitsch, J. J. Weigand, R. Wolf, *Angew. Chem. Int. Ed.* **2019**, *58*, 18931; b) F. Dielmann, A. Timoshkin, M. Piesch, G. Balázs, M. Scheer, *Angew. Chem. Int. Ed.* **2017**, *56*, 1671.
[70] O. J. Scherer, J. Braun, G. Wolmershäuser, *Chem. Ber.* **1990**, *123*, 471.
[71] O. J. Scherer, T. Mohr, G. Wolmershäuser, *J. Organomet. Chem.* **1997**, *529*, 379.
[72] M. Di Vaira, C. A. Ghilardi, S. Midollini, L. Sacconi, *J. Am. Chem. Soc.* **1978**, *100*, 2550.
[73] L. Y. Goh, C. K. Chu, R. C. S. Wong, T. W. Hambley, *Dalton Trans.* **1989**, 1951.
[74] O. J. Scherer, H. Sitzmann, G. Wolmershäuser, *J. Organomet. Chem.* **1984**, *268*, C9-C12.
[75] M. E. Barr, L. F. Dahl, *Organometallics* **1991**, *10*, 3991.
[76] M. Scheer, U. Becker, M. H. Chisholm, J. C. Huffman, F. Lemoigno, O. Eisenstein, *Inorg. Chem.* **1995**, *34*, 3117.
[77] O. J. Scherer, G. Berg, G. Wolmershäuser, *Chem. Ber.* **1995**, *128*, 635.
[78] N. C. Zanetti, R. R. Schrock, W. M. Davis, *Angew. Chem. Int. Ed.* **1995**, *34*, 2044.
[79] C. E. Laplaza, W. M. Davis, C. C. Cummins, *Angew. Chem. Int. Ed.* **1995**, *34*, 2042.
[80] O. J. Scherer, T. Brück, *Angew. Chem. Int. Ed.* **1987**, *26*, 59.
[81] E. Urneúzÿius, W. W. Brennessel, C. J. Cramer, J. E. Ellis, P. von Ragué Schleyer, *Science* **2002**, *295*, 832.
[82] O. J. Scherer, H. Sitzmann, G. Wolmershäuser, *Angew. Chem. Int. Ed.* **1985**, *24*, 351.
[83] M. Di Vaira, L. Sacconi, *Angew. Chem. Int. Ed.* **1982**, *21*, 330.
[84] J. Bai, A. V. Virovets, M. Scheer, *Angew. Chem. Int. Ed.* **2002**, *41*, 1737.
[85] a) J. Bai, A. V. Virovets, M. Scheer, *Science* **2003**, *300*, 781; b) M. Scheer, J. Bai, B. P. Johnson, R. Merkle, A. V. Virovets, C. E. Anson, *Eur. J. Inorg. Chem.* **2005**, 4023.
[86] a) M. Scheer, L. J. Gregoriades, A. V. Virovets, W. Kunz, R. Neueder, I. Krossing, *Angew. Chem. Int. Ed.* **2006**, *45*, 5689; b) M. Scheer, A. Schindler, R. Merkle, B. P. Johnson, M. Linseis, R. Winter, C. E. Anson, A. V. Virovets, *J. Am. Chem. Soc.* **2007**, *129*, 13386; c) M. Scheer, A. Schindler, C. Gröger, A. V. Virovets, E. V. Peresypkina, *Angew. Chem. Int. Ed.* **2009**, *48*, 5046; d) M. Scheer, A. Schindler, J. Bai, B. P. Johnson, R. Merkle, R. Winter, A. V. Virovets, E. V. Peresypkina, V. A. Blatov, M. Sierka, H. Eckert, *Chem. Eur. J.* **2010**, *16*, 2092; e) F. Dielmann, A. Schindler, S. Scheuermayer, J. Bai, R. Merkle, M. Zabel, A. V. Virovets, E. V. Peresypkina, G. Brunklaus, H. Eckert, M. Scheer, *Chem. Eur. J.* **2012**, *18*, 1168; f) C. Schwarzmaier, A. Schindler, C. Heindl, S. Scheuermayer, E. V. Peresypkina, A. V. Virovets, M. Neumeier, R. Gschwind, M. Scheer, *Angew. Chem. Int. Ed.* **2013**, *52*, 10896; g) H. Brake, E. Peresypkina, C. Heindl, A. V. Virovets, W. Kremer, M. Scheer, *Chem. Sci.* **2019**, *10*, 2940.
[87] C. Heindl, E. Peresypkina, A. V. Virovets, I. S. Bushmarinov, M. G. Medvedev, B. Krämer, B. Dittrich, M. Scheer, *Angew. Chem. Int. Ed.* **2017**, *56*, 13237.
[88] F. Dielmann, R. Merkle, S. Heinl, M. Scheer, *Z. Naturforsch. B* **2009**, 3.
[89] a) F. Dielmann, C. Heindl, F. Hastreiter, E. V. Peresypkina, A. V. Virovets, R. M. Gschwind, M. Scheer, *Angew. Chem. Int. Ed.* **2014**, *53*, 13605; b) F. Dielmann, M. Fleischmann, C. Heindl, E. V. Peresypkina, A. V. Virovets, R. M. Gschwind, M. Scheer, *Chem. Eur. J.* **2015**, *21*, 6208; c) C. Heindl, S. Heinl, D. Lüdeker, G. Brunklaus, W. Kremer, M. Scheer, *Inorganica Chim. Acta* **2014**, *422*, 218; d) C. Heindl, E. V. Peresypkina, A. V. Virovets, W. Kremer, M. Scheer, *J. Am. Chem. Soc.* **2015**, *137*, 10938.
[90] S. Heinl, E. Peresypkina, J. Sutter, M. Scheer, *Angew. Chem. Int. Ed.* **2015**, *54*, 13431.
[91] C. Schwarzmaier, S. Heinl, G. Balázs, M. Scheer, *Angew. Chem. Int. Ed.* **2015**, *54*, 13116.
[92] C. Schwarzmaier, *Ph.D. Thesis*, University of Regensburg, Regensburg, **2012**.
[93] M. Eberl, *Ph.D. thesis*, University of Regensburg, Regensburg, **2011**.

2. Research Objectives

First investigations of the coordination chemistry of the P_4 butterfly complex [{Cp'''Fe(CO)$_2$}$_2$(μ,η$^{1:1}$-P_4)] towards Lewis acids have already been performed. Based on the results obtained, it was claimed that the P_4 butterfly complex can be considered as an inorganic dppm derivative. This assertion is mostly correct, but in some cases, it could also be shown that [{Cp'''Fe(CO)$_2$}$_2$(μ,η$^{1:1}$-P_4)] is not a pure spectator ligand. In these rare examples, under certain conditions, either the P_4 framework or the stabilizing iron fragments were rearranged. Therefore, the objectives for this work were to:

- Investigation of the coordination behavior of [{Cp'''Fe(CO)$_2$}$_2$(μ,η$^{1:1}$-P_4)] towards transition metal-based Lewis acids;
- Determination of the reaction conditions for the rearrangement of the P_4 butterfly complex.

Based on the results obtained in the synthesis of supramolecular aggregates with [Cp*Fe(η^5-P_5)] and coinage metals, the new building blocks [Cp^{Bn}Fe(η^5-P_5)] and [Cp^{BIG}Fe(η^5-P_5)] were introduced into supramolecular chemistry. Especially the use of the sterically more demanding Cp^{Bn} and Cp^{BIG} ligands enabled the formation of larger spherical aggregates. For this reason, we were interested in whether it is possible to form even larger aggregates by further increasing the steric demand of the Cp^R ligand attached to the pentaphosphaferrocene.

Preliminary results in the synthesis of an alkyl substituted pentabiphenylcyclopentadienyl ligand were presented in my master thesis. However, the first attempts to attach the super bulky Cp^R ligand to iron failed. Instead, only a remarkably stable cyclopentadienyl radical could be isolated. Based on these results the following research tasks arise:

- Study the reactivity of the cyclopentadienyl radical;
- Optimization of the reaction conditions to obtain iron complexes with a super bulky Cp^R ligand;
- Synthesis of a super bulky pentaphosphaferrocene derivative;
- Probe the potential of the super bulky pentaphosphaferrocene derivative as a building block in supramolecular chemistry.

Preface

The following chapter has already been published: The article is reprinted with permission of Wiley-VCH. License Number: 5024271270361.

English version: 'Rearrangement of a P_4 Butterfly Complex – The Formation of a Homoleptic Phosphorus–Iron Sandwich Complex'

Angew. Chem. Int. Ed. **2017***, 56,* 7312–7317.

German version: 'Umwandlung eines P_4-Butterfly-Komplexes – die Bildung eines homoleptischen Phosphor-Eisen-Sandwich-Komplexes'

Angew. Chem. **2017***, 129,* 7418–7423.

Authors

Julian Müller, Sebastian Heinl, Christoph Schwarzmaier, Gábor Balázs, Martin Keilwerth, Karsten Meyer, Manfred Scheer.

Author contribution

The main part of the preparation of the manuscript was done by J. Müller. Parts of the introduction and parts of the discussion of compound **2** were written by C. Schwarzmaier. G. Balázs performed the DFT calculations and contributed the corresponding parts in the manuscript and the Supporting Information. C. Schwarzmaier described the synthesis and characterization (NMR, IR, MS, EA, X-Ray, EPR, Evans-NMR) of compound **2** in his PhD thesis. Primarily investigations on compound **3** were performed by S. Heinl. The optimization of the synthesis of **3**, synthesis of **4** and **5**, and the characterization (NMR, IR, MS, EA, X-Ray) of **3**, **4**, and **5** was done by J. Müller. The characterization (NMR, IR, MS, EA, X-Ray) of **3** was already part of J. Müller's master thesis. Samples for the Mößbauer measurements of **2**, **3**, and **5** were provided by J. Müller. The measurement and interpretation of Mößbauer spectra of **2**, **3**, and **5** were performed by M. Keilwerth. The corresponding part in the Supporting Information was written by M. Keilwerth. and K. Meyer. M. Scheer supervised the research and revised the manuscript.

Acknowledgements

This work was supported by the Deutsche Forschungsgemeinschaft (DFG, Sche 384/32-1).

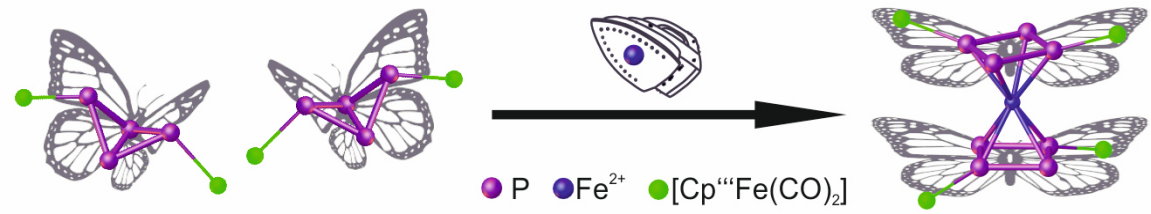
P
Fe2+
[Cp‘‘‘Fe(CO)2]

3. Rearrangement of a P_4 Butterfly Complex – The Formation of a homoleptic Phosphorus-Iron Sandwich Complex

Abstract: *The versatile coordination behavior of the P_4 butterfly complex [{Cp'''Fe(CO)$_2$}$_2$($\mu,\eta^{1:1}$-P_4)] (**1**, Cp''' = η^5-$C_5H_2{}^tBu_3$) towards different iron(II) compounds is presented. The reaction of **1** with [$FeBr_2$·dme] (dme = dimethoxyethane) leads to the chelate complex [{Cp'''Fe(CO)$_2$}$_2$($\mu_3,\eta^{1:1:2}$-P_4){$FeBr_2$}] (**2**), whereas, in the reaction with [Fe(CH_3CN)$_6$][PF_6]$_2$, an unprecedented rearrangement of the P_4 butterfly structural motif leads to the cyclo-P_4 moiety in {(Cp'''Fe(CO)$_2$)$_2$($\mu_3,\eta^{1:1:4}$-P_4)}$_2$Fe][PF_6]$_2$ (**3**). Complex **3** represents the first fully characterized "carbon-free" sandwich complex containing cyclo-P_4R_2 ligands in a homoleptic-like iron–phosphorus-containing molecule. Alternatively, **2** can be transformed into **3** by halogen abstraction and subsequent coordination of **1**. The additional isolated side products, [{Cp'''Fe(CO)$_2$}$_2$($\mu_3,\eta^{1:1:2}$-P_4){Cp'''Fe(CO)}][PF_6] (**4**) and [{Cp'''Fe(CO)$_2$}$_2$($\mu_3,\eta^{1:1:4}$-P_4){Cp'''Fe}][PF_6] (**5**), give insight into the stepwise activation of the P_4 butterfly moiety in **1**.*

3.1. Introduction

The activation of small molecules has been an area of great interest over the last years. The conversion of molecules such as dinitrogen or carbon dioxide under mild reaction conditions could be the answer to an ever-expanding energy demand.[1] But also the activation of other molecules such as white phosphorus (P_4) is of particular interest, since P_4 is an important industrial starting material.[2] The activation of P_4 can be mediated by main group elements[3] as well as by transition metals.[4] One of the first degradation steps is the formation of a tetraphosphabicyclo[1.1.0]butane unit.[5] This so-called butterfly framework can either be stabilized by one[5,6] or two[7] covalently bound metal fragments or organic substituents.[8] These butterfly complexes can be further converted by P–P bond cleavage between the two "bridgehead" phosphorus atoms. Scherer et al. reported the formation of a formal $P_4{}^{4-}$ ligand by an oxidative addition of a P–P bond in [{Cp*Co(CO)}(η^2-P_4)] (**A**, Cp* = η^5-$C_5(CH_3)_5$) to a [Cp*Co(CO)] fragment, which leads to [{Cp*Co(CO)}$_2$($\mu,\eta^{2:2}$-P_4)] (**B**) (Scheme 3.1).[6a] Rather unselective activation processes of P_4 butterfly complexes proceed via photolysis[9] or thermolysis.[6d,9b,10] However, successive decarbonylation and P–P bond cleavage of [{Cp''Fe(CO)$_2$}$_2$($\mu,\eta^{1:1}$-P_4)] (**C**, Cp'' = η_5-$C_5H_3{}^tBu_2$) was reported under photolytic conditions,[7a] whereas the thermolysis of [{Cp'''Fe(CO)$_2$}$_2$($\mu,\eta^{1:1}$-P_4)] (**1**, Cp''' = η^5-$C_5H_2{}^tBu_3$) leads to the *catena*-P_4 ligand containing complex **G** and the pentaphosphaferrocene derivative **H**.[11]

Further, we could recently show that **1** is able to act as a bidentate ligand itself. This unique feature arises from the spatial proximity of the two "wing-tip" phosphorus atoms and their electronical properties. Thus, **1** chelates on [Cu(CH_3CN)$_4$][BF_4] to give the monoadduct [{Cp'''Fe(CO)$_2$}$_2$($\mu_3,\eta^{1:1:2}$-P_4){Cu(CH_3CN)}][BF_4] (**I**) and the spiro compound [{(Cp'''Fe(CO)$_2$)$_2$($\mu_3,\eta^{1:1:2}$-P_4)}$_2$Cu][BF_4] (**J**) (Scheme 3.1).[12] Both complexes still bear the intact P_4-butterfly as ligand. We supposed that the reaction outcome might change if a less

electron-rich transition metal moiety is used instead of Cu^{I}. Thus, we chose iron(II) compounds as promising candidates, since most of the previously discussed activation reactions proceed in the presence of d^6 metals. Furthermore, chelate complexes of iron(II) halides have drawn special interest because of their use as catalysts in different processes. Gibson et al. investigated the use of $[(R_2EC_2H_4ER_2)FeX_2]$ (E = N, P;X = Cl, Br; R = alkyl or aryl) complexes as catalysts for the controlled polymerization of styrene and acrylate monomers.[13] Moreover, Tyler et al. reported on the catalytic activity of $[(dppe)_2FeCl_2]$ (dppe = $Ph_2PC_2H_4PPh_2$) for the direct generation of ammonia from hydrogen and dinitrogen.[14]

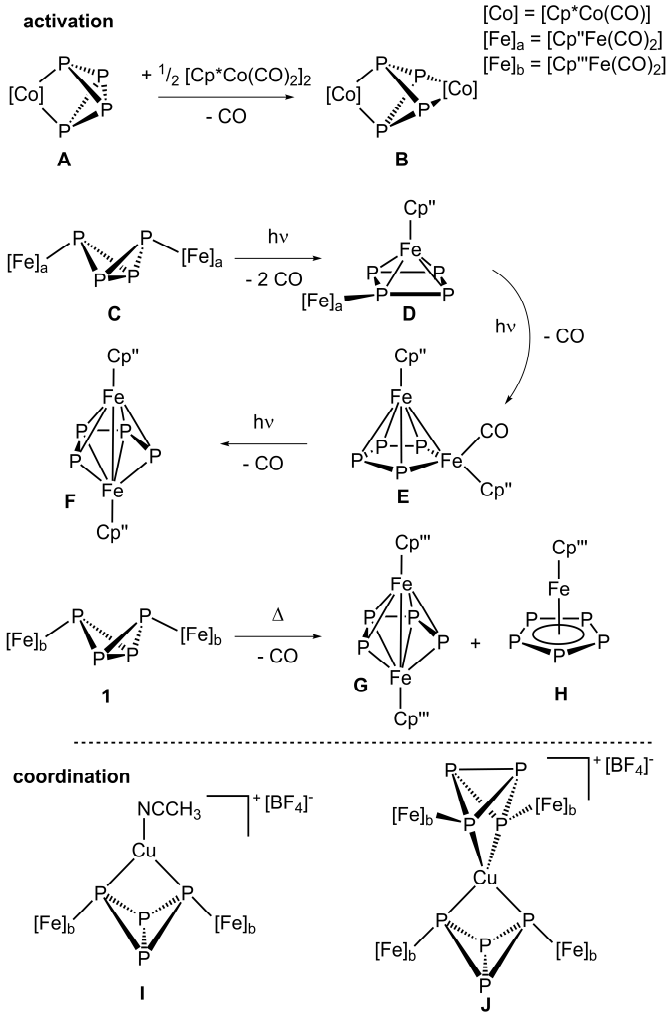

Scheme 3.1. Transformation reactions of selected P_4 butterfly complexes (**1** and **A** – **H**) and representation of the coordination compounds of **1** with $[Cu(CH_3CN)_4][BF_4]$ (**I** and **J**).

Herein we report on the detailed studies of the versatile coordination behavior of the butterfly complex **1** towards different iron(II) compounds as Lewis acids. Depending on the nature of the anion, either chelate complexes are obtained or an unprecedented isomerization of the butterfly unit occurs by the unique formation of a homoleptic-like complex containing aromatic *cyclo*-P_4R_2 ligands (R = Cp'''$Fe(CO)_2$) (Scheme 3.2).[15]

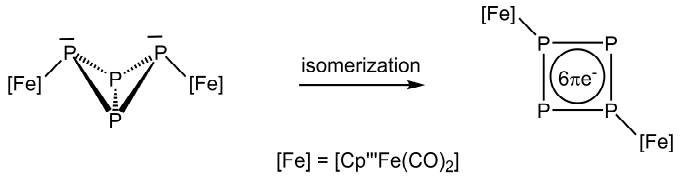

Scheme 3.2. Schematic representation of the isomerization process of **1.**

3.2. Results and Discussion

The reaction of [$FeBr_2$·dme] with **1** in a 1:1 ratio ((i) in Scheme 3.3) leads to [{Cp'''$Fe(CO)_2$}$_2$(μ_3,$\eta^{1:1:2}$-P_4){$FeBr_2$}] (**2**) in a 52% isolated crystalline yield ($^{31}P\{^1H\}$ NMR shows a quantitative conversion of **1**). Complex **2** is paramagnetic and ^{31}P NMR as well as EPR silent. The effective magnetic moment of **2** in solution was determined by the Evans method[16] giving μ_{eff} = 6.1 μ_B, which corresponds approximately to four unpaired electrons. The μ_{eff} value of **2** is slightly larger than that of [($R_2PC_2H_4PR_2$)$FeCl_2$] (R = alkyl or aryl) (μ_{eff} = 5.0 – 5.5 μ_B).[13] DFT calculations at the BP86/def2-TZVP level show that the quintet spin state is the ground state of **2** with the triplet and the singlet spin states lying higher in energy with 67.94 and 98.82 kJmol^{-1}, respectively. Furthermore, the formation of **2** from [$FeBr_2$·dme] and **1** is exothermic by −64.03 kJmol^{-1}. The Mößbauer spectrum shows doublets for the central and the terminal iron atoms (central Fe: δ = 0.73(3) mms^{-1} and ΔE_q = 2.33(1) mms^{-1}; two terminal iron atoms: δ = 0.12(3) mms^{-1} and ΔE_q =

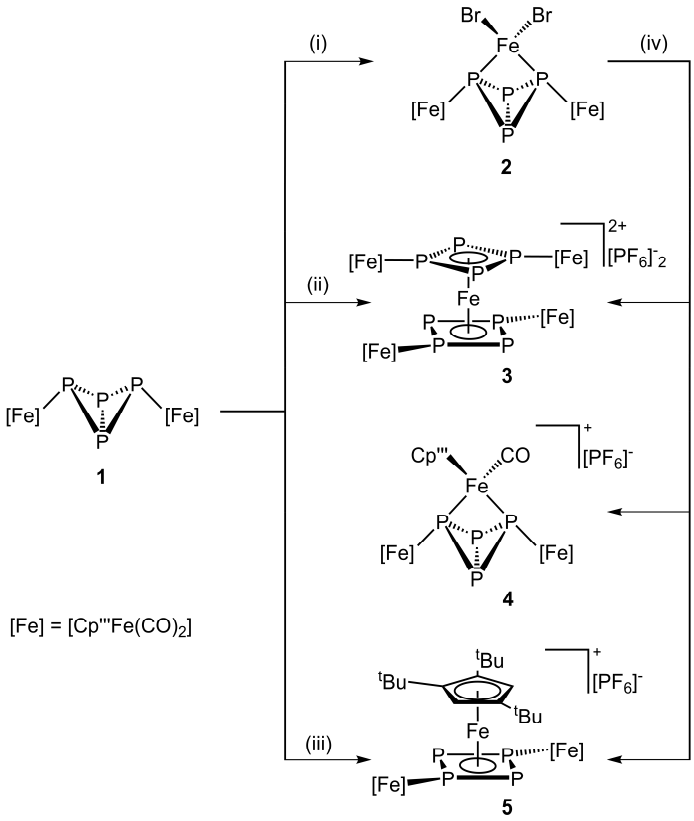

Scheme 3.3. Synthesis of the products starting from **1**:
(i) **1** + [$FeBr_2$·dme]; (ii) **1** + 0.5 [$Fe(CH_3CN)_6$][PF_6]$_2$; (iii) **1** + 0.5 [{Cp'''Fe(μ-Br)}$_2$] + $TlPF_6$; (iv) **1** + **2** + $TlPF_6$.

1.73(4) mms^{-1}). These values are in good agreement with the calculated ones[17] and indicate an iron(II) high-spin configuration for the central iron and an iron(II) low-spin configuration for the terminal iron atoms.[18] The IR spectrum (KBr) of **2** shows two strong absorption bands at $\tilde{\nu}$ = 2029 and 1983 cm^{-1}, which are about 30 cm^{-1} blue-shifted compared to **1**.

The molecular structure of **2** (Figure 3.1) reveals that the Lewis acidic Fe3 atom is coordinated by two terminal bromine atoms and the "wing-tip" phosphorus atoms of the butterfly ligand **1** in a distorted tetrahedral manner. The dihedral angle between the planes defined by the atoms Br1–Fe3–Br2 and P1–Fe3–P2 is 85.35(2)°. The P1–Fe3–P2 bond angle of 70.27(3)° is smaller than the corresponding bond angles in the chelate complexes **I** (75.19(2)°) and **J** (72.51(3)° and 72.71(3)°).[12] The P–$Fe_{cent.}$ distances (2.4823(8) Å and 2.4364(7) Å) compare well with those found in [$(Cy_2PC_2H_4PCy_2)FeCl_2$] (Cy = cyclohexyl, 2.461(1) Å and 2.466(1) Å).[13] The P–P (2.2057(9) – 2.2216(10) Å) and P–$Fe_{term.}$ (2.2634(7) and 2.2861(8) Å) distances are similar to the ones of **J** exhibiting a similar coordination environment of the Lewis acid, nicely exemplifying the potential of **1** to serve as a small bite angle chelate ligand for different Lewis acids.

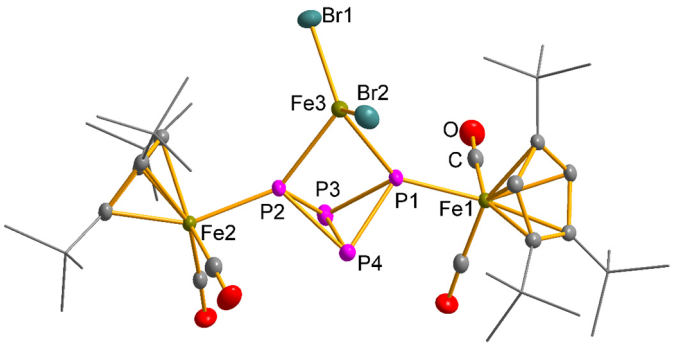

Figure 3.1. Structure of **2** in the crystal. Solvent molecules and H atoms are omitted for clarity. Ellipsoids are set at 50% probability.

By switching from tightly coordinated Br ligands to substitutionally more labile CH_3CN ligands on Fe, we speculated that the reaction of **1** with $[Fe(CH_3CN)_6][PF_6]_2$ would lead to a similar complex formation than in the case of $[Cu(CH_3CN)_4][BF_4]$ (formation of **I** and **J**). But, to our surprise, the reaction of two equivalents of **1** with one equivalent of $[Fe(CH_3CN)_6][PF_6]_2$ ((ii) in Scheme 3.3) leads to the quantitative formation (according to $^{31}P\{^1H\}$ NMR) of the unprecedented sandwich complex $[\{(Cp'''Fe(CO)_2)_2(\mu_3,\eta^{1:1:4}\text{-}P_4)\}_2Fe][PF_6]_2$ (**3**) isolated in a 68% crystalline yield. Obviously, an isomerization has occurred by transforming the butterfly P_4R_2 ligand into the 6π-aromatic P_4R_2 ligand (Scheme 3.2) to form the unique homoleptic-like octaphosphorus iron sandwich complex **3**. After the homoleptic decaphosphatitanocene dianion synthesized by Ellis et al.[19] this is another unique example for an all-phosphorus ligand containing sandwich complex.

Single-crystal X-ray diffraction reveals that the central Fe atom in **3** is coordinated by two planar *cyclo*-P_4 units (Figure 3.2). Each *cyclo*-P_4 unit is substituted by two bulky [Cp'''Fe(CO)$_2$] fragments. The P–P distances vary from 2.1406(10) Å to 2.1547(10) Å and are between a P–P single (2.20–2.25 Å) and a P–P double bond (2.00–2.05 Å), which compares well to the P–P distances found in the isolated P_4^{2-} anion in $Cs_2P_4{\cdot}2NH_3$ (2.146(1) Å and 2.1484(9) Å).[20] The *cyclo*-P_4R_2 (R = Cp'''Fe(CO)$_2$) units in **3** are slightly distorted from the symmetric square geometry with P–P–P bond angles of 82.76(4)°/82.88(4)° and 97.11(4)°/97.24(4)°. Due to the geometry analogy of the two *cyclo*-P_4 units in **3** and $Cs_2P_4{\cdot}2NH_3$, we propose that the *cyclo*-P_4 units in **3** can be formally described as aromatic 6 π-electron-containing R_2P_4 ligands. The two *cyclo*-P_4 planes in **3** are parallel to each other but twisted along the $P_{4,cent.}$-Fe-$P_{4,cent.}$ axis with a torsion angle of 60°. Interestingly, for the hypothetical $[Fe(P_4)_2]^{2-}$ dianion containing square *cyclo*-P_4 ligands, a staggered conformation (torsion angle of 45°; D_{4d} symmetry) has been predicted by DFT studies.[21] The distances between the *cyclo*-P_4 plane centroids and Fe3 are 1.7648(7) Å and 1.7759(7) Å, thus being slightly longer than the calculated ones for the $[Fe(P_4)_2]^{2-}$ anion (1.739 Å).[21] The $Fe_{term.}$–P distances vary from 2.2255(9) Å to 2.2317(9) Å and are slightly longer than the corresponding distance in **D** (2.211(1) Å) (Scheme 3.1)[7a] but are shorter than those in **1** (2.348(2) Å and 2.3552(19) Å).[11]

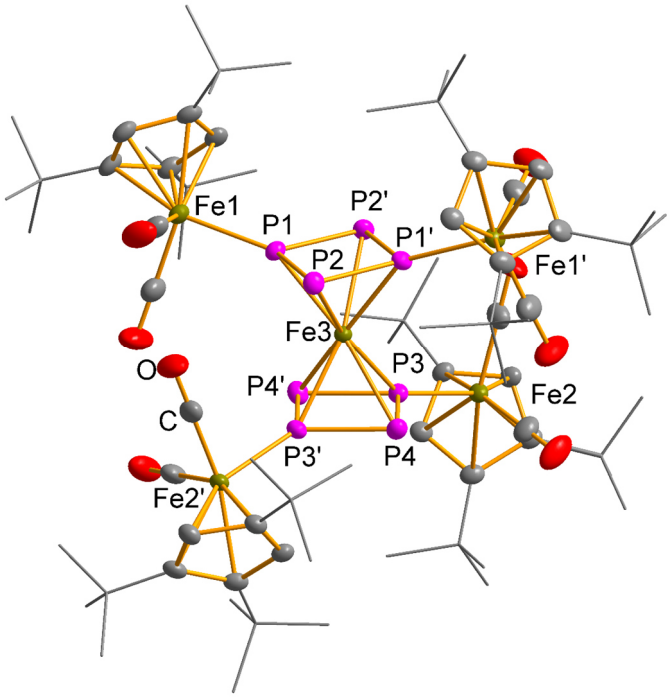

Figure 3.2. Cationic part of the structure of **3** in the crystal. H atoms and solvent molecules are omitted for clarity. Ellipsoids are set at 50% probability.

To obtain a deeper insight into the formation of **3** and its electronic structure, DFT calculations at the BP86/def2-TZVP level were performed, which show that the reaction of $[Fe(CH_3CN)_6]^{2+}$ (quintet spin state) with **1** is exothermic by −118.76 kJmol^{-1} indicating the preferred formation of **3**. The inspection of the natural charge distribution in **3** shows that

the *cyclo*-P_4 ligand is a good electron donor but a weak acceptor. This becomes obvious by comparing the charge distribution in **3** and the free planar ligand [{Cp'''Fe(CO)$_2$}$_2$(P_4)] (**L**). While each *cyclo*-P_4 unit in **3** bears an overall positive charge of 0.47, in the free ligand **L**, it bears a partial negative charge of −0.50. Further stabilization arises from the [Cp'''Fe(CO)$_2$] substituents, which additionally dissipate the overall twofold positive charge in **3**, each bearing a partial positive charge of 0.44. The Wiberg Bond Index (WBI) of the P–P bonds (0.97 on average) as well as of the $Fe_{term.}$–P bonds (0.91 on average) are close to unity. In contrast, the WBI of the $Fe_{cent.}$–P bonds are considerably lower (0.63 on average) indicating the π-type coordination of the *cyclo*-P_4 units in **3**. Both, the highest occupied (HOMO) and the lowest unoccupied (LUMO) molecular orbital are mainly iron-centered non-bonding orbitals, while the HOMO−1 and HOMO−2 orbitals are Fe–P bonding orbitals (Figure 3.3).

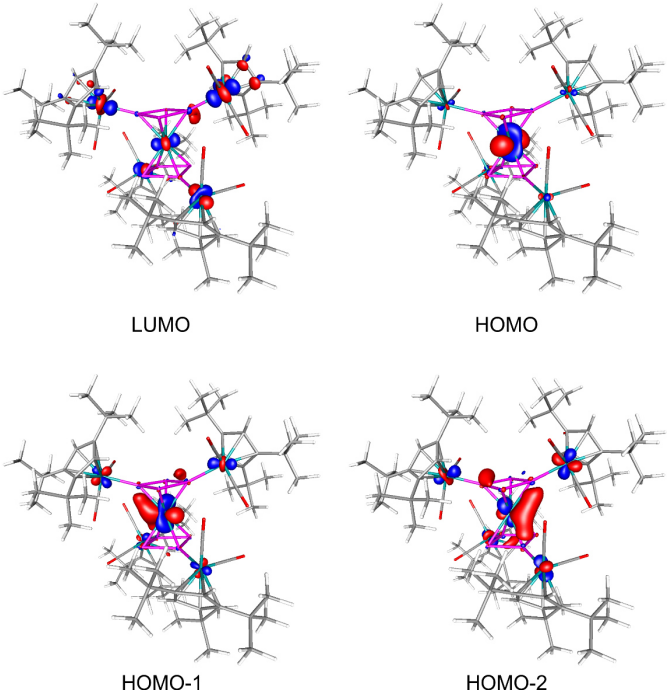

Figure 3.3. Frontier molecular orbitals in **3** at the BP86/def2-TZVP level.

In the $^{31}P\{^1H\}$ NMR spectrum (CD_2Cl_2) of **3**, two multiplets at δ = 91.7 ppm and 114.3 ppm corresponding to an AA'BB' spin system were observed, which could be confirmed by simulation (Figure 3.4; for coupling constants cf. Table S3.2).[17] The downfield shifted signal is assigned to the atoms P1, P1', P3, P3' and the upfield shifted signal to P2, P2', P4, P4', respectively. The Mößbauer spectrum shows doublets for the central iron atom ($Fe_{cent.}$: δ = 0.47(3) mms^{-1}; ΔE_q = 0.58(4) mms^{-1}) indicating an iron(II) low-spin configuration. The signals with an isomer shift of δ = 0.13(8) mms^{-1} and a ΔE_q = 1.83(3) mms^{-1} are assigned to the four terminal iron atoms,[18] and are in good agreement with the calculated ones.[17]

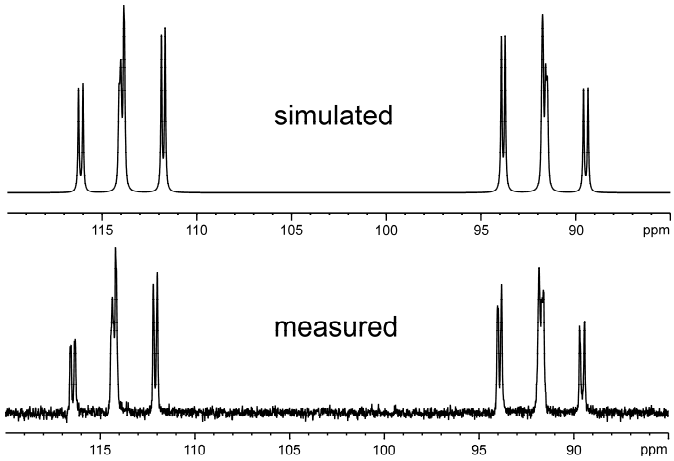

Figure 3.4. Experimental (bottom) and simulated (top) $^{31}P\{^1H\}$ NMR spectrum of **3** in CD_2Cl_2 at 300K.

Furthermore, we investigated if complex **2** can serve as a precursor for the synthesis of **3**. Therefore, one equivalent of **2** was treated with 4 equivalents of $TlPF_6$ in the presence of one equivalent of **1** ((iv) in Scheme 3.3) under ultrasonic conditions. The formation of **3** was confirmed by $^{31}P\{^1H\}$ NMR spectroscopy (yields vary from 50% to 12% according to the $^{31}P\{^1H\}$ NMR). However, this approach does not lead exclusively to **3**, but also to the minor products $[\{Cp'''Fe(CO)_2\}_2(\mu_3,\eta^{1:1:2}\text{-}P_4)\{Cp'''Fe(CO)\}][PF_6]$ (**4**) and $[\{Cp'''Fe(CO)_2\}_2(\mu_3,\eta^{1:1:4}\text{-}P_4)\{Cp'''Fe\}][PF_6]$ (**5**) and other side products that could not yet be characterized.[22] The formation of the side products may originate from the fragmentation of the ligand **1**.

An X-ray structure analysis of **4** reveals an intact P_4 butterfly structural motif (Figure 3.5), coordinating to the [Cp'''Fe(CO)] fragment by the two "wing-tip" phosphorus atoms. The P–P distances in the P_4 butterfly moiety are within 2.1974(8) – 2.2327(8) Å and lie in the range of P–P single bonds. The P–$Fe_{cent.}$ distances with 2.2985(10) Å and 2.3224(10) Å

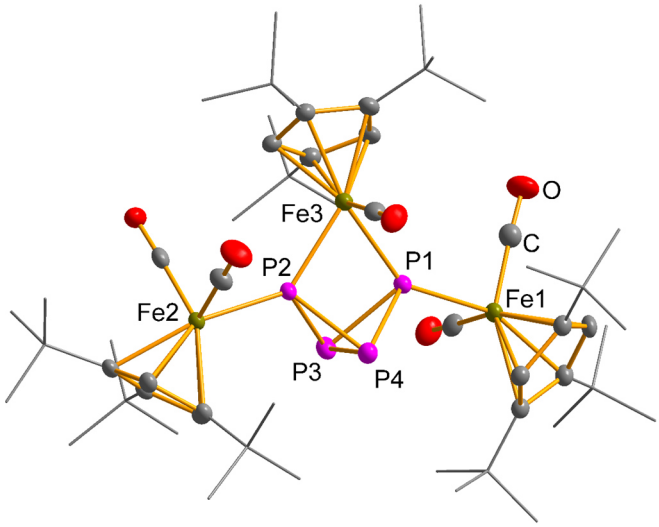

Figure 3.5. Cationic part of the molecular structure of **4**. H atoms and solvent molecules are omitted for clarity. Ellipsoids are set at 50% probability.

are significantly shorter than those in **2** (2.4823(8) Å and 2.4364(7) Å). In the $^{31}P\{^1H\}$ NMR spectrum (CD_2Cl_2), the multiplets at δ = 15.8, 69.7 and 137.4 ppm with an integral ratio of 1:1:2 are assigned to the P_4Fe part of the cation of **4**. The ESI mass spectrum (CH_3CN) shows the molecular ion peak of the cation of **4** at m/z = 1131.4.

In addition to the formation of **5** as a minor product ((iv) in Scheme 3.3), we were able to develop a rational synthetic procedure for the synthesis of **5** ((iii) in Scheme 3.3). Therefore, complex **1** was treated with one equivalent of [{Cp'''Fe(μ-Br)}$_2$] and three equivalents of $TlPF_6$, to give **5** in a 24% crystalline yield (quantitative according to the $^{31}P\{^1H\}$ NMR). A single-crystal X-ray structural analysis reveals that the former P_4 butterfly unit has again been transformed to an aromatic *cyclo*-R_2P_4 unit, which coordinates η^4 to a [Cp'''Fe] fragment (Figure 3.6). The P–P distances vary from 2.1361(9) Å to 2.1516(7) Å and the P–P–P bond angles from 82.98(3)° to 96.60(3)° and are very similar to those observed in **3** (2.1406(10) – 2.1547(10) Å; 82.76(4)°/82.88(4)° and 97.11(4)°/97.24(4)°). In addition, the distance between the central iron atom and the center of the *cyclo*-P_4 unit (1.7610(5) Å) is almost equal to those in **3** (1.7648(7) Å and 1.7759(7) Å). The $^{31}P\{^1H\}$ NMR spectrum (CD_2Cl_2) shows three multiplets, due to the hindered rotation of the substituents at δ = 45.6 ppm (assigned to P3), 56.8 ppm (assigned to P1 and P4) and 78.9 ppm (assigned to P2) for **5**. A similar behavior has been reported for [Cp'''Co{1,3-P_2(^{t}BuC)$_2$}].[23] The Mößbauer spectrum reveals doublets for the central and the terminal iron atoms (central Fe atom: δ = 0.43(3) mms^{-1} and ΔE_q = 1.62(4) mms^{-1}; two terminal iron atoms: δ = 0.13(8) mms^{-1} and ΔE_q = 1.75(3) mms^{-1}). These values are in good agreement with the calculated ones[17] and indicate an iron(II) low-spin configuration for all iron atoms.[18]

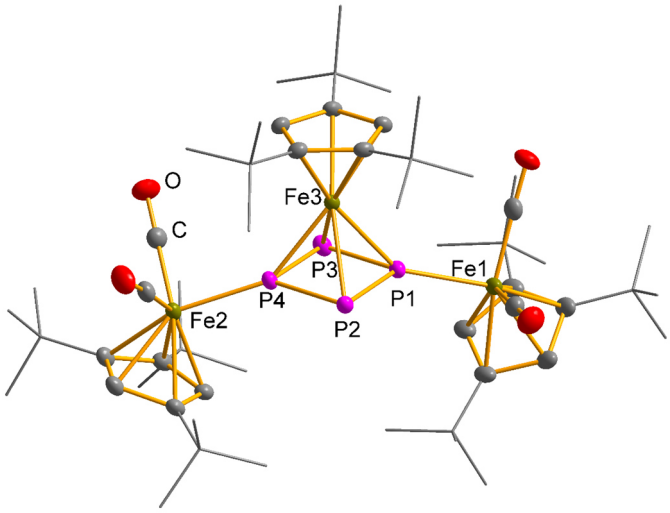

Figure 3.6. Cationic part of the structure of **5** in the crystal. H atoms and solvent molecules are omitted for clarity. Ellipsoids are set at 50% probability.

According to the DFT calculations, the electronic structure of **5** is similar to that of **3**. On the other hand, the elimination of one CO ligand from **4** to form **5** is thermodynamically

disfavored by 72.73 kJmol^{-1}. This indicates that complex **4** is probably not an intermediate in the formation of **5**.

3.3. Conclusion

Summing up, we showed that the butterfly complex [{Cp'''Fe(CO)$_2$}$_2$(μ,η$^{1:1}$-P$_4$)] (**1**) can serve as a bidentate ligand with a small bit angle to form the coordination compound [{Cp'''Fe(CO)$_2$}$_2$(μ$_3$,η$^{1:1:2}$-P$_4$){FeBr$_2$}] (**2**) in the reaction with [FeBr$_2$·dme]. More importantly, it was demonstrated that the P$_4$R$_2$ butterfly unit of **1** can be unprecedentedly transformed into *cyclo*-P$_4$R$_2$ units (R = Cp'''Fe(CO)$_2$) by coordination towards suitable iron(II) salts as Lewis acids. Thus, **1** forms with [Fe(CH$_3$CN)$_6$][PF$_6$]$_2$ [{(Cp'''Fe(CO)$_2$)$_2$(μ$_3$,η$^{1:1:4}$-P$_4$)}$_2$Fe][PF$_6$]$_2$ (**3**) the first example of a homoleptic-like sandwich complex with *cyclo*-P$_4$R$_2$ ligands (R = Cp'''Fe(CO)$_2$). Additionally, an alternative synthetic approach for **3** was found, using **2** as starting material along with TlPF$_6$ and **1**. Beside the formation of **3**, the two minor products [{Cp'''Fe(CO)$_2$}$_2$(μ$_3$,η$^{1:1:2}$-P$_4$){Cp'''Fe(CO)}][PF$_6$] (**4**) and [{Cp'''Fe(CO)$_2$}$_2$(μ$_3$,η$^{1:1:4}$-P$_4$){Cp'''Fe}][PF$_6$] (**5**) could be characterized, highlighting that the stepwise P$_4$ butterfly transformation is strongly connected to the steric hindrance and the electronic nature of the used iron(II) compound. Moreover, the isomerization of the P$_4$-butterfly ligand to the aromatic *cyclo*-P$_4$R$_2$ moiety represents a further, so far unknown step in the activation of P$_4$.

3.4. Reference

[1] a) N. Hazari, *Chem. Soc. Rev.* **2010**, *39*, 4044-4056; b) I. Mellone, F. Bertini, L. Gonsalvi, A. Guerriero, M. Peruzzini, *CHIMIA International Journal for Chemistry* **2015**, *69*, 331-338; c) Z. Turner, *Inorganics* **2015**, *3*, 597; d) R. A. Henderson, *Transition Met. Chem.* **1990**, *15*, 330-336; e) V. P. Indrakanti, J. D. Kubicki, H. H. Schobert, *Energy & Environmental Science* **2009**, *2*, 745-758; f) X. Yin, J. R. Moss, *Coord. Chem. Rev.* **1999**, *181*, 27-59.

[2] H. Diskowski, T. Hofmann, in *Ullmann's Encyclopedia of Industrial Chemistry*, Wiley-VCH Verlag GmbH & Co. KGaA, **2000**.

[3] a) M. Scheer, G. Balázs, A. Seitz, *Chem. Rev.* **2010**, *110*, 4236-4256; b) N. A. Giffin, J. D. Masuda, *Coord. Chem. Rev.* **2011**, *255*, 1342-1359; c) S. Khan, S. S. Sen, H. W. Roesky, *Chem. Commun.* **2012**, *48*, 2169-2179.

[4] a) B. M. Cossairt, N. A. Piro, C. C. Cummins, *Chem. Rev.* **2010**, *110*, 4164-4177; b) M. Caporali, L. Gonsalvi, A. Rossin, M. Peruzzini, *Chem. Rev.* **2010**, *110*, 4178-4235.

[5] a) A. P. Ginsberg, W. E. Lindsell, *J. Am. Chem. Soc.* **1971**, *93*, 2082-2084; b) I. Krossing, L. van Wüllen, *Chem. Eur. J.* **2002**, *8*, 700-711.

[6] a) O. J. Scherer, M. Swarowsky, G. Wolmershaeuser, *Organometallics* **1989**, *8*, 841-842; b) M. Scheer, C. Troitzsch, P. G. Jones, *Angew. Chem.* **1992**, *104*, 1395-1397; c) B. Zarzycki, F. M. Bickelhaupt, U. Radius, *Dalton Trans.* **2013**, *42*, 7468-7481; d) S. Dürr, D. Ertler, U. Radius, *Inorg. Chem.* **2012**, *51*, 3904-3909.

[7] a) O. J. Scherer, G. Schwarz, G. Wolmershäuser, *Z. Anorg. Allg. Chem.* **1996**, *622*, 951-957; b) C. Schwarzmaier, A. Y. Timoshkin, G. Balázs, M. Scheer, *Angew. Chem. Int. Ed.* **2014**, *53*, 9077-9081; for the unsymmetric substitution by a nucleophile/electrophile approach cf.: c) D. Holschumacher, T. Bannenberg, K. Ibrom, C. G. Daniliuc, P. G. Jones, M. Tamm, *Dalton Trans.* **2010**, *39*, 10590–10592; d) J. E. Borger, A. W. Ehlers, M. Lutz, J. C. Slootweg, K. Lammertsma, *Angew. Chem. Int. Ed*. **2014**, *53*, 12836 –12839; e) J. E. Borger, A. W. Ehlers, M. Lutz, J. C. Slootweg, K. Lammertsma, *Angew. Chem. Int. Ed.* **2017**, *56*, 285–290.

[8] a) A. R. Fox, R. J. Wright, E. Rivard, P. P. Power, *Angew. Chem.* **2005**, *117*, 7907-7911; b) B. M. Cossairt, C. C. Cummins, *New J. Chem.* **2010**, *34*, 1533-1536; c) S. Heinl, S. Reisinger, C. Schwarzmaier, M. Bodensteiner, M. Scheer, *Angew. Chem. Int. Ed. Engl.* **2014**, *53*, 7639-7642; d) S. Heinl, G. Balázs, A. Stauber, M. Scheer, *Angew. Chem. Int. Ed*. **2016**, *55*, 15524-15527.

[9] a) M. Scheer, U. Becker, *J. Organomet. Chem.* **1997**, *545–546*, 451-460; b) M. Scheer, U. Becker, E. Matern, *Chem. Ber.* **1996**, *129*, 721-724; c) O. J. Scherer, R. Winter, G. Wolmershäuser, *Z. Anorg. Allg. Chem.* **1993**, *619*, 827-835; d) O. J. Scherer, J. Vondung, G. Wolmershäuser, *Angew. Chem. Int. Ed.* **1989**, *28*, 1355-1357.

[10] a) O. J. Scherer, T. Brück, G. Wolmershäuser, *Chem. Ber.* **1988**, *121*, 935-938; b) M. Scheer, U. Becker, J. C. Huffman, M. H. Chisholm, *J. Organomet. Chem.* **1993**, *461*, C1-C3; c) M. Scheer, C. Troitzsch, L. Hilfert, M. Dargatz, E. Kleinpeter, P. G. Jones, J. Sieler, *Chem. Ber.* **1995**, *128*, 251-257; d) O. J. Scherer, J. Schwalb, H. Swarowsky, G. Wolmershäuser, W. Kaim, R. Gross, *Chem. Ber.* **1988**, *121*, 443-449; e) O. J. Scherer, J. Schwalb, G. Wolmershäuser, W. Kaim, R. Groß, *Angew. Chem. Int. Ed. Engl.* ***1986****, 25, 363–364*; f) O. J. Scherer, H. Sitzmann, G. Wolmershäuser, *J. Organomet. Chem.* **1984**, *268*, C9-C12; g) O. J. Scherer, H. Sitzmann, G. Wolmershäuser, *Angew. Chem. Int. Ed. Engl.* ***1985****, 24, 351–353*; h) O. J. Scherer, H. Swarowsky, G. Wolmershäuser, W. Kaim, S. Kohlmann, *Angew. Chem.* **1987**, *99*, 1178-1179; i) C. Eichhorn, O. J. Scherer, T. Sögding, G. Wolmershäuser, *Angew. Chem. Int. Ed.* **2001**, *40*, 2859-2861.

[11] O. J. Scherer, T. Hilt, G. Wolmershäuser, *Organometallics* **1998**, *17*, 4110-4112.

[12] C. Schwarzmaier, S. Heinl, G. Balázs, M. Scheer, *Angew. Chem. Int. Ed.* **2015**, *54*, 13116-13121.

[13] R. K. O'Reilly, M. P. Shaver, V. C. Gibson, A. J. P. White, *Macromolecules* **2007**, *40*, 7441-7452.

[14] J. D. Gilbertson, N. K. Szymczak, D. R. Tyler, *J. Am. Chem. Soc.* **2005**, *127*, 10184-10185.

[15] The lone pairs of the two wing-tip P atoms of the butterfly complex and the 2 electrons of the afterwards opened bridge-head P-P bond results in the 6 π-electrons of the aromatic P_4R_2 system.

[16] G. A. Bain, J. F. Berry, *J. Chem. Educ.* **2008**, *85*, 532.

[17] For details cf. the Supporting Informations.

[18] D. W. H. Rankin, N. W. Mitzel, C. A. Morrison, *Structural Methods in Molecular Inorganic Chemistry*, John Wiley & Sons, Ltd, **2013**.

[19] E. Urneúzÿius, W. W. Brennessel, C. J. Cramer, J. E. Ellis, P. von Ragué Schleyer, *Science* **2002**, *295*, 832-834.

[20] F. Kraus, J. C. Aschenbrenner, N. Korber, *Angew. Chem.* **2003**, *115*, 4162-4165.

[21] Z. Li, C. Zhao, L. Chen, *J. Mol. Struc. THEOCHEM* **2007**, *810*, 1-6.

[22] The yields of reaction path (iv) may vary, which can be rationalized by the unselective fragmentation of **1**.

[23] E.-M. Rummel, M. Eckhardt, M. Bodensteiner, E. V. Peresypkina, W. Kremer, C. Gröger, M. Scheer, *Eur. J. Inorg. Chem.* **2014**, 1625-1637

3.5. Supporting Information

Synthesis and Characterization:

General Remarks:

All manipulations were performed with rigorous exclusion of oxygen and moisture using Schlenk-type glassware on a dual manifold Schlenk line with Argon inert gas or glove box filled with N_2 containing a high-capacity recirculator (<0.1 ppm O_2). Solvents were dried using a MB SPS-800 device of company MBRAUN, degassed and saturated with argon. Mass spectrometry was performed using a Waters Micromass LCT (ESI-MS) and a JEOL AccuTOF GCX (FD-MS), respectively. Elemental analysis (CHN) was determined using a Vario micro cube and Vario EL III instrument. Infrared spectroscopy was performed using a Bruker ALPHA Platinum-ATR-Spectrometer or a VARIAN FTS-800 FT-IR spectrometer.

Thallium(I) hexafluorophosphate, 97% was purchased by ABCR and used without further purification. $[\{Cp'''Fe(CO)_2\}_2(\mu,\eta^{1:1}\text{-}P_4)]$ (**1**)[1], $[Fe(CH_3CN)_6][PF_6]_2$[2] and $[\{Cp'''Fe(\mu\text{-}Br)\}_2]$[3] were synthesized following literature-known routes.

Synthesis of $[\{Cp'''Fe(CO)_2\}_2(\mu_3,\eta^{1:1:2}\text{-}P_4)FeBr_2]$ (2)

To a suspension of 38 mg $[FeBr_2\cdot dme]$ (0.123 mmol) in 5 ml dichloromethane is given a solution of 100 mg $[\{Cp'''Fe(CO)_2\}_2(\mu,\eta^{1:1}\text{-}P_4)]$ (**1**) (0.123 mmol) in 5 ml dichloromethane. The reaction mixture is stirred for 10 minutes resulting in a dark red colored solution. The solution is filtered via cannula and concentrated in vacuum (2 ml). Storing the solution at −28 °C yields **2** as a dark red crystalline solid.

Crystalline yield: 60 mg (0.058 mmol, 52%)

Analytical data of **2**:

NMR (CD_2Cl_2, 298 K)	^1H: δ [ppm] = −3.4 (s br, 9H, -($C_4\underline{H}_9$)), −2.2 (s br, 18H, -$(C_4H_9)_2$), −20.1 (s br, 2H, $C_5\underline{H}_2{}^t Bu_3$).
Evans method	μ_{eff} [μ_B] = 6.13.
Spin	N = 5.2.
IR (KBr)	$\tilde{\nu}$ [cm^{-1}] = 1983 (vs), 1929 (vs)
Elemental analysis ($C_{38}H_{58}Br_2Fe_3O_4P_4\cdot(CH_2Cl_2)_{0.5}$)	Calculated: C 43.11, H 5.54 Found: C 43.12, H 5.65
Mass spectrometry (FD, toluene)	m/z: 733.3 (100%) $[\{Cp'''Fe\}_2P_5]^+$, 1253.4 (10%) $[\{Cp'''Fe(CO)_2\}_3P_8 - CO - 2H]^+$, 1283.3 (5%) $[\{Cp'''Fe(CO)_2\}_3P_8]^+$.

Synthesis of $[\{\{Cp'''Fe(CO)_2\}_2(\mu_3,\eta^{1:1:4}\text{-}P_4)\}_2Fe]^{2+}[PF_6]^-_2$ (3):

A red suspension of 200 mg (0.246 mmol) $[\{Cp'''Fe(CO)_2\}_2(\mu,\eta^{1:1}\text{-}P_4)]$ (**1**) and 76 mg (0.129 mmol) $[Fe(CH_3CN)_6][PF_6]_2$ in 20 ml dichloromethane is stirred for 16 h at room temperature. The resulting brownish reaction mixture is filtered over diatomaceous earth and concentrated in vacuum. Brown blocks of **3** can be obtained by layering the solution with hexane.

Yield (according to NMR): quantitative
Yield (crystalline): 165 mg (0.084 mmol, 68%)

Analytical data for **3**:

NMR (CD_2Cl_2, 298 K) 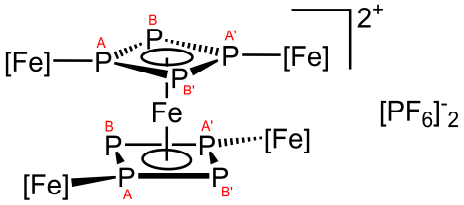 [Fe] = $Cp'''Fe(CO)_2$	^1H: δ [ppm] = 1.41 (s, 9H, -($C_4\underline{H}_9$)), 1.48 (s, 18H, -(C_4H_9)$_2$), 5.38 (s, 2H, $C_5\underline{H}_2{}^tBu_3$). $^{31}P\{^1H\}$: δ [ppm] = −143.84 (sept., 2P, $\underline{P}F_6$, $^1J_{PF}$ = 710 Hz), 91.7 (m, 4P, $\underline{P}_B/\underline{P}_{B'}$, $^1J_{AB}$ = 354.4 Hz, $^1J_{AB'}$ = 354.8 Hz, $^2J_{BB'}$ = 2.1 Hz), 114.3 (m, 4P, $\underline{P}_A/\underline{P}_{A'}$, $^2J_{AA'}$ = 8.0 Hz)
IR (crystalline)	$\tilde{\nu}$ [cm^{-1}] = 1978 (s), 2001(vs, br), 2026 (s), 2043 (s)
Elemental analysis ($C_{76}H_{116}F_{12}Fe_5O_8P_{10}\cdot(CH_2Cl_2)_2$)	Calculated: C 43.69, H 5.64 Found: C 43.78, H 5.66
Mass spectrometry (ESI, CH_3CN)	m/z: 1829.1 (1%) $[M - PF_6]^+$, 1339.0 (7%) $[M - (Cp'''Fe(CO)_2) - 2PF_6]^+$, 993.9 (39%) $[M - 2(Cp'''Fe(CO)_2) - 2PF_6]^+$, 965.9 (7%) $[M - 2(Cp'''Fe(CO)_2) - CO - 2PF_6]^+$, 937.9 (39%) $[M - 2(Cp'''Fe(CO)_2) - 2CO - 2PF_6]^+$, 841.1 (12%) $[M - 2PF_6]^{2+}$, 655.5 (7%) $[M - (Cp'''Fe(CO)_2) - CO - 2PF_6]^{2+}$, 345.1 (100%) $[Cp'''Fe(CO)_2]^+$, 330.2 (32%) $[(Cp'''Fe(CO)_2) - CH_3]^+$, 317.1 (27%) $[Cp'''FeCO]^+$.

Alternative synthesis of $[\{\{Cp'''Fe(CO)_2\}_2(\mu_3,\eta^{1:1:4}\text{-}P_4)\}_2Fe]^{2+}[PF_6]^-_2$ (3):

A suspension of 51 mg $[\{Cp'''Fe(CO)_2\}_2(\mu_3,\eta^{1:1:2}\text{-}P_4)FeBr_2]$ (**2**) (0.050 mmol), 41 mg $[\{Cp'''Fe(CO)_2\}_2(\mu,\eta^{1:1}\text{-}P_4)]$ (**1**) (0.050 mmol) and 75 mg $TlPF_6$ (0.215 mmol) in 20 ml dichloromethane is treaded in the ultrasonic bath for 2 h. The resulting dark brown reaction mixture is filtered over diatomaceous earth.

Yield (according to ^{31}P-NMR; PPh_3 as standard):

$[\{\{Cp'''Fe(CO)_2\}_2(\mu_3,\eta^{1:1:4}\text{-}P_4)\}_2Fe]^{2+}[PF_6]^-_2$ (**3**): 50 - 12%
$[\{\{Cp'''Fe(CO)_2\}_2(\mu_3,\eta^{1:1:2}\text{-}P_4)\}(Cp'''Fe(CO))]^+[PF_6]^-$ (**4**): 8 - 1%
$[\{\{Cp'''Fe(CO)_2\}_2(\mu_3,\eta^{1:1:4}\text{-}P_4)\}FeCp''']^+[PF_6]^-$ (**5**): 1 - 0%

Analytical data for **4** :

NMR (CD_2Cl_2, 298 K)	^{31}P: δ [ppm] = −143.84 (sept., 1P, $\underline{P}F_6$, $^1J_{PF}$ = 710 Hz), 15.8 (m, 1P), 69.7 (m, 1P), 137.4 (m, 2P)
Mass spectrometry (ESI, CH3CN)	m/z: 1131.4 (100%) $[M - PF_6]^+$, 1103.4 (55%) $[M - CO - PF_6]^+$,

Synthesis of $[\{\{Cp'''Fe(CO)_2\}_2(\mu_3,\eta^{1:1:4}\text{-}P_4)\}FeCp''']^+[PF_6]^-$ (5):

In a spindle flask, a suspension of 50 mg $[\{Cp'''Fe(\mu\text{-}Br)\}_2]$ (0.068 mmol), 110 mg $[\{Cp'''Fe(CO)_2\}_2(\mu,\eta^{1:1}\text{-}P_4)]$ (**1**) (0.135 mmol) and 71 mg $TlPF_6$ (0.203 mmol) in 20 ml dichloromethane is treated in the ultrasonic bath for 16 h. The solvent is removed under vacuum. The remaining solid is taken up in toluene, filtered over diatomaceous earth and dried in vacuum. The residue is solved in thf and layered underneath hexane to yield **5** as dark green blocks.

Yield (according to NMR): quantitative
Yield (crystalline): 40 mg (0.026 mmol, 24 %)

Analytical data for **5**:

NMR (CD_2Cl_2, 298 K) 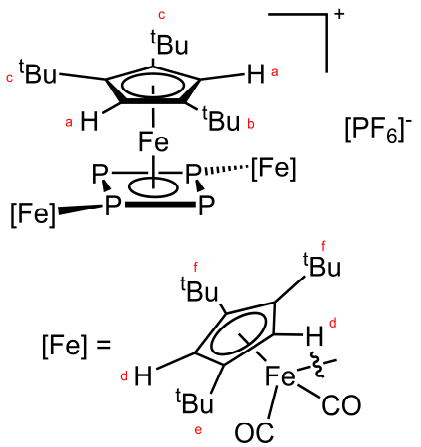 	^{1}H: δ [ppm] = 1.14 (s , 9H, b), 1.39 (s, 18H, c), 1. 41 (s , 18H, e), 1.47 (s, 36H, f), 5.36 (s br, 4H, d), 5.38 (s, 2H, a). ^{31}P: δ [ppm] = -143.84 (sept., 1P, $\underline{P}F_6$, $^1J_{PF}$ = 710 Hz), 45.6 (m, 1P, 4), 56.8 (m, 2P, 1 & 3), 78.9 (m, 1P, 2)
IR (crystalline)	$\tilde{\nu}$ [cm^{-1}] = 1972 (vs, br), 2017 (vs), 2028 (s)
Elemental analysis $(C_{55}H_{87}Fe_3O_4P_5F_6 \cdot (C_4H_8O)_2)$	Calculated: C 54.32, H 7.45 Found: C 54.64, H 7.15
Mass spectrometry (ESI, CH_3CN)	m/z: 1047.36 (2 %) $[M - 2CO - PF_6]^+$, 1103.27 (100 %) $[M - PF_6]^+$.

Crystallographic Details

General remarks:

Single crystal structure analyses were performed using Agilent Technologies diffractometer GV1000, Titan^{S2} diffractometer (**4**), SuperNova, Single source at offset, Atlas diffractometer. (**2**, **3**, **5**). Frames integration and data reduction were performed with the CrysAlisPro[4] software package. Using the software Olex2[5] the structure solution was carried out using the programs ShelXT[6] (Sheldrick, 2015). Least squares refinements on F_0^2 were performed using SHELXL-2014[7] (Sheldrick, 2015). Further details are given in Table S3.1.

In **2** a dichloromethane molecule was refined to a chemical occupancy 62:38. In **3** one disordered *tert*-butyl group was refined to a chemical occupancy 74:26 and a solvent mask was used to squeeze a disordered dichloromethane molecule. The single crystal analysis of **4** reveals a disordered central P_4 – Fe unit. The main part (94%) of the structure shows a P_4 – butterfly motive that coordinates a [Cp'''Fe(CO)] – fragment in a η^2 fashion. The minor part (6%) shows a *cyclo*-P_4 unit that coordinates a [Cp'''Fe] – fragment in a η^4 fashion. Additionally, a solvent mask was used to squeeze a disordered tetrahydrofurane molecule. In **5** the PF_6^- anion is disordered and was refined to a chemical occupancy 80:20.

Crystallographic data and details of the diffraction experiments are given in Table S3.1. CIF files with comprehensive information on the details of the diffraction experiments and full tables of bond lengths and angles for **2**, **3**, **4** and **5** are deposited in Cambridge Crystallographic Data Centre under the deposition codes CCDC 1531887-1531890.

Table S3.1: Crystallographic data and details of diffraction experiments for **2**, **3**, **4** and **5**.

Compound	**2** · 2 CH_2Cl_2	**3**	**4**	**5** · 2 thf
CCDC number	1531887	1531888	1531889	1531890
Formula	$C_{40}H_{62}Br_2Cl_4Fe_3O_4P_4$	$C_{76}H_{116}F_{12}Fe_5O_8P_{10}$	$C_{59.9375}H_{95}F_6Fe_3O_{5.9375}P_{4.9875}$	$C_{59}H_{95}F_6Fe_3O_5P_5$
$D_{calc.}$/ g cm^{-3}	1.571	1.372	1.315	1.291
μ/mm^{-1}	12.056	8.122	6.679	6.668
Formula Weight	1199.94	1974.63	1346.62	1320.74
Color	red	black	clear brown	dark green
Shape	plate	block	block	block
Size/mm^3	0.24×0.09×0.02	0.17×0.11×0.09	0.38×0.15×0.14	0.26×0.19×0.13
T/K	123.01(10)	123.01(10)	123.00(10)	123.01(10)
Crystal System	monoclinic	monoclinic	monoclinic	triclinic
Space Group	$P2_1/c$	C2/c	C2/c	$P\bar{1}$
a/Å	21.2045(2)	24.5485(5)	36.5561(6)	10.2890(3)
b/Å	13.33220(10)	15.9348(3)	10.4827(2)	15.2465(3)
c/Å	19.7875(2)	24.6752(5)	35.5465(6)	21.6807(5)
α/°	90	90	90	89.7792(19)
β/°	114.8930(10)	97.9544(18)	92.6951(15)	87.626(2)
γ/°	90	90	90	89.0826(19)
V/Å^3	5074.27(9)	9559.5(3)	13606.6(4)	3397.70(14)

Z	4	4	8	2
Z'	1	0.5	1	1
Wavelength/Å	1.54178	1.54184	1.54184	1.54184
Radiation type	Cu Kα	Cu Kα	Cu Kα	Cu Kα
Θ_{min}/°	4.034	3.617	2.420	3.540
Θ_{max}/°	70.815	74.113	74.817	74.251
Measured Refl.	27122	27896	42206	38720
Independent Refl.	9502	9308	13367	13415
Reflections Used	8749	8304	12752	12399
R_{int}	0.0268	0.0271	0.0298	0.0284
Parameters	541	550	777	784
Restraints	0	24	72	222
Largest Peak	0.508	1.376	0.483	0.830
Deepest Hole	-0.517	-2.355	-0.413	-1.308
GooF	1.020	1.047	1.034	1.062
wR_2 (all data)	0.0650	0.1306	0.0788	0.1227
wR_2	0.0627	0.1260	0.0777	0.1188
R_1 (all data)	0.0291	0.0547	0.0328	0.0452
R_1	0.0257	0.0485	0.0312	0.0421

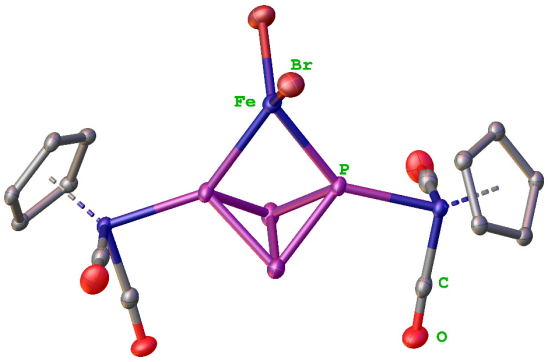

Figure S3.1: Molecular structure of compound **2**. Hydrogen atoms, ^{t}Butyl-groups and two solvent molecules dcm are omitted for clarity. Thermal ellipsoids are shown at 50% probability level.

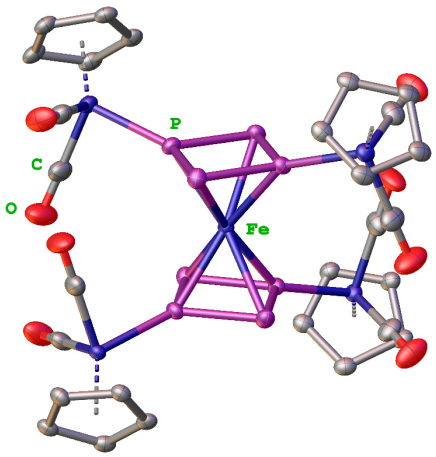

Figure S3.2: Molecular structure of compound **3**. Hydrogen atoms, ^{t}Butyl-groups, and the counter anions PF_6^- are omitted for clarity. Thermal ellipsoids are shown at 50% probability level.

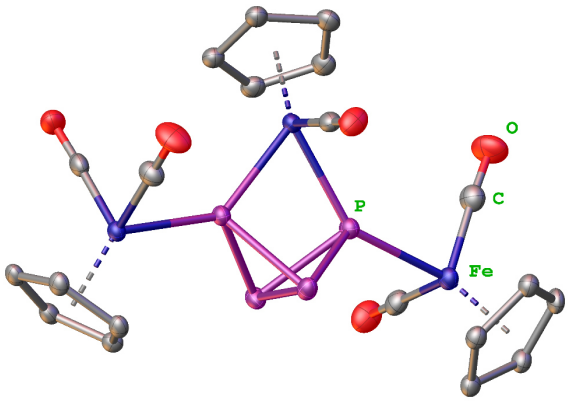

Figure S3.3: Main part of the molecular structure of compound **4**. Hydrogen atoms, ^{t}Butyl-groups, a solvent molecule thf and the counter anion PF_6^- are omitted for clarity. Thermal ellipsoids are shown at 50% probability level.

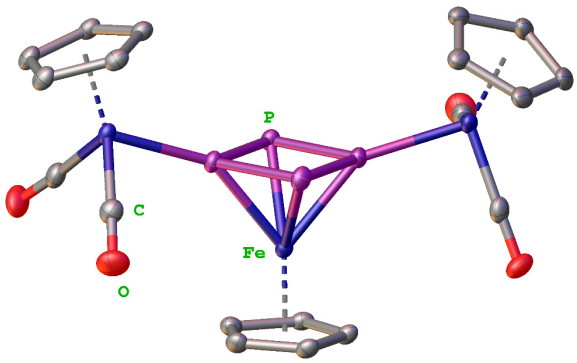

Figure S3.4: Molecular structure of compound **5**. Hydrogen atoms, ^{t}Butyl-groups, a solvent molecule thf and the counter anion PF_6^- are omitted for clarity. Thermal ellipsoids are shown at 50% probability level.

Mößbauer Spectra

General remarks:

^{57}Fe Mößbauer spectra were recorded on a WissEl Mößbauer spectrometer (MRG-500) at 77 K in constant acceleration mode. ^{57}Co/Rh was used as the radiation source. WinNormos for Igor Pro software has been used for the quantitative evaluation of the spectral parameters (least-squares fitting to Lorentzian peaks). The minimum experimental line widths were 0.20 mm·s^{-1}. The temperature of the samples was controlled by an MBBC-HE0106 MÖSSBAUER He/N_2 cryostat within an accuracy of ±0.3 K. Isomer shifts were determined relative to α-iron at 298 K.

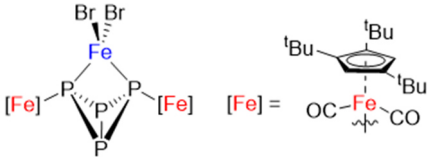

Species 1:
Isomer shift δ = 0.12(3) mms^{-1}
Quadrupole splitting ΔE_Q = 1.73(4) mms^{-1}
Γ_{FWHM} = 0.30(1) mms^{-1}
Relative Area 67%

Species 2:
Isomer shift δ = 0.73(3) mms^{-1}
Quadrupole splitting ΔE_Q = 2.33(1) mms^{-1}
Γ_{FWHM} = 0.31(8) mms^{-1}
Relative Area 33%

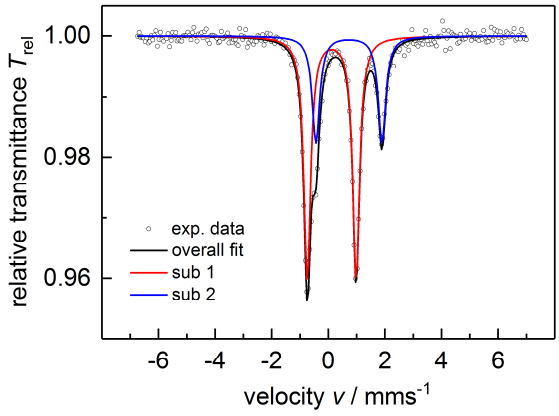

Figure S3.5. Zero-filled ^{57}Fe Mößbauer spectrum of **2**, recorded on a micro-crystalline, solid sample at 77 K.

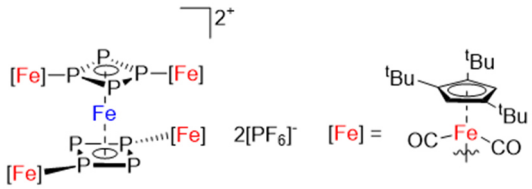

Species 1:
Isomer shift δ = 0.12(8) mms^{-1}
Quadrupole splitting ΔE_Q = 1.81(3) mms^{-1}
Γ_{FWHM} = 0.34(7) mms^{-1}
Relative Area 75%

Species 2:
Isomer shift δ = 0.47(3) mms^{-1}
Quadrupole splitting ΔE_Q = 0.57(4) mms^{-1}
Γ_{FWHM} = 0.29(8) mms^{-1}
Relative Area 25%

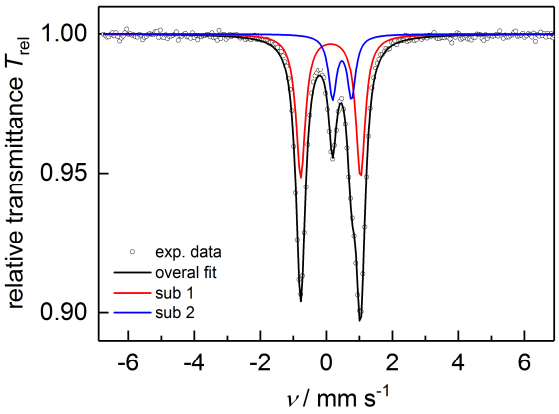

Figure S3.6. Zero-filled ^{57}Fe Mößbauer spectrum of **3**, recorded on a micro-crystalline, solid sample at 77 K.

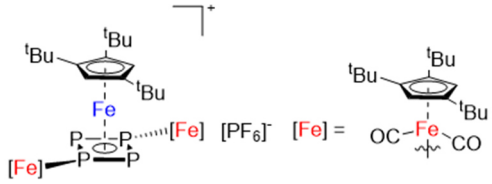

Species 1:
Isomer shift δ = 0.13(8) mms^{-1}
Quadrupole splitting ΔE_Q = 1.75(3) mms^{-1}
Γ_{FWHM} = 0.31(1) mms^{-1}
Relative Area 62%

Species 2:
Isomer shift δ = 0.43(3) mms^{-1}
Quadrupole splitting ΔE_Q = 1.62(4) mms^{-1}
Γ_{FWHM} = 0.28(8) mms^{-1}
Relative Area 38%

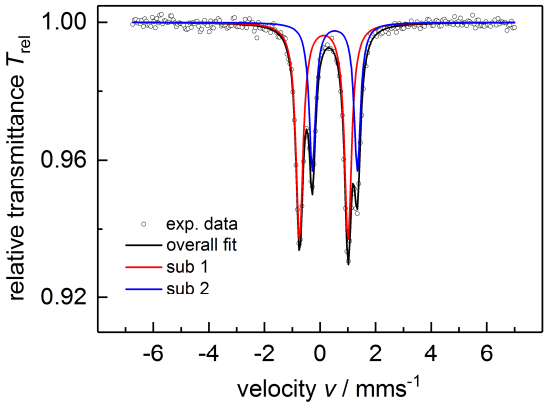

Figure S3.7. Zero-filled ^{57}Fe Mößbauer spectrum of **5**, recorded on a micro-crystalline, solid sample at 77 K.

^{1}H NMR and ^{31}P NMR Spectroscopy

General remarks:

^{1}H and ^{31}P NMR spectra were recorded on a Bruker Avance III HD 400 (^{1}H: 400.130 MHz, ^{31}P: 161.976 MHz). The chemical shifts are reported in ppm relative to external TMS (^{1}H) and H_3PO_4 (^{31}P). The ^{31}P NMR simulation was performed with the simulation tool of Bruker TopSpin 3.0.

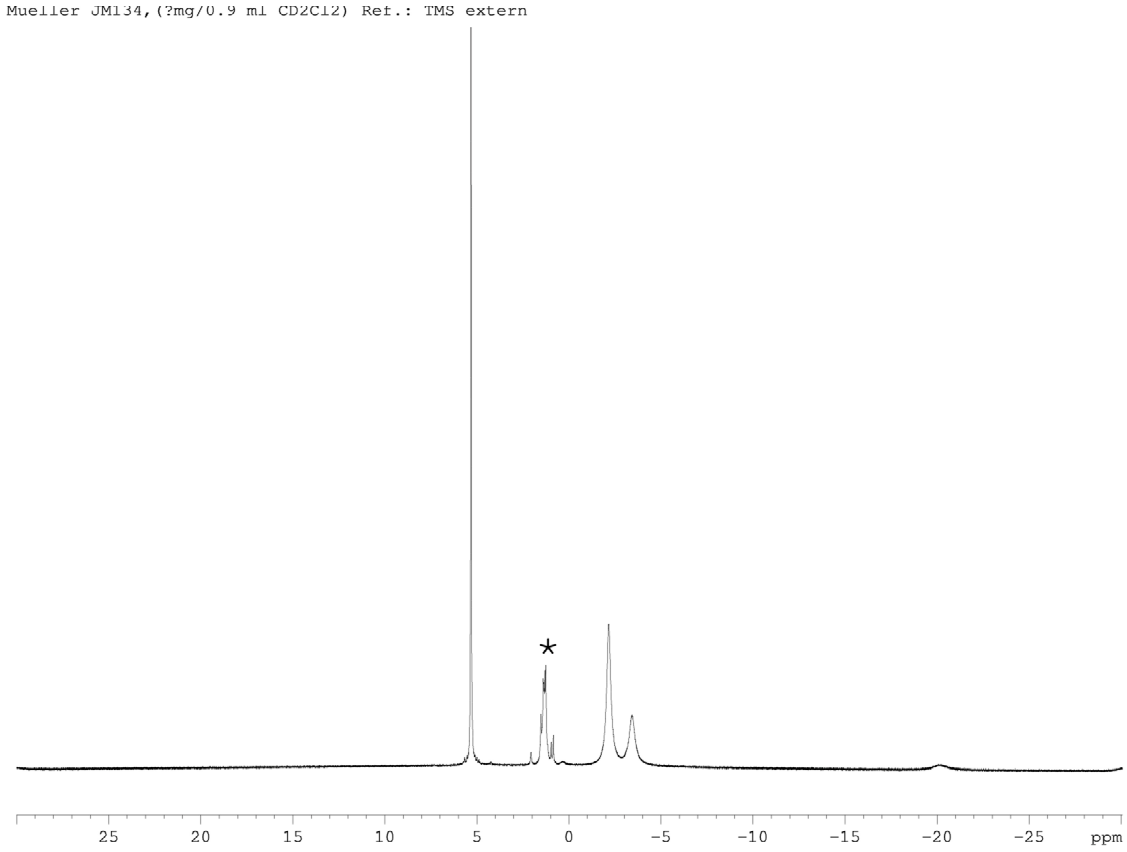

Figure S3.8. ^{1}H NMR spectrum of [{Cp'''Fe(CO)$_2$}$_2$(μ_3,$\eta^{1:1:2}$-P$_4$)FeBr$_2$] (**2**) in CD_2Cl_2. The marked signal (*) arise from impurities.

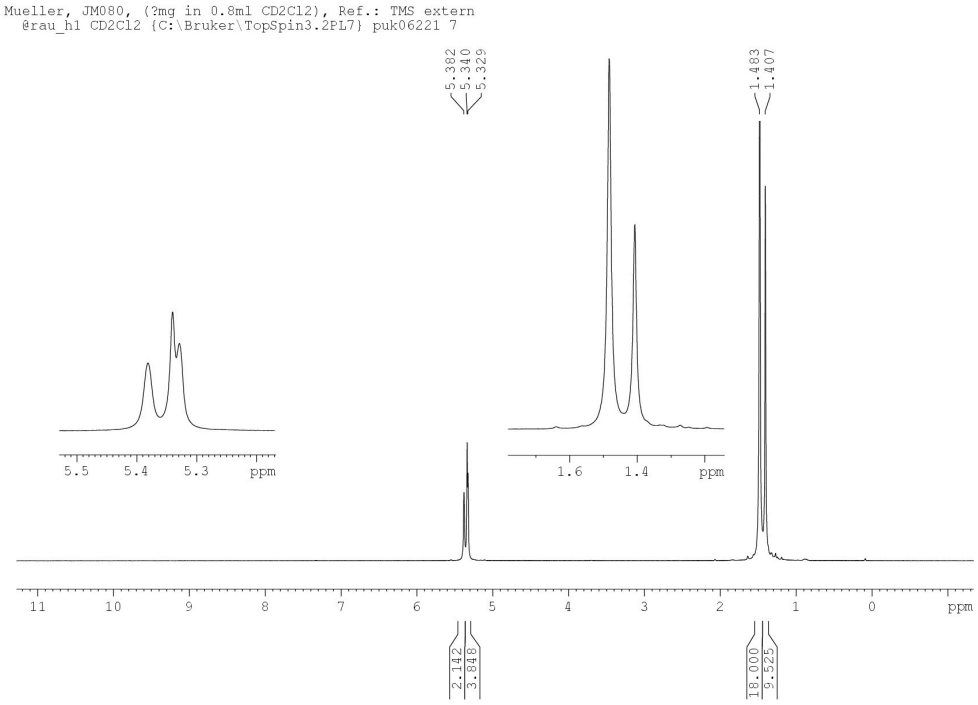

Figure S3.9: ^{1}H NMR spectrum of [{{Cp'''Fe(CO)$_2$}$_2$(μ_3,$\eta^{1:1:4}$-P$_4$)}$_2$Fe]$^{2+}$[PF$_6$]$^{-}_2$ (**3**) in CD_2Cl_2.

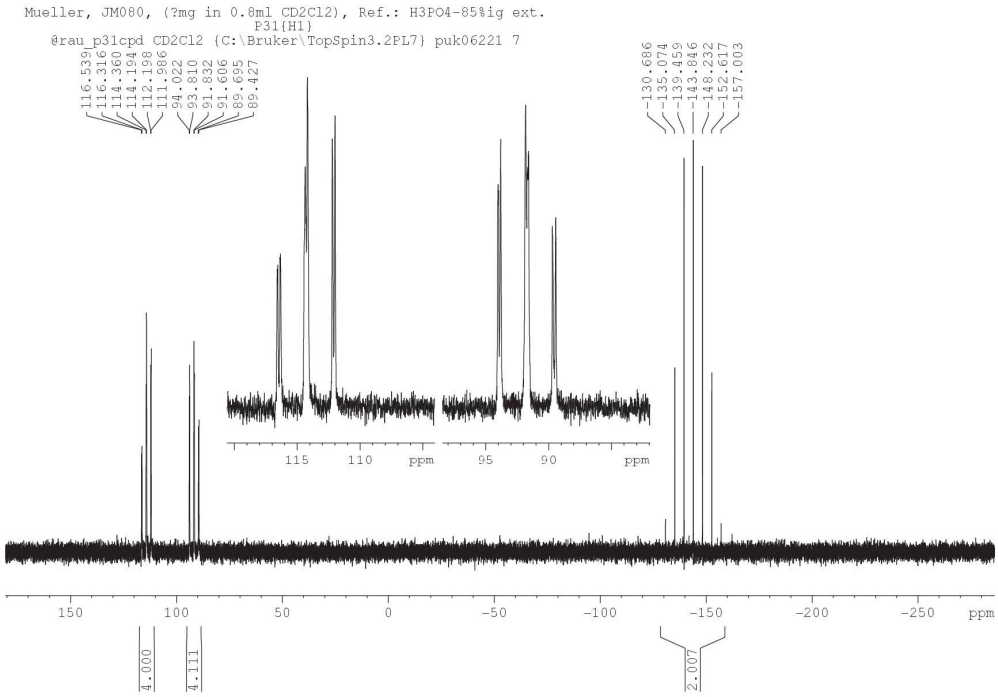

Figure S3.10: $^{31}P\{^1H\}$ NMR spectrum of $[\{\{Cp'''Fe(CO)_2\}_2(\mu_3,\eta^{1:1:4}\text{-}P_4)\}_2Fe]^{2+}[PF_6]^-_2$ (**3**) in CD_2Cl_2.

Table S3.2: Calculated coupling constants of **3**.

Chemical shift [ppm]		Coupling constants [Hz]	
AA'	113.8	$^1J_{AB}$	354.4
BB'	91.7	$^1J_{AB'}$	354.8
		$^1J_{AA'}$	8.0
		$^1J_{BB'}$	2.1

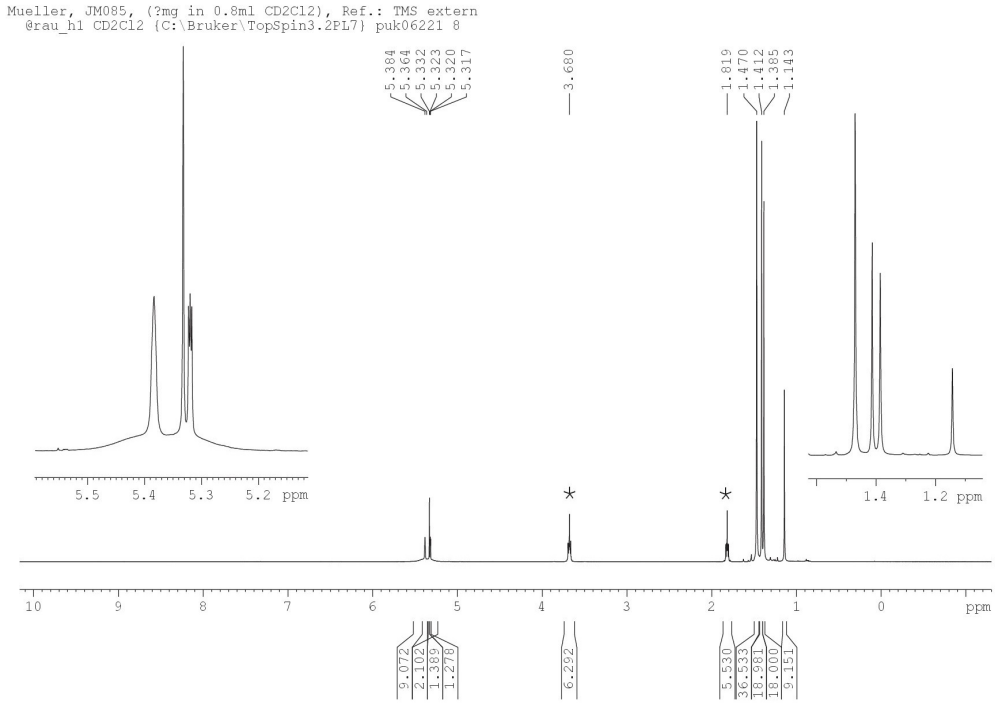

Figure S3.11: ^1H NMR spectrum of $[\{\{Cp'''Fe(CO)_2\}_2(\mu_3,\eta^{1:1:4}\text{-}P_4)\}FeCp'''][PF_6]^-$ (**5**) in CD_2Cl_2. The marked signals (*) correspond to thf.

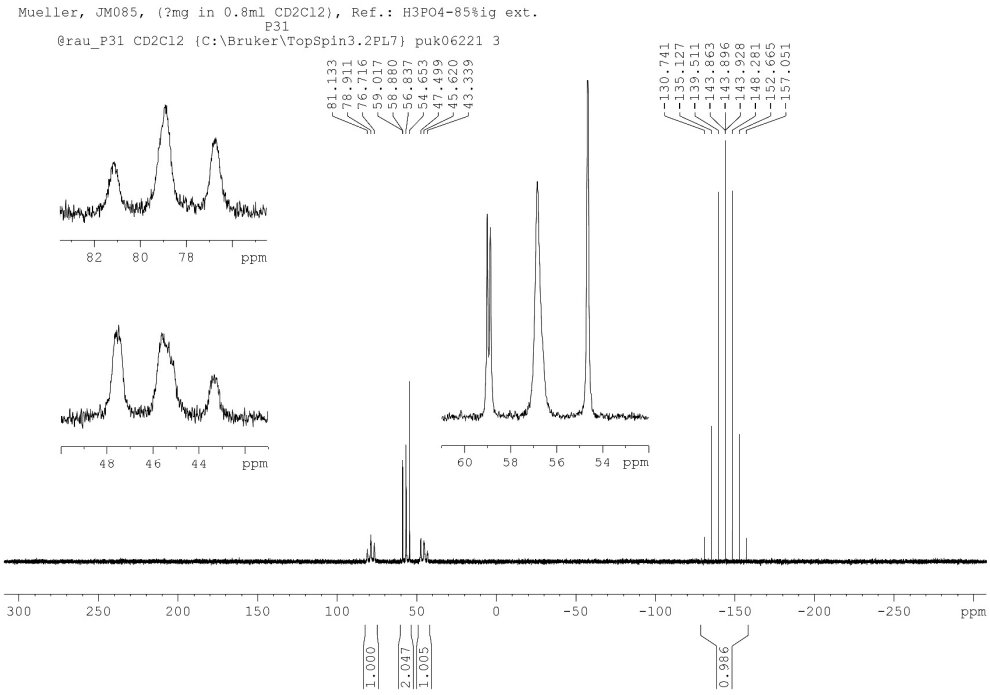

Figure S3.12: ^{31}P NMR spectrum of [{{Cp'''Fe(CO)$_2$}$_2$(μ_3,$\eta^{1:1:4}$-P_4)}FeCp'''][PF_6]$^-$ (**5**) in CD_2Cl_2.

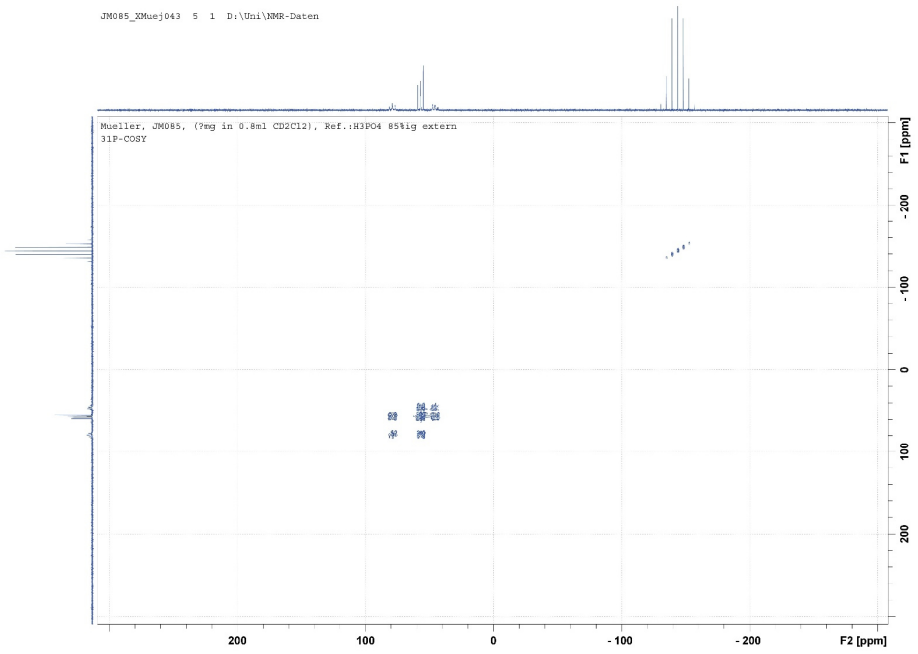

Figure S3.13: ^{31}P–^{31}P cosy NMR spectrum of [{{Cp'''Fe(CO)$_2$}$_2$(μ_3,$\eta^{1:1:4}$-P_4)}FeCp'''][PF_6]$^-$ (**5**) in CD_2Cl_2.

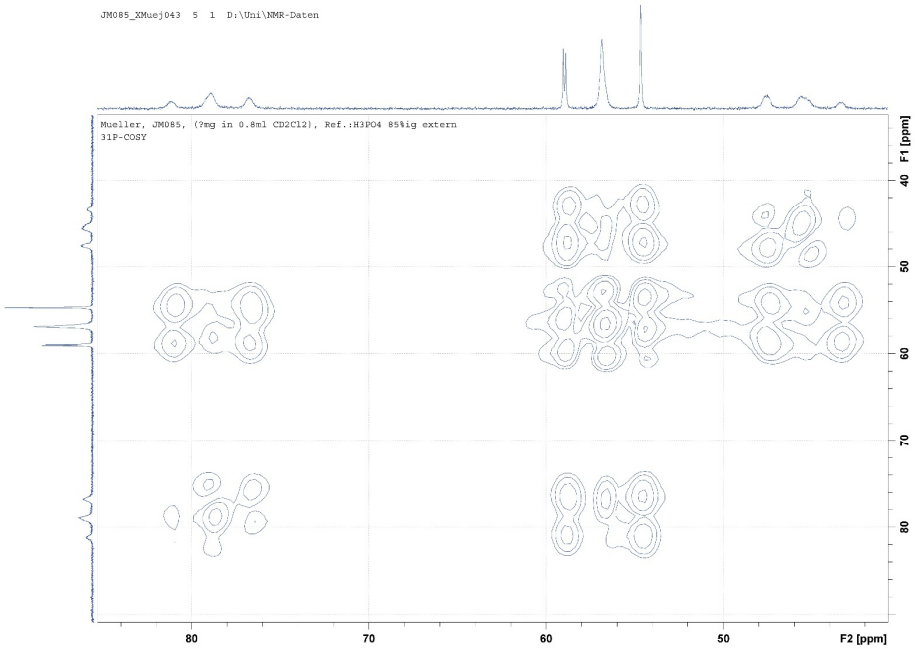

Figure S3.14: Detail of ^{31}P–^{31}P cosy NMR spectrum of [{{Cp'''Fe(CO)$_2$}$_2$(μ_3,$\eta^{1:1:4}$-P_4)}FeCp'''$]^+[PF_6]^-$ (**5**) in CD_2Cl_2.

Computational Details

All calculations have been performed with the TURBOMOLE program package[8] at the RI[9]-BP86[10] //def2-TZVP[9b, 11] level of theory. To speed up the geometry optimization the Multipole Accelerated Resolution-of-the-Identity (MARI-J)[9, 12] approximation has been used. The final energy of the molecules was determined by single point calculations without using the RI formalism.

For the calculation of the Mößbauer parameters of complexes **2**, **3** and **5**, the geometry has been optimized at the RI-BP86/def2-TZVP level in TURBOMOLE followed by single point calculations using ORCA.[13] In the single point calculations the B3LYP[10a-d, 14] functuional together with the core-property basis set CP(PPP) basis set[15] for Fe and def2-TZVP for all other atoms has been used. The isomer shift (δ) was calculated according to the formulae δ = α(ρ(0) - C) + β, with α = -0.366, C = 11810 and β = 2.852. ρ(0) represents the calculated electron density on Fe. The values of the parameters α, β and C depends from the functional and basis set used and were taken from the reference [16].

Table S3.3: Total energy of the computed compounds, at the BP86/def2-TZVP level.

Compound	Total energy (Hartree)
[{Cp'''Fe(CO)$_2$}$_2$(μ,η^1:η^1-P_4)] (**1**)	-5678.390385
[{Cp'''Fe(CO)$_2$}$_2$(*cyclo*-μ,η^1:η^1-P_4)] [a)]	-5678.331718
$[Fe(MeCN)_6]^{2+}$ (quintet)	-2060.454259
MeCN	-132.8114966
[{{Cp'''Fe(CO)$_2$}$_2$(μ_3,$\eta^{1:1:4}$-P_4)}$_2$Fe]$^{2+}$	-12620.41128

[$FeBr_2$(dme)] (quintet)	-6721.972694
dme	-308.9928029
[{{Cp'''Fe(CO)$_2$}$_2$(μ_3,η^1:η^1:η^2-P_4)}$FeBr_2$] (**2**) (quintet)	-12091.39466
[{{Cp'''Fe(CO)$_2$}$_2$(μ_3,$\eta^{1:1:4}$-P_4)}FeCp'''$]^+$	-7607.750829
[{{Cp'''Fe(CO)$_2$}$_2$(μ_3,$\eta^{1:1:2}$-P_4)}Fe(CO)Cp'''$]^+$	-7721.143842

a) Single point calculation (unrestricted singlet) using the geometry as found in the optimized structure of **3**.

Table S3.4: Relative energy of [{{Cp'''Fe(CO)$_2$}$_2$(μ_3,η^1:η^1:η^2-P_4)}$FeBr_2$] in different spin states. Calculated at the BP86/def2-TZVP level.

	Singlet	Triplet	Quintet
Relative energy (kJ·mol^{-1})	94.82	67.94	0.00

Table S3.5: NPA charges (natural population analysis) condensed to fragments. Calculated at the BP86/def2-TZVP level.

	Cp'''Fe(CO)$_2$	{Cp'''Fe(CO)$_2$}$_2$$P_4$	P_4	$Fe_{central}$	Cp'''
[{{Cp'''Fe(CO)$_2$}$_2$(μ_3,$\eta^{1:1:4}$-P_4)}$_2$Fe]$^{2+}$	0.44	1.35	0.47	-0.70	-
[{{Cp'''Fe(CO)$_2$}$_2$(μ_3,$\eta^{1:1:4}$-P_4)}FeCp'''$]^+$	0.36	1.09	0.37	-0.23	0.13
[{{Cp'''Fe(CO)$_2$}$_2$(μ_3,$\eta^{1:1:2}$-P_4)}Fe(CO)Cp'''$]^+$	0.35	1.01	0.31	-0.25	0.11
[{{Cp'''Fe(CO)$_2$}$_2$(μ_3,η^1:η^1:η^2-P_4)}$FeBr_2$] (**2**)	0.20	0.36	-0.03	0.64	-
[{Cp'''Fe(CO)$_2$}$_2$(*cyclo*-μ,η^1:η^1-P_4)] [a]	0.25	0.00	-0.50	-	-
[{Cp'''Fe(CO)$_2$}$_2$(μ,η^1:η^1-P_4)] (**1**)	0.06	-	-0.12	-	-

a) Single point calculation (unrestricted singlet) using the geometry as found in the optimized structure of **3**.

Table S3.6: Reaction energies for selected transformations, calculated at the BP86/def2-TZVP level.

Transformation	Energy (kJ·mol^{-1}) [a]
2 [{Cp'''Fe(CO)$_2$}$_2$(μ,η^1:η^1-P_4)] (**1**) + [Fe(MeCN)$_6$]$^{2+}$ = [{{Cp'''Fe(CO)$_2$}$_2$(μ_3,$\eta^{1:1:4}$-P_4)}$_2$Fe]$^{2+}$ (**3**) + 6 MeCN	-118.76
[{Cp'''Fe(CO)$_2$}$_2$(μ,η^1:η^1-P_4)] (**1**) + [$FeBr_2$(dme)] = [{{Cp'''Fe(CO)$_2$}$_2$(μ_3,η^1:η^1:η^2-P_4)}$FeBr_2$] (**2**) + dme	-64.03
[{Cp'''Fe(CO)$_2$}$_2$(μ,η^1:η^1-P_4)] (**1**) = [{Cp'''Fe(CO)$_2$}$_2$(*cyclo*-μ,η^1:η^1-P_4)] (**L**) [b]	154.03
[{{Cp'''Fe(CO)$_2$}$_2$(μ_3,$\eta^{1:1:2}$-P_4)}Fe(CO)Cp'''$]^+$ = [{{Cp'''Fe(CO)$_2$}$_2$(μ_3,$\eta^{1:1:4}$-P_4)}FeCp'''$]^+$ + CO	72.73

a) The SCF energies without any corrections have been used.
b) Single point calculation (unrestricted singlet) on the R_2P_4 ligand using the geometry as found in the optimized structure of 3.

Table S3.7. Calculated and experimental Isomer shifts (δ / mm·s^{-1}) and Quadrupole splitting (QS / mm·s^{-1}). For labeling see Figure S3.15.

	2 (quintet spin state)		**3**		**5**	
	δ	QS	δ	QS	δ	QS
Fe	0.53	2.33	0.41	0.89	0.49	2.11
Fe	0.07	1.94	0.08	1.99	0.08	1.93
Experiment						
Fe	0.73(3)	2.33(1)	0.47(3)	0.57(4)	0.43(3)	1.62(4)
Fe	0.12(3)	1.73(4)	0.12(8)	1.81(3)	0.13(8)	1.75(3)

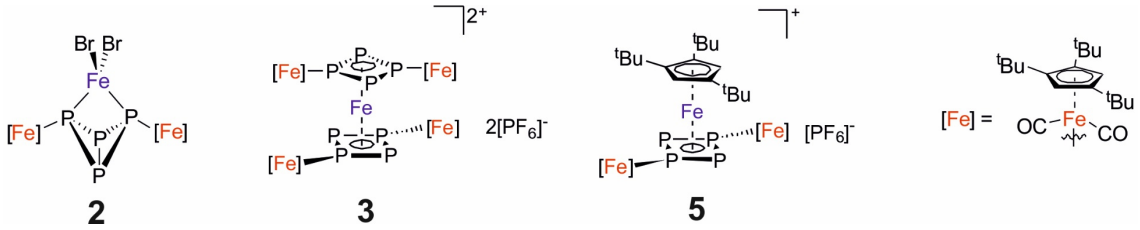

Figure S3.15. Labeling scheme for Mößbauer parameters.

Table S3.8. Cartesian coordinates of the optimized geometry of [{Cp'''Fe(CO)$_2$}$_2$(μ,η$^{1:1}$-P$_4$)] (**1**) at the RI-BP86/def2-TZVP level of theory.

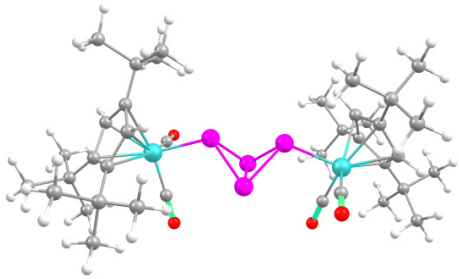

Atom	x	y	z
Fe	3.6563096	-0.0573871	-0.5344296
Fe	-3.5734605	0.0642978	-0.4911500
P	1.4346193	-0.0654399	0.2647336
P	0.0423094	-1.0594926	-1.1801880
P	0.0415403	1.1307841	-1.0388112
P	-1.3489100	-0.0406703	0.2657766
O	2.8109966	0.6288459	-3.2347408
O	3.3927000	-2.8855592	-1.1742666
O	-3.3668258	2.9682208	-0.5831879
O	-2.6867526	-0.1596906	-3.2559047
C	5.5102127	1.0350403	-0.6010401
C	4.5086423	1.8167075	0.1559351
C	4.1304033	0.9963559	1.2720522
C	4.8289777	-0.2409639	1.2718196
C	5.6617437	-0.2020968	0.1037312
C	-4.7127112	-1.7776976	-0.4803460
C	-5.6180990	-0.6223178	-0.6132905
C	-5.3989513	0.1760080	0.5583415
C	-4.4397767	-0.4243692	1.4361342
C	-4.0204704	-1.6087487	0.7701563
C	6.4837770	1.3450573	-1.7587498
C	7.7968236	1.8612014	-1.1138994
C	6.0084302	2.3725379	-2.7996436
C	6.8180991	0.0549650	-2.5451511
C	3.4730836	-1.7579433	-0.9018176
C	3.1198023	0.3824773	-2.1415637
C	-3.4183000	1.8080024	-0.5349206
C	-3.0194488	-0.0880064	-2.1445757
C	4.0139968	3.2765072	0.0584701
C	5.2192597	4.2314600	0.2340569
C	3.2505116	3.6038173	-1.2412143
C	3.0364269	3.5865582	1.2161150
C	4.8767901	-1.2604866	2.4029248
C	5.7989346	-0.6650447	3.4980009
C	3.4825907	-1.5096892	3.0051671
C	5.4728452	-2.6007301	1.9365130
C	-4.5625208	-3.1191714	-1.2285756
C	-5.5495885	-4.1136225	-0.5620716
C	-4.8311948	-3.0913229	-2.7429043
C	-3.1341998	-3.6854571	-1.0509118
C	-6.7373342	-0.2551977	-1.6128545
C	-7.8199530	-1.3606072	-1.6060930
C	-7.4438476	1.0464173	-1.1671987
C	-6.2385368	0.0039946	-3.0497165
C	-4.1407382	0.0091335	2.8667694
C	-5.4366332	-0.2090204	3.6878872
C	-3.7484030	1.4975101	2.9384466
C	-3.0170797	-0.8418571	3.4844882
H	3.3910026	1.2798022	2.0127792
H	6.3260392	-1.0031998	-0.2004338
H	-5.9090101	1.1108168	0.7640857
H	-3.2751462	-2.2967939	1.1529159
H	8.2165244	1.1159085	-0.4233977
H	7.6377924	2.7903500	-0.5509510
H	8.5438083	2.0613872	-1.8966510

H	6.7850493	2.4750614	-3.5719375
H	5.8471505	3.3681932	-2.3737814
H	5.0870636	2.0499933	-3.3009071
H	7.3352290	-0.6948350	-1.9324396
H	7.4898786	0.3059170	-3.3783840
H	5.9127854	-0.4046799	-2.9636918
H	5.9367037	4.1649204	-0.5919544
H	5.7572355	4.0176707	1.1692580
H	4.8615185	5.2707712	0.2795022
H	2.9807581	4.6707130	-1.2462119
H	2.3195471	3.0230693	-1.2954248
H	3.8271194	3.4015196	-2.1467764
H	2.6899265	4.6250201	1.1179420
H	3.5149461	3.4894502	2.2012933
H	2.1487486	2.9386790	1.1871007
H	5.8911864	-1.3700029	4.3377614
H	5.3939735	0.2796575	3.8877167
H	6.8071465	-0.4675789	3.1056735
H	2.8002232	-1.9516453	2.2666923
H	3.0202808	-0.5828058	3.3718845
H	3.5635348	-2.2006666	3.8573883
H	5.5142523	-3.3004139	2.7837633
H	6.4993007	-2.4831566	1.5600557
H	4.8658777	-3.0650574	1.1481827
H	-6.5934491	-3.7909561	-0.6688380
H	-5.3363035	-4.2194209	0.5111276
H	-5.4500268	-5.1048754	-1.0292124
H	-5.8597797	-2.8098966	-2.9903965
H	-4.6679604	-4.1010278	-3.1473749
H	-4.1449514	-2.4133092	-3.2660181
H	-3.0469792	-4.6213463	-1.6207549
H	-2.8991709	-3.9243773	-0.0056567
H	-2.3715230	-2.9883253	-1.4236062
H	-8.6706415	-1.0485071	-2.2299937
H	-8.1946882	-1.5367034	-0.5871796
H	-7.4536480	-2.3146521	-2.0012323
H	-8.2306953	1.2896249	-1.8949907
H	-6.7516595	1.8996080	-1.1353807
H	-7.9239280	0.9427621	-0.1835729
H	-5.6870027	-0.8376556	-3.4757343
H	-5.5799140	0.8824708	-3.0725129
H	-7.0992093	0.2087608	-3.7045329
H	-5.7591044	-1.2596361	3.6487168
H	-6.2610666	0.4145341	3.3131417
H	-5.2629214	0.0557806	4.7415912
H	-3.6225188	1.8021326	3.9881379
H	-4.5180015	2.1450145	2.4944692
H	-2.8014818	1.6799189	2.4124878
H	-3.2899000	-1.9071261	3.5191295
H	-2.8312844	-0.5145814	4.5179538
H	-2.0787274	-0.7395847	2.9208763

Table S3.9. Cartesian coordinates of the optimized geometry of [{Cp'''Fe(CO)$_2$}$_2$(μ_3,$\eta^{1:1:2}$-P$_4$){FeBr$_2$}] (quintet spin state) (**2**) at the RI-BP86/def2-TZVP level of theory.

Atom	x	y	z
Fe	3.6598980	-0.0734301	-0.7126951
Fe	-3.5684331	0.1537144	-0.5729372
P	1.4491616	-0.1509725	-0.0337023
P	0.0116909	-0.8895508	-1.5755774
P	0.0627249	1.2663717	-1.0985041
P	-1.3394429	-0.0638404	0.0262573
Fe	0.0883134	-0.6322741	1.8797801
Br	0.5516481	1.0259461	3.5020328
Br	-0.3192312	-2.9064098	2.3784027
O	2.9043514	0.7905080	-3.3924709
O	3.5015611	-2.8625325	-1.5480384
O	-3.3174510	3.0576695	-0.6885313
O	-2.8266355	-0.0879263	-3.3817299
C	5.4899486	1.0642492	-0.6991895
C	4.4796395	1.7580677	0.1276846
C	4.1216372	0.8371963	1.1735203

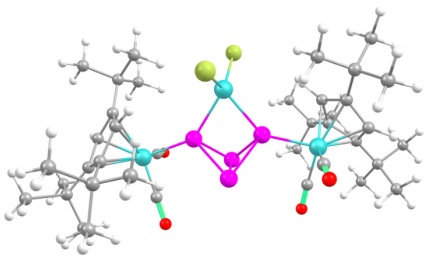

C	4.8565192	-0.3770278	1.0686043
C	5.6716471	-0.2245964	-0.1015700
C	-4.6500328	-1.7144071	-0.4383027
C	-5.5869257	-0.6069666	-0.7287263
C	-5.4519379	0.3100967	0.3623256
C	-4.5325614	-0.1733726	1.3501920
C	-4.0394338	-1.4010325	0.8274013
C	6.4567382	1.4853731	-1.8280237
C	7.7713151	1.9308196	-1.1338282
C	5.9864973	2.6135013	-2.7613597
C	6.7868578	0.2788718	-2.7390565
C	3.5436311	-1.7586103	-1.1948964
C	3.1821360	0.4715831	-2.3112473
C	-3.3886517	1.9020774	-0.6207453
C	-3.1146530	-0.0108928	-2.2598302
C	3.9765435	3.2165993	0.1627262
C	5.1807362	4.1531688	0.4271296
C	3.2176186	3.6560629	-1.1057942
C	3.0013938	3.4169733	1.3444713
C	4.9594889	-1.4795358	2.1138212
C	5.7974016	-0.8928891	3.2802213
C	3.5804078	-1.8965607	2.6495484
C	5.6874680	-2.7179795	1.5615144
C	-4.4179006	-3.1155896	-1.0406506
C	-5.3550942	-4.0859255	-0.2733153
C	-4.6769715	-3.2617211	-2.5492479
C	-2.9617296	-3.5771991	-0.8059926
C	-6.6979482	-0.3965772	-1.7826002
C	-7.7398588	-1.5318608	-1.6339397
C	-7.4518253	0.9258787	-1.5085829
C	-6.2036628	-0.3052472	-3.2402191
C	-4.3664929	0.3962036	2.7543167
C	-5.7521501	0.2919581	3.4427846
C	-3.9332433	1.8743548	2.7278371
C	-3.3537307	-0.4206494	3.5692647
H	3.3831057	1.0416997	1.9441809
H	6.3533278	-0.9820388	-0.4717488
H	-6.0003620	1.2416432	0.4491390
H	-3.2951316	-2.0203536	1.3205782
H	8.1938851	1.1174712	-0.5271526
H	7.6135763	2.7954592	-0.4759682
H	8.5152421	2.2123086	-1.8937136
H	6.7674008	2.7907311	-3.5153386
H	5.8253503	3.5618334	-2.2390336
H	5.0682106	2.3458186	-3.2989064
H	7.2920846	-0.5357391	-2.2046673
H	7.4677870	0.6086706	-3.5363662
H	5.8827708	-0.1265508	-3.2124472
H	5.9009806	4.1700017	-0.3989345
H	5.7164177	3.8553239	1.3402492
H	4.8170661	5.1810864	0.5710364
H	2.9406002	4.7168605	-1.0141576
H	2.2890802	3.0790357	-1.2147064
H	3.7970768	3.5407228	-2.0249426
H	2.6451152	4.4566234	1.3362749
H	3.4841502	3.2420919	2.3160859
H	2.1188590	2.7661981	1.2793248
H	5.9394195	-1.6585125	4.0569952
H	5.2910679	-0.0326754	3.7396465
H	6.7901895	-0.5659970	2.9373495
H	2.9686749	-2.3655778	1.8674949
H	3.0164897	-1.0450162	3.0553490
H	3.7002514	-2.6274204	3.4622838
H	5.7543585	-3.4825359	2.3483451
H	6.7145971	-2.4851448	1.2440665
H	5.1522801	-3.1640791	0.7123355
H	-6.4139146	-3.8241267	-0.4017046
H	-5.1313335	-4.0810140	0.8024769
H	-5.2101257	-5.1107360	-0.6458383
H	-5.7202008	-3.0807290	-2.8293183
H	-4.4397925	-4.2937318	-2.8457297
H	-4.0323922	-2.5970974	-3.1393951
H	-2.8385800	-4.5894587	-1.2168913
H	-2.6786422	-3.6238685	0.2527273
H	-2.2467001	-2.9185509	-1.3176224
H	-8.5971135	-1.3324131	-2.2935651
H	-8.1138151	-1.5896156	-0.6013896

H	-7.3356482	-2.5141666	-1.9025090
H	-8.2280237	1.0559637	-2.2756512
H	-6.7857852	1.7985732	-1.5654980
H	-7.9529572	0.9254323	-0.5302794
H	-5.6082633	-1.1655249	-3.5542595
H	-5.5962880	0.5979814	-3.3843239
H	-7.0716666	-0.2348700	-3.9127391
H	-6.1096295	-0.7476830	3.4625019
H	-6.5082281	0.9055265	2.9318505
H	-5.6760749	0.6451257	4.4814368
H	-3.9197171	2.2765109	3.7511903
H	-4.6222569	2.4936410	2.1354146
H	-2.9225731	1.9832961	2.3123040
H	-3.6622558	-1.4709939	3.6711839
H	-3.2596627	0.0020068	4.5792749
H	-2.3532590	-0.4030834	3.1151705

Table S3.10. Cartesian coordinates of the optimized geometry of [{{Cp'''Fe(CO)$_2$}$_2$(μ_3,$\eta^{1:1:4}$-P$_4$)}$_2$Fe]$^{2+}$ (**3**) at the RI-BP86/def2-TZVP level of theory.

Atom	x	y	z
Fe	-0.0718815	-0.0044005	0.2705416
P	-1.4832345	-0.0190746	2.0953062
P	-0.0935448	-1.6720088	1.9742062
P	1.2305801	0.9094630	-1.4989447
P	-0.9165556	1.2310928	-1.4789392
P	1.4038464	-0.0924557	2.0417596
P	0.0039187	1.5669657	2.0581017
P	-1.4808450	-0.8713655	-1.4382398
P	0.6620043	-1.1929477	-1.5539181
Fe	-2.1720533	3.0162380	-2.1387520
Fe	-3.6302210	-0.0046690	2.8202304
Fe	1.8702025	-3.0095184	-2.1790750
Fe	3.5186210	-0.2360126	2.9007758
O	-3.3121608	3.4247175	0.5113683
O	-3.4492694	2.8296166	3.5030791
O	-4.2728349	1.1440990	-2.9325065
O	-4.6102371	0.5302886	0.1244577
C	-0.5359209	3.9282566	-3.1600402
H	0.4660178	3.5137256	-3.1899772
C	-1.5501352	3.6451758	-4.1370181
C	-2.3715037	5.0828875	-2.5046969
H	-3.0337238	5.7312157	-1.9414747
C	-3.5650727	-0.7834279	4.8467452
C	-4.8466997	-0.2287235	4.5226978
H	-5.3059154	0.6013354	5.0496825
C	-2.7494454	4.3962501	-3.7068752
C	-1.0007910	4.8393553	-2.1676927
C	-5.4754077	-0.9401020	3.4456165
C	-0.1570939	5.6026207	-1.1606715
C	-3.3748277	-1.8329659	3.9038267
H	-2.4842389	-2.4490160	3.8491795
C	-2.8364107	3.2373091	-0.5259210
C	-4.5156806	-1.9925802	3.0462662
C	-3.4951070	1.7126439	3.2148095
C	-4.1090101	4.7517851	-4.3453114
C	-1.2032755	2.8784553	-5.4273233
C	-2.0654223	1.6217776	-5.6582485
H	-1.8826114	0.8809618	-4.8672867
H	-1.7916673	1.1631664	-6.6191283
H	-3.1373008	1.8305792	-5.6866932
C	-3.4346903	1.8780302	-2.6274362
C	-4.2138914	0.2952465	1.1855702
C	-4.6344404	-3.2268479	2.1299145
C	-2.7477123	-0.5072776	6.0980953
C	-4.8318687	-2.8961827	0.6374690
H	-5.6987632	-2.2602397	0.4436534
H	-4.9744483	-3.8308360	0.0765540
H	-3.9411427	-2.3953002	0.2321375
C	-3.4582337	-1.2732720	7.2465669
H	-4.4788199	-0.8993620	7.4089139
H	-2.8968060	-1.1397945	8.1820644
H	-3.5163601	-2.3501702	7.0352133
C	-1.3124828	-1.0393461	5.9587924

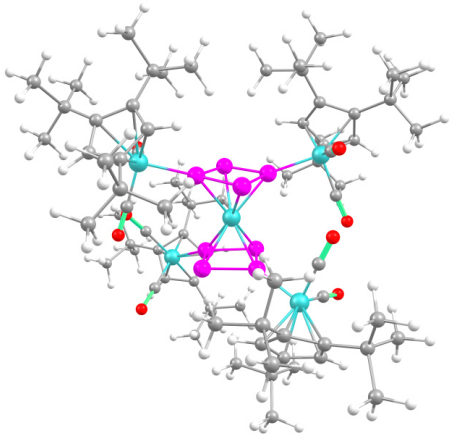

H	-1.2880620	-2.1273618	5.8051661
H	-0.7527693	-0.8289525	6.8801992
H	-0.7851907	-0.5595707	5.1218394
C	-3.3557487	-4.0889453	2.2237851
H	-2.4591023	-3.5465105	1.8884643
H	-3.4736570	-4.9627614	1.5690367
H	-3.1795154	-4.4670880	3.2405258
C	-5.1855587	4.9708820	-3.2553036
H	-5.3516278	4.0632124	-2.6590065
H	-6.1353864	5.2267453	-3.7434891
H	-4.9498955	5.7978535	-2.5735240
C	-3.8843498	6.1065673	-5.0735975
H	-3.5498220	6.8867525	-4.3759008
H	-4.8311656	6.4377797	-5.5226755
H	-3.1399980	6.0253602	-5.8760059
C	-6.9515279	-0.6241928	3.1263519
C	-1.3157827	3.8506543	-6.6279428
H	-2.3423329	4.1829062	-6.8146679
H	-0.9617293	3.3455370	-7.5377490
H	-0.6911429	4.7421153	-6.4748591
C	-2.7079340	0.9904828	6.4487083
H	-2.1541156	1.5663864	5.6954822
H	-2.2049655	1.1288154	7.4158477
H	-3.7133879	1.4232758	6.5436627
C	-4.7012060	3.7469519	-5.3473498
H	-4.0664029	3.5869796	-6.2241985
H	-5.6549747	4.1493403	-5.7157553
H	-4.9189575	2.7767124	-4.8836847
C	-7.2259569	0.8926552	3.2647020
H	-7.0543229	1.2729885	4.2796233
H	-8.2818845	1.0839394	3.0316454
H	-6.6168411	1.4799535	2.5639998
C	-5.7939210	-4.1116718	2.6532867
H	-5.6479654	-4.3710321	3.7115076
H	-5.8213579	-5.0486293	2.0794448
H	-6.7736911	-3.6338847	2.5514881
C	0.2671572	2.4057431	-5.3862533
H	0.9733939	3.2464468	-5.3365170
H	0.4848204	1.8538782	-6.3102941
H	0.4618785	1.7292338	-4.5415977
C	-7.4637884	-1.0334914	1.7355802
H	-6.9249740	-0.5201420	0.9289983
H	-8.5202674	-0.7419389	1.6555425
H	-7.4194516	-2.1125558	1.5594114
C	-7.7896615	-1.3613408	4.2072299
H	-7.6590537	-2.4499338	4.1599744
H	-8.8554281	-1.1415938	4.0530637
H	-7.5192052	-1.0302910	5.2195590
O	2.2276998	-3.8775872	0.5839753
O	2.7304775	-2.6404491	4.3603019
O	4.2340521	-1.2931124	-2.2318465
O	4.5283095	-1.8800176	0.7158795
C	0.4278526	-3.5879766	-3.6426747
H	-0.5111488	-3.0700856	-3.8038276
C	1.6480748	-3.2767115	-4.3342986
C	1.9890188	-5.0130491	-2.8254085
H	2.4634794	-5.8016167	-2.2519867
C	3.6395785	1.1437310	4.5817682
C	4.7877132	0.2909241	4.4952154
H	5.0981419	-0.3977887	5.2738458
C	2.6653964	-4.2094555	-3.8023203
C	0.5989559	-4.6743057	-2.7376112
C	5.5188803	0.5070527	3.2790826
C	-0.4984819	-5.4799784	-2.0604403
C	3.6201340	1.8530722	3.3469882
H	2.8573455	2.5721773	3.0687909
C	2.0744430	-3.5105143	-0.5018355
C	4.7545901	1.5237608	2.5262482
C	3.0127460	-1.6782816	3.7873985
C	4.0973434	-4.6161867	-4.2095431
C	1.6470220	-2.2955733	-5.5226910
C	2.6283171	-1.1167965	-5.3643044
H	2.3288147	-0.4782079	-4.5213840
H	2.6066036	-0.5021513	-6.2755303
H	3.6620324	-1.4316766	-5.2035133
C	3.3002002	-1.9742775	-2.2085720
C	4.1048133	-1.1997696	1.5498508

C	5.0742144	2.3457954	1.2638609
C	2.8392909	1.4352664	5.8416412
C	5.2099286	1.5066924	-0.0214861
H	5.9518307	0.7087749	0.0533859
H	5.5082041	2.1616914	-0.8525716
H	4.2437351	1.0546834	-0.2860421
C	3.7312512	2.3775505	6.6954135
H	4.6763830	1.8928825	6.9772684
H	3.2011301	2.6480938	7.6195635
H	3.9682290	3.3049350	6.1553699
C	1.5198921	2.1559633	5.5259508
H	1.6866934	3.1173911	5.0197863
H	0.9840314	2.3701607	6.4608427
H	0.8658460	1.5422964	4.8913110
C	3.9501812	3.3699419	0.9967857
H	2.9803202	2.8809507	0.8247213
H	4.1990596	3.9330686	0.0874834
H	3.8454276	4.0972108	1.8142440
C	4.8902633	-5.1298093	-2.9833962
H	4.9853162	-4.3584237	-2.2070746
H	5.9029585	-5.4042758	-3.3074377
H	4.4509242	-6.0276339	-2.5306489
C	3.9264285	-5.8039740	-5.1977620
H	3.3835563	-6.6380224	-4.7320136
H	4.9179910	-6.1705260	-5.4981789
H	3.3852771	-5.5100652	-6.1060468
C	6.9199612	-0.1297813	3.1548237
C	1.9431108	-3.0842839	-6.8221598
H	2.9593167	-3.4906962	-6.8527624
H	1.8297924	-2.4142957	-7.6861623
H	1.2375212	-3.9175326	-6.9498254
C	2.5505852	0.1588477	6.6508129
H	1.8806111	-0.5195539	6.1065419
H	2.0640353	0.4259559	7.5991749
H	3.4679473	-0.3905568	6.9034324
C	4.9712541	-3.5413411	-4.8770653
H	4.5569412	-3.1725031	-5.8201313
H	5.9471967	-3.9879159	-5.1125119
H	5.1582633	-2.6878561	-4.2136932
C	6.9338224	-1.5469846	3.7771907
H	6.6982230	-1.5504294	4.8487686
H	7.9430466	-1.9677026	3.6758114
H	6.2378327	-2.2247357	3.2644361
C	6.3624815	3.1653465	1.5270421
H	6.2599234	3.7855544	2.4289455
H	6.5443398	3.8371608	0.6763195
H	7.2509407	2.5365057	1.6464354
C	0.2418856	-1.6785196	-5.6977470
H	-0.5200879	-2.4354080	-5.9312751
H	0.2695573	-0.9749285	-6.5402462
H	-0.0767048	-1.1166878	-4.8078260
C	7.5106738	-0.2661490	1.7416270
H	6.9106911	-0.9256670	1.1025692
H	8.5082302	-0.7188180	1.8281142
H	7.6416173	0.6948647	1.2348764
C	7.8623714	0.7713555	4.0012693
H	7.9211924	1.7932919	3.6054745
H	8.8756494	0.3458287	3.9915181
H	7.5302244	0.8295087	5.0470852
C	-1.5846648	-4.5687594	-1.4673448
H	-1.1805106	-3.9389339	-0.6614879
H	-2.3922804	-5.1827828	-1.0452050
H	-2.0358944	-3.9132212	-2.2252583
C	-1.1285155	-6.3578282	-3.1754608
H	-1.5723956	-5.7416771	-3.9697281
H	-1.9222058	-6.9861035	-2.7471021
H	-0.3823773	-7.0223397	-3.6331364
C	0.0565127	-6.4027924	-0.9615091
H	0.7984746	-7.1114635	-1.3551068
H	-0.7628720	-6.9994324	-0.5378384
H	0.5148644	-5.8380186	-0.1391123
C	-1.0154793	6.2621040	-0.0672926
H	-1.7458557	6.9688749	-0.4855228
H	-0.3673226	6.8350528	0.6099463
H	-1.5539449	5.5209583	0.5379763
C	0.8952574	4.6944292	-0.5063899

H	0.4215575	3.9038580	0.0938183
H	1.5342819	5.2900417	0.1601445
H	1.5505462	4.2187471	-1.2500520
C	0.5640268	6.7163860	-1.9668805
H	1.2233951	6.2928896	-2.7374595
H	1.1787152	7.3240228	-1.2878915
H	-0.1551308	7.3847251	-2.4606766

Table S3.11. Cartesian coordinates of the optimized geometry of [{{Cp'''Fe(CO)$_2$}$_2$(μ_3,$\eta^{1:1:2}$-P_4)}Fe(CO)Cp'''$]^+$ (**4**) at the RI-BP86/def2-TZVP level of theory.

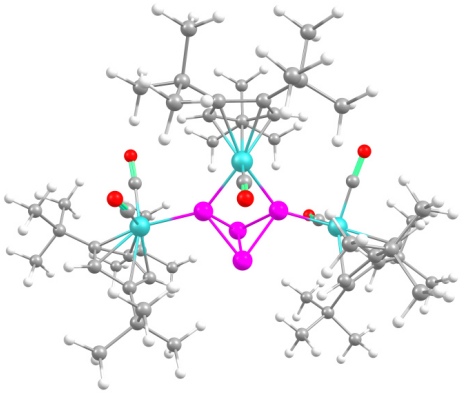

Atom	x	y	z
Fe	0.2453578	0.3706075	-3.5892470
Fe	-1.2243634	-0.5676636	3.4086284
Fe	1.9801784	0.3043288	0.3966330
P	0.3779165	0.1327181	-1.2682966
P	-0.1049722	-0.1315492	1.3629261
P	-1.3797938	0.9117114	-0.1346920
P	-1.0556718	-1.2887330	-0.3080457
O	2.4630365	-1.5050282	-3.8158592
O	1.5340066	3.1794890	0.4714604
O	-1.5916301	-3.3396040	2.5822157
O	2.0091054	2.6865283	-3.4971024
O	1.2593184	-1.2905367	4.7409143
C	-1.8887928	0.1218320	-3.7617187
H	-2.5534109	-0.1264800	-2.9414843
C	-1.2621208	-0.8531462	-4.6119653
C	-2.5974127	1.0811044	3.2547986
H	-2.7153249	1.7081154	2.3778482
C	-1.5730541	1.4499243	-4.1651155
C	-1.8641510	0.2608994	5.2334695
H	-1.3155929	0.1507217	6.1627080
C	3.2034944	-0.8066928	1.7115935
C	3.5516410	-0.8047750	-0.5222488
C	-3.3776811	-0.0951520	3.5080782
C	-0.4468070	-0.0878669	-5.5793129
C	1.3107690	1.7636481	-3.4759630
C	3.8851182	0.4226932	1.4198179
C	4.1168104	0.4227636	-0.0357784
C	-1.4572498	-2.2259729	2.8715086
C	-0.6519224	1.2934653	-5.2532640
H	-0.2029914	2.1185922	-5.7965748
C	-1.6856250	-2.3359806	-4.5528289
C	3.0316470	-1.6030120	0.5367969
C	-1.6901796	1.3492525	4.3220313
C	-2.8796873	-0.6499745	4.7856269
C	1.7112118	2.0272240	0.4510110
C	-4.6205278	-0.4162890	2.6502678
C	4.9985842	1.2976818	-0.9554957
C	-0.9499063	2.6487456	4.5903354
C	-2.2730769	2.7505631	-3.7728185
C	-2.7472417	-2.5527567	-3.4518717
H	-2.3677619	-2.3098272	-2.4488011
H	-3.0336901	-3.6132774	-3.4420113
H	-3.6593018	-1.9668814	-3.6346036
C	0.3172712	-0.4251450	-6.8792304
C	1.5641289	-0.7805140	-3.7025363
C	-5.8779630	-0.2907257	3.5477334
H	-5.9266927	-1.0569205	4.3277442
H	-6.7767592	-0.3961850	2.9236734
H	-5.9201869	0.6950563	4.0326853
C	-3.3427256	-1.7607358	5.7542363
C	6.4636822	1.2149375	-0.4583577
H	6.6129981	1.7098427	0.5071375
H	7.1215839	1.7096727	-1.1874124
H	6.7924211	0.1700735	-0.3624455
C	-2.3805417	-2.7061919	-5.8871125
H	-3.2175737	-2.0249739	-6.0967719
H	-2.7875340	-3.7245182	-5.8113053
H	-1.7016222	-2.6855312	-6.7452747
C	-0.6945664	-0.2284373	-8.0409682
H	-1.5461926	-0.9165505	-7.9684588
H	-0.1903035	-0.4137429	-9.0001306
H	-1.0877157	0.7977384	-8.0575606

C	-4.7928114	0.6352940	1.5321021
H	-4.9284028	1.6499656	1.9327832
H	-5.6930147	0.3876177	0.9531796
H	-3.9449387	0.6413329	0.8318297
C	-0.3316885	3.2217778	3.3070785
H	0.4365533	2.5503701	2.9031078
H	0.1431494	4.1904357	3.5159866
H	-1.0833901	3.3884115	2.5228316
C	0.9281928	-1.8335633	-6.9848210
H	1.6808115	-2.0170006	-6.2080845
H	1.4371275	-1.9177291	-7.9553740
H	0.1831336	-2.6340223	-6.9474911
C	-4.5832369	-1.7924835	1.9570150
H	-3.7795683	-1.8240311	1.2073517
H	-5.5347697	-1.9594594	1.4317067
H	-4.4355308	-2.6245719	2.6497913
C	2.7299901	-3.0944041	0.4810809
C	-3.4370947	2.4761020	-2.8056093
H	-4.1789367	1.7962455	-3.2494005
H	-3.9489759	3.4193628	-2.5693215
H	-3.0914203	2.0412332	-1.8570471
C	-4.2792436	-1.0776737	6.7878104
H	-3.7581702	-0.2746075	7.3277831
H	-4.6134096	-1.8206155	7.5258935
H	-5.1703562	-0.6448942	6.3159921
C	-4.0758584	-2.9625443	5.1337148
H	-5.0126491	-2.6898930	4.6386743
H	-4.3332263	-3.6654197	5.9386718
H	-3.4448842	-3.5056525	4.4191729
C	4.5598458	2.7704352	-1.0747087
H	3.5844847	2.8467555	-1.5688285
H	5.2887216	3.3153863	-1.6926736
H	4.4902271	3.2836853	-0.1136263
C	-2.1370621	-2.3458005	6.5284539
H	-1.4141387	-2.8226239	5.8530718
H	-2.5025522	-3.1146253	7.2227079
H	-1.6077791	-1.5991703	7.1339162
C	-0.5292001	-3.3097976	-4.2526128
H	0.2943199	-3.2374233	-4.9678702
H	-0.9055694	-4.3426075	-4.2790813
H	-0.1253048	-3.1279260	-3.2470421
C	1.4824185	0.5699433	-7.0986419
H	1.1461492	1.6083059	-7.2131347
H	2.0063135	0.3034678	-8.0265535
H	2.2119830	0.5286007	-6.2786664
C	0.1433739	2.4662710	5.6571660
H	-0.2746744	2.1511647	6.6239149
H	0.6591073	3.4219206	5.8243131
H	0.8975235	1.7298670	5.3484728
C	-2.0080917	3.6468715	5.1313466
H	-2.7964626	3.8366650	4.3894203
H	-1.5250786	4.6058174	5.3676146
H	-2.4829961	3.2703757	6.0484686
C	4.4168648	1.2705093	2.5945112
C	5.0057104	0.7282207	-2.3920122
H	5.4263696	-0.2859682	-2.4368795
H	5.6299149	1.3729316	-3.0257009
H	4.0013300	0.7114293	-2.8335036
C	0.2989265	-0.9719400	4.1745634
C	2.1189105	-3.5092394	-0.8673101
H	1.1518933	-3.0135923	-1.0372970
H	1.9473742	-4.5951068	-0.8809580
H	2.7807299	-3.2697001	-1.7102553
C	3.4188911	1.2475387	3.7719813
H	2.4407502	1.6432639	3.4667196
H	3.8045895	1.8821199	4.5820466
H	3.2754527	0.2446670	4.1904291
C	5.7241524	0.5884941	3.0803696
H	5.5353783	-0.4469705	3.3966702
H	6.1294845	1.1388311	3.9420432
H	6.4943135	0.5677983	2.2994516
C	4.0903165	-3.8210106	0.6499696
H	4.7889245	-3.5510086	-0.1544473
H	3.9404988	-4.9103909	0.6209594
H	4.5614787	-3.5673293	1.6101098
C	4.7056321	2.7526901	2.3036546

H	5.5078297	2.8985704	1.5737466
H	5.0327569	3.2351939	3.2359356
H	3.8104362	3.2831717	1.9540890
C	1.7965174	-3.5320439	1.6188612
H	2.2087117	-3.2878503	2.6077561
H	1.6462775	-4.6204330	1.5858118
H	0.8119878	-3.0576942	1.5224095
C	-2.8642884	3.3538357	-5.0730753
H	-2.0789757	3.6366983	-5.7875362
H	-3.4351458	4.2610748	-4.8300612
H	-3.5447342	2.6479542	-5.5702235
C	-1.3086876	3.7748074	-3.1452217
H	-0.8796126	3.3982569	-2.2065467
H	-1.8486325	4.7064111	-2.9229024
H	-0.4833431	4.0267192	-3.8248146
H	3.5638900	-1.1050798	-1.5634909
H	2.9042241	-1.1095307	2.7090964

Table S3.12. Cartesian coordinates of the optimized geometry of [{{Cp'''Fe(CO)$_2$}$_2$(μ$_3$,η$^{1:1:4}$-P$_4$)}FeCp'''$]^+$ (**5**) at the RI-BP86/def2-TZVP level of theory.

Atom	x	y	z
Fe	-0.7552629	-0.7782083	-1.7698822
Fe	1.4381817	-3.2222064	1.1196008
Fe	-1.8570417	3.1188579	-0.1246378
P	0.1793839	-1.5582885	0.1670092
P	-1.0673716	0.9828443	-0.3360746
P	-1.9015617	-0.9243093	0.2926045
P	0.9767386	0.3212539	-0.5517416
O	2.8902488	-3.4387173	-1.4032174
O	-4.6310320	2.2174823	-0.0501054
O	-0.2271368	-5.5121268	0.4322714
O	-1.8689073	3.4657283	-3.0227677
C	1.7093593	-2.0562347	2.9073253
H	1.3189552	-1.0538791	3.0398371
C	-1.2103331	-0.0649502	-3.6827186
H	-1.4455845	0.9655472	-3.9240848
C	-0.3316363	3.6190051	1.2989579
H	0.5197923	2.9835327	1.5115404
C	-1.4378595	-2.2990874	-3.0662884
C	-2.1892503	-1.0578340	-3.3053956
C	3.1150654	-3.8227601	2.3366284
C	1.0015939	-3.2427062	3.2483186
C	-0.0488426	-1.9783627	-3.3118536
H	0.7709566	-2.6811248	-3.2203243
C	0.0995301	-0.6227090	-3.7296904
C	-0.3380153	4.6418385	0.2918317
C	3.0093875	-2.3488482	2.3705443
C	1.8753406	-4.3139418	2.8645737
H	1.6426040	-5.3663812	2.9901294
C	-2.6059866	-4.0009802	-1.5083293
H	-1.9472997	-3.7650202	-0.6631455
H	-2.8934375	-5.0594975	-1.4253825
H	-3.5084469	-3.3945805	-1.4014305
C	-3.6860439	-0.7406575	-3.4946433
C	0.3747915	-4.5533613	0.6699728
C	-2.4067234	4.5231340	1.3425481
H	-3.4351325	4.7303210	1.6212050
C	1.3363032	0.0121089	-4.3475689
C	-3.5191312	2.5335522	-0.0941137
C	-1.5775607	3.5468805	1.9836654
C	-1.6968663	5.2256267	0.3112740
C	4.2537033	-4.8339668	2.0832590
C	-1.0398735	-2.0528278	4.1431823
H	-0.4442576	-1.2395118	4.5812225
H	-1.9357017	-2.1773167	4.7674046
H	-1.3672120	-1.7435211	3.1403544
C	5.3553374	-4.4056892	1.0991838
H	4.9587396	-4.2173455	0.0934418
H	6.0814703	-5.2262710	1.0132154
H	5.9123475	-3.5230418	1.4285424
C	2.6368896	-0.6170030	-3.8212677
H	2.7487687	-0.4510206	-2.7406794
H	3.5009086	-0.1615345	-4.3261251

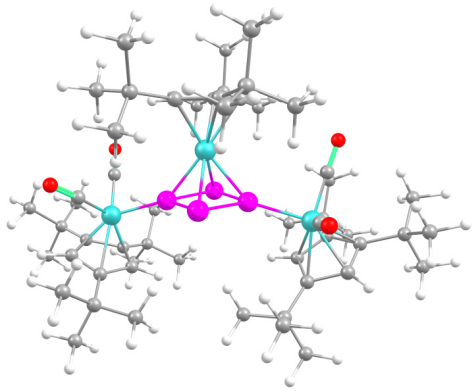

H	2.6782016	-1.6982287	-4.0110242
C	-1.1784979	-4.5012715	3.6172882
H	-1.6164809	-4.2687064	2.6376995
H	-2.0041003	-4.6322874	4.3308159
H	-0.6564964	-5.4652678	3.5420346
C	-3.9524383	0.7610924	-3.2649600
H	-3.6343652	1.0645317	-2.2605728
H	-5.0298659	0.9572426	-3.3526643
H	-3.4470421	1.3988237	-4.0003642
C	-0.6426421	-4.6918744	-2.8665849
H	-0.9639179	-5.7233100	-2.6676415
H	0.0941533	-4.4235646	-2.0995063
H	-0.1417864	-4.6821490	-3.8448779
C	0.9758173	4.9894115	-1.9250379
H	0.8899992	3.9453920	-2.2542119
H	1.9283835	5.3804462	-2.3104700
H	0.1697746	5.5606221	-2.3911319
C	-2.3673431	6.4591070	-0.3295702
C	1.2353511	-0.2591995	-5.8726678
H	1.2116295	-1.3374773	-6.0840188
H	2.1068448	0.1711047	-6.3872890
H	0.3285827	0.1922293	-6.2993106
C	4.8969416	-5.1195514	3.4677191
H	5.3398047	-4.2190572	3.9116441
H	5.6939201	-5.8680652	3.3534852
H	4.1568634	-5.5179572	4.1758758
C	4.5679278	-1.1035545	0.7181177
H	5.0051943	-2.0293219	0.3362046
H	5.3429636	-0.3245774	0.6751211
H	3.7565127	-0.8006696	0.0411178
C	3.4280161	0.1464581	2.5235184
H	2.5737112	0.3935457	1.8771388
H	4.1894995	0.9242303	2.3745095
H	3.1095184	0.1939517	3.5747063
C	-3.2646819	2.1257801	3.2403586
H	-4.0709787	2.8331307	3.0011411
H	-3.4918311	1.6922127	4.2246197
H	-3.2847237	1.3144272	2.5001207
C	-2.7714344	-4.2345333	-4.0176180
H	-3.7528497	-3.7493623	-4.0261461
H	-2.9416848	-5.3176864	-3.9315262
H	-2.2854475	-4.0470952	-4.9857222
C	-3.8843319	6.2175633	-0.5172084
H	-4.0786152	5.3711633	-1.1897539
H	-4.3335877	7.1132098	-0.9672786
H	-4.4135054	6.0398539	0.4276168
C	5.2179949	-1.4415334	3.1520163
H	4.8540554	-1.5116904	4.1871565
H	5.9033273	-0.5840439	3.0939967
H	5.7984935	-2.3433289	2.9334022
C	0.2394303	-3.7066008	5.5347376
H	0.7712326	-4.6680595	5.5644467
H	-0.6218647	-3.7759191	6.2144220
H	0.9151116	-2.9291464	5.9185730
C	2.1464527	4.1756765	0.0913172
H	2.3164317	4.2568300	1.1742803
H	3.0681925	4.4999352	-0.4106544
H	1.9893155	3.1173237	-0.1644660
C	-1.8824255	3.8777616	4.4032176
H	-0.9177498	4.4023351	4.4546983
H	-2.0603406	3.3945569	5.3745993
H	-2.6719266	4.6267054	4.2495875
C	-0.8041771	1.7621299	3.5847064
H	-0.7390789	1.0100654	2.7852277
H	-1.0516755	1.2439617	4.5213555
H	0.1845334	2.2256042	3.7153494
C	3.6871283	-6.1694562	1.5436959
H	2.9996436	-6.6613745	2.2436064
H	4.5204757	-6.8655861	1.3781890
H	3.1698914	-6.0332869	0.5844210
C	-1.8277122	6.9017917	-1.6994958
H	-0.7795795	7.2154439	-1.6678516
H	-2.4106688	7.7691041	-2.0398180
H	-1.9398600	6.1167935	-2.4583175
C	-2.1927291	7.6253265	0.6802662
H	-1.1358670	7.8643127	0.8542016

H	-2.6503021	7.3854597	1.6504236
H	-2.6840555	8.5270607	0.2877888
C	2.3260574	-3.3197783	-0.3988025
C	4.0453549	-1.2240824	2.1638175
C	-0.2525085	-3.3712896	4.1013140
C	0.9811375	5.0717235	-0.3861813
C	-1.8373452	3.3154592	-1.8753008
C	-4.0375717	-1.0329082	-4.9783321
H	-3.4113114	-0.4322578	-5.6530688
H	-5.0887454	-0.7688111	-5.1666498
H	-3.9007939	-2.0878282	-5.2413667
C	-1.8769942	-3.7628828	-2.8449937
C	1.3780368	1.5320375	-4.1194537
H	0.4826068	2.0329934	-4.5124403
H	2.2497917	1.9635976	-4.6320194
H	1.4655076	1.7639889	-3.0482697
C	-1.8861599	2.8101320	3.2782355
C	-4.6580369	-1.4999456	-2.5762302
H	-4.6814474	-2.5760866	-2.7740993
H	-5.6771949	-1.1222994	-2.7423526
H	-4.4110145	-1.3448745	-1.5164094
C	1.3172615	6.5108441	0.0786785
H	0.6076073	7.2558031	-0.2967475
H	2.3145043	6.7869401	-0.2922007
H	1.3357103	6.5787203	1.1759219

Reference

[1] C. Schwarzmaier, A. Y. Timoshkin, G. Balázs, M. Scheer, *Angew. Chem. Int. Ed.* **2014**, *53*, 9077-9081.
[2] J. K. Clegg, J. Cremers, A. J. Hogben, B. Breiner, M. M. J. Smulders, J. D. Thoburn, J. R. Nitschke, *Chem. Sci.* **2013**, *4*, 68-76.
[3] M. Wallasch, G. Wolmershäuser, H. Sitzmann, *Angew. Chem. Int. Ed.* **2005**, *44*, 2597-2599.
[4] CrysAlisPro Software System, Agilent Technologies UK Ltd, Yarnton, Oxford, **2014**.
[5] O. V. Dolomanov, L. J. Bourhis, R. J. Gildea, J. A. K. Howard, H. Puschmann, *J. Appl. Crystallogr.* **2009**, *42*, 339-341.
[6] G. M. Sheldrick, *Acta Crystallographica Section A* **2015**, *71*, 3-8.
[7] G. Sheldrick, *Acta Crystallographica Section C* **2015**, *71*, 3-8.
[8] a) R. Ahlrichs, M. Bär, M. Häser, H. Horn, C. Kölmel, *Chem. Phys. Lett.* **1989**, *162*, 165-169; b) O. Treutler, R. Ahlrichs, *J. Chem. Phys.* **1995**, *102*, 346-354.
[9] a) K. Eichkorn, O. Treutler, H. Öhm, M. Häser, R. Ahlrichs, *Chem. Phys. Lett.* **1995**, *242*, 652-660; b) K. Eichkorn, F. Weigend, O. Treutler, R. Ahlrichs, *Theor. Chem. Acc.* **1997**, *97*, 119-124.
[10] a) P. A. M. Dirac, *Proc. R. Soc. London, Ser. A* **1929**, *123*, 714-733; b) J. C. Slater, *Phys. Rev.* **1951**, *81*, 385-390; c) S. H. Vosko, L. Wilk, M. Nusair, *Can. J. Phys.* **1980**, *58*, 1200-1211; d) A. D. Becke, *Phys. Rev. A* **1988**, *38*, 3098-3100; e) J. P. Perdew, *Phys. Rev. B* **1986**, *33*, 8822-8824; Erratum: J. P. Perdew *Phys. Rev.* B **1986, *34*,** 7406.
[11] A. Schäfer, C. Huber, R. Ahlrichs, *J. Chem. Phys.* **1994**, *100*, 5829-5835.
[12] M. Sierka, A. Hogekamp, R. Ahlrichs, *J. Chem. Phys.* **2003**, *118*, 9136-9148.
[13] a) ORCA - An ab initio, DFT and semiempirical SCF-MO package. Version 3.0.; b) F. Neese, *WIREs Comput. Mol. Sci.* **2012**, *2*, 73-78.
[14] a) A. D. Becke, *J. Chem. Phys.* **1993**, *98*, 5648-5652; b) C. Lee, W. Yang, R. G. Parr, *Phys. Rev. B* **1988**, *37*, 785-789.
[15] F. Neese, *Inorg. Chim. Acta* **2002**, *337*, 181-192.
[16] M. Römelt, S. Ye, F. Neese, *Inorg. Chem.* **2009**, *48*, 784-785.

Preface

The following chapter has already been published: The article is reprinted with permission of Wiley-VCH. License Number: 5024271423292.

English version: 'Coordination Behavior of a P_4 -Butterfly Complex towards Transition Metal Lewis Acids: Preservation versus Rearrangement'

Chem. Eur. J. ***2021****, 27, 3675.*

Authors

Julian Müller, Manfred Scheer.

Author contribution

J. Müller prepared the manuscript and performed the synthesis and characterization of the herein presented compounds. M. Scheer supervised the research and revised the manuscript.

Acknowledgements

This work was supported by the Deutsche Forschungsgemeinschaft (DFG, Sche 384/38-1). We thank Martin Weber for the measurement and evaluation of the cyclic voltammograms. Open access funding enabled and organized by Projekt DEAL.

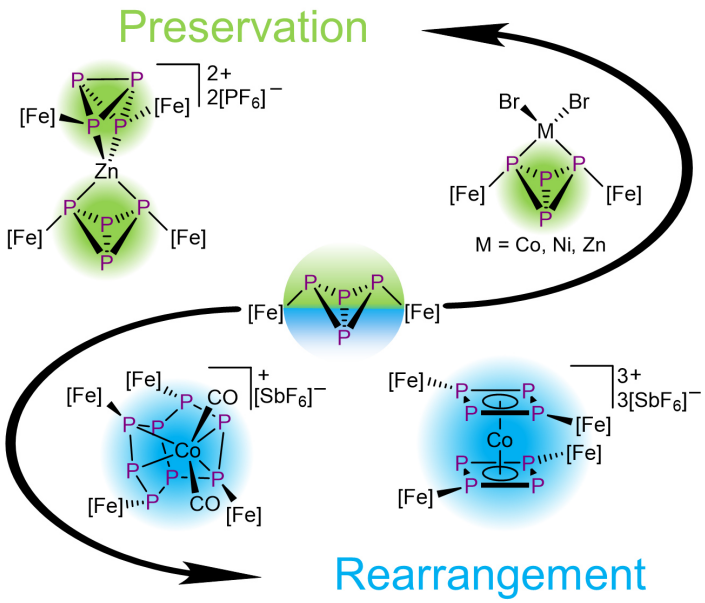
Preservation
2+
2[PF6]−
[Fe]
[Fe]
Zn
[Fe]
[Fe]
Br
Br
M
[Fe]
[Fe]
M = Co, Ni, Zn
[Fe]
[Fe]
[Fe]
CO
+
[SbF6]−
Co
[Fe]
CO
[Fe]
[Fe]
3+
3[SbF6]−
Co
[Fe]
[Fe]
Rearrangement

4. Coordination Behavior of a P_4-Butterfly Complex towards Transition Metal Lewis Acids: Preservation versus Rearrangement

Abstract: *The reactivity of the P_4 butterfly complex [{Cp'''Fe(CO)$_2$}$_2$(μ,η$^{1:1}$-P_4)] (**1**, Cp''' = η^5-$C_5H_2{}^tBu_3$) towards divalent Co, Ni and Zn salts is investigated. The reaction with the bromide salts leads to [{Cp'''Fe(CO)$_2$}$_2$(μ$_3$,η$^{2:1:1}$-P_4){MBr_2}] (M = Co (**2Co**), Ni (**2Ni**), Zn (**2Zn**)) in which the P_4 butterfly scaffold is preserved. The use of the weakly ligated Co complex [Co(NCCH$_3$)$_6$][SbF_6]$_2$, results in the formation of [{(Cp'''Fe(CO)$_2$)$_2$(μ$_3$,η$^{4:1:1}$-P_4)}$_2$Co][SbF_6]$_3$ (**3**), which represents the second example of a homoleptic-like octaphospha-metalla-sandwich complex. The formation of the threefold positively charged complex **3** occurs via redox processes, which among others also enables the formation of [{Cp'''Fe(CO)$_2$}$_4$(μ$_5$,η$^{4:1:1:1:1}$-P_8){Co(CO)$_2$}][SbF_6] (**4**), bearing a rare octaphosphabicyclo[3.3.0]octane unit as a ligand. On the other hand, the reaction with [Zn(NCCH$_3$)$_4$][PF_6]$_2$ yields the spiro complex [{(Cp'''Fe(CO)$_2$)$_2$(μ$_3$,η$^{2:1:1}$-P_4)}$_2$Zn][PF_6]$_2$ (**5**) under preservation of the initial structural motif.*

4.1. Introduction

Oligophosphorus compounds are a versatilely useable class of compounds and are therefore in the focus of current research. As they typically exhibit several sterically accessible lone pairs, these compounds show a manifold coordination chemistry.[1–3] Some of the most prominent representatives are the bis(diphenyl) phosphines of the type $Ph_2P(CH_2)_nPPh_2$ (dppm, n = 1; dppe, n = 2; dppp, n = 3) that can act as monodentate,[4] chelating bidentate[5–9] or non-chelating bidentate[6,9] ligands. Due to their preference to form chelate complexes with small bite angles, these ligands are especially useful in homogeneous catalysis.[2,3,10] Compounds with a higher phosphorus content show an even more diverse coordination chemistry. For example, the monoanionic P_3 chain [$^tBu_2$P-P-P$^tBu_2$]$^-$ is able to coordinate up to two [Cr(CO)$_4$] fragments in an η$^{2:1}$ fashion,[11] while linear tetraphosphides can undergo a [4+1] cycloaddition to give five membered metalla-cycles.[12] Furthermore, cyclic systems of tetraphosphines[13] and pentaphosphines[14] can also act as bidentate ligands. Here, regardless of the ring size, the oligophosphines always stabilize the metal center in a 1,3-coordination mode. However, the highest diversity of coordination modes is found for phosphorus ligands that do not bear any organic substituents.[1] These so called P_n ligands are usually obtained by reactions of white phosphorus (P_4) with either main group or transition metal moieties.[15] One of the first steps in the activation of the tetrahedral P_4 molecule is the formation of a tetraphosphabicyclo[1.1.0]butane unit[16,17] which can be stabilized by forming either mononuclear[16,18] or binuclear[19,20,21,22] P_4 butterfly complexes.

Our group could show that the P_4 butterfly complex [{Cp'''Fe(CO)$_2$}$_2$(μ,η$^{1:1}$-P_4)] (**1**, Cp''' = η^5-$C_5H_2{}^tBu_3$) also fulfils the requirements of a bidentate ligand (Figure 4.1, top left), which mimics the dppm ligand.[23,24] In **1**, the central P_4 butterfly unit coordinates the Lewis acids via its two “wing-tip” phosphorus atoms. This results in complexes that can best be

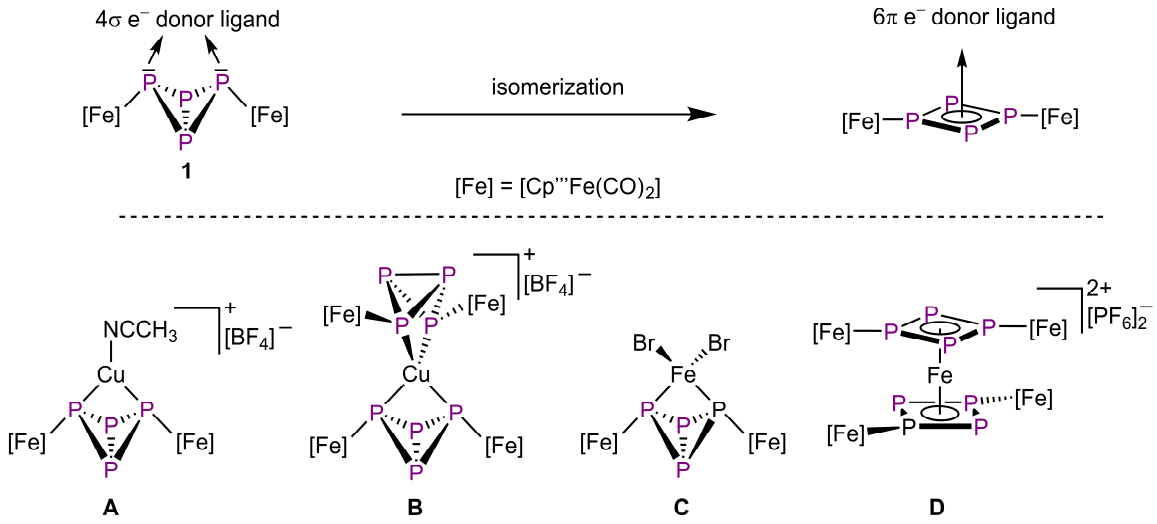

Figure 4.1. Top: Schematic illustration of the isomerization of [{Cp'''Fe(CO)$_2$}$_2$(μ,η$^{1:1}$-P$_4$)] (**1**). Bottom: Examples of coordination compounds **A** – **D** synthesized from **1**.

compared with the corresponding dppm complexes since they exhibit a very similar geometry, steric bulk and bite angle. However, in contrast to dppm, we could also show that **1** is electronically very flexible. On the one hand, **1** can act as a 4σ-electron donor. This is demonstrated in the case of [Cu(NCCH$_3$)$_4$][BF$_4$], where the monoadduct [{Cp'''Fe(CO)$_2$}$_2$(μ$_3$,η$^{2:1:1}$-P$_4$){Cu(NCCH$_3$)}][BF$_4$] (**A**) as well as the spiro compound [{{Cp'''Fe(CO)$_2$}$_2$(μ$_3$,η$^{2:1:1}$-P$_4$)}$_2$Cu][BF$_4$] (**B**) can be obtained, depending on the stoichiometry (Figure 4.1).[23] On the other hand, reactivity studies with Fe^{II} salts have shown that the reaction outcome is strongly dependent on the nature of the ligands since the ligands influence the electron affinity of the metal center. Therefore, the reaction with [FeBr$_2$·dme] (dme = dimethoxyethane) yields the neutral coordination compound [{Cp'''Fe(CO)$_2$}$_2$(μ$_3$,η$^{2:1:1}$-P$_4$){FeBr$_2$}] (**C**).[24] However, performing the same reaction in the presence of an Fe^{II} salt with more labile acetonitrile ligands, an isomerization of the butterfly unit to an aromatic *cyclo*-P$_4$[Fe]$_2$ entity ([Fe] = [Cp'''Fe(CO)$_2$]) is observed, which now acts as a 6π-electron donor (Figure 4.1, top right). This leads to the formation of the first octaphosphorus-iron-sandwich complex [{(Cp'''Fe(CO)$_2$)$_2$(μ$_3$,η$^{4:1:1}$-P$_4$)}$_2$Fe][PF$_6$]$_2$ (**D**). The conditions of the isomerization of **1** are still not fully understood. However, the results with Fe^{II} have shown, that the reactivity is strongly dependent on the nature of the ligands of the Lewis acid. To investigate this phenomenon further and to rationalize under what conditions what kind of coordination behavior is to be expected, we investigated the reaction of the butterfly complex **1** with various divalent transition metal compounds.

Herein, we report on detailed studies of the coordination behavior of the butterfly complex **1** towards 3d transition metal-based Lewis acids. A preservation of the P$_4$ butterfly framework is observed in most of the reactions. However, it could also be shown that **1** has a high tendency to rearrange in the presence of weakly ligated d^6 metals, which yields

complexes that contain *cyclo*-$P_4[Fe]_2$ units ([Fe] = Cp'''Fe(CO)$_2$) or the rare octaphosphabicyclo[3.3.0]octane unit as ligands.

4.2. Result and Discussion

The reactions of **1** with 1.1 equivalents of the divalent bromide salts $CoBr_2$, [$NiBr_2$·dme] or $ZnBr_2$ lead to the formation of [{Cp'''Fe(CO)$_2$}$_2$(μ_3,$\eta^{2:1:1}$-P_4){MBr_2}] (M=Co (**2Co**), Ni (**2Ni**), Zn (**2Zn**)), respectively, which can be isolated in moderate crystalline yields (Scheme 4.1).

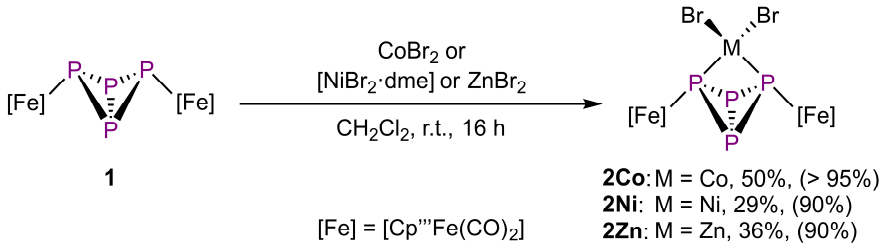

Scheme 4.1. Syntheses of the coordination compounds with divalent bromide salts starting from **1**. The displayed yields correspond to the isolated crystalline yield referred to **1**. The number in brackets gives the yield according to the ^{31}P NMR spectroscopy of the reaction mixtures.

The molecular structures of **2Co**, **2Ni** and **2Zn** (Figure 4.2, Figure S4.2 and Figure S4.3) reveal that the P_4 butterfly unit is still intact and coordinates the Lewis acidic metal atom always via the two "wing-tip" phosphorus atoms. The metal centers are coordinated in a distorted tetrahedral fashion, which is indicated by the twist angles of the P1-M1-P2 plane to the Br1-M1-Br2 plane of 86.15(1)° (**2Co**), 84.39(4)° (**2Ni**) and 85.92(2)° (**2Zn**), respectively. The trend in the covalence radii[25] of Fe (r_{Fe} = 1.16 Å), Co (r_{Co} = 1.11 Å), Ni (r_{Ni} = 1.10 Å) and Zn (r_{Zn} = 1.18 Å) is nicely reflected in the metal phosphorus bond lengths of **C** (2.4364(7)/2.4823(8) Å),[24] **2Co** (2.3614(11)/2.3959(11) Å), **2Ni** (2.3389(15)/-2.3607(14) Å), **2Zn** (2.4479(6)/2.5002(6) Å). However, the P–Ni bond lengths of **2Ni** are longer compared to the ones in the square planar complex [(dppm)$NiBr_2$] (2.143(2) Å and 2.152(2) Å).[8] The deviation of the geometry of the nickel center (d^8 configuration) from the preferred square planar geometry ([(dppm)$NiBr_2$]) to a distorted tetrahedral geometry (**2Ni**) must be caused by the steric bulk of **1** that does not allow a square planar geometry at the nickel atom. With 70.102(18)° the bite angle of the P_4 butterfly unit in **2Zn** is almost

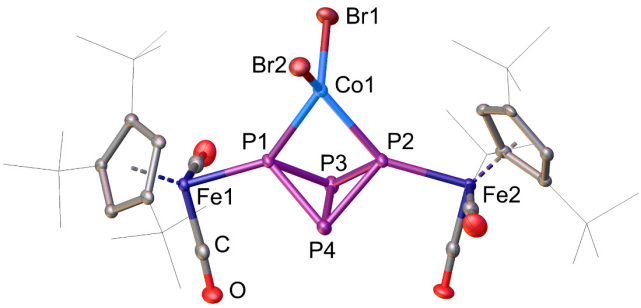

Figure 4.2. Molecular structure of **2Co** in the solid state exemplifying the structural core of **2Ni** and **2Zn** as well (cf. Figure S4.2 and Figure S4.3). Hydrogen atoms and CH_2Cl_2 molecules are omitted for clarity. Atomic displacement parameters (ADPs) are shown at 50% probability level.

identical with the corresponding angle in **C** (70.27(3)°).[24] The cobalt and nickel analogues exhibit a slightly larger bite angle of 73.55(4)° (**2Co**) and 72.08(5)° (**2Ni**). However, the bite angle in **2Ni** is smaller compared to the one in [(dppm)$NiBr_2$] (75.62(8)°).[8] In all three compounds the P–P bond lengths are in the range of a common P–P single bond as it was observed for **C**.[24]

The ^{1}H NMR spectra (CD_2Cl_2) of **2Co**, **2Ni** and **2Zn** each show three signals for the two magnetically equivalent Cp''' ligands. The ^{1}H NMR spectrum of **2Zn** reveals two broad singlets at δ = 1.42 ppm and d = 1.37 ppm with an integral ratio of 18:9 which can be assigned to the three ^{t}Bu groups. The broad signal with an integral of 2 at δ = 5.11 ppm can be assigned to the two aryl H atoms of the Cp''' ligands. Since compound **2Co** and **2Ni** are paramagnetic, the signals in the ^{1}H NMR spectra are strongly shifted. The ^{1}H NMR spectrum of **2Co** exhibits three broad signals at δ = −3.7, −5.8 and −26.1 ppm with an integral ratio of 18:9:2. In the case of **2Ni**, the signals with an integral ratio of 9:18:2 are shifted to δ = 3.9, 3.3 and −15.8 ppm, respectively.

The ^{31}P{^{1}H} NMR spectrum of **2Zn** in CD_2Cl_2 reveals two sharp triplets of an A_2X_2 spin system at δ = −43.1 ppm and δ = −309.6 ppm ($^1J_{PP}$ = 198 Hz). In comparison to the chemical shifts of **2Zn**, the signals of **1** (δ = −81.4 ppm and δ = −325.0 ppm)[19,22] and **A** (δ = −73.2 ppm and δ = −313.7 ppm)[23] are shifted to lower ppm values.

The ^{31}P{^{1}H} NMR spectrum (CD_2Cl_2) of the reaction solution of **2Zn** reveals an additional set of signals at δ = 137.3, 69.3 and 16.0 ppm corresponding to a byproduct (coupling constants are summarized in Table S4.4).[24,26] The integral ratio of main product to side product is 10:1. Despite several attempts, the exact structure of this byproduct could not be clarified yet, but according to the chemical shift as well as the coupling pattern, the presence of a *cyclo*-P_4 unit is very likely. The formation of this byproduct may be attributed to a partial fragmentation of **1** as this can generate metal species that can be coordinated by **1**. The formation of *cyclo*-P_4 containing complexes, induced by a partial fragmentation of **1**, has already been observed.[24]

The ^{31}P{^{1}H} NMR spectrum of **2Ni** in CD_2Cl_2 shows only one very broad signal at δ = −267.3 ppm ($\omega_{½}$ = 575 Hz) while **2Co** is ^{31}P NMR silent. During the synthesis of **2Ni** a diamagnetic byproduct is formed which can be observed in the ^{31}P{^{1}H} NMR spectrum (CD_2Cl_2) of the reaction solution in form of an AA'XX' spin system at δ = 97.4 ppm and 198.8 ppm. The corresponding coupling constants are summarized in Table S4.3. The chemical shifts and coupling pattern point towards the presence of a cyclic P_4 unit instead of a P_4-butterfly core. Regardless of numerous attempts, the nature of the byproduct could not be unambiguously clarified so far.

Although **2Co** and **2Ni** are paramagnetic, they are EPR silent, indicating the presence of high spin d^7 and d^8 configurations, respectively. The same behavior was observed for

complex **C** where a high spin d^6 configuration could be verified for the central iron atom.[24] According to the applied Evans method[27] compound **2Co** possesses an effective magnetic moment of μ_{eff} = 4.8 μ_B. Although the value is higher than 3.9 μ_B, which is expected for three unpaired electrons, it is in good agreement with experimentally found values of tetrahedrally coordinated Co^{II} complexes (μ_{eff} = 4.3 – 4.7 μ_B).[28] Complex **2Ni** exhibits an effective magnetic moment of μ_{eff} = 2.7 μ_B that fits to two unpaired electrons. However, this value is smaller compared to other tetrahedrally coordinated Ni^{II} compounds that have magnetic moments within the range of μ_{eff} = 3.3 – 4.0 μ_B.[29] On the other hand, complexes of $[NiX_2L]$ (X = Cl, Br, I; L = bis-diphosphines) are mainly described to be diamagnetic caused by the square planar geometry.[7,8,30]

The unexpected formation of the sandwich complex **D** in the reaction of **1** with $[Fe(NCCH_3)_6][PF_6]_2$,[24] inspired us to investigate the reaction of **1** with M^{II} compounds containing labile ligands. Therefore, we reacted two equivalents of **1** with 1.05 equivalents of $[M(NCCH_3)_n][X]_2$ (M = Co, n = 6, X = PF_6, SbF_6, Scheme 4.2; M = Ni, n = 6, X = PF_6, SbF_6, Scheme 4.3; M = Zn, n = 4, X = PF_6, Scheme 4.4). Based on ^{31}P NMR spectroscopic investigations, the reaction of **1** with $[Co(NCCH_3)_6][X]_2$ (X = PF_6, SbF_6) leads to the formation of a variety of products (Scheme 4.2). The use of the salt with the better soluble hexafluorophosphate anion only allowed the characterization of the already known compounds $[\{Cp'''Fe(CO)_2\}_2(\mu_3,\eta^{4:1:1}\text{-}P_4)(Cp'''Fe)][PF_6]$[24] (**E**) and $[Cp'''Fe(CO)_3][PF_6]$ (**F**) by single crystal X-ray structure analysis, ^{31}P NMR spectroscopy and mass spectrometry (see supporting information). However, switching to the less soluble hexafluoroantimonate anion additionally allows the isolation of $[\{(Cp'''Fe(CO)_2)_2(\mu_3,\eta^{4:1:1}\text{-}P_4)\}_2Co][SbF_6]_3$ (**3**) (3%) and few crystals of $[\{Cp'''Fe(CO)_2\}_4(\mu_5,\eta^{4:1:1:1:1}\text{-}P_8)\{Co(CO)_2\}][SbF_6]$ (**4**). The central P_8 unit of **4** is a rare example of an octaphosphabicyclo[3.3.0]octane unit which must have been formed by a dimerization of **1** in the presence of a $[Co(CO)_2]^{3+}$ unit. Complex **3** however, contains two *cyclo*-$P_4[Fe]_2$ units that coordinate the central cobalt atom in an η^4

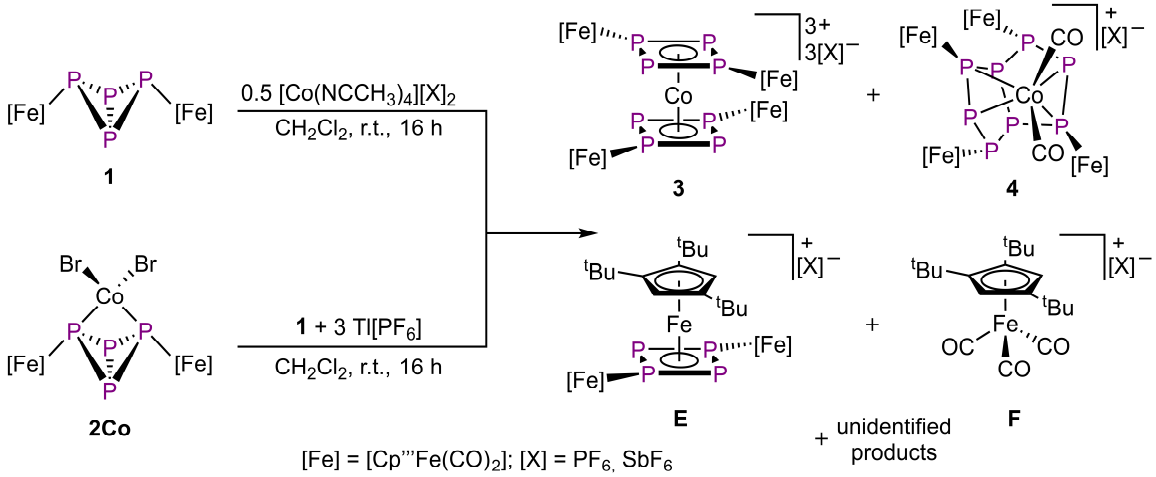

Scheme 4.2. Coordination complexes derived from **1** in the presence of labile ligated cobalt centers.

coordination mode each. Therefore, **3** represents the second example of a homoleptic-like octaphospha-metalla-sandwich complex.[24] The threefold positive charge of **3** indicates that the central cobalt atom must be in the oxidation state of +III. Hence, **3** is isoelectronic to **D**,[24] which shows that the isomerization has a high tendency to occur in the presence of weakly ligated d^6 metals. The charge of the complex also reveals that redox processes are involved in the formation of **3**. Surprisingly, the cyclic voltammogram of $[Co(NCCH_3)_6][PF_6]_2$ in CH_2Cl_2 reveals that the Co^{2+} ion can only be reduced electrochemically, but not oxidized (Figure S4.33). On the other hand, **1** can be both oxidized and reduced electrochemically but both processes are irreversible (Figure S4.34). Therefore, the Co^{3+} ion is most likely produced chemically by a reduction of **1** during the reaction. However, the use of an excess of **1** as well as the addition of $[Cp_2Fe][PF_6]$ as an electron acceptor did not enhance the formation of **3** significantly. The driving force for this oxidation is most likely the isomerization of the butterfly units to the aromatic *cyclo*-$P_4[Fe]_2$ units (see Figure 4.1, top), since DFT calculations showed that the analogue reaction of $[Fe(NCCH_3)_6]^{2+}$ and **1** is exothermic by −118.76 kJ/mol.[24] The redox processes must also induce a degradation of **1**, since all characterized side products indicate a partial decomposition of **1**. The tendency of butterfly complexes to decompose and rearrange in the presence of reactive species or under harsh reaction conditions has already been discussed in the literature.[19,20,24] Despite intensive efforts it was not possible to identify other products of this reaction that would allow a better insight into the reaction pathway. This is mainly hindered by the very similar solubility of all the products since all are charged and bear the well soluble Cp''' ligand.

The single-crystal X-ray structure analysis of **3** reveals that the P_4 butterfly units have isomerized into *cyclo*-P_4 units that coordinate as 6 π-electron donors to the central Co

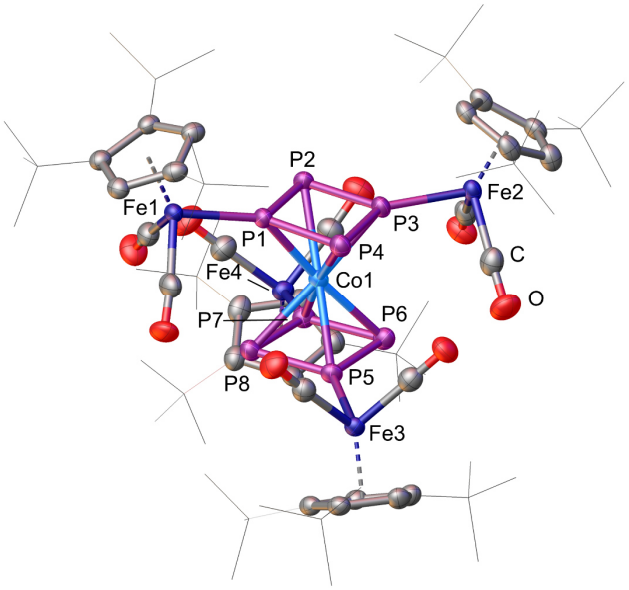

Figure 4.3. Cationic part of the molecular structures of **3**. The three SbF_6^- anions, hydrogen atoms and solvent molecules are omitted for clarity. ADPs are shown at 50% probability level.

atom (Figure 4.3). The P–P bond lengths vary from 2.135(2) to 2.154(2) Å and are between a P–P single (≈2.22 Å)[25] and a P=P double bond (≈2.04 Å).[31] Compared to other *cyclo*-P_4^{2-}containing compounds, the P–P bond lengths of **3** are in good agreement.[24,32,33] The geometry of the *cyclo*-P_4 units is with P-P-P angles from 83.17(8) to 96.62(8)° slightly distorted compared to the square P_4^{2-} anion of $[Cs_2P_4{\cdot}2NH_3]$ (89.76(4) and 90.24(4)°).[33] The deformation is most likely induced by the two sterically demanding [Fe] fragments that stabilize each *cyclo*-P_4 unit. However, compared to the analogue iron complex **D**,[24] the P-P-P angles of **3** are slightly closer to the ideal value of 90°. The planar P_4 rings in **3** (sums of the P-P-P angles are 359.95 and 359.96°) are almost parallel with an $P_{4,cent.}$-Co-$P_{4,cent.}$ angle of 178.00(7)°. The two *cyclo*-P_4 units are in an eclipsed conformation while **D** shows an intermediate state between the staggered and the eclipsed conformation.[24] However, DFT calculations have predicted that the hypothetical $[(P_4)_2Co^{III}]^-$ anion containing square *cyclo*-P_4 ligands has a staggered conformation (D_{4d} symmetry).[34] The Fe–P distances vary from 2.1972(17) to 2.2055(17) Å and are shorter than the corresponding distances in **D** (2.2255(9) to 2.2317(9) Å)[24] and **1** (2.348(2) and 2.3552(19) Å).[19]

The ^{1}H NMR spectrum (CD_3CN) of **3** shows three broad signals for the magnetically equivalent Cp''' ligands at δ = 6.01, 1.44 and 1.39 ppm with an integral ratio of 2:9:18. The $^{31}P\{^1H\}$ NMR spectrum (CD_3CN) of **3** reveals an AA'XX' spin system at δ = 196.8 and 144.1 ppm (coupling constants are summarized in Table S4.5). Compared to the iron containing complex **D** (δ = 114.3 and 91.7 ppm in CD_2Cl_2)[24] the signals of **3** are strongly shifted downfield.

The molecular structure of **4** reveals the formation of a mono-cationic complex that contains an octaphospha-bicyclo[3.3.0]octane cage (Figure 4.4), which can be derived

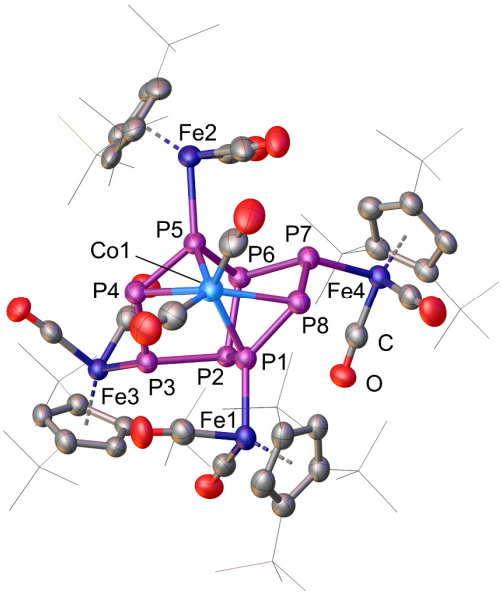

Figure 4.4. Cationic part of the molecular structures of **4**. The SbF_6^- anion and hydrogen atoms are omitted for clarity. ADPs are shown at 50% probability level.

from the realgar structure type with a $[Co(CO)_2]^{3+}$ fragment inserted into the P4–P8 bond. The P_8 unit can also be described as two fused P_5 rings that are twisted due to the coordination of the $[Co(CO)_2]^{3+}$ fragment. The only comparable complex with a yet more symmetrical P_8 unit is $[K(dme)]_2[(Cp'''Co)_2(\mu,\eta^{3:3}\text{-}P_8)]$.[35] However, the dicobalt complex consists of two allylic subunits (P–P bond length of 2.1519(6)–2.1580(6) Å) that are connected via P–P single bonds (2.1947(6)–2.2247(6) Å),[35] while the P–P bond lengths in **4** vary from 2.1928(17) Å to 2.2308(18) Å. The only exceptions are the P1–P8 (2.116(2) Å) and P4–P5 (2.111(2) Å) bonds that are shorter due to the side-on coordination of the cobalt atom. The four Co–P bond lengths in **4** are not equal. The distances to the phosphorus atoms that are also coordinated by an iron fragment are shorter (Co1–P1 (2.2553(1) Å), Co1–P5 (2.2551(17) Å) compared to the substituent free P atoms P4 (2.4058(18) Å) and P8 (2.4098(17) Å). The Fe–P distances vary from 2.2996(15) Å to 2.3115(15) Å and are slightly shortened compared to the ones in **1**.[19]

The question whether the central $[M(CO)_2]$ fragment in **4** contains an iron or a cobalt atom cannot be unambiguously clarified by single crystal structure analysis. Therefore, a solution of **4** was investigated by ESI mass spectrometry, where the presence of cobalt was confirmed by the detection of the molecular ion peak at m/z = 1743.4. The $^{31}P\{^1H\}$ NMR spectrum of **4** in thf-d_8 shows an AA'MM'OO'XX' spin system at δ = 303.9, 234.2, −151.4 and −272.9 ppm (coupling constants are summarized in Table S4.6). Due to the diamagnetic nature of **4**, it can be concluded that **4** also contains cobalt in the oxidation state +III, which means that the ligand constitutes a P_8^{6-} unit.

Since the reaction of **1** with $[Co(NCCH_3)_6][X]_2$ (X = PF_6, SbF_6) leads to the formation of several side products, we investigated if the selectivity is increased when starting the reaction with compound **2Co** (Scheme 4.2). Therefore, **2Co** was treated with **1** and an excess (3 equivalents) of Tl[PF_6] in order to eliminate the two bromido ligands by the formation of TlBr. This should lead to vacancies in the coordination sphere of the Co^{II} center while it is still bound to **1**. However, the $^{31}P\{^1H\}$ NMR spectrum of the reaction mixture indicates that this alternative reaction pathway does not lead to an increased selectivity, since the obtained NMR spectrum is comparable to the one of the reaction of **1** with $[Co(NCCH_3)_6][X]_2$.

The reaction of **1** with $[Ni(NCCH_3)_6][X]_2$ (X = PF_6, SbF_6) leads also to the formation of several products (Scheme 4.3; $^{31}P\{^1H\}$ NMR of the reaction mixture is depicted in Figure S4.27). Despite several attempts, only the nickel-free fragmentation products **E** and **F** could be isolated and characterized, which were also observed in the analogue reaction with $[Co(NCCH_3)_6][X]_2$. The appearance of these degradation products indicates that **1** partially decomposes during the reaction with $[Ni(NCCH_3)_6][X]_2$ which might also be induced by redox processes.

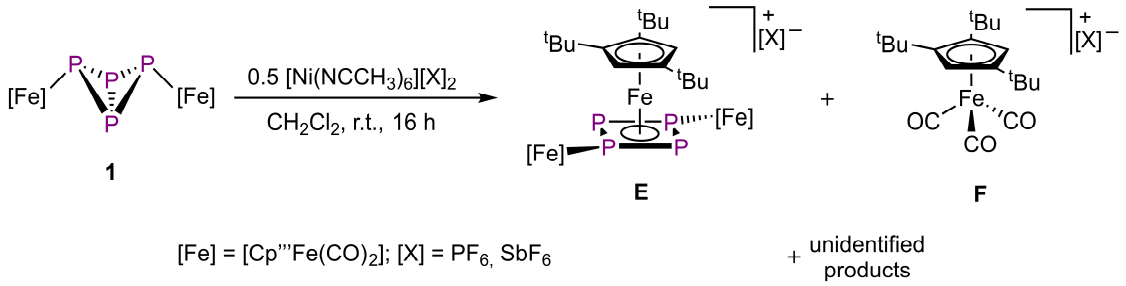

Scheme 4.3. Coordination complexes derived from **1** in the presence of $[Ni(NCCH_3)_6][X]_2$ (X = PF_6, SbF_6).

In contrast, stirring **1** with $[Zn(NCCH_3)_4][PF_6]_2$ leads to the quantitative formation of $[\{(Cp'''Fe(CO)_2)_2(\mu_3,\eta^{2:1:1}\text{-}P_4)\}_2Zn][PF_6]_2$ (**5**; Scheme 4.4; 68%, >95% according to ^{31}P NMR spectroscopy). The spiro complex **5** bears two still intact P_4 butterfly units that coordinate the central zinc atom. The preservation of the P_4 butterfly scaffold can be explained by the electronic properties of Zn^{II} that has a d^{10} configuration. Therefore, the isomerization to *cyclo*-P_4 units (6π-electron donors) is not expected, but the preservation of the P_4 butterfly scaffold (4σ-electron donor) enables the formation of a stable 18 valence electron complex. The existence of such spiro complexes was already observed for **B**.[23]

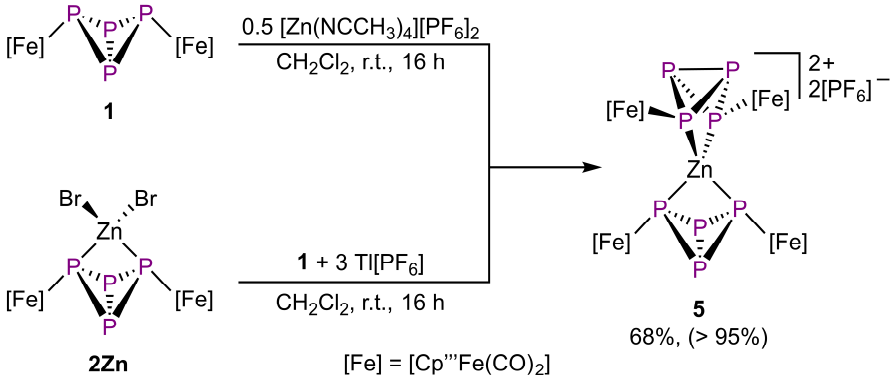

Scheme 4.4. Coordination complexes derived from **1** in the presence of the labile ligated Lewis acid of zinc. The displayed yields correspond to the isolated crystalline yield referred to **1**. The number in brackets gives the yield according to the ^{31}P NMR spectroscopy of the reaction mixtures.

The molecular structure of **5** reveals that the central Zn^{2+} cation is coordinated by two butterfly units (Figure 4.5). The distorted tetrahedral geometry at Zn1 is indicated by a twist angle of the Zn1-P1-P2 plane to the Zn1-P1'-P2' plane of 75.5814(5)°. This twist angle is slightly larger than the one in **B** (74.882(2)°)[23] but much smaller than the one in $[Zn\{\eta^2\text{-}((P(^iPr)_2)_2N\}_2]$ (87.53(5)°).[36] The Zn–P bond lengths of 2.4471(11) and 2.4536(11) Å are in good agreement with the ones of complex **2Zn** (2.4479(6), 2.5002(6) Å). The bite angle of 73.34(3)° is approx. 3° larger compared to **2Zn** which can be explained by the steric repulsion of the four [Fe] fragments. With 2.2102(15)–2.2252(15) Å the distances between the "wing-tip" and the "bridge-head" P atoms are in the region of P–P single bonds, while the P3–P4 bond (2.1803(16) Å) has a slight double bond character. Compared to **1**,[19] the P–P bond lengths are slightly elongated which indicates a widening of the P_4 butterfly scaffold during coordination of the Zn^{2+} cation. At the same time, the Fe–P distances

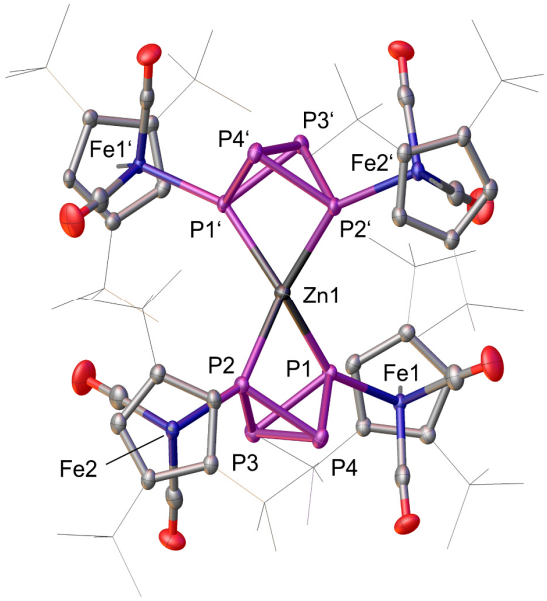

Figure 4.5. Cationic part of the molecular structures of **5**. The two PF_6^- anions, hydrogen atoms and solvent molecules are omitted for clarity. ADPs are shown at 50% probability level.

(2.2806(12), 2.2832(12) Å) are slightly shortened compared to the free ligand complex **1** (2.348(2), 2.3552(19) Å).[19]

The ^{1}H NMR spectrum (CD_2Cl_2) of **5** shows the characteristic signals for the magnetically equivalent Cp''' ligands at δ = 5.00, 1.45 and 1.42 ppm. The $^{31}P\{^1H\}$ NMR spectrum (CD_2Cl_2) of **5** reveals an AA'A''A'''XX'X''X''' spin system at δ = −13.2 and −295.3 ppm (coupling constants are summarized in Table S4.8) for the cation and a septet at δ = −143.8 ppm for the two PF_6^- anions.

Moreover, we were also interested in whether **5** can also be formed starting from **2Zn**. Therefore, **2Zn** is treated with the halogen abstractor Tl[PF_6] in the presence of **1**. The quantitative formation of **5** was confirmed by ^{31}P NMR spectroscopy.

4.3. Conclusion

We have reported on the versatile coordination behavior of the butterfly complex **1**. On the one hand, **1** acts as a bidentate ligand for divalent bromide salts to give complexes **2Co**, **2Ni**, and **2Zn**. In these compounds the P_4 butterfly unit coordinates the Lewis acids via the two “wing-tip” phosphorus atoms. Thereby, the exhibited bite angles are comparable to analogue dppm complexes. On the other hand, however, the formation of two unidentified side products, which exhibit an altered P_4 scaffold and occur during the synthesis of **2Ni** and **2Zn**, indicates that complex **1** is electronically highly flexible. This behavior is especially emphasized in the reaction with [$Co(NCCH_3)_6$][SbF_6]$_2$, which leads to **3** as the second example of a homoleptic octaphospha-metal-sandwich complex. Here, the P_4 ligands act as 6π-electron donors, which is enabled by isomerization to aromatic *cyclo*-P_4

ligands. However, surprisingly the starting material $[Co(NCCH_3)_6][SbF_6]_2$ gets at least partly oxidized from Co^{II} to Co^{III} which also leads to an unselective degradation of **1** and the formation of several byproducts, like the monocationic compound **4**, a product of a dimerization of **1** in the presence of a $[Co(CO)_2]^{3+}$ fragment. Complex **4** contains a P_8 unit which represents a rare all-phosphorus derivative of bicyclo[3.3.0]octane. The reaction of **1** and $[Zn(NCCH_3)_4][PF_6]_2$ leads to the formation of the spiro complex **5** that still bears intact P_4 butterfly units. However, this outcome highlights that the isomerization is not dependent on the nature of the ligand only, but also strongly related with electronic properties of the metal. Therefore, this study clearly shows that the rearrangement of **1** is feasible in the presence of weakly ligated d^6 metals only.

4.4. Reference

[1] K. H. Whitmire, *Coord. Chem. Rev.* **2018**, *376*, 114.
[2] J. A. Gillespie, D. L. Dodds, P. C. J. Kamer, *Dalton Trans.* **2010**, *39*, 2751.
[3] S. M. Mansell, *Dalton Trans.* **2017**, *46*, 15157.
[4] a) L.-S. Luh, U. B. Eke, L.-K. Liu, *Organometallics* **1995**, *14*, 440; b) Y. B. Malysheva, D. V. Moiseev, A. V. Gushchin, V. A. Dodonov, *Russ. J. Gen. Chem.* **2005**, *75*, 1766; c) D. V. Moiseev, Y. B. Malysheva, A. S. Shavyrin, Y. A. Kurskii, A. V. Gushchin, *J. Organomet. Chem.* **2005**, *690*, 3652.
[5] B. Gabor, S. Holle, P. W. Jolly, R. Mynott, *J. Organomet. Chem.* **1994**, *466*, 201.
[6] S. M. Jing, V. Balasanthiran, V. Pagar, J. C. Gallucci, T. V. RajanBabu, *J. Am. Chem. Soc.* **2017**, *139*, 18034.
[7] M. Schultz, F. Eisenträger, C. Regius, F. Rominger, P. Hanno-Igels, P. Jakob, I. Gruber, P. Hofmann, *Organometallics* **2012**, *31*, 207.
[8] J. A. S. Bomfim, F. P. de Souza, C. A. L. Filgueiras, A. G. de Sousa, M. T. P. Gambardella, *Polyhedron* **2003**, *22*, 1567.
[9] A. M. Messinis, S. L. J. Luckham, P. P. Wells, D. Gianolio, E. K. Gibson, H. M. O'Brien, H. A. Sparkes, S. A. Davis, J. Callison, D. Elorriaga, O. Hernandez-Fajardo, R. B. Bedford, *Nat Catal* **2019**, *2*, 123.
[10] a) M.-N. Birkholz, Z. Freixa, van Leeuwen, Piet W. N. M., *Chem. Soc. Rev.* **2009**, *38*, 1099; b) van Leeuwen, Piet W. N. M., P. C. J. Kamer, J. N. H. Reek, P. Dierkes, *Chem. Rev.* **2000**, *100*, 2741; c) P. Dierkes, van Leeuwen, Piet W. N. M., *Dalton Trans.* **1999**, 1519.
[11] V. Balema, H. Goesmann, E. Matern, G. Fritz, *Z. Anorg. Allg. Chem.* **1996**, *622*, 35.
[12] a) H. Binder, B. Schuster, W. Schwarz, K. W. Klinkhammer, *Z. Anorg. Allg. Chem.* **1999**, *625*, 699; b) D. Bongert, H.-D. Hausen, W. Schwarz, G. Heckmann, H. Binder, *Z. Anorg. Allg. Chem.* **1996**, *622*, 1167; c) S. Gómez-Ruiz, B. Gallego, E. Hey-Hawkins, *Dalton Trans.* **2009**, 2915; d) S. Gómez-Ruiz, R. Wolf, E. Hey-Hawkins, *Dalton Trans.* **2008**, 1982; e) K. Issleib, F. R. Krech, E. Lapp, *Synth. React. Inorg. Met. Org. Chem.* **1977**, *7*, 253.
[13] A. Forster, C. S. Cundy, M. Green, F. Stone, *Inorganic and Nuclear Chemistry Letters* **1966**, *2*, 233.
[14] a) M. A. Bush, V. R. Cook, P. Woodward, *Chem. Commun.* **1967**, 630; b) S. J. Geier, D. W. Stephan, *Chem. Commun.* **2008**, 2779; c) D. M. Yufanyi, T. Grell, E. Hey-Hawkins, *Eur. J. Inorg. Chem.* **2019**, *2019*, 1557.
[15] a) B. M. Cossairt, N. A. Piro, C. C. Cummins, *Chem. Rev.* **2010**, *110*, 4164; b) M. Scheer, G. Balázs, A. Seitz, *Chem. Rev.* **2010**, *110*, 4236; c) M. Caporali, L. Gonsalvi, A. Rossin, M. Peruzzini, *Chem. Rev.* **2010**, *110*, 4178.
[16] A. P. Ginsberg, W. E. Lindsell, *J. Am. Chem. Soc.* **1971**, *93*, 2082.
[17] I. Krossing, L. van Wüllen, *Chem. Eur. J.* **2002**, *8*, 700.
[18] a) S. Dürr, D. Ertler, U. Radius, *Inorg. Chem.* **2012**, *51*, 3904; b) O. J. Scherer, M. Swarowsky, H. Swarowsky, G. Wolmershäuser, *Angew. Chem. Int. Ed.* **1988**, *27*, 694.
[19] O. J. Scherer, T. Hilt, G. Wolmershäuser, *Organometallics* **1998**, *17*, 4110.
[20] O. J. Scherer, G. Schwarz, G. Wolmershäuser, *Z. Anorg. Allg. Chem.* **1996**, *622*, 951.
[21] a) S. Pelties, D. Herrmann, B. de Bruin, F. Hartl, R. Wolf, *Chem. Commun.* **2014**, *50*, 7014; b) S. Heinl, M. Scheer, *Chem. Sci.* **2014**, *5*, 3221.
[22] C. Schwarzmaier, A. Y. Timoshkin, G. Balázs, M. Scheer, *Angew. Chem. Int. Ed.* **2014**, *53*, 9077.
[23] C. Schwarzmaier, S. Heinl, G. Balázs, M. Scheer, *Angew. Chem. Int. Ed.* **2015**, *54*, 13116.
[24] J. Müller, S. Heinl, C. Schwarzmaier, G. Balázs, M. Keilwerth, K. Meyer, M. Scheer, *Angew. Chem. Int. Ed.* **2017**, *56*, 7312.
[25] P. Pyykkö, M. Atsumi, *Chem. Eur. J.* **2009**, *15*, 186.

[26] These signals were mistakenly assigned to $[\{Cp'''Fe(CO)_2\}_2(\mu_3,\eta^{2:1:1}\text{-}P_4)\{Cp'''Fe(CO)\}]^+$ in the previous work.
[27] a) D. F. Evans, *J. Chem. Soc.* **1959**, 2003; b) G. A. Bain, J. F. Berry, *J. Chem. Educ.* **2008**, *85*, 532.
[28] B. N. Figgis, R. S. Nyholm, *J. Chem. Soc.* **1954**, 12.
[29] A. B. P. Lever, *Inorg. Chem.* **1965**, *4*, 763.
[30] a) C. Ercolani, J. V. Quagliano, L. M. Vallarino, *Inorganica Chim. Acta* **1973**, *7*, 413; b) G. R. van Hecke, W. D. Horrocks, *Inorg. Chem.* **1966**, *5*, 1968.
[31] P. Pyykkö, M. Atsumi, *Chem. Eur. J.* **2009**, *15*, 12770.
[32] a) A. Cavaillé, N. Saffon‐Merceron, N. Nebra, M. Fustier‐Boutignon, N. Mézailles, *Angew. Chem. Int. Ed.* **2018**, *57*, 1874; b) U. Chakraborty, J. Leitl, B. Muhldorf, M. Bodensteiner, S. Pelties, R. Wolf, *Dalton Trans.* **2018**, *47*, 3693; c) F. Dielmann, A. Timoshkin, M. Piesch, G. Balázs, M. Scheer, *Angew. Chem. Int. Ed.* **2017**, *56*, 1671; d) M. Modl, S. Heinl, G. Balázs, F. Delgado Calvo, M. Caporali, G. Manca, M. Keilwerth, K. Meyer, M. Peruzzini, M. Scheer, *Chem. Eur. J.* **2019**, *25*, 6300; e) M. Piesch, S. Reichl, M. Seidl, G. Balázs, M. Scheer, *Angew. Chem. Int. Ed.* **2019**, *58*, 16563; f) O. J. Scherer, R. Winter, G. Wolmershäuser, *Z. Anorg. Allg. Chem.* **1993**, *619*, 827.
[33] F. Kraus, J. C. Aschenbrenner, N. Korber, *Angew. Chem. Int. Ed.* **2003**, *42*, 4030.
[34] Z. Li, C. Zhao, L. Chen, *J. Mol. Struct. THEOCHEM* **2007**, *810*, 1.
[35] M. Piesch, M. Seidl, M. Scheer, *Chem. Sci.* **2020**, *11*, 6745.
[36] D. A. Dickie, R. A. Kemp, *Organometallics* **2014**, *33*, 6511.

4.5. Supporting Information

Synthesis and Characterization

General Remarks:

All manipulations were performed with rigorous exclusion of oxygen and moisture using Schlenk-type glassware on a dual manifold Schlenk line with Argon inert gas or glove box filled with N_2 or Ar containing a high-capacity recirculator (<0.1 ppm O_2). All solvents were dried using a MB SPS-800 device of company MBRAUN, degassed and saturated with argon. Mass spectrometry was performed using a Waters Micromass LCT (ESI-MS) and a Jeol AccuTOF GCX (LIFDI-MS), respectively. Elemental analysis (CHN) was determined using a Vario micro cube. Infrared spectroscopy was performed using a Thermo Scientific Nicolet iS5. spectrometer. The X-Band EPR measurements were carried out with a MiniScope MS400 device with a frequency of 9.44 GHz and a rectangular resonator TE102 of the company Magnettech GmbH.

$CoBr_2$ (97%), Tl[PF_6] (97%) and NO[SbF_6] (97%) were purchased by abcr. NO[PF_6] (96%) was bought from Alfa Aesar. All commercially available chemicals were used without further purification. Compound [{Cp'''Fe$(CO)_2$}$_2$($\mu,\eta^{1:1}$-P_4)][1] (**1**) and [$NiBr_2$·dme][2] were synthesized according to literature known procedures.

Synthesis of [{Cp'''Fe$(CO)_2$}$_2$($\mu_3,\eta^{2:1:1}$-P_4){$CoBr_2$}] (2Co)

0.200 g of compound **1** (0.246 mmol, 1eq) and 0.059 g of $CoBr_2$ (0.270 mmol, 1.1eq) are suspended in 20 ml of CH_2Cl_2. The mixture is stirred for 16 hours at room temperature and filtered over diatomaceous earth to give a brown reddish solution. The solution is concentrated in vacuum and stored at –35 °C to give pure **2Co** as dark brown crystalline solid.

Yield: 0.131 g (0.126 mmol, 50%)

Analytical data of **2Co**:

NMR (CD_2Cl_2, 298 K)	^{1}H: δ [ppm] = –26.1 (s br, 4H, $C_5\underline{H}_2{}^t Bu_3$), −5.8 (s br, 18H, -($C_4\underline{H}_9$)), –3.7 (s br, 36H, -($C_4\underline{H}_9$)$_2$). Due to the paramagnetic character of the sample no signal in the ^{31}P NMR spectrum could be obtained in a region of +600 to −600 ppm.
Evans method	μ_{eff} [μ_B] = 4.8.
IR (CH_2Cl_2)	$\tilde{\nu}$ [cm^{-1}] = 1978 (s), 2016 (m), 2024 (vs).

Elemental analysis ($C_{38}H_{58}Br_2CoFe_2O_4P_4 \cdot (CH_2Cl_2)_{1.5}$)	Calculated: C 40.88, H 5.30 Found: C 40.73, H 5.25.
Mass spectrometry (LIFDI, toluene)	m/z: 1032.9 (100%) $[M]^+$.

Synthesis of [{Cp'''Fe(CO)$_2$}$_2$(μ_3,$\eta^{2:1:1}$-P$_4$){NiBr$_2$}] (2Ni)

In the absence of light, 0.050 g of compound **1** (0.061 mmol, 1eq) and 0.020 g of [$NiBr_2$·dme] (0.065 mmol, 1.1eq) are suspended in 5 ml of CH_2Cl_2. The mixture is stirred for 16 hours at room temperature and filtered over diatomaceous earth to give a dark red solution. The solution is concentrated in vacuo and stored at –35 °C to give **2Ni** as dark red crystalline solid. However, these crystals contain always traces of a diamagnetic side product.

Yield: 0.021 g which correspond to 0.018 g of **2Ni** (0.018 mmol, 29%)

Analytical data of **2Ni**:

NMR (CD_2Cl_2, 298 K)	^{1}H: δ [ppm] = –15.8(s br, 4H, $C_5\underline{H}_2{}^t Bu_3$), 3.3 (s br, 36H, -($C_4\underline{H}_9$)$_2$), 3.9 (s br, 18H, -($C_4\underline{H}_9$)). ^{31}P{^{1}H}: δ [ppm] = –267.3 (br, $\omega_{½}$ = 575 Hz).
Evans method	μ_{eff} [μ_B] = 2.7.
IR (CH_2Cl_2)	$\tilde{\nu}$ [cm^{-1}] = 1978 (s), 2017 (m), 2024 (vs).
Mass spectrometry (LIFDI, toluene)	m/z: 1031.9 (100%) $[M]^+$, 424.1 (35%) $[Cp'''Fe(CO)_2Br]^+$.

Analytical data of the byproduct:

NMR (CD_2Cl_2, 298 K)	^{31}P{^{1}H}: δ [ppm] = 97,4 (m, 1P), 198.8 (m, 1P). Coupling constants are summarized in Table S4.3.

Synthesis of [{Cp'''Fe(CO)$_2$}$_2$(μ_3,$\eta^{2:1:1}$-P$_4$){ZnBr$_2$}] (2Zn)

0.100 g of compound **1** (0.123 mmol, 1eq) and 0.030 g of $ZnBr_2$ (0.065 mmol, 1.1eq) are suspended in 10 ml of CH_2Cl_2. The mixture is stirred for 16 hours at room temperature to give a dark yellow solution. The solvent is evaporated. The obtained residue is taken up in 10 ml of toluene and filtered over diatomaceous earth. The solvent of the filtrate is removed in vacuo to give analytically pure powder of **2Zn**. Dark yellow crystals of **2Zn** can be obtained by storing a concentrated CH_2Cl_2 solution at –35 °C.

Yield: 0.046 g (0,044 mmol, 36%)

Analytical data of **2Zn**:

NMR (CD_2Cl_2, 298 K)	^{1}H: δ [ppm] = 1.37 (s br,18, -($C_4\underline{H}_9$)), 1.41 (s, 36H, -($C_4\underline{H}_9)_2$), 5.11 (s br, 4H, $C_5\underline{H}_2{}^t Bu_3$). $^{31}P\{^1H\}$: δ [ppm] = –309,6 (t, 2P, $P_{\text{"bridge-head"}}$, $^1J_{PP}$ = 198 Hz), –43.1 (t, 2P, $P_{\text{"wing-tip"}}$, $^1J_{PP}$ = 198 Hz). $^{13}C\{^1H\}$: δ [ppm] = 31.7 (s, -(C($\underline{C}H_3)_3$)), 31.4 (s, -(C($\underline{C}H_3)_3$)), 33.3 (s, -(C($\underline{C}H_3)_3$)), 33.9 (s, -($\underline{C}(CH_3)_3$)), 89.0 (s, $\underline{C}_2H_2C_3{}^t Bu_3$), 110.6 (s, $C_2H_2\underline{C}_3{}^t Bu_3$), 112.6 (s, $C_2H_2\underline{C}_3{}^t Bu_3$), 212.9 (br s, $\underline{C}O$)
IR (CH_2Cl_2)	$\tilde{\nu}$ [cm^{-1}] = 1976 (vs), 2014(s) 2023 (vs).
Elemental analysis ($C_{38}H_{58}Br_2ZnFe_2O_4P_4 \cdot (CH_2Cl_2)$)	Calculated: C 41.65, H 5.38 Found: C 41.68, H 5.38.
Mass spectrometry (LIFDI, toluene)	m/z: 959.1 (100%) $[M - Br]^+$, 893.0 (61%) $[M - Zn - Br]^+$, 814.2 (11%) $[M - Zn - 2Br]^+$, 758.2 (12%) $[M - Zn - 2Br – 2CO]^+$, 469.1 (97%) $[Cp'''Fe(CO)_2P_4]^+$, 424.1 (14%), $[Cp'''Fe(CO)_2Br]^+$, 345.2 (13%) $[Cp'''Fe(CO)_2]^+$.

Analytical data of the byproduct that is present in the reaction mixture:[3,4]

NMR (CD_2Cl_2, 298 K)	$^{31}P\{^1H\}$: δ [ppm] = 16,0 (m, 1P), 69.3 (m, 1P), 137.3 (m, 1P). Coupling constants are summarized in Table S4.4.

Synthesis of $[M(NCCH_3)_n][X]_2$ [M = Co, n = 6, X = PF_6, SbF_6; M = Ni, n = 6, X = PF_6, SbF_6; M = Zn, n = 4, X = PF_6]

3,762 mmol of NO[X] (2 eq) is dissolved in 20 ml of CH_3CN and added to a suspension of 1.976 mmol of metal powder (1.05 eq) in 10 ml of CH_3CN. The reaction flask is connected to an overpressure outlet and stirred for 20 h at room temperature in the case of cobalt and nickel. The reaction with zinc powder is stirred for 3 h at room temperature. The obtained suspension is reduced to half by evaporation in vacuo. To remove the remaining metal powder the mixture is filtered over diatomaceous earth to give a clear solution. Storing a concentrated solution at –35 °C gives crystalline $[M(NCCH_3)_n][X]_2$.

$[Co(NCCH_3)_6][PF_6]_2$: Yield: 0.676 g (1.137 mmol, 61%) as orange needles
$[Co(NCCH_3)_6][SbF_6]_2$: Yield: 0.828 g (1.066 mmol, 54%) as orange needles
$[Ni(NCCH_3)_6][PF_6]_2$: Yield: 0.599 g (1.007 mmol, 51%) as blue needles
$[Ni(NCCH_3)_6][SbF_6]_2$: Yield: 0.860 g (1.108 mmol, 51%) as blue needles
$[Zn(NCCH_3)_4][PF_6]_2$: Yield: 0.977 g (0.903 mmol, 48%) as colorless needles

Synthesis of $[\{(Cp'''Fe(CO)_2)_2(\mu_3,\eta^{4:1:1}\text{-}P_4)\}_2Co][SbF_6]_3$ (3) and $[\{Cp'''Fe(CO)_2\}_4(\mu_5,\eta^{4:1:1:1:1}\text{-}P_8)\{Co(CO)_2\}][SbF_6]$ (4)

Reaction pathway 1:

0.200 g of compound **1** (0.246 mmol, 2eq) and 0.095 g of $[Co(NCCH_3)_6][SbF_6]_2$ (0.123 mmol, 1.05eq) are suspended in 5 ml of CH_2Cl_2. The mixture is stirred for 16 hours at room temperature during which a fluffy orange precipitate is formed. The overlaying solution is decanted and filtered over diatomaceous earth. The orange precipitate that remains on the frit and in the reaction flask is washed two times with a small amount of CH_2Cl_2. The CH_2Cl_2 solutions are combined (The $^{31}P\{^1H\}$ NMR spectrum is depicted in Figure S4.24). The orange precipitated is taken up in CH_3CN and filtered over diatomaceous earth to give a dark orange solution (The $^{31}P\{^1H\}$ NMR spectrum is depicted in Figure S4.25). Both solutions are evaporated to dryness, taken up in 2 ml of 1,3-difluorbenzene and layered under hexane.

The layering of the formerly CH_3CN solution gives orange blocks of **3** that are covered with a black oil. The oil can be removed by washing with small amounts of CH_2Cl_2.

The layering of the formerly CH_2Cl_2 filtrate gives a dark brown oil and a very small amount of dark red needles of **4**.

Yield of **3**: 0.010 g (0,004 mmol, 3%)
Yield of **4**: < 0.005 g (< 1%)
Yield of $[Cp'''Fe(CO)_3][SbF_6]$: < 0.005 g (< 1%)
Yield of $[\{Cp'''Fe(CO)_2\}_2(\mu_3,\eta^{4:1:1}\text{-}P_4)(Cp'''Fe)][SbF_6]$: < 0.005 g (< 1%)

Reaction pathway 2:

0.050 g of **2Co** (0.048 mmol, 1eq), 0.039 g of **1** (0.048 mmol, 1eq) and 0.051 g of $TlPF_6$ (0.145 mmol, 3eq) are suspended in 10 ml of CH_2Cl_2. The mixture is stirred for 16 h at room temperature and filtered over diatomaceous earth. ^{31}P NMR spectroscopy indicates an identical reaction outcome as described in reaction pathway 1.

Analytical data of **3**:

NMR (CD_3CN, 298 K)	^1H: δ [ppm] = 1.39 (s br, 36H, -($C_4\underline{H}_9$)), 1.44 (s, 72H, -($C_4\underline{H}_9$)$_2$), 6.01 (s br, 8H, $C_5\underline{H}_2{}^t\text{Bu}_3$). $^{31}P\{^1H\}$: δ [ppm] = 144,1 (m, 4P), 196.8 (m, 4P). Coupling constants are summarized in Table S4.5.
IR (CH_2Cl_2)	$\tilde{\nu}$ [cm^{-1}] = 2008 (m), 2043(s)

Mass spectrometry (ESI, CH_3CN)	m/z: 1939.2 (< 1%) $[M + SbF_6 + OH]^+$, 1703.3 (< 1%) $[M + O]^+$, 1577.1 (< 1%) $[M - Cp'''Fe(CO)_2 + SbF_6]^+$, 1359.2 (1%) $[M - Cp'''Fe(CO)_2 + OH]^+$, 1331.2 (< 1%) $[M - Cp'''Fe(CO)_2 + OH - CO]^+$, 997.0 (7%) $[M - 2Cp'''Fe(CO)_2]^+$, 852.2 (100%) $[M + OH]^{2+}$, 671.1 (31%) $[M - Cp'''Fe(CO)_2]^{2+}$, 386.2 (90%) $[Cp'''Fe(CO)_2(NCCH_3)]^+$, 330.2 (13%) $[Cp'''Fe(NCCH_3)]^+$, 244.9 $[SbF_6]^-$.

Analytical data of **4**:

NMR (thf-d_8, 298 K)	$^{31}P\{^1H\}$: δ [ppm] = 303.9 (m, 2P), 234.2 (m, 2P), −151.4 (m, 2P), −272.9 (m, 2P).
NMR (CD_3CN, 298 K)	$^{31}P\{^1H\}$: δ [ppm] = 308.2 (m, 2P), 234.4 (m, 2P), −151.5 (m, 2P), −272.0 (m, 2P). Coupling constants are summarized in Table S4.6.
Mass spectrometry (ESI, CH_3CN)	m/z: 1743.3 (3%) $[M]^+$, 1715.3 (< 1%) $[M - CO]^+$, 1687.3 (< 1%) $[M - 2CO]^+$, 1659.3 (1%) $[M – 3CO]^+$, 1159.3 (14%) $[\{Cp'''Fe(CO)_2\}_2P_4 + Cp'''Fe(CO)_2]^+$, 1131.3 (8%) $[\{Cp'''Fe(CO)_2\}_2P_4 + Cp'''Fe(CO)]^+$, 1103.3 (9%) $[\{Cp'''Fe(CO)_2\}_2P_4 + Cp'''Fe]^+$, 852.2 (2%) $[\{(Cp'''Fe(CO)_2)_2P_4\}_2(Co) + OH]^{2+}$, 823.3 (< 1%) $[\{Cp'''Fe(CO)_2\}_2P_2 – CO - H]^+$, 386.2 (23%) $[Cp'''Fe(CO)_2(NCCH_3)]^+$, 373.1 (100%) $[Cp'''Fe(CO)_3]^+$, 330.2 (20%) $[Cp'''Fe(NCCH_3)]^+$, 244.9 $[SbF_6]^-$.

Analytical data of the side product in the CH_3CN washing solution:

NMR (CD_2Cl_2, 298 K)	$^{31}P\{^1H\}$: δ [ppm] = 171.0 (m, 2P), 97.9 (m, 1P), 87.7 (m, 2P), 77.0 (m, 2P), −51.9 (m br, 1P). Coupling constants are summarized in Table S4.7.
NMR (CD_3CN, 298 K)	$^{31}P\{^1H\}$: δ [ppm] = 165.0 (m, 2P), 99.8 (m, 1P), 87.6 (m, 2P), 78.0 (m, 2P), −53.9 (m br, 1P).

Analytical data of $[Cp'''Fe(CO)_3][SbF_6]$:

Mass spectrometry (ESI, CH_3CN)	m/z: 373.1 $[M]^+$

Reaction of 1 and $[Ni(NCCH_3)_6][X]_2$ (X = PF_6, SbF_6)

0.150 g of compound **1** (0.1842 mmol, 2eq) and 0.0967 mmol of $[Ni(NCCH_3)_6][X]_2$ (1.05 eq) are suspended in 20 ml of CH_2Cl_2 and stirred for 16 hours at room temperature. The mixture is evaporated in vacuo to half the volume and filtered over diatomaceous earth to give a brown solution. This solution is investigated by $^{31}P\{^1H\}$ NMR spectroscopy (see Figure S4.27). The rest of the solution is evaporated to dryness, taken up in 1,3-difluorbenzene and layered under pentane to give a brown oil of an unknown composition and small amounts of pale brown needles of $[Cp'''Fe(CO)_3][X]$.

Yield of $[Cp'''Fe(CO)_3][X]$: < 0.005 g (< 1%)
Yield of $[\{Cp'''Fe(CO)_2\}_2(\mu_3,\eta^{1:1:4}\text{-}P_4)(Cp'''Fe)][X]$: ≈ 1% (according to ^{31}P NMR spectroscopy)

Synthesis of $[\{(Cp'''Fe(CO)_2)_2(\mu_3,\eta^{2:1:1}\text{-}P_4)\}_2Zn][PF_6]_2$ (5)

Reaction pathway 1:

0.100 g of compound **1** (0.123 mmol, 2eq) and 0.050 g of $[Zn(NCCH_3)_4][PF_6]_2$ (0.065 mmol, 1.05eq) are suspended in 10 ml of CH_2Cl_2. The mixture is stirred for 16 hours at room temperature and filtered over diatomaceous earth to give a dark yellow solution. The solution is concentrated in vacuo and stored at –35 °C to give **5** as dark yellow crystalline solid.

Yield: 0.083 g (0,042 mmol, 68%)

Reaction pathway 2:

0.050 g of **2Zn** (0.048 mmol, 1eq), 0.039 g of **1** (0.048 mmol, 1eq) and 0.051 g of $TlPF_6$ (0.145 mmol, 3eq) are suspended in 10 ml of CH_2Cl_2. The mixture is stirred for 16 h at room temperature and filtered over diatomaceous earth. ^{31}P NMR spectroscopy indicates an identical reaction outcome as described in reaction pathway 1.

Analytical data of **5**:

NMR (CD_2Cl_2, 298 K)	^1H: δ [ppm] = 1.42 (s br, 36H, -($C_4\underline{H}_9$)), 1.45 (s, 72H, -($C_4\underline{H}_9$)$_2$), 5.00 (s br, 8H, $C_5\underline{H}_2{}^t\text{Bu}_3$). $^{31}P\{^1H\}$: δ [ppm] = –295,3 (m, 4P, $P_{\text{"bridge-head"}}$),–143.8 (sept, 2P, $\underline{P}F_6^-$), –13.2 (m, 4P, $P_{\text{"wing-tip"}}$). Coupling constants are summarized in Table S4.8.

	$^{13}C\{^1H\}$: δ [ppm] = 31.8 (s, -(C(<u>C</u>H$_3$)$_3$)), 32.6 (s, -(C(<u>C</u>H$_3$)$_3$)), 33.4 (s, -(C(<u>C</u>H$_3$)$_3$)), 33.8 (s, -(<u>C</u>(CH$_3$)$_3$)), 89.0 (s, <u>C</u>$_2$H$_2$C$_3$^{t}Bu$_3$), 111.4 (s, C$_2$H$_2$<u>C</u>$_3$^{t}Bu$_3$), 113.9 (s, C$_2$H$_2$<u>C</u>$_3$^{t}Bu$_3$), 211.8 (br s, <u>C</u>O)
IR (CH_2Cl_2)	$\tilde{\nu}$ [cm^{-1}] = 1989 (s), 2023 (vs), 2030 (s)
Elemental analysis ($C_{76}H_{116}F_{12}Fe_4O_8P_{10}Zn \cdot CH_2Cl_2$)	Calculated: C 44.70, H 5.75 Found: C 44.87, H 5.64
Mass spectrometry (ESI, CH_3CN)	m/z: 1131.3 (9%) [{Cp'''Fe(CO)$_2$}$_2$P$_4$ + Cp'''Fe(CO)]$^+$, 1103.3 (10%) [{Cp'''Fe(CO)$_2$}$_2$P$_4$ + Cp'''Fe]$^+$, 1075.4 (1%) [{Cp'''Fe(CO)$_2$}$_2$P$_4$ + Cp'''Fe - CO]$^+$, 1019.4 (1%) [{Cp'''Fe(CO)$_2$}$_2$P$_4$ + Cp'''Fe - 3CO]$^+$, 991.4 (< 1%) [{Cp'''Fe(CO)$_2$}$_2$P$_4$ + Cp'''Fe - 4CO]$^+$, 358.2 (14%) [Cp'''Fe(CO)(NCCH$_3$)]$^+$, 330.2 (100%) [Cp'''Fe(NCCH$_3$)]$^+$, 144.9 [PF$_6$]$^-$.

Crystallographic Details

General remarks:

Single crystal structure analyses were performed using either Rigaku (formerly Agilent Technologies) diffractometer GV50, TitanS2 diffractometer (**2Ni**, **2Zn**, **3**, **4**, [Cp'''Fe(CO)$_3$][PF$_6$], [Cp'''Fe(CO)$_3$][SbF$_6$]) or SuperNova, Single source at offset, Atlas diffractometer (**2Co**) or a Gemini Ultra diffractometer (Oxford diffraction) with an AtlasS2 detector (**5**) with Cu-K*α* radiation (λ = 1.54178 Å). Frames integration and data reduction were performed with the CrysAlisPro[5] software package. All structures were solved ether by ShelXT[6] (**2Ni**, **2Zn**, **3**, **4**, **5**, [Cp'''Fe(CO)$_3$][PF$_6$]) or ShelXS[7] (**2Co**, [Cp'''Fe(CO)$_3$][PF$_6$]) using the software Olex2[8] and refined by full-matrix least-squares method against F^2 in anisotropic approximation using ShelXL[6]. Hydrogen atoms were refined in calculated positions using riding on pivot atom model. Further details are given in Table S4.1 and Table S4.2.

CCDC-2026542 (**2Co**), CCDC-2026543 (**2Ni**), CCDC-2026544 (**2Zn**), CCDC-2026545 (**3**), CCDC-2026546 (**4**), CCDC-2026547 (**5**), CCDC-2026548 (**[Cp'''Fe(CO)$_3$][PF$_6$]**), and CCDC-2026549 (**[Cp'''Fe(CO)$_3$][SbF$_6$]**) contain the supplementary crystallographic data for this paper. These data can be obtained free of charge at: www.ccdc.cam.ac.uk/conts/retrieving.html (or from the Cambridge Crystallographic Data Centre, 12 Union Road, Cambridge CB2 1EZ, UK; Fax: + 44-1223-336-033; e-mail: deposit@ccdc.cam.ac.uk).

Table S4.1. Crystallographic data and details of diffraction experiments for **2Co**, **2Ni**, **2Zn** and **3**.

Compound	**2Co** · 2(CH_2Cl_2)	**2Ni** · 2(CH_2Cl_2)	**2Zn** · 2(CH_2Cl_2)	**3** · 2.61($C_6H_4F_2$) · 0.8(C_6H_{14})
Formula	$C_{40}H_{62}Br_2Cl_4CoFe_2O_4P_4$	$C_{40}H_{62}Br_2Cl_4Fe_2NiO_4P_4$	$C_{40}H_{62}Br_2Cl_4Fe_2O_4P_4Zn$	$C_{96.46}H_{137.64}CoF_{23.22}Fe_4O_8P_8Sb_3$
CCDC number	2026542	2026543	2026544	2026545
$D_{calc.}$/ g cm^{-3}	1.585	1.577	1.587	1.577

μ/mm^{-1}	12.405	10.240	10.368	12.199
Formula Weight	1203.02	1202.80	1209.46	2761.74
Color	dark brown	dark brown	clear yellow	clear dark orange
Shape	plate	plate	plate	irregular
Size/mm^3	0.13×0.11×0.04	0.10×0.08×0.04	0.33×0.15×0.03	0.26×0.19×0.11
T/K	123.01(10)	122.94(18)	122.96(11)	122.93(19)
Crystal System	monoclinic	monoclinic	monoclinic	monoclinic
Space Group	$P2_1/c$	$P2_1/c$	$P2_1/c$	$P2_1/c$
a/Å	21.1398(6)	21.1466(7)	21.1695(4)	14.5876(2)
b/Å	13.2714(3)	13.2685(2)	13.31570(10)	27.7347(4)
c/Å	19.7648(6)	19.8156(7)	19.7952(4)	29.2809(4)
α/°	90	90	90	90
β/°	114.622(4)	114.327(4)	114.868(2)	100.9578(13)
γ/°	90	90	90	90
V/Å^3	5040.9(3)	5066.3(3)	5062.62(16)	11630.5(3)
Z	4	4	4	4
Z'	1	1	1	1
Wavelength/Å	1.54184	1.54184	1.54184	1.54184
Radiation type	Cu K_α	Cu K_α	Cu K_α	Cu K_α
Θ_{min}/°	4.141	4.045	4.040	3.463
Θ_{max}/°	72.952	73.966	74.487	67.079
Measured Refl's.	18681	24114	28759	79709
Ind't Refl's	9630	9793	9842	20695
Refl's with I > 2(I)	8451	7622	9533	16742
R_{int}	0.0399	0.0564	0.0261	0.0782
Parameters	541	542	542	1559
Restraints	0	0	0	550
Largest Peak	0.772	1.114	0.607	1.835
Deepest Hole	-0.645	-0.742	-0.514	-2.029
GooF	1.098	1.035	1.082	1.045
wR_2 (all data)	0.1062	0.1274	0.0752	0.1993
wR_2	0.1024	0.1152	0.0746	0.1885
R_1 (all data)	0.0537	0.0717	0.0283	0.0823
R_1	0.0455	0.0509	0.0275	0.0691

Table S4.2. Crystallographic data and details of diffraction experiments for **4**, **5**, [Cp'''Fe(CO)$_3$][PF$_6$] and [Cp'''Fe(CO)$_3$][SbF$_6$].

Compound	**4**	**5** · 4(CH_2Cl_2)	[Cp'''Fe(CO)$_3$][PF$_6$]	[Cp'''Fe(CO)$_3$][SbF$_6$]
Formula	$C_{90.5}CoF_6Fe_4H_{146}O_{10}P_8Sb$	$C_{80}H_{124}Cl_8F_{12}Fe_4O_8P_{10}Zn$	$C_{20}H_{29}F_6FeO_3P$	$C_{20}H_{29}F_6FeO_3Sb$
CCDC number	2026546	2026547	2026548	2026549
$D_{calc.}$/ g cm^{-3}	1.316	1.481	1.467	1.657
μ/mm^{-1}	8.850	8.546	6.408	14.129
Formula Weight	2159.90	2323.85	518.25	609.03
Color	dark brown	clear yellow	dark brown	dark yellow
Shape	needle	plate	irregular	needle
Size/mm^3	0.20×0.09×0.04	0.45×0.14×0.06	0.62×0.39×0.34	0.45×0.08×0.07
T/K	123.00(10)	123(1)	123.00(10)	123.00(10)
Crystal System	triclinic	orthorhombic	orthorhombic	monoclinic
Flack Parameter	-	-0.006(3)	-0.007(4)	-
Hooft Parameter	-	-0.0058(16)	-0.012(3)	-
Space Group	*P*-1	*Pba2*	$P2_12_12_1$	$P2_1/c$
a/Å	14.1898(4)	17.45470(10)	10.1272(3)	10.89360(10)
b/Å	19.3435(4)	21.0632(2)	14.0681(4)	12.39000(10)
c/Å	20.7967(4)	14.17520(10)	16.4718(5)	18.0885(2)
α/°	96.846(2)	90	90	90
β/°	95.481(2)	90	90	91.2600(10)
γ/°	104.082(2)	90	90	90
V/Å^3	5451.1(2)	5211.54(7)	2346.75(12)	2440.85(4)
Z	2	2	4	4
Z'	1	0.5	1	1
Wavelength/Å	1.54184	1.54184	1.54184	1.54184

Radiation type	Cu K_α	Cu K_α	Cu K_α	Cu K_α
Θ_{min}/°	3.238	4.198	4.133	4.059
Θ_{max}/°	66.600	71.769	74.186	73.958
Measured Refl's.	56856	34731	5871	13817
Ind't Refl's	19063	9438	3987	4773
Refl's with I > 2(I)	13306	9100	3861	4452
R_{int}	0.0953	0.0393	0.0287	0.0255
Parameters	1073	594	289	336
Restraints	204	19	0	28
Largest Peak	0.991	0.491	0.246	0.437
Deepest Hole	-0.655	-0.908	-0.454	-0.391
GooF	1.027	1.033	1.045	1.037
wR_2 (all data)	0.1880	0.0978	0.0867	0.0527
wR_2	0.1703	0.0962	0.0854	0.0517
R_1 (all data)	0.0893	0.0377	0.0340	0.0227
R_1	0.0651	0.0358	0.0327	0.0205

X–ray diffraction on Crystals of **2Co**

In the crystal structure of [{Cp'''Fe(CO)$_2$}$_2$(μ_3,$\eta^{2:1:1}$-P_4){$CoBr_2$}] · 2(CH_2Cl_2) (**2Co**) a chlorine atom of one the CH_2Cl_2 molecules is disordered over two positions and was refined to an occupancy of 50:50.

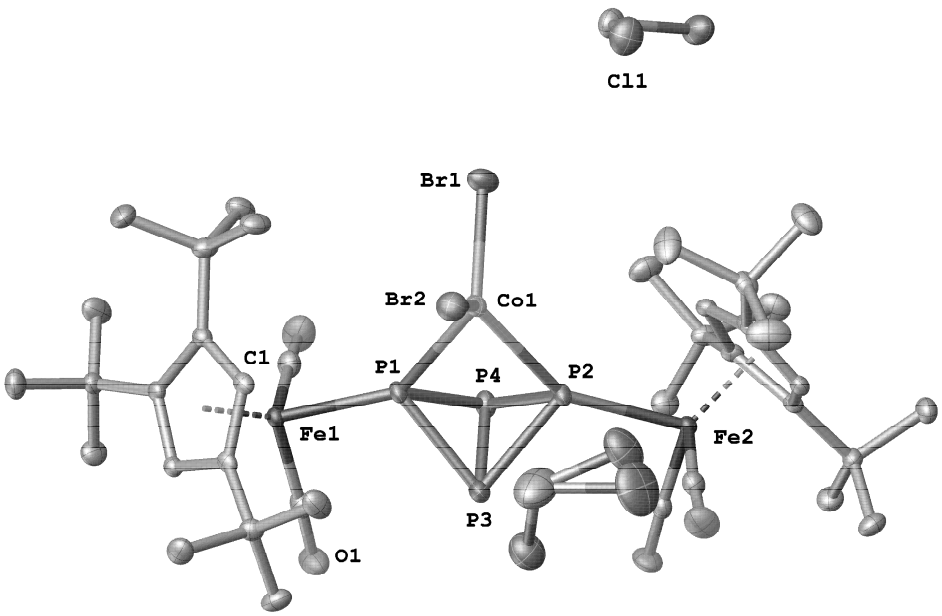

Figure S4.1. Molecular structure of **2Co** · 2(CH_2Cl_2) in the crystal. Hydrogen atoms are omitted for clarity. ADPs are drawn at 50% probability level. Selected bond length [Å] and angles [°] are: P1-P3 2.2183(13), P1-P4 2.2034(13), P2-P3 2.2113(13), P2-P4 2.2210(14), P3-P4 2.1926(14), P1···P2 2.8481(13), Co-P1 2.3614(11), Co-P2 2.3959(11), Co-Br1 2.3669(7), Co-Br2 2.3753(8), P1-Fe1 2.2538(11), P2-Fe2 2.2768(11). Br1-Co-Br2 114.80(3), Br1-Co-P1 112.97(4) Br1-Co-P2 111.85(4), Br2-Co-P1 114.37(4), Br2-Co-P2 122.67(4), P1-Co-P2 73.55(4).

X–ray diffraction on Crystals of **2Ni**

In the crystal structure of [{Cp'''Fe(CO)$_2$}$_2$(μ_3,$\eta^{2:1:1}$-P_4){$NiBr_2$}] · 2(CH_2Cl_2) (**2Ni**) a chlorine atom of one the CH_2Cl_2 molecules is disordered over two positions and was refined to an occupancy of 65:35.

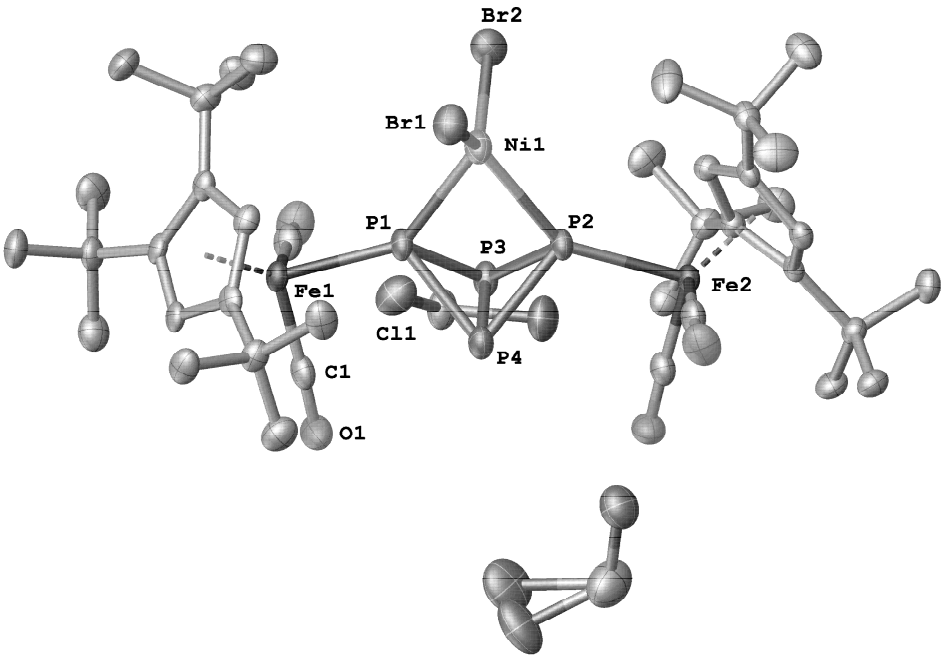

Figure S4.2. Molecular structure of **2Ni** · 2(CH_2Cl_2) in the crystal. Hydrogen atoms are omitted for clarity. ADPs are drawn at 50% probability level. Selected bond length [Å] and angles [°] are: P1-P3 2.1888(15), P1-P4 2.2108(17), P2-P3 2.2047(16), P2-P4 2.2073(18), P3-P4 2.2156(17), Ni-P1 2.3389(15), Ni-P2 2.3607(14), Ni-Br1 2.3629(10), Ni-Br2 2.3591(9), P1-Fe1 2.2622(13), P2-Fe2 2.2802(12), Br1-Ni-Br2 123.81(4), Br1-Ni-P1 107.25(5), Br1-Ni-P2 104.08(4), Br2-Ni-P1 112.88(4), Br2-Ni-P2 124.47(5), P1-Ni-P2 72.08(5).

X–ray diffraction on Crystals of **2Zn**

In the crystal structure of [{Cp'''Fe(CO)$_2$}$_2$(μ_3,$\eta^{2:1:1}$-P_4){$ZnBr_2$}] · 2(CH_2Cl_2) (**2Zn**) a chlorine atom of one the CH_2Cl_2 molecules is disordered over two positions and was refined to an occupancy of 66:34.

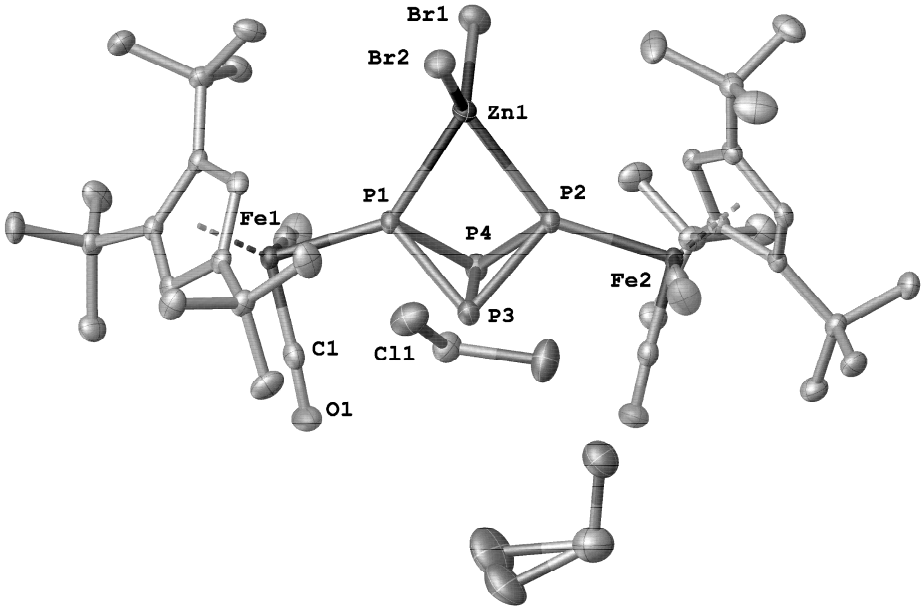

Figure S4.3. Molecular structure of **2Zn** · $2(CH_2Cl_2)$ in the crystal. Hydrogen atoms are omitted for clarity. ADPs are drawn at 50% probability level. Selected bond length [Å] and angles [°] are: P1-P3 2.2137(7), P1-P4 2.1993(7), P2-P3 2.2087(7), P2-P4 2.2143(8), P3-P4 2.2010(8), P1···P2 2.8420(8), Zn-P1 2.4479(6), Zn-P2 2.5002(6), Zn-Br1 2.3629(4), Zn-Br2 2.3655(4), P1-Fe1 2.2583(6), P2-Fe2 2.2827(6), Br1-Zn-Br2 117.21(1), Br1-Zn-P1 112.46(2), Br1-Zn-P2 110.28(2), Br2-Zn-P1 115.15(2), Br2-Zn-P2 122.77(2), P1-Zn-P2 70.10(2).

X–ray diffraction on Crystals of **3**

The X-ray diffraction experiment of $[\{(Cp'''Fe(CO)_2)_2(\mu_3,\eta^{4:1:1}\text{-}P_4)\}_2Co][SbF_6]_3$ · $2.61(C_6H_4F_2)$ · $0.8(C_6H_{14})$ (**3**) suffers from disorder of the hole cation, all anions as well as one hexane molecule (Figure S4.4). The cation as well one SbF_6^- anion is disordered over two position with an occupancy of 97:3. For the discussion of the bond length as well as the angles only the main component was taken into account (Figure S4.5). Due to the low occupancy of the minor part, only the heavy atom scaffold (P, Fe, Co) as well as one Sb atom could be refined (Figure S4.6). The already mentioned SbF_6^- anion is disordered in total over three position with an occupancy of 60:37:3. The other two anions were refined with occupancies of 55:44 and 80:20 over two positions, respectively. One position of the three o-dfb ($C_6H_4F_2$) solvent molecules is only 61% occupied. The hexane position is occupied in 80% while one CH_3 group is also disordered over two positions with an occupancy of 50:30.

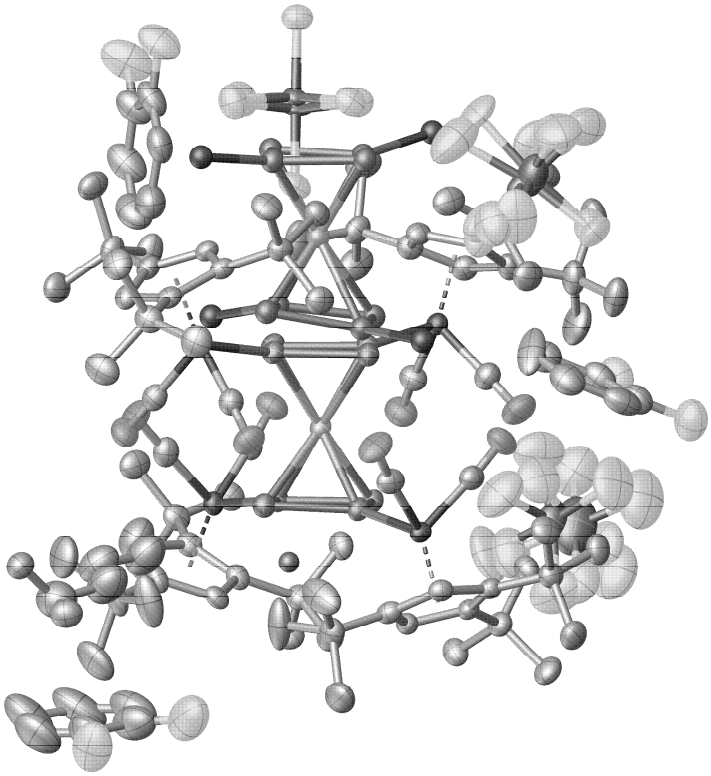

Figure S4.4. Asymmetric unit of **3** · 2.61($C_6H_4F_2$) · 0.8(C_6H_{14}) in the solid state displaying all the disordered parts. Hydrogen atoms are omitted for clarity. ADPs are drawn at 50% probability level.

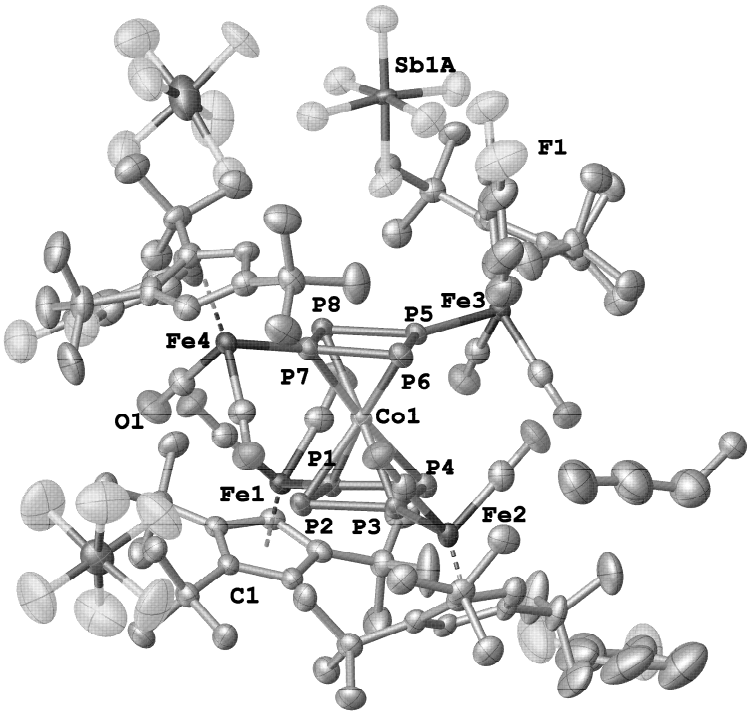

Figure S4.5. Part 1 of the Molecular structure of **3** · 2.61($C_6H_4F_2$) · 0.8(C_6H_{14}) in the crystal. Hydrogen atoms are omitted for clarity. ADPs are drawn at 50% probability level. Selected bond length [Å] and angles [°] are: P1-P2 2.151(2), P2-P3 2.147(2), P3-P4 2.137(2), P1-P4 2.139(2), P5-P6 2.135(2), P6-P7 2.137(2), P7-P8 2.154(2), P5-P8 2.151(2), Fe1-P1 2.2007(17), Fe2-P3 2.1972(17), Fe3-P5 2.2055(17), Fe4-P7 2.2013(18), Co1-P1 2.2685(17), Co1-P2 2.3589(17), Co1-P3 2.2749(17), Co1-P4 2.3581(19), Co1-P5 2.2691(17), Co1-P6 2.3636(18), Co1-P7 2.270(2), Co1-P8 2.3486(19); P4-P1-P2 96.45(8), P1-P2-P3 83.17(8), P2-P3-P4 96.62(8), P3-P4-P1 83.71(8), P8-P5-P6 96.25(8), P5-P6-P7 84.20(8), P6-P7-P8 96.09(9), P7-P8-P5 83.42(8), P2-P1-Fe1 130.59(9), P4-P1-Fe1 132.03(9), P2-P3-Fe2 132.72(8), P4-P3-Fe2 130.33(9), P6-P5-Fe3 130.38(9), P8-P5-Fe3 132.73(9), P6-P7-Fe4 131.11(9), P8-P7-Fe4 131.51(9).

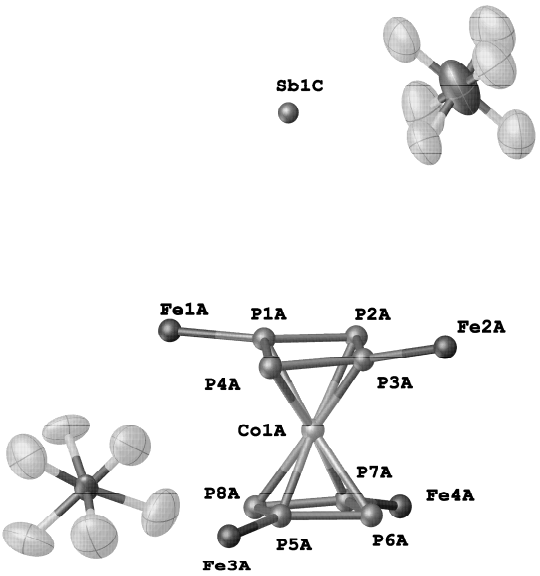

Figure S4.6. Part 2 of the Molecular structure of **3** · 2.61($C_6H_4F_2$) · 0.8(C_6H_{14}) in the crystal. Due to the occupancy of the cation as well as one SbF_6^- anion of only 3%, only the heavy atom scaffold can be refined.

X–ray diffraction on Crystals of **4**

In the crystal structure of [{Cp'''Fe(CO)$_2$}$_4$(μ_5,$\eta^{4:1:1:1:1}$-P_8){Co(CO)$_2$}][SbF_6] (**4**) the SbF_6^- anion is disordered over two positions with an occupancy of 52:48.

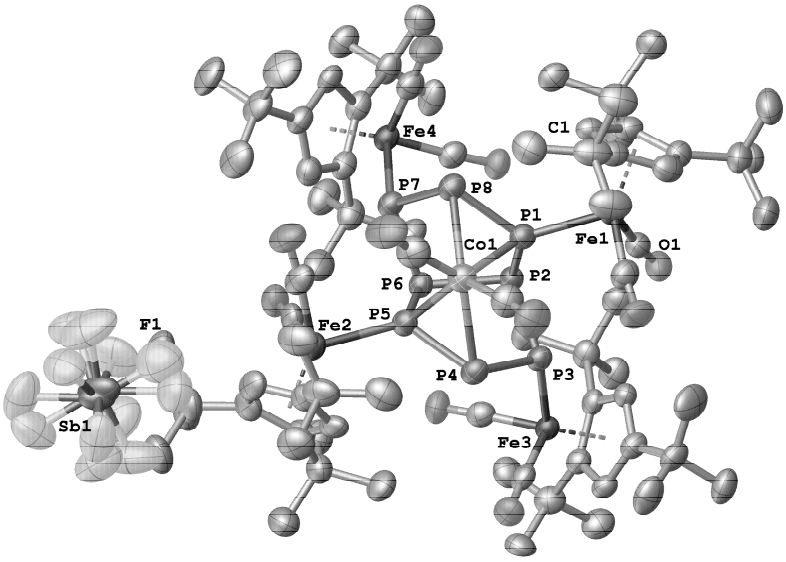

Figure S4.7. Molecular structure of **4** in the crystal. Hydrogen atoms are omitted for clarity. ADPs are drawn at 50% probability level. Selected bond length [Å] and angles [°] are: P1-P2 2.2075(18), P1-P8 2.116(2), P2-P3 2.2046(19), P2-P6 2.1928(17), P3-P4 2.2308(18), P4-P5 2.111(2), P5-P6 2.2162(18), P6-P7 2.2075(19), P7-P8 2.2246(19), Fe1-P1 2.3022(15), Fe2-P5 2.3115(15), Fe3-P3 2.3101(16), Fe4-P7 2.2996(15), Co1-P1 2.2553(15), Co1-P4 2.4058(18), Co1-P5 2.2551(17), Co1-P8 2.4098(17); P8-P1-P2 108.49(8), P1-P2-P6 100.16(7), P1-P2-P3 89.22(7), P6-P2-P3 104.79(7), P2-P3-P4 101.39(7), P3-P4-P5 107.60(8), P4-P5-P6 108.24(7), P5-P6-P7 89.17(7), P5-P6-P2 100.48(7), P2-P6-P7 105.03(8), P6-P7-P8 101.37(7), P7-P8-P1 107.51(8).

X–ray diffraction on Crystals of **5**

The crystal structure of $[\{(Cp'''Fe(CO)_2)_2(\mu_3,\eta^{2:1:1}\text{-}P_4)\}_2Zn][PF_6]_2 \cdot 4(CH_2Cl_2)$ (**5**) contains half of the molecule in the asymmetric unit. The chlorine atom of one the CH_2Cl_2 molecules is disordered over two positions and was refined to an occupancy of 52:48.

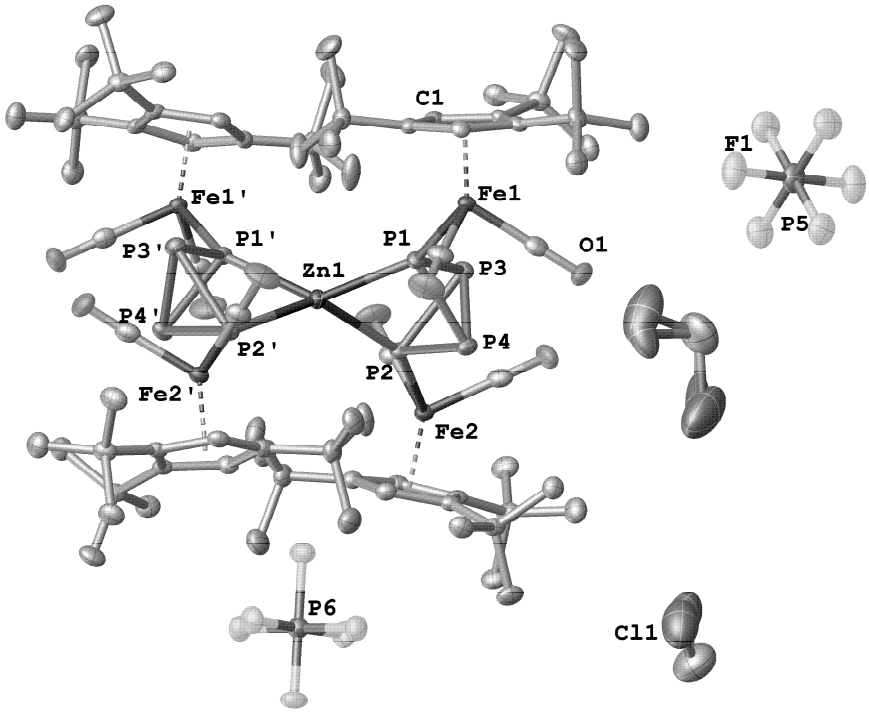

Figure S4.8. Molecular structure of **5** · $4(CH_2Cl_2)$ in the crystal. Hydrogen atoms are omitted for clarity. ADPs are drawn at 50% probability level. Selected bond length [Å] and angles [°] are: P1-P3 2.2152(15), P1-P4 2.2214(15), P2-P3 2.2252(15), P2-P4 2.2102(15), P3-P4 2.1803(16), Zn1-P1 2.4536(11), Zn1-P2 2.4471(11), Fe1-P1 2.2832(12), Fe2-P2 2.2806(12); P1-Zn1-P1' 137.35(6), P1-Zn1-P2 73.34(3), P1-Zn1-P2' 123.68(4), P2-Zn1-P2' 136.79(6), P2-Zn1-P1' 123.68(4).

X–ray diffraction on Crystals of $[Cp'''Fe(CO)_3][PF_6]$

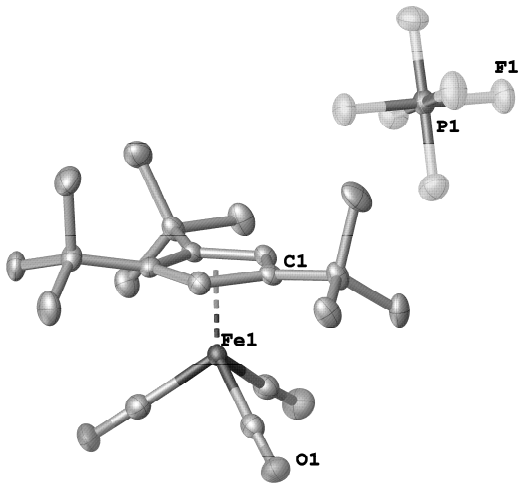

Figure S4.9. Molecular structure of $[Cp'''Fe(CO)_3][PF_6]$ in the crystal. Hydrogen atoms are omitted for clarity. ADPs are drawn at 50% probability level.

X–ray diffraction on Crystals of $[Cp'''Fe(CO)_3][SbF_6]$

In the crystal structure of $[Cp'''Fe(CO)_3][SbF_6]$ the SbF_6^- anion is disordered over two positions with an occupancy of 55:45.

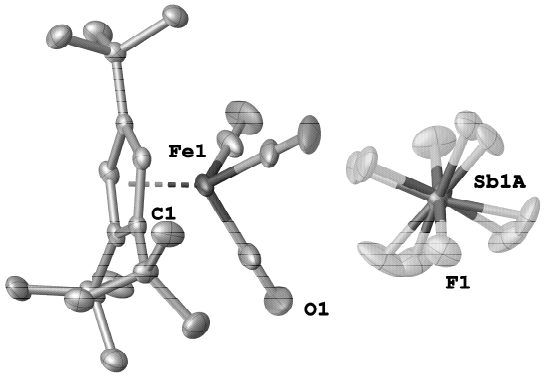

Figure S4.10. Molecular structure of $[Cp'''Fe(CO)_3][SbF_6]$ in the crystal. Hydrogen atoms are omitted for clarity. ADPs are drawn at 50% probability level.

NMR Spectroscopy

General remarks:

^1H, ^{31}P and ^{13}C NMR spectra were recorded on a Bruker Avance III HD 400 (^1H: 400.130 MHz, ^{31}P: 161.976 MHz, ^{13}C: 100.655 MHz) at 298 K. The chemical shifts are reported in ppm relative to external TMS (^1H, ^{13}C) and H_3PO_4 (^{31}P). The ^{31}P NMR simulation was performed with the simulation tool of Bruker TopSpin (Version 4.0.8.).

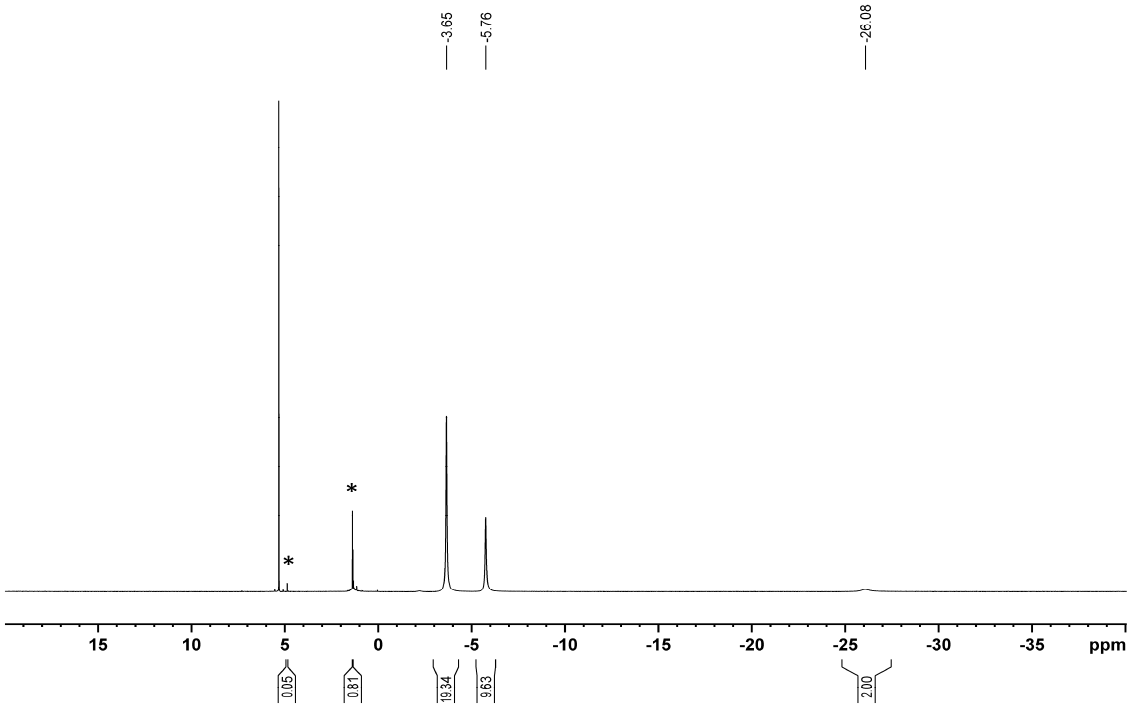

Figure S4.11. ^1H NMR spectrum of **2Co** in CD_2Cl_2. Impurities are marked with *.

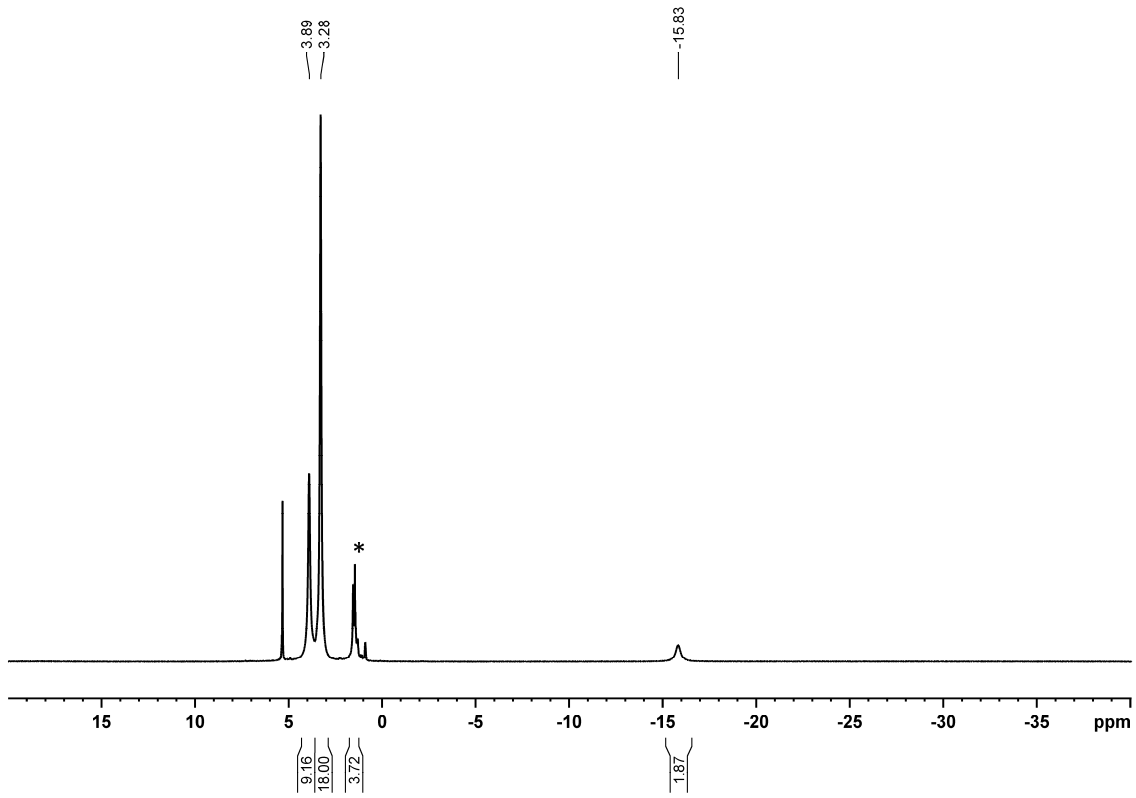

Figure S4.12. ^{1}H NMR spectrum of **2Ni** in CD_2Cl_2. Impurities are marked with *.

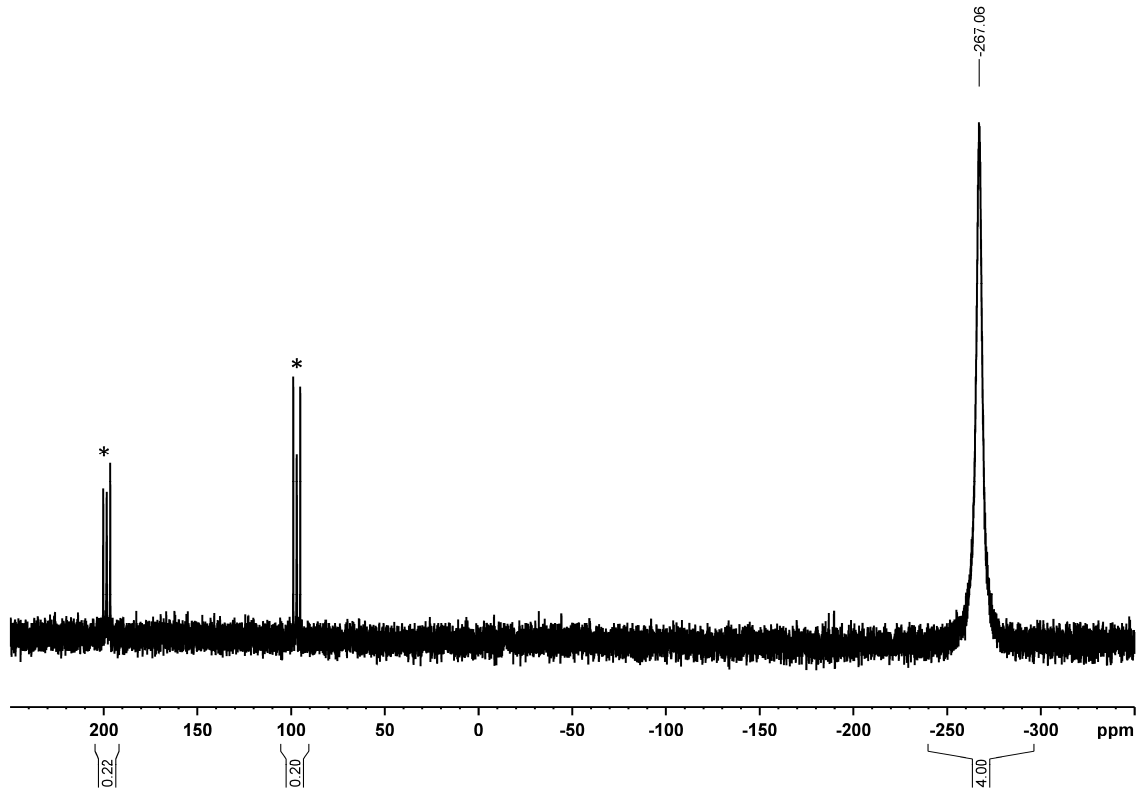

Figure S4.13. $^{31}P\{^{1}H\}$ NMR spectrum of **2Ni** in CD_2Cl_2. The signals marked with * belong to an unknown side product.

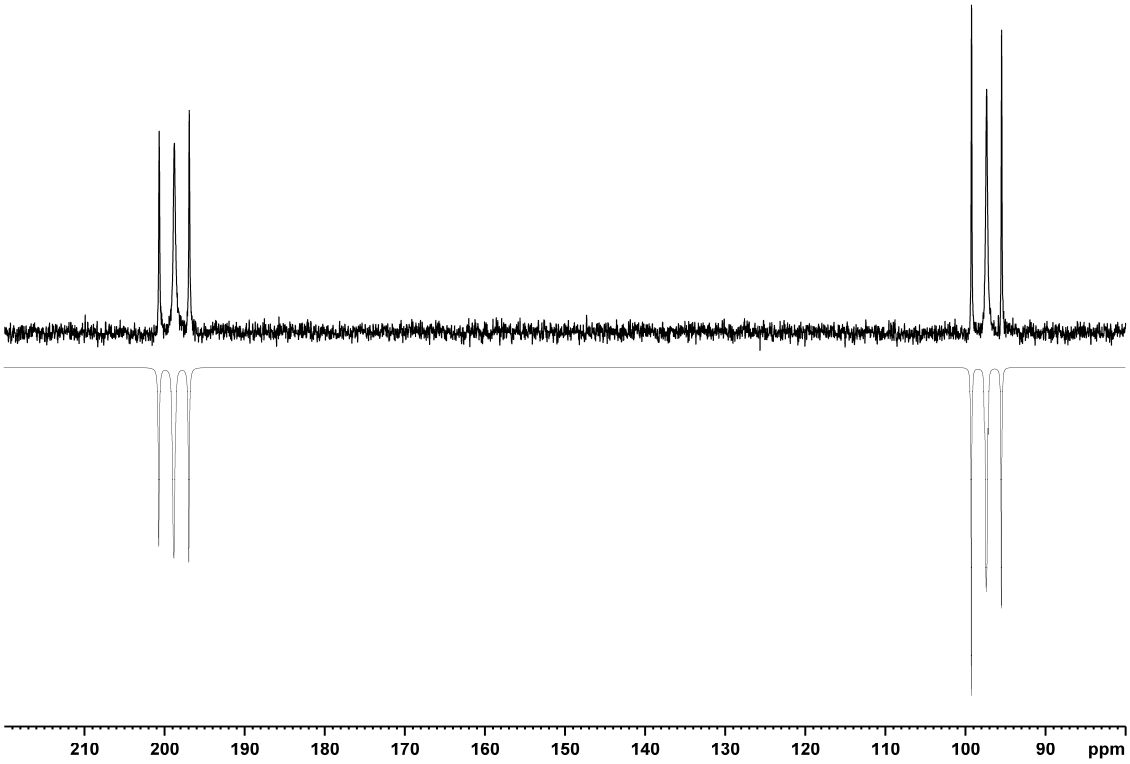

Figure S4.14. Simulated $^{31}P\{^{1}H\}$ NMR spectrum of the AA'XX' spin system in the reaction of **2Ni**.

Table S4.3. Calculated coupling constants of the AA'XX' spin system with a R-factor of 2.53%.

Chemical shift [ppm]		Coupling constants [Hz]			
AA'	198.8	$^{2}J_{AA'}$	-0.4	$^{1}J_{A'X}$	282.0
XX'	97.3	$^{1}J_{AX}$	322.1	$^{1}J_{A'X'}$	326.0
		$^{1}J_{AX'}$	286.3	$^{2}J_{XX'}$	-28.0

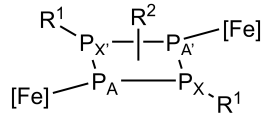

Scheme S4.1. Postulated structure of the byproduct based on the coupling constants obtained by the simulation. R^1 and R^2 are possible pattern for substitution.

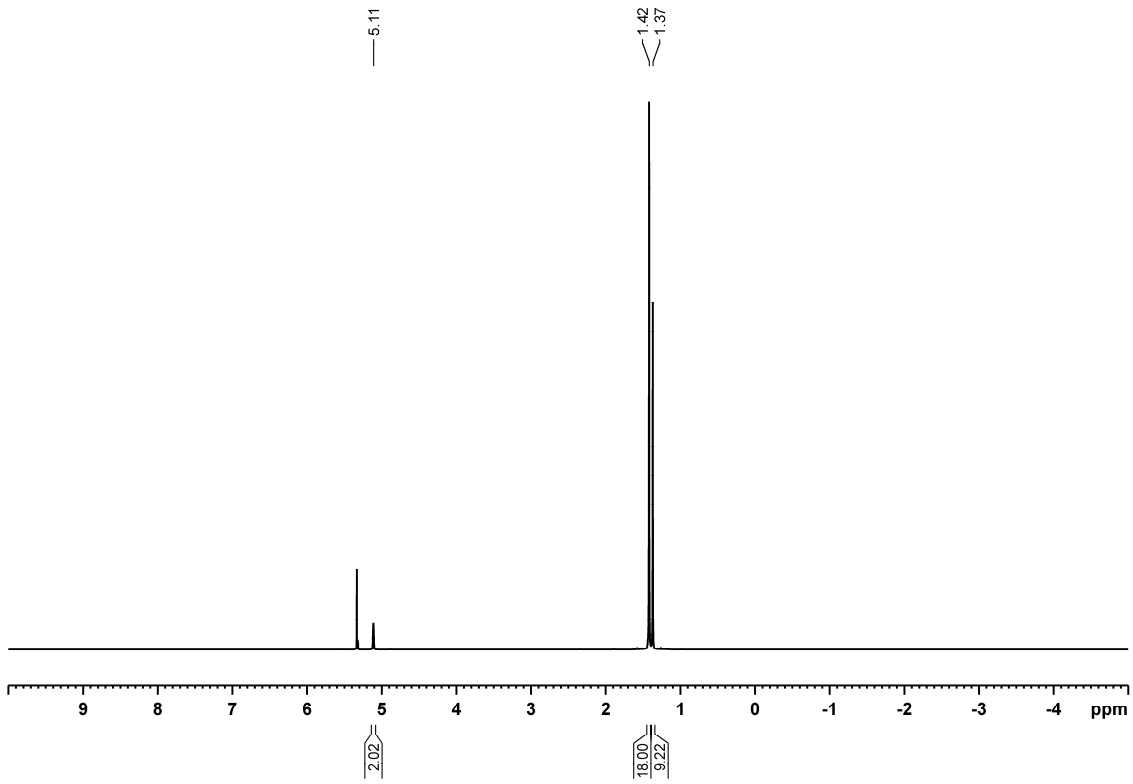

Figure S4.15. ^{1}H NMR spectrum of **2Zn** in CD_2Cl_2.

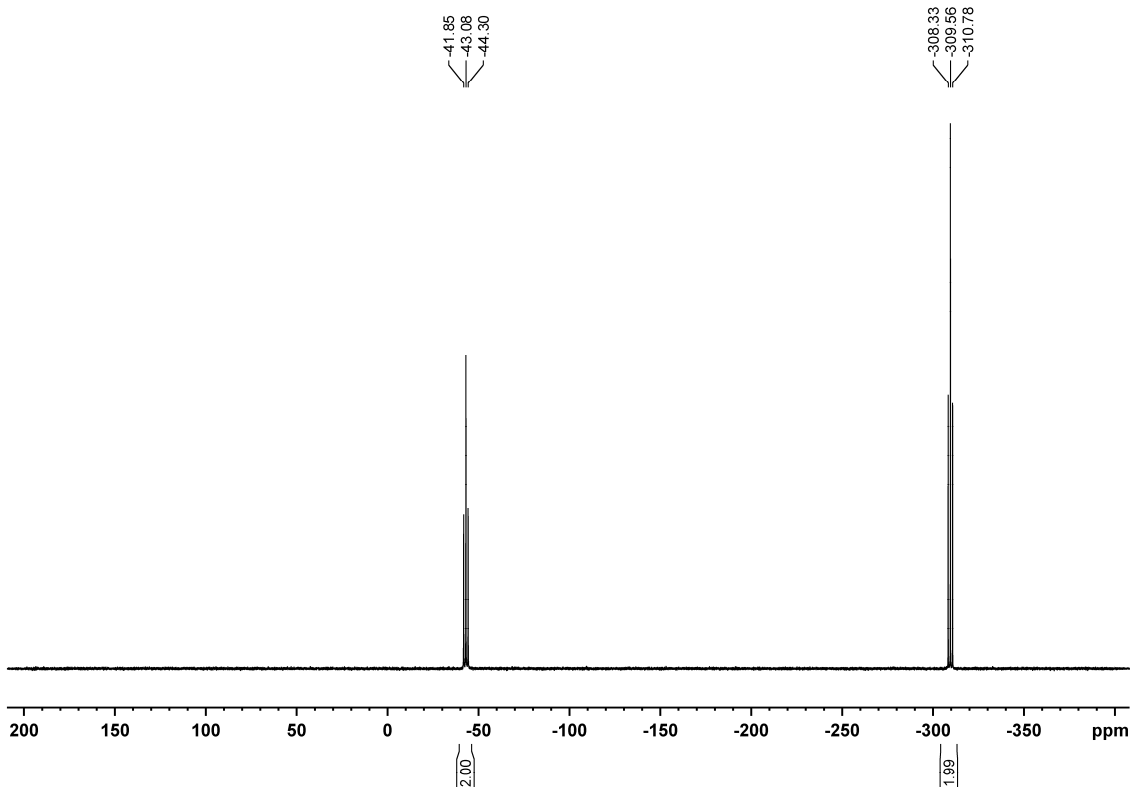

Figure S4.16. $^{31}P\{^{1}H\}$ NMR spectrum of **2Zn** in CD_2Cl_2.

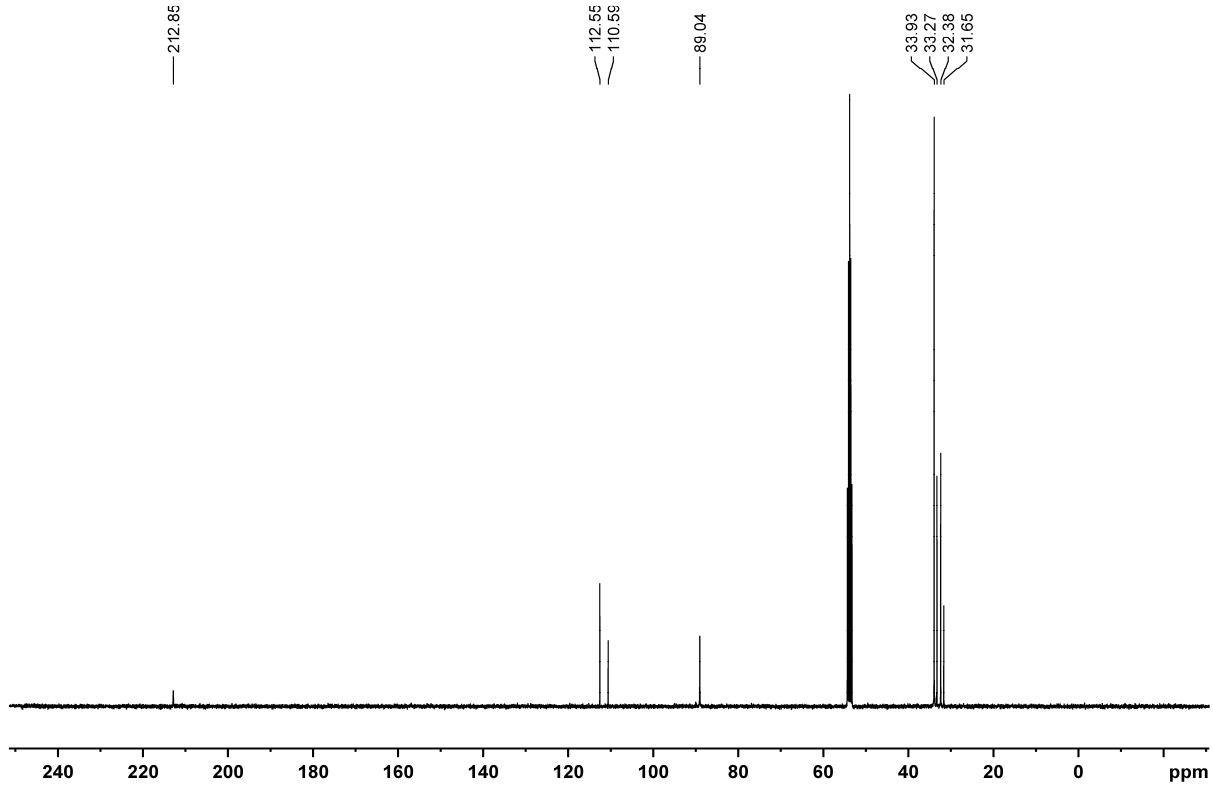

Figure S4.17. $^{13}C\{^1H\}$ NMR spectrum of **2Zn** in CD_2Cl_2.

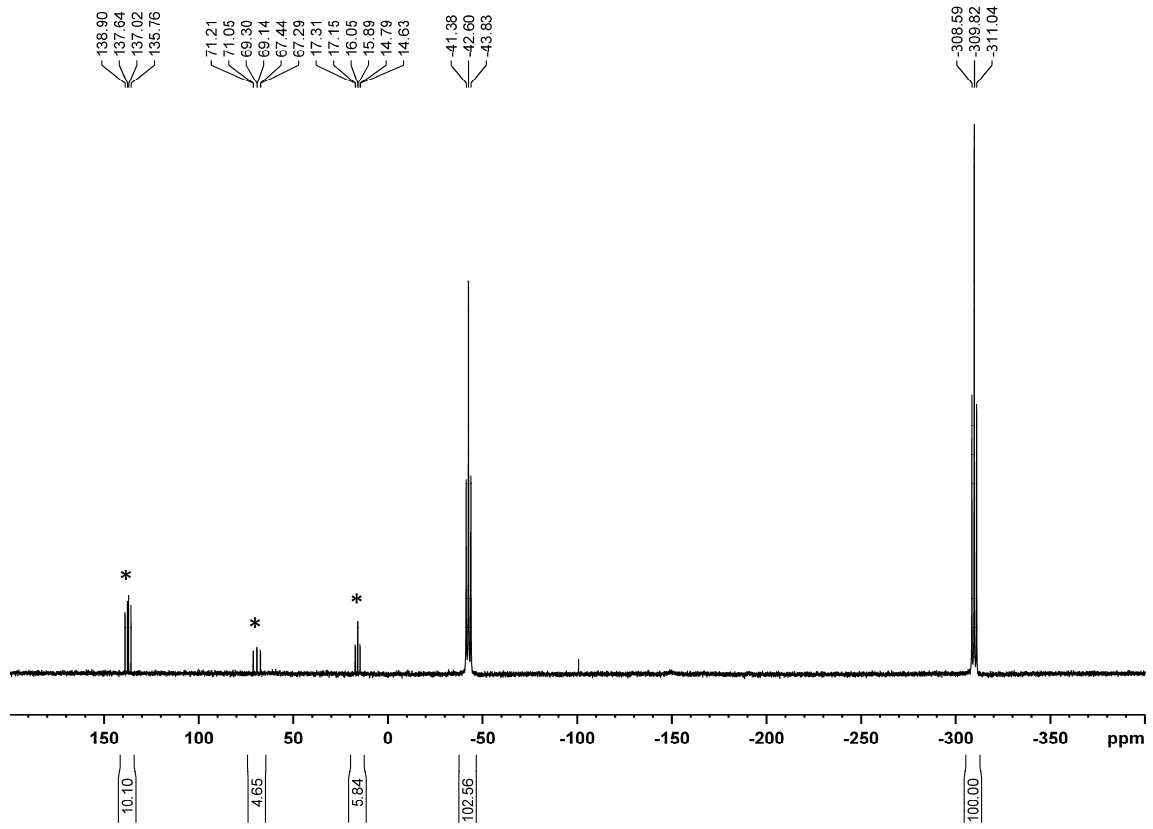

Figure S4.18. Reaction $^{31}P\{^1H\}$ NMR spectrum of the synthesis of **2Zn** in CD_2Cl_2. The signals marked with * belong to an unknown side product.

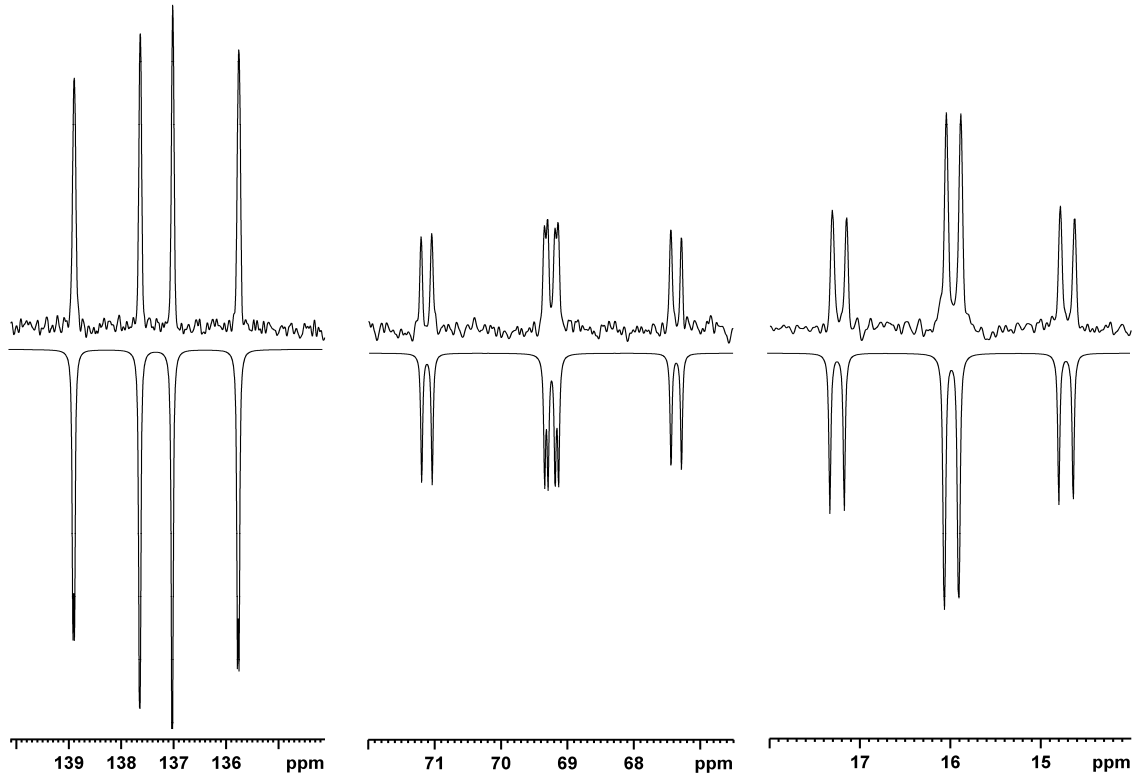

Figure S4.19. Simulated $^{31}P\{^1H\}$ NMR spectrum of the A_2MX spin system in the reaction of **2Zn**. These Signals were mistakenly assigned to $[\{Cp'''Fe(CO)_2\}_2(\mu_3,\eta^{1:1:2}\text{-}P_4)\{Cp'''Fe(CO)\}]^+$ in the previous work.[4]

Table S4.4. Calculated coupling constants of the A_2MX spin system with a R-factor of 0.29%.

Chemical shift [ppm]		Coupling constants [Hz]	
A	137.3	$^1J_{AM}$	304.7
M	69.3	$^1J_{AX}$	204.3
X	15.9	$^2J_{MX'}$	25.5

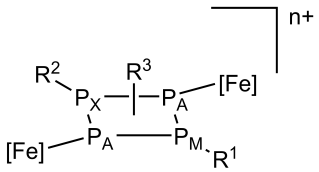

Scheme S4.2. Postulated structure of the byproduct based on the coupling constants obtained by the simulation. R^1, R^2 and R^3 are possible pattern for substitution.

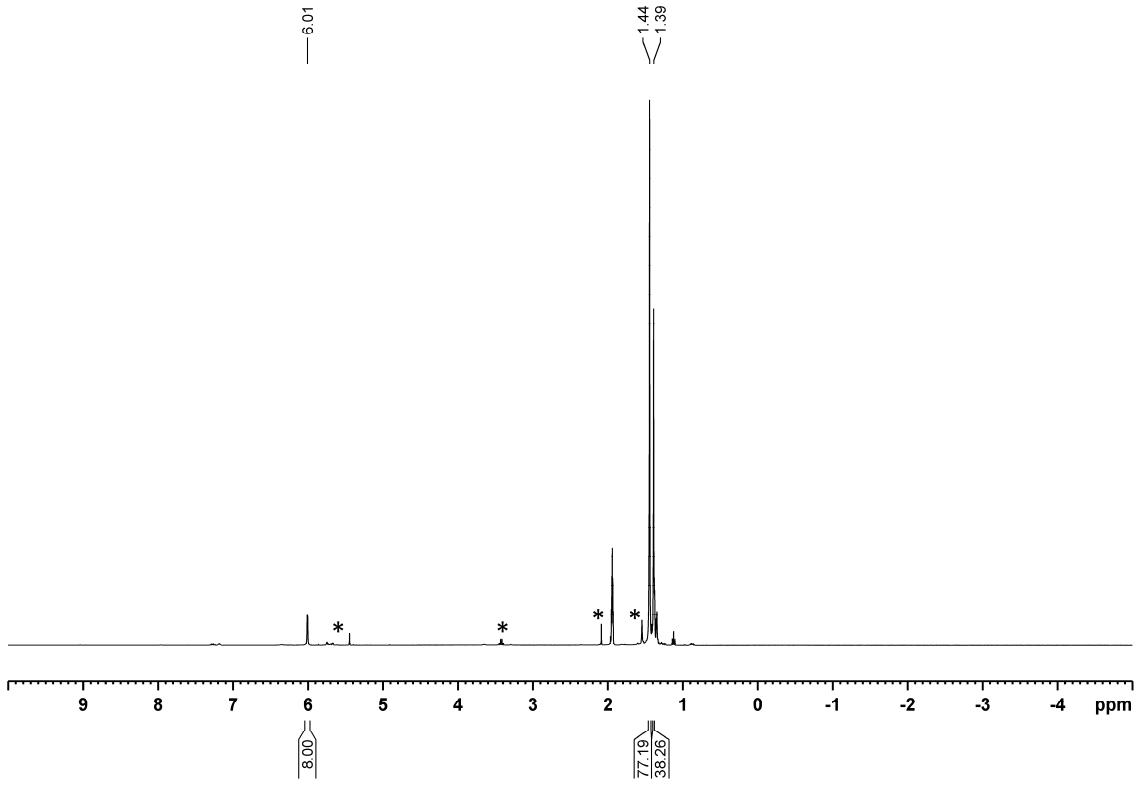

Figure S4.20. ^{1}H NMR spectrum of **3** in CD_3CN. Impurities are marked with *.

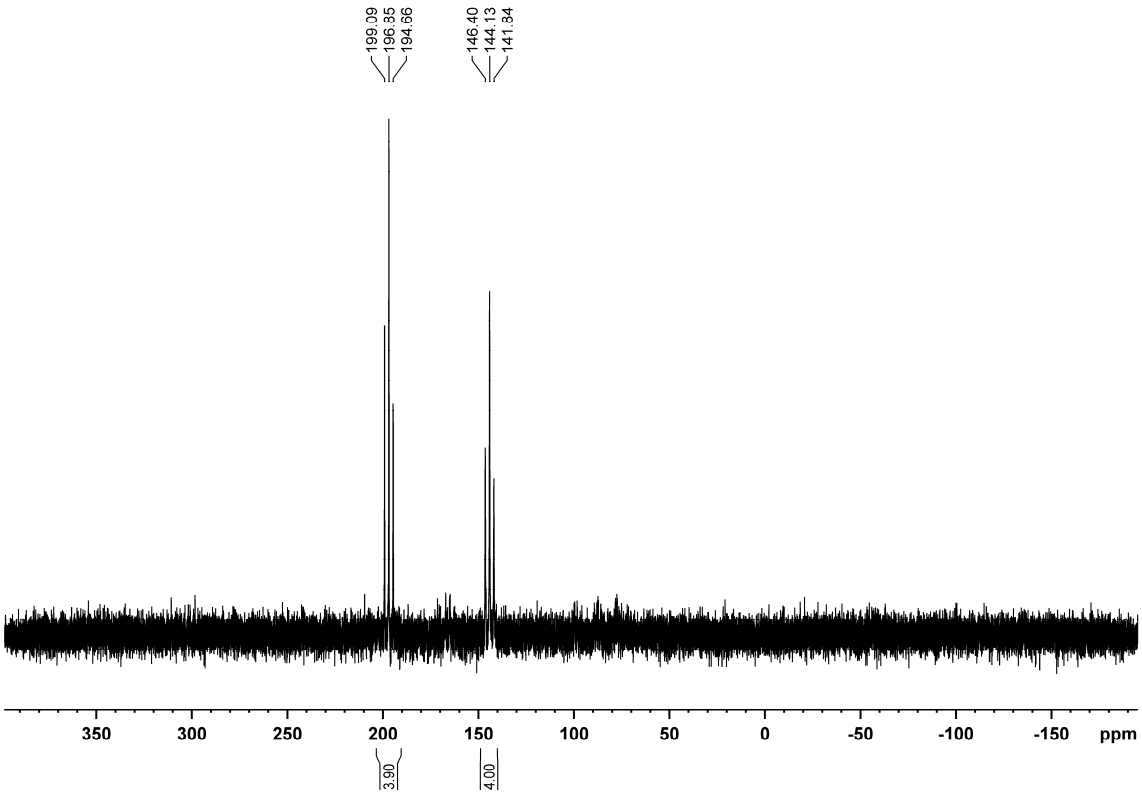

Figure S4.21. 31P{1H} NMR spectrum of **3** in CD3CN.

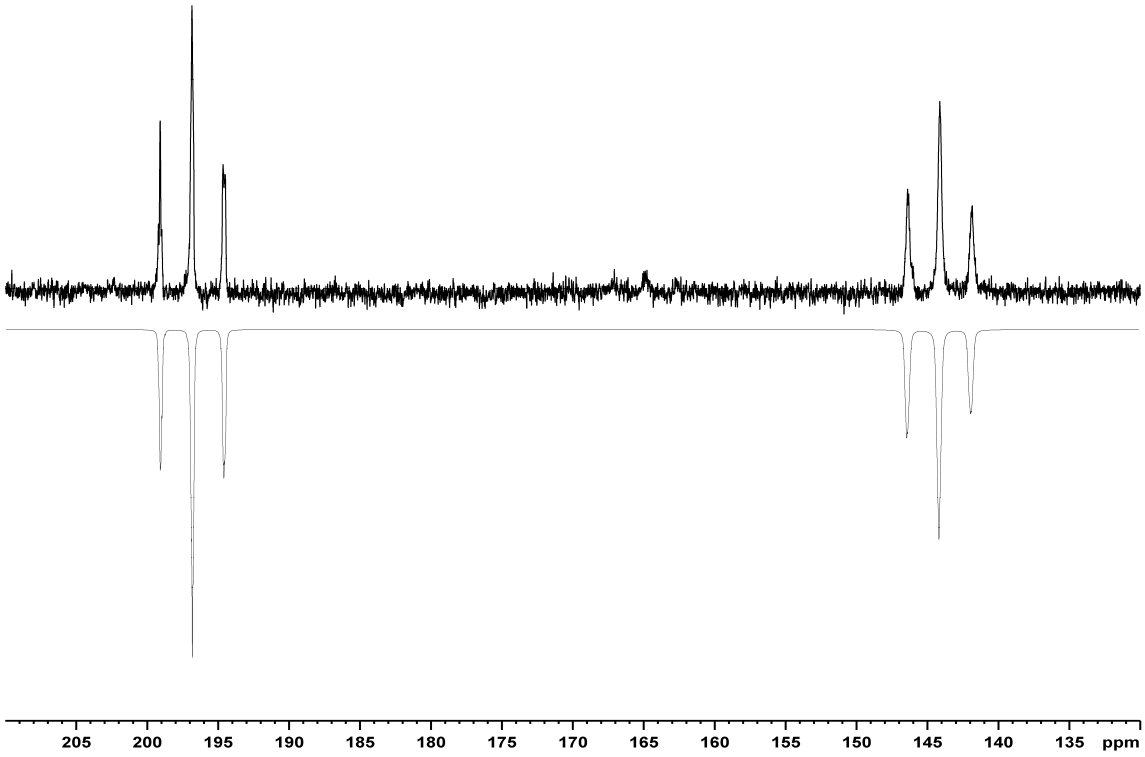

Figure S4.22. Simulated $^{31}P\{^{1}H\}$ NMR spectrum of **3** (AA'XX' spin system).

Table S4.5. Calculated coupling constants of the cation of **3** (AA'XX' spin system) with a R-factor of 3.68%.

Chemical shift [ppm]		Coupling constants [Hz]			
AA'	196.7	$^{2}J_{AA'}$	20.8	$^{1}J_{AX'}$	366.7
XX'	144.2	$^{2}J_{XX'}$	-16.8	$^{1}J_{AX}$	363.2

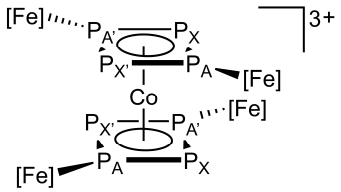

Scheme S4.3. Schematic view of the cation of **3** for the NMR assignment.

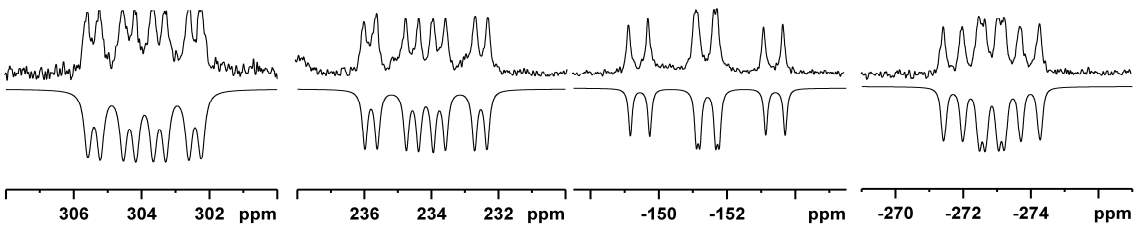

Figure S4.23. Simulated $^{31}P\{^{1}H\}$ NMR spectrum of **4** (AA'MM'OO'XX' spin system).

Table S4.6. Calculated coupling constants of the cation of **4** (AA'MM'OO'XX' spin system) with a R-factor of 2.31%.

Chemical shift [ppm]		Coupling constants [Hz]					
AA'	303.9	$^1J_{AO}$	316.2	$^1J_{A'O'}$	309.9	$^2J_{AM}$	62.2
MM'	234.2	$^1J_{AX'}$	166.5	$^1J_{A'X}$	172.6	$^2J_{OX}$	92.8
OO'	−151.4	$^1J_{MO}$	328.3	$^1J_{M'O'}$	332.0	$^2J_{A'M'}$	57.9
XX'	−272.9	$^1J_{MX}$	202.7	$^1J_{M'X'}$	197.4	$^2J_{O'X'}$	91.6

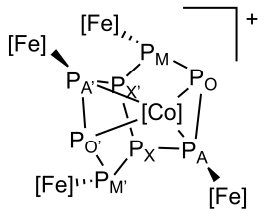

Scheme S4.4. Schematic view of the cation of **4** for the NMR assignment.

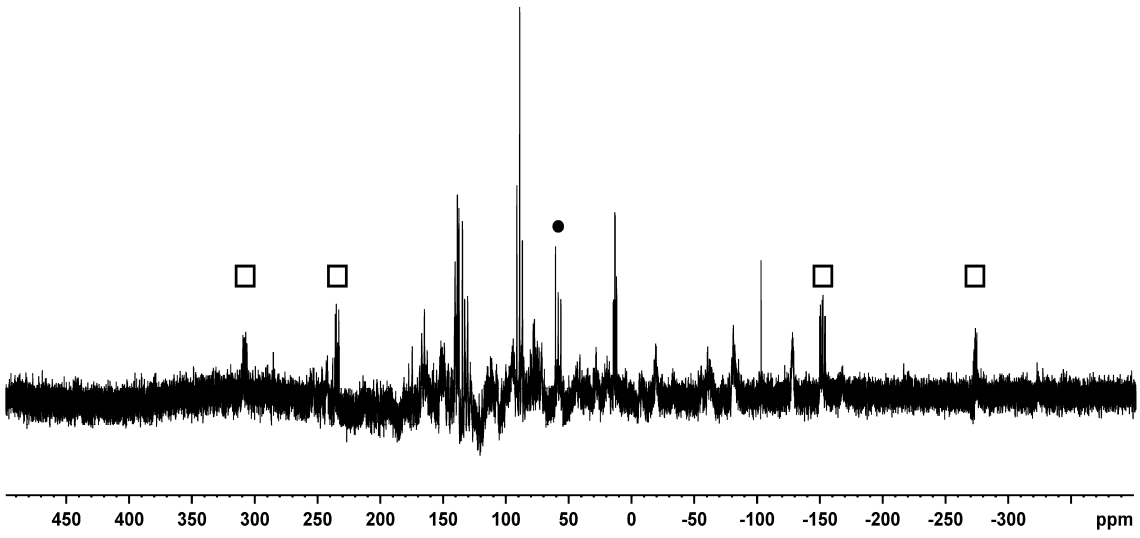

Figure S4.24. CH_2Cl_2 washing solution of the reaction of **1** and $[Co(NCCH_3)_6][SbF_6]_2$ in CD_3CN. The signal marked with a square (□) can be assigned to **4** while the signal marked with a dot (●) is part of the signal that can be assigned to the cation of $[\{Cp'''Fe(CO)_2\}_2(\mu_3,\eta^{1:1:4}\text{-}P_4)(Cp'''Fe)]^+$.[4]

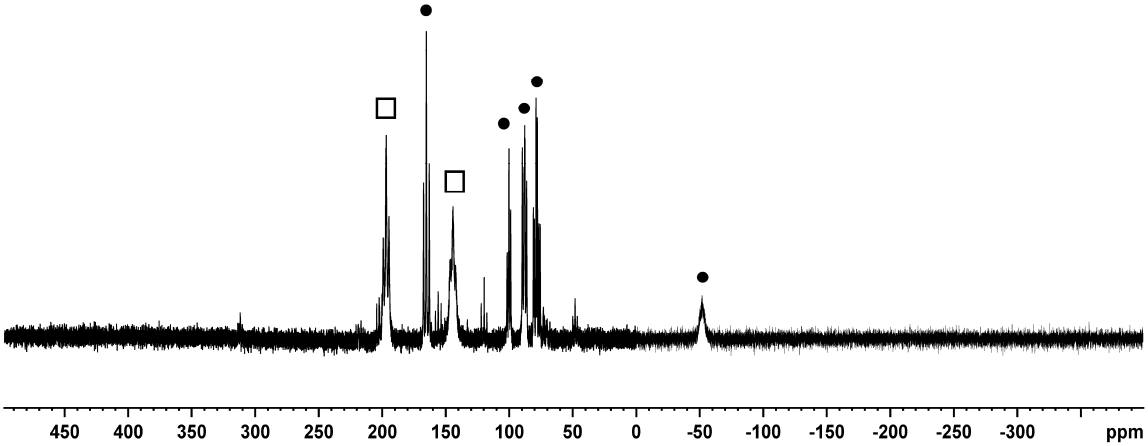

Figure S4.25. CH_3CN washing solution of the reaction of **1** and $[Co(NCCH_3)_6][SbF_6]_2$ in CD_3CN. The signal marked with a square (□) can be assigned to **3** while signals marked with a dot (●) indicate the formation of an unknown side product.

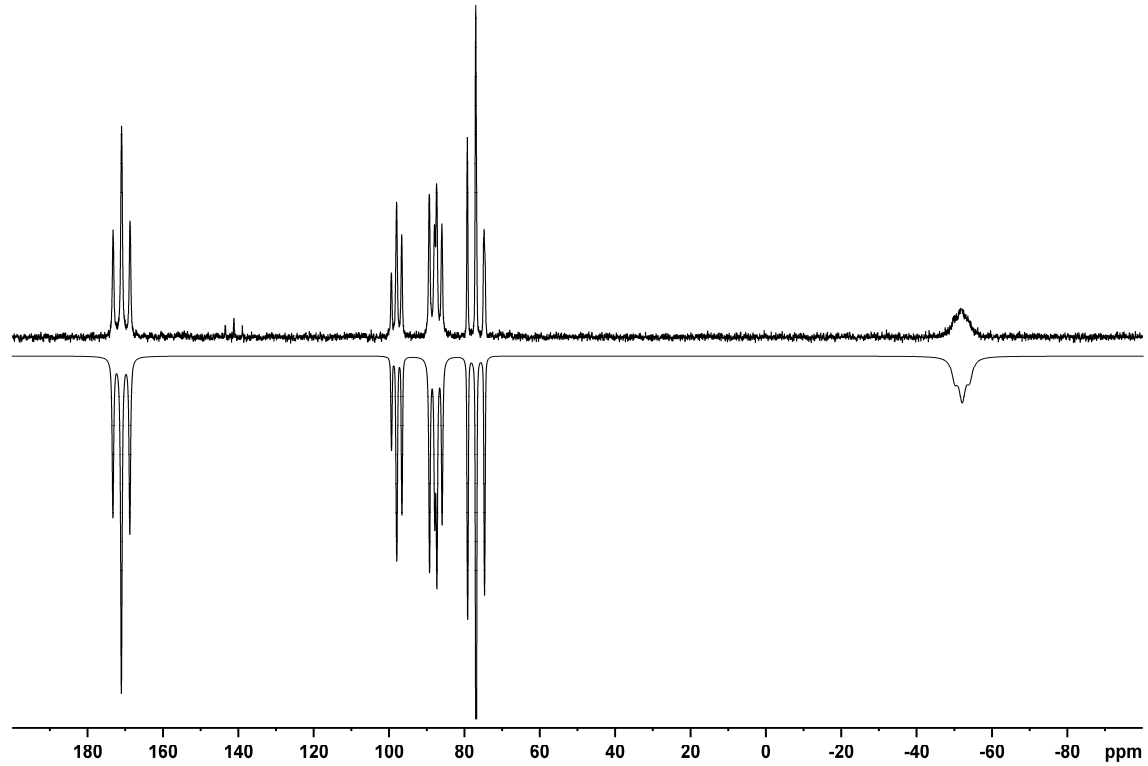

Figure S4.26. Simulated $^{31}P\{^1H\}$ NMR spectrum of the side product marked with a dot (●) in CD_2Cl_2 ($A_2MN_2O_2X$ spin system) (see Figure S4.25).

Table S4.7. Calculated coupling constants of the $A_2MN_2O_2X$ spin system with a R-factor of 1.15%.

Chemical shift [ppm]		Coupling constants [Hz]			
A	171.0	$^2J_{AM}$	11.8	$^2J_{MO}$	20.0
M	97.9	$^2J_{AN}$	17.9	$^2J_{MX}$	17.4
N	87.7	$^1J_{AO}$	363.0	$^2J_{NO}$	20.5
O	77.0	$^2J_{AX}$	16.7	$^1J_{NX}$	318.6
X	–51.9	$^1J_{MN}$	223.4	$^2J_{OX}$	17.5

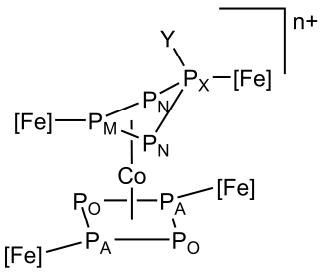

Scheme S4.5. Postulated structure of the byproduct based on the coupling constants obtained by the simulation. The nature of Y is still unclear. However, the formation of a hydroxy species (Y = OH) is very likely.

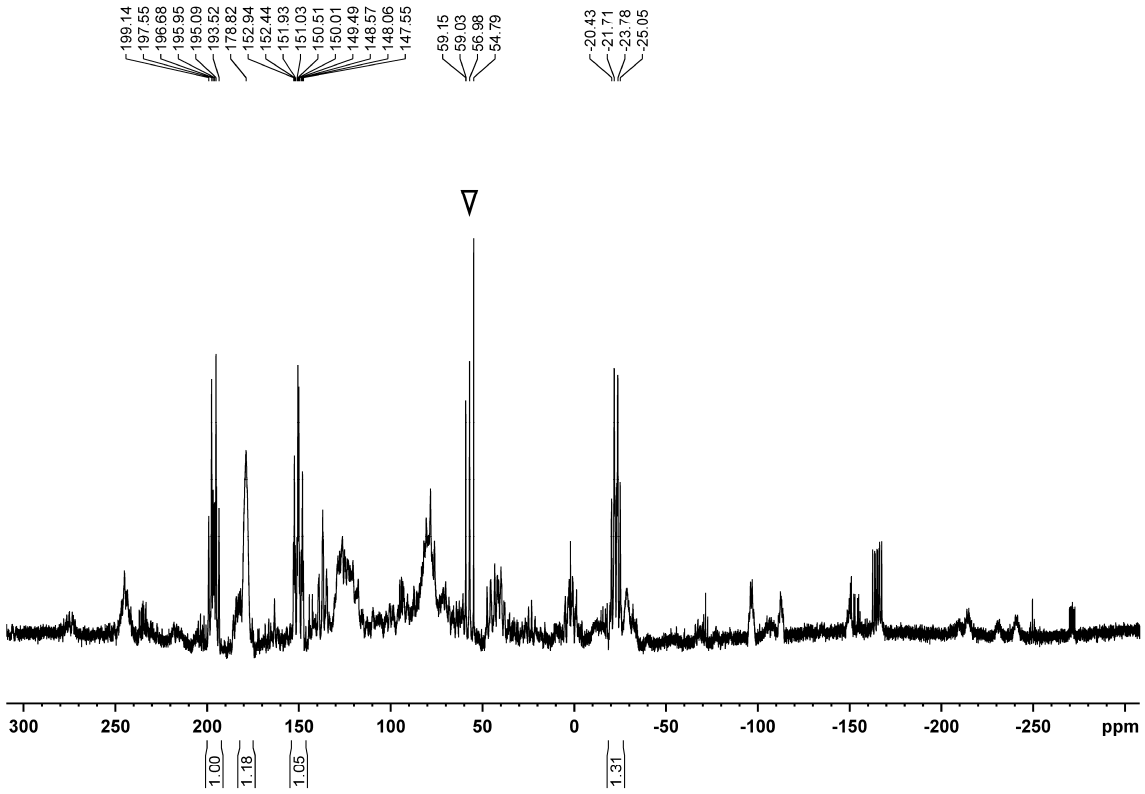

Figure S4.27. Reaction $^{31}P\{^1H\}$ NMR spectrum of the reaction of **1** and $[Ni(NCCH_3)_6][SbF_6]_2$ in CD_2Cl_2. The signal marked with a triangle is part of the signal that can be assigned to the cation of $[\{Cp'''Fe(CO)_2\}_2(\mu_3,\eta^{1:1:4}\text{-}P_4)(Cp'''Fe)]^+$.[4]

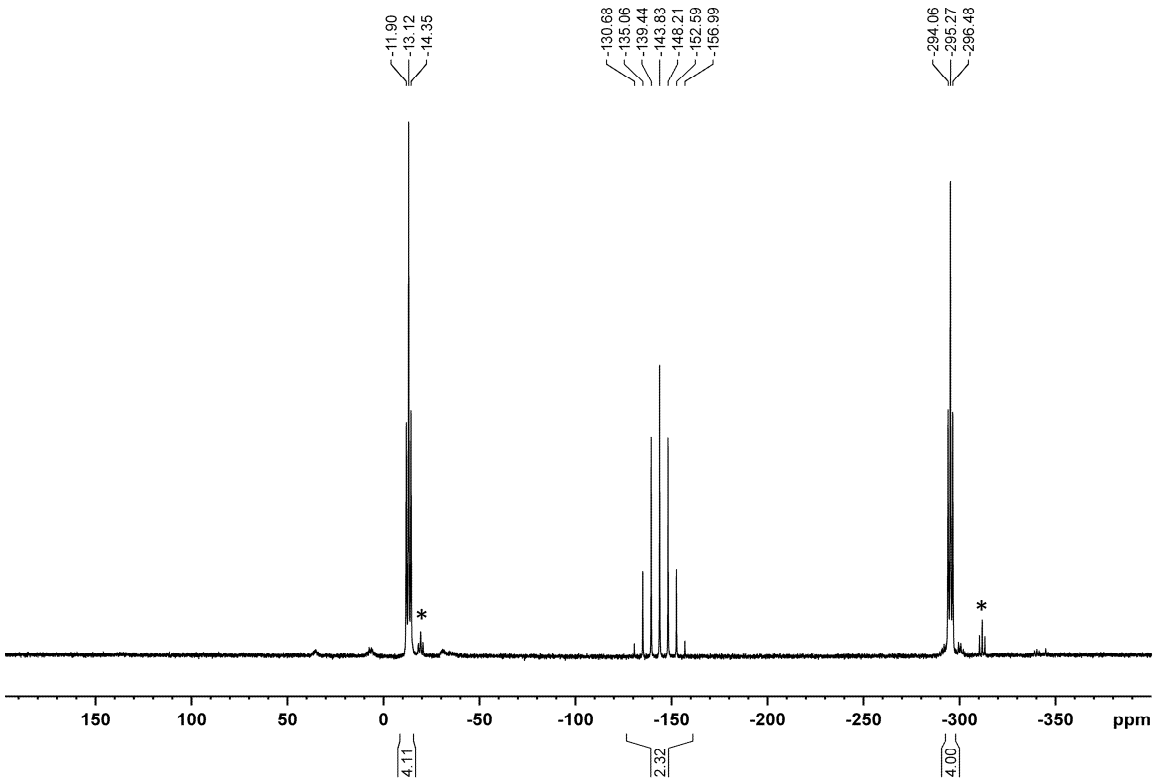

Figure S4.28. $^{31}P\{^1H\}$ NMR spectrum of the reaction solution of **5** in CD_2Cl_2. The marked signals are assigned to the starting material.

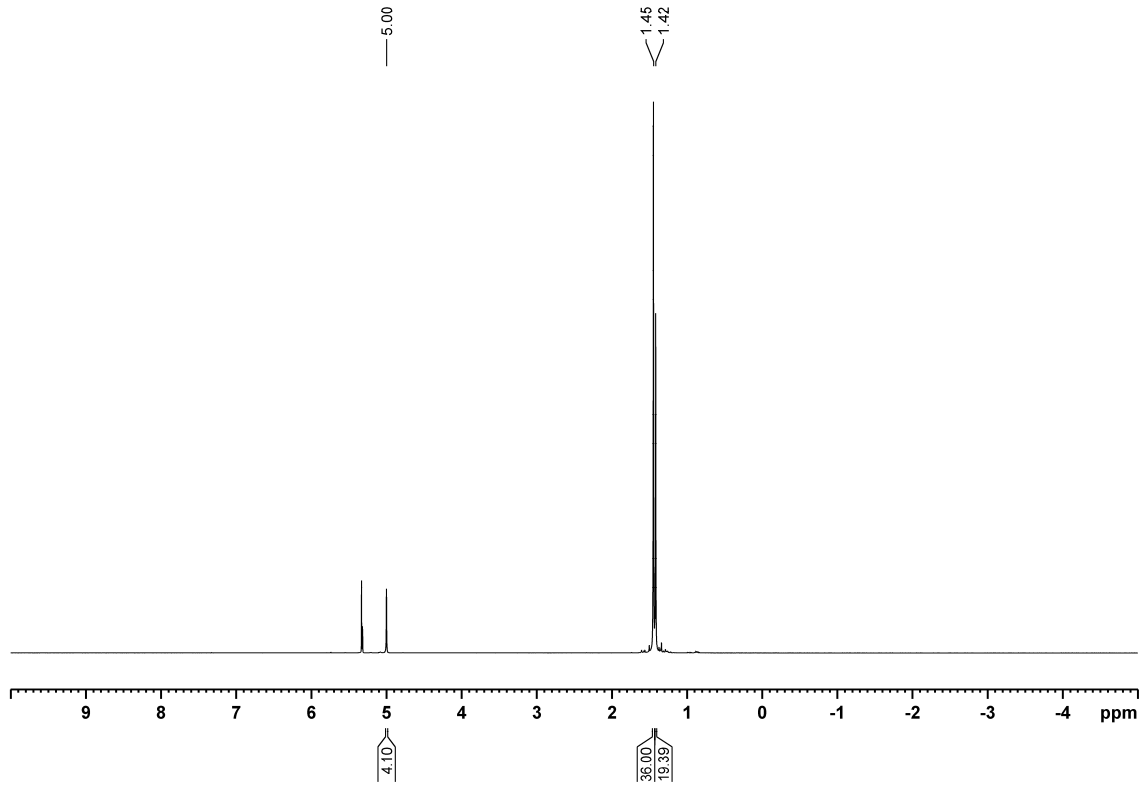

Figure S4.29. ^1H NMR spectrum of **5** in CD_2Cl_2.

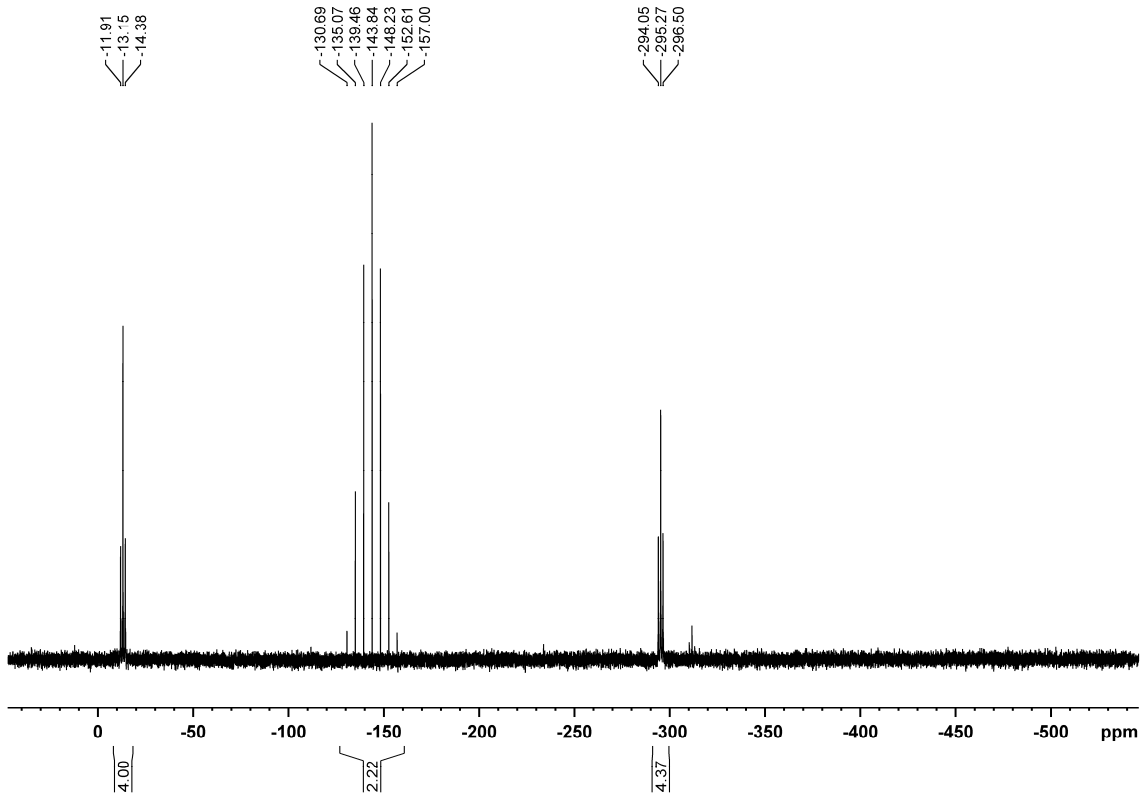

Figure S4.30. $^{31}P\{^{1}H\}$ NMR spectrum of **5** in CD_2Cl_2.

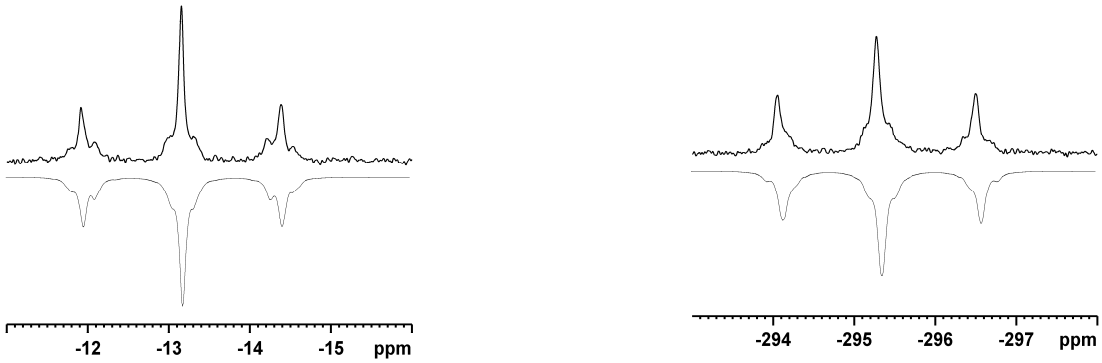

Figure S4.31. Simulated $^{31}P\{^{1}H\}$ NMR spectrum of **5** (AA'A''A'''XX'X''X''' spin system).

Table S4.8. Calculated coupling constants of the cation of **5** (AA'A''A'''XX'X''X''' spin system) with a R-factor of 0.59%.

Chemical shift [ppm]		Coupling constants [Hz]					
AA'A''A'''	295.2	$^{2}J_{AA'}$	36.0	$^{2}J_{A''A'''}$	27.7	$^{2}J_{AA''}$	-25.8
XX'X''X'''	-13.1	$^{1}J_{AX}$	198.8	$^{1}J_{A''X'''}$	199.0	$^{2}J_{AA'''}$	-1.5
		$^{1}J_{A'X}$	197.1	$^{1}J_{A'''X'''}$	198.6	$^{2}J_{AA''}$	-43.3
		$^{1}J_{XX'}$	150.2	$^{1}J_{X''X'''}$	149.5	$^{2}J_{A'A'''}$	-33.4

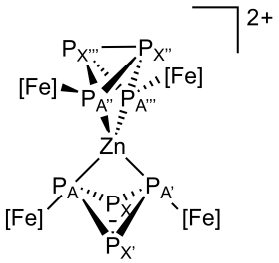

Scheme S4.6. Schematic view of the cation of **5** for the NMR assignment.

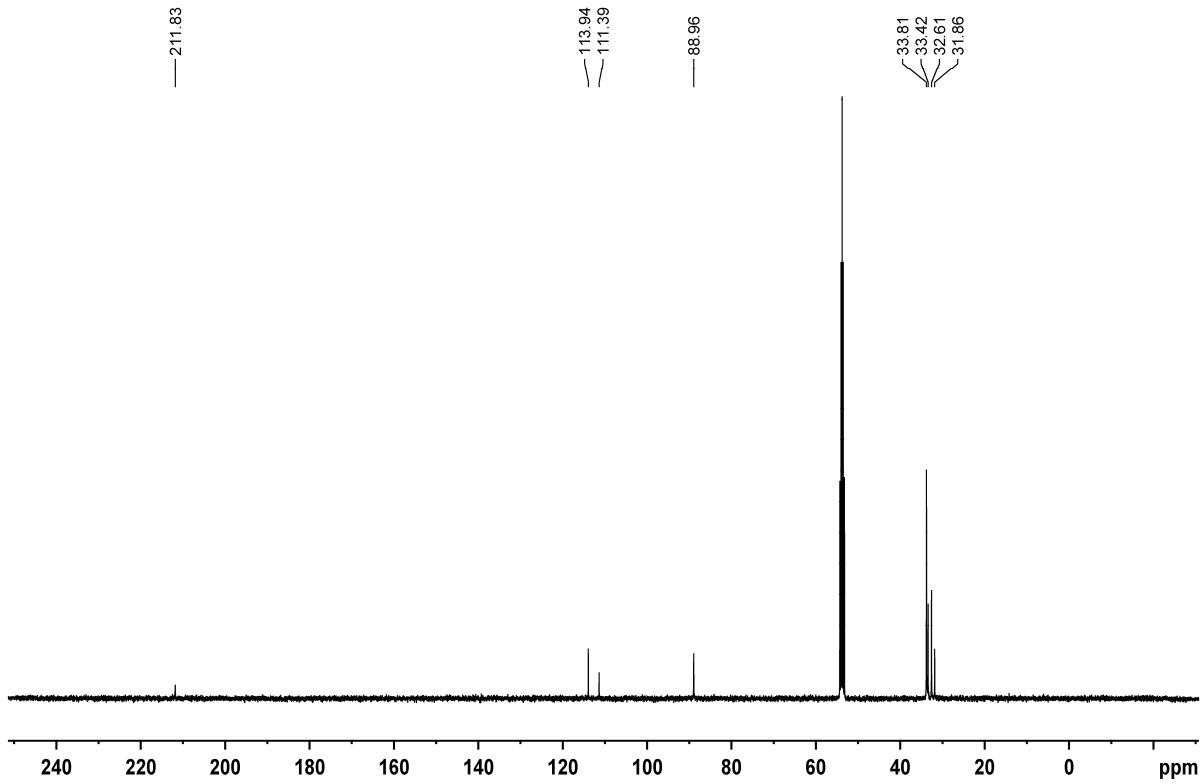

Figure S4.32. $^{13}C\{^1H\}$ NMR spectrum of **5** in CD_2Cl_2.

Magnetic Measurements in Solution (Evans Method)

Magnetic susceptibilities χ_{meas} and effective magnetic moments μ_{eff} of paramagnetic compounds in solution were determined by ^1H NMR spectroscopy using the Evans method[9] with pure solvent as internal reference according to equation[10] (1) and (3). The diamagnetic contributions were considered in equation (2) while χ_{dia} is determined from literature known values that are summarized in [11]. ^1H NMR spectra were recorded on a Bruker Avance III HD 400 (^1H: 400.130 MHz) spectrometer.

Equations:

$$\chi_{meas} = \frac{3 \cdot \Delta f}{1000 \cdot f \cdot c} \qquad (1)$$

$$\chi_{para} = \chi_{meas} - \chi_{dia} \quad (2)$$

$$\mu_{eff} = 798 \cdot \sqrt{T \cdot \chi_{para}} \quad (3)$$

Where

χ_{meas} is the measured molar susceptibility of the sample in $m^3 \cdot mol^{-1}$,

χ_{dia} is the diamagnetic molar susceptibility of the sample in $m^3 \cdot mol^{-1}$,

χ_{para} is the paramagnetic molar susceptibility of the sample in $m^3 \cdot mol^{-1}$,

Δf is the chemical shift difference between solvent in presence of paramagnetic solute and pure solvent in Hz,

f is the operating frequency of NMR spectrometer in Hz,

c is the concentration of paramagnetic sample in $mol \cdot L^{-1}$,

T is the absolute temperature in K, and

μ_{eff} is the effective magnetic moment in μ_B.

Cyclic Voltammetry

General Remarks:

For the cyclic voltammetry measurements, a cell of 5 ml volume was used. The cell was filled with a CH_2Cl_2 solution of 0.01 mmol of the analyte and 750 mg of the conducting salt $[(^nBu)_4N][PF_6]$. The setup contains three electrodes: the working electrode as well as the counter electrodes are each Pt wires, while the reverence electrode is made from Ag wire. Ferrocene was used as an internal standard.

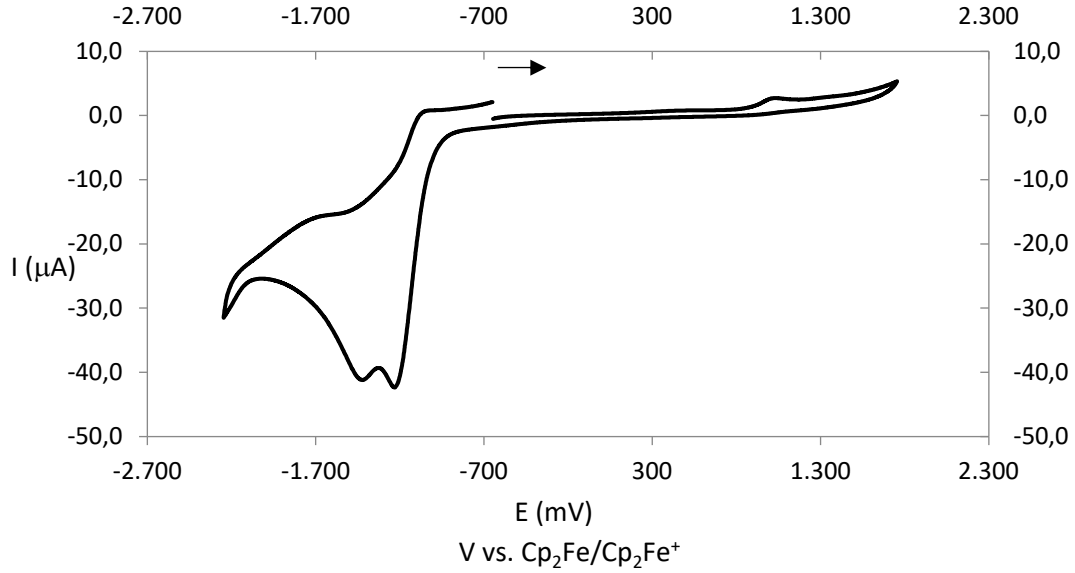

Figure S4.33. Cyclic voltammogram of $[Co(NCCH_3)_6][PF_6]_2$.

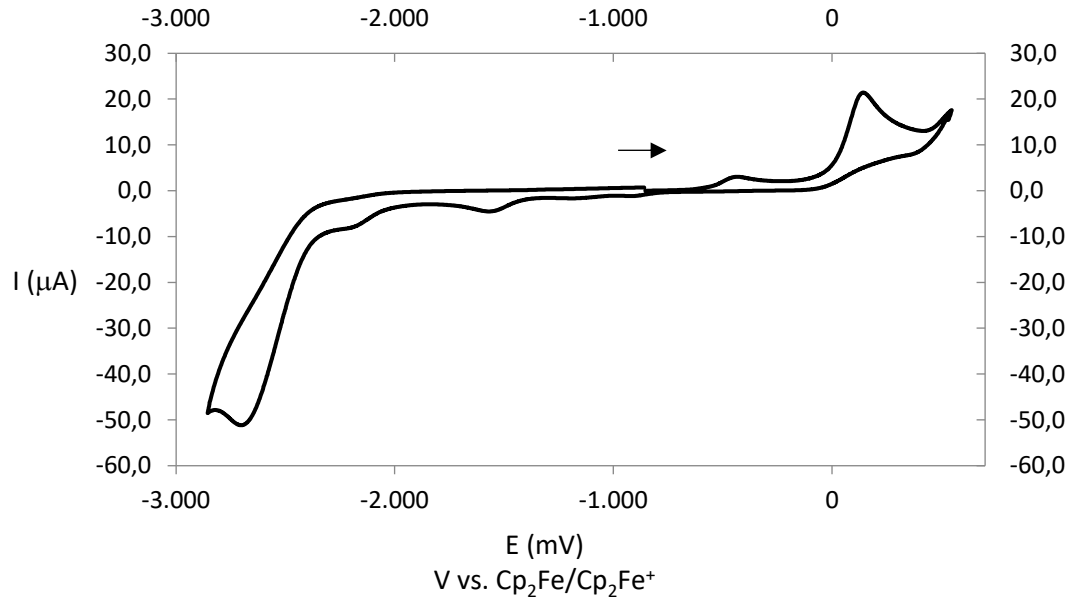

Figure S4.34. Cyclic voltammogram of **1**.

Reference:

[1] C. Schwarzmaier, A. Y. Timoshkin, G. Balázs, M. Scheer, *Angew. Chem. Int. Ed.* **2014**, *53*, 9077.
[2] M. Scheer, G. Balazs, *Präparative Metallorganische Chemie Für Fortgeschritttene*, **2013**.
[3] These signals were mistakenly assigned to $[\{Cp'''Fe(CO)_2\}_2(\mu_3,\eta^{1:1:2}\text{-}P_4)\{Cp'''Fe(CO)\}]^+$ in the previous work.
[4] J. Müller, S. Heinl, C. Schwarzmaier, G. Balázs, M. Keilwerth, K. Meyer, M. Scheer, *Angew. Chem. Int. Ed.* **2017**, *56*, 7312.
[5] *CrysAlisPro Software System*, Agilent Technologies UK Ltd, Yarnton, Oxford, **2014**.
[6] G. Sheldrick, *Acta Crystallographica Section C* **2015**, *71*, 3.
[7] G. M. Sheldrick, *Acta Crystallographica Section A* **2015**, *71*, 3.
[8] O. V. Dolomanov, L. J. Bourhis, R. J. Gildea, J. A. K. Howard, H. Puschmann, *J. Appl. Crystallogr.* **2009**, *42*, 339.
[9] D. F. Evans, *J. Chem. Soc.* **1959**, 2003.
[10] G. J. P. Britovsek, V. C. Gibson, S. K. Spitzmesser, K. P. Tellmann, A. J. P. White, D. J. Williams, *Dalton Trans.* **2002**, 1159.
[11] G. A. Bain, J. F. Berry, *J. Chem. Educ.* **2008**, *85*, 532.

Preface

The following chapter has already been published: The article is reprinted with permission from the Royal Society of Chemistry.

'From a P_4 Butterfly Scaffold to *cyclo*- and *catena*-P_4 Units'

Chem. Commun. ***2021****, 57, 2257*.

Authors

Julian Müller, Gábor Balázs, Manfred Scheer.

Author contribution

J. Müller prepared the manuscript and performed the synthesis and characterization of the herein presented compounds. G. Balázs performed all DFT calculations and contributed the corresponding parts in the manuscript and the Supporting Information. M. Scheer supervised the research and revised the manuscript.

Acknowledgement

This work was supported by the Deutsche Forschungsgemeinschaft (Sche 384/38-1).

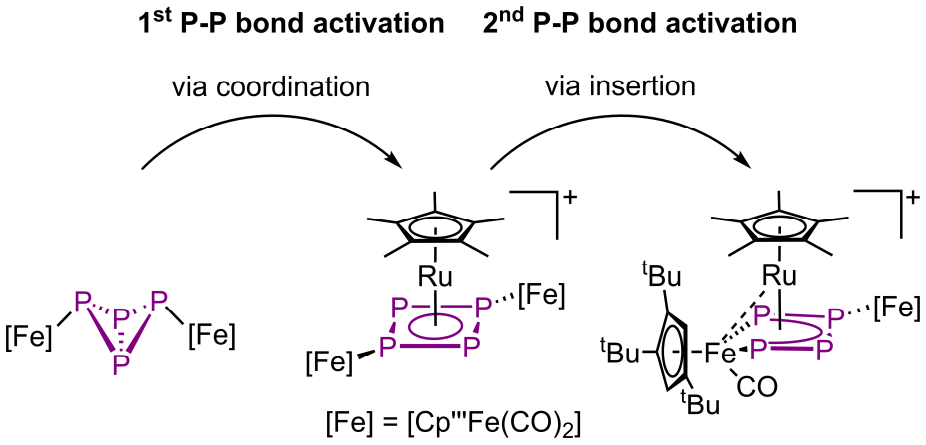
1st P-P bond activation
2nd P-P bond activation
via coordination
via insertion
[Fe]
[Fe]
Ru
[Fe]
[Fe]
+
tBu
Ru
[Fe]
tBu
Fe
CO
tBu
+
[Fe] = [Cp'''Fe(CO)2]

5. From a P_4 Butterfly Scaffold to *cyclo*- and *catena*-P_4 Units

Abstract: *The reactivity of [{Cp'''Fe(CO)$_2$}$_2$(μ,η$^{1:1}$-P$_4$)] (**1**) towards half-sandwich complexes of Ru(II), Rh(III), and Ir(III) is studied. The coordination of these Lewis acids leads to a rearrangement of the P$_4$ butterfly unit to form complexes with either an aromatic cyclo-P$_4$R$_2$ unit (R = Cp'''Fe(CO)$_2$) or a catena-tetraphosphaene entity.*

5.1. Introduction

The activation of small molecules is an active research topic. This research area focuses mainly on inert molecules such as H_2,[1,2] N_2,[1,3] CO_2,[4] and CH_4[1]since their functionalization might be important to solve e.g. energy problems. However, this research area also includes highly reactive compounds such as white phosphorus (P_4) where the focus is to control its reactivity. In industrial applications, P_4 is an important starting material for the synthesis of organophosphorus derivatives. However, their synthesis proceeds via multistep reactions with low atom economic efficiency. To increase the sustainability, a direct and selective functionalization is desired. Therefore, the degradation of tetrahedral P_4 in the presence of reactive main group compounds[5] and transition metal complexes[6] is investigated (Scheme 5.1, left). Typically, harsh reaction conditions are needed to generate these reactive metal species.[7,8–12] In the field of P_4 conversion, work was done by the Scherer group, e.g. by showing that the photolysis of [Cp''Fe(CO)$_2$]$_2$ (Cp'' = η^5-$C_5H_3{}^tBu_2$) in the presence of P_4 leads to [Cp''$_2$Fe$_2$(CO)$_n$P$_4$] (n = 3, 4 type **A**, n = 2 type **B**, n = 1 and n = 0 type **D**) by successive decarbonylation (Scheme 5.1, left).[8] Comparable results were obtained via thermolytic reactions of P_4 with [Cp'''Fe(CO)$_2$]$_2$[9] (Cp''' = η^5-$C_5H_2{}^tBu_3$), [Cp*Co(CO)]$_2$[13] (Cp* = η^5-C_5Me_5) and [Cp*Co(^{i}Pr$_2$Im)(η^2-C_2H_4)][10,14] (^{i}Pr$_2$Im = 1,3-di-isopropylimidazolein-2-ylidene), respectively. The thermolysis of [Cp*Ni(CO)]$_2$ leads to complexes of the type **E**.[15] In molten $GaCl_3$, P_4 can also be converted by in situ generated Ph_2P^+,[12] leading to the insertion of phosphonium cations into several P–P bonds to form cationic $P_4(PPh_2)$ (type **A**), $P_4(PPh_2)_2$ (type **C**) and $P_4(PPh_2)_3$ (type **F**) compounds.

Conversions of P_4 at mild conditions is an overall goal in this chemistry, which can be achieved with coordinative unsaturated complexes,[16,17] like the triple-decker complex [(Cp'''Co)$_2$(μ-C_7H_8)].[18] In solution it dissociates into the 14-valence-electron (VE) fragment [Cp'''Co] and reacts readily with complexes bearing intact tetrahedral P_4 units to *cyclo*-P_4 (type **B**) containing derivatives.[16] On the other hand we showed that the formation of the butterfly complex [{Cp'''Fe(CO)$_2$}$_2$(μ,η$^{1:1}$-P$_4$)][9] (**1**) by the reaction of [Cp'''Fe(CO)$_2$]$_2$ with P_4 does not need thermal activation and already occurs quantitatively at room temperature.[19] The reactivity of **1** is very versatile, since the reaction with PhC≡CPh or P≡C^{t}Bu gives access to triphospholyl- and tetraphospholyl-containing iron complexes.[20] We could also show that **1** has the properties of a chelate ligand (Scheme 5.1, right, coordination type

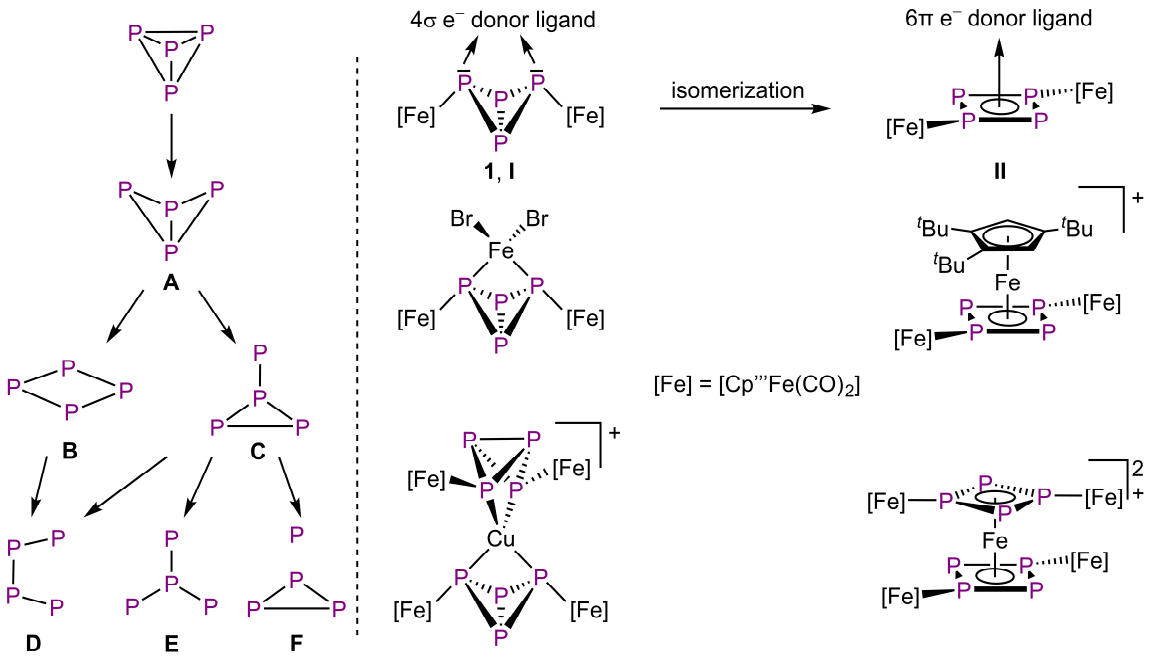

Scheme 5.1. Left: Schematic overview of a first steps of the successive degradation of the P_4 tetrahedron. Charges and lone pairs of electrons are omitted for the sake of simplicity. Right: Donor capabilities of **1** and the resulting complexes.

I).[21–23] Here, the P_4 butterfly scaffold coordinates to various transition metal-based Lewis acids via the two ‘‘wing tip’’ phosphorus atoms. However, in the presence of a d^6 metal Lewis acid like Fe(II) that bears ligands that can easily be substituted, an unusual isomerization of the butterfly unit (4σ e^- donor, coordination type **I**) to an aromatic *cyclo*-P_4R_2 unit (6π e^- donor, R = [Cp’’’Fe(CO)$_2$], coordination type **II**) is observed, giving access to the unique homoleptic octaphosphorus sandwich complex [{(Cp’’’Fe(CO)$_2$)$_2$(μ_3,$\eta^{4:1:1}$-P_4)}$_2$Fe][PF_6]$_2$.[22] To obtain deeper insight into the isomerization reaction of **1**, it was reacted with various 3d metal Lewis acids to give mainly coordination as a chelating ligand, but in one case an isomerization via a redoxreaction to Co(III) occurred.[23] Since the availability of $3d^6$ metal-based Lewis acids like Fe(II) and Co(III) is limited, the question to use 4d and 5d transition metal complexes, which typically yield products with a higher stability, came into mind. This might alter the reaction outcome in general. Herein, we report on the reactivity of **1** towards Ru(II)-, Rh(III)-, and Ir(III)-based Lewis acids, surprisingly leading exclusively to an isomerization to form *cyclo*- and also *catena*-P_4 containing complexes.

5.2. Results and Discussion

A method to generate unsaturated transition metal fragments in solution is to treat the corresponding metal halide precursor with an excess of a thallium(I) salt that bears a weakly coordinating anion to eliminate poorly soluble thallium(I) halides. This was used to generate the solvent-stabilized (CH_3CN or CH_2Cl_2) species ‘‘[CymRu][PF_6]$_2$’’ (Cym = *para*-cymene) and ‘‘[Cp*M][PF_6]$_2$’’ (M = Rh, Ir) in situ. These metal fragments react smoothly

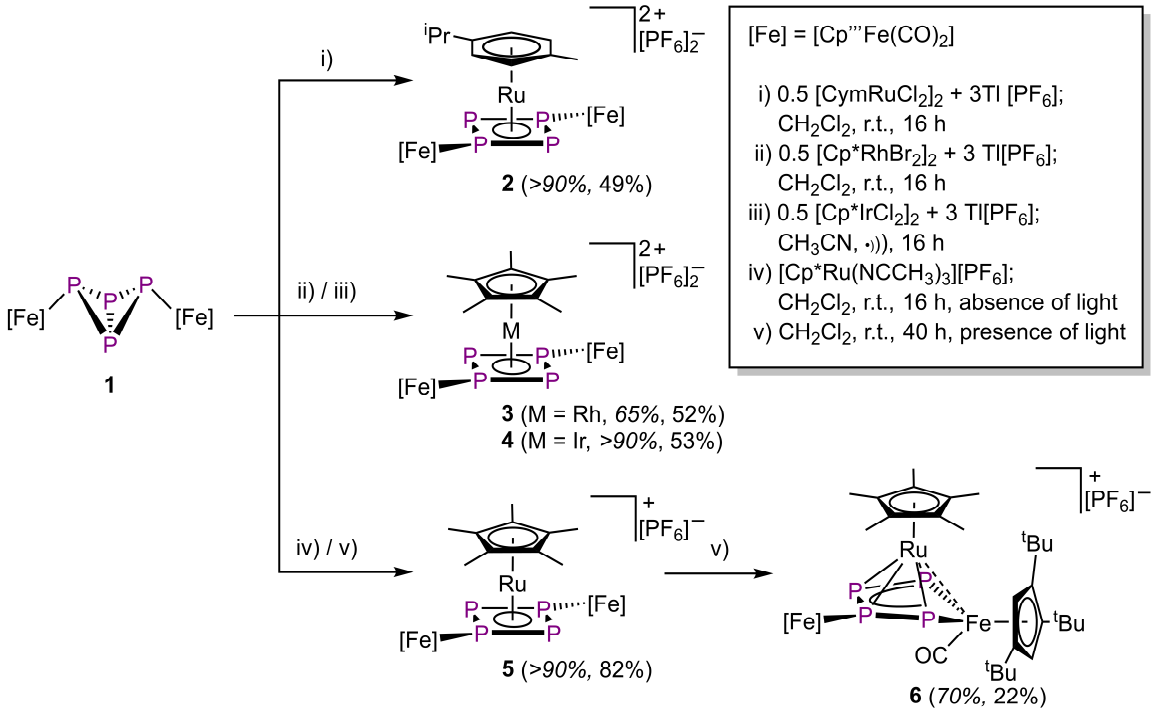

Scheme 5.2. Synthesis of the isomerization products starting from **1**. The yields in italics are based on the ^{31}P NMR spectra of the crude reaction mixture, while the second value refers to the isolated yield.

with **1** leading to $[\{Cp'''Fe(CO)_2\}_2(\mu_3,\eta^{4:1:1}\text{-}P_4)(LM)][PF_6]_2$ (**2**: LM = CymRu; **3**: LM = Cp*Rh; **4**: LM = Cp*Ir; Scheme 5.2). Complexes **2**–**4** feature all *cyclo*-P_4R_2 units that coordinate the central $[LM]^{2+}$ fragments. This finding reveals that the isomerization of the P_4 butterfly moiety (4σ e^- donor, coordination type **I**) to a *cyclo*-P_4R_2 ligand (6π e^- donor, coordination type **II**) is a general feature, not only bound to 3d metals, if the 18 VE rule can be fulfilled and a d^6 metal is present. The molecular structures of **2**–**4** shows, that the central metal atom is coordinated in an η^4 fashion by the *cyclo*-P_4R_2 unit (Figure 5.1). The similar covalent radii of Ru (r_{Ru} = 1.25 Å), Rh (r_{Rh} = 1.25 Å), and Ir (r_{Ir} = 1.22 Å) lead to similar M–$P_{4,cent.}$ distances of 1.8890(2) Å in **2**, 1.8939(3) Å in **3** and 1.8915(2) Å in **4**.[24] Compared to $[\{Cp'''Fe(CO)_2\}_2(\mu_3,\eta^{4:1:1}\text{-}P_4)(Cp'''Fe)][PF_6]$, the distances are approx. 0.13 Å longer

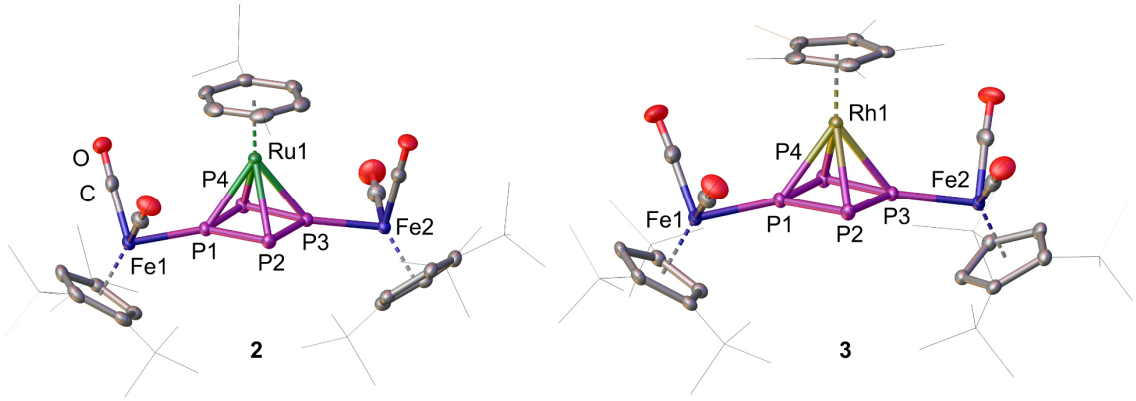

Figure 5.1. Cationic parts of the molecular structures in solid state of **2** and **3**. The structural core of **3** exemplifies the one of **4** as well. Hydrogen atoms are omitted for clarity. A.d.p. are shown at 50% probability level.

(1.7609(5) Å) which is attributed to the smaller covalent radius of Fe (r_{Fe} = 1.16 Å).[22] The P–P bond lengths are with 2.1356(7)–2.1481(7) Å (**2**), 2.1433(8)–2.1459(8) Å (**3**), and 2.1488(6)–2.1518(6) Å (**4**) in the range between a P–P single (2.20–2.25 Å) and a P=P double bond (2.00–2.05 Å). These bond lengths are in good agreement with the determined P–P distances in the isolated *cyclo*-P_4^{2-} anion (2.146(1) and 2.1484(9) Å) in $Cs_2P_4{\cdot}2NH_3$[25] as well as in other complexes with formal P_4^{2-} ligands.[16,22,23,26] The *cyclo*-P_4 units exhibit similar diamond-shaped geometries in all three complexes, which was also found in the other complexes derived from **1**.[22,23]

The ^{1}H NMR spectrum of **2** in CD_2Cl_2 shows two singlets at δ = 1.33 and 1.45 ppm and a multiplet at δ = 5.66 ppm with an integral ratio of 18:36:4 for the two Cp''' ligands. The signals at δ = 1.35, 2.59, and 6.71 ppm can be assigned to the Cym ligand. The ^{1}H NMR spectra of **3** and **4** show similar signals for the Cp''' ligands while the singlet of the Cp* signal can be detected at δ = 2.46 (**3**, CD_2Cl_2) and 2.64 ppm (**4**, CD_3CN), respectively. The ^{31}P{^{1}H} NMR spectra of **2** and **4** show each an AA'XX' spin system for the cation (**2** in CD_2Cl_2: δ = 148.9 and 102.9 ppm; **4** in CD_3CN: δ = 102.3 and 62.7 ppm).‡ The cation of **3** shows two signals at δ = 169.8 and 121.1 ppm that are part of an AA'MM'X spin system (X corresponds to Rh) caused by the NMR-active ^{103}Rh nuclei (*I* = 1/2, 100% natural abundance).‡ However, the ^{31}P{^{1}H} NMR spectrum of the reaction solution of **3** reveals an additional set of signals at δ = 201.7, 157.7 and 125.7 ppm corresponding to a byproduct (AA'MNX spin system, X corresponds to Rh),‡ in a ratio of **3** to the byproduct of approximately 2:1. Despite several attempts, the exact structure of the byproduct could not be clarified yet, but, according to the NMR features, the presence of a *cyclo*-P_4 unit bound to a ^{103}Rh core is very likely.

The reaction of **1** and $[Cp^*Ru(NCCH_3)_3][PF_6]$ in the absence of light yields $[\{Cp'''Fe(CO)_2\}_2(\mu_3,\eta^{4:1:1}\text{-}P_4)(Cp^*Ru)][PF_6]$ (**5**). During this reaction, all acetonitrile ligands are substituted by **1**, while the P_4 core isomerizes to a cyclic P_4 unit. Despite numerous attempts, it was not possible to isolate **5** in crystalline form. However, the ^{31}P{^{1}H} NMR spectrum of **5** in CD_2Cl_2 shows an AA'XX' spin system at δ = 82.0 and 51.6 ppm unambiguously confirms its identity.‡ The chemical shift values as well as the spin system compare well to that found for **2**–**4** and $[\{Cp'''Fe(CO\}_2)_2(\mu_3,\eta^{4:1:1}\text{-}P_4)(Cp'''Fe)][PF_6]$[22,23] (δ = 78.9, 56.8 and 45.6 ppm).

Performing the reaction of **1** with $[Cp^*Ru(NCCH_3)_3][PF_6]$ in the presence of light, a different reaction outcome is observed. Surprisingly, the main product is not **5**, but a subsequent CO elimination, followed by the insertion of the [Cp'''Fe(CO)] fragment into one of the adjacent P–P bonds, leads to $[\{Cp'''Fe(CO)_2\}\{Cp'''Fe(CO)\}(\mu_3,\eta^{4:2:1}\text{-}P_4)(Cp^*Ru)][PF_6]$ (**6**) in moderate yield (22%, 70% according to ^{31}P NMR spectroscopy). Complex **6** features a metallo-tetraphosphaene unit and represents a formally twofold activated P_4 butterfly complex **1**. The formation of **6** also highlights the high diversity in different binding modes

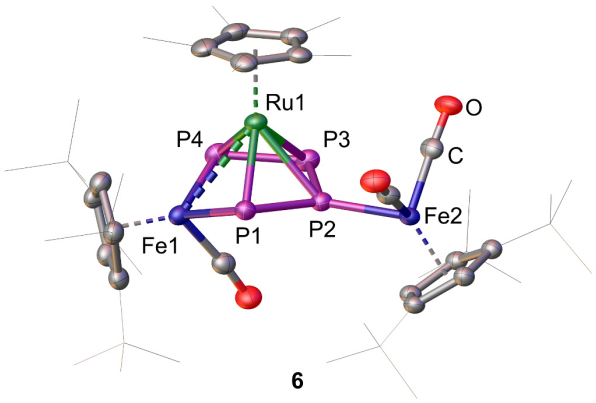

Figure 5.2. Cationic part of the 1*S*-2*R*-3*R*-4*R*-5*S* enantiomer of **6** in the solid state. Hydrogen atoms are omitted for clarity. A.d.p. are shown at 50% probability level.

of the P_4 unit in **1**. Furthermore, **6** should be handled with caution, as further treatment with UV light leads to subsequent transformations and finally to decomposition.

The insertion of Fe1 into the P1–P4 bond leads to the formation of the 1*S*-2*R*-3*R*-4*R*-5*S* configuration (Figure 5.2) while insertion into the P3–P4 bond leads to the formation of the 1*R*-2*S*-3*S*-4*S*-5*R* configuration (Figure S5.5, ESI†). The two enantiomers form a racemate and are both present in the solid state structure. The central FeP_4 metallacycle reveals an envelope conformation with an almost planar *catena*-P_4 unit (dihedral angle P1-P2-P3-P4 of 7.73(3)°). The three Fe–P distances vary from 2.2413(6) to 2.2539(6) Å and are in the range of typical Fe–P single bonds.[21–24] The P–P bond distances vary from 2.1335(8) to 2.1446(8) Å and are in a range between a P–P single and a P=P double bond. The [Cp*Ru] fragment is located over the center of the metallocycle with two shorter Ru–P distances (Ru1–P1: 2.3592(5); Ru1–P4: 2.3513(6) Å) and two longer Ru–P distances (Ru1–P2: 2.4454(5); Ru1–P3: 2.4469(6) Å). This results in a shift of the ruthenium fragment towards the [Cp'''Fe1(CO)] fragment and raises the question of a Ru–Fe interaction. While the Ru1–Fe1 distance of 2.9052(4) Å is longer than a predicted single bond (2.41 Å),[24] the distance is still significantly smaller than the sum of the van der Waals radii (4.90 Å).[27] A complex similar to **6** is for example the dirhodium complex [(Cp$^+$Rh(CO))(μ,η$^{4:2}$-P_4){Cp$^+$Rh}] (**III**, Cp$^+$ = η^5-C_5Me_4Et).[11] Although, **III** has two electrons more than **6**, the P–P bond lengths (2.150(3)–2.160(3) Å) are comparable. However, in **III**, no metal–metal interaction was observed since the η^4-coordinated [Cp$^+$Rh] fragment is located over the center of the P_4 chain. The complex [K(dme)$_2$][(^{Mes}BIAN)Co(μ,η$^{4:2}$-P_4)Ga(nacnac)][28] (**IV**, dme = dimethoxyethane, ^{Mes}BIAN = 1,2-bis(2,4,6-dimethylphenylimino)acenaphthene, nacnac = CH[CMeN(2,6-^{i}Pr$_2$C$_6$H$_3$)]$_2$) exhibits a similar, however main group-based, heteroatomic core, but without significant metal–metal interaction. The bond lengths (2.1198(7)–2.1286(7) Å) are comparable to the ones in **6**. A similar carbon-based complex is [{CpFe(CO)}{μ,μ$^{4:2}$-(CR-(CH)$_2$-CR)}(Cp*Ru)] (R = CMe$_2$OH) where the [Cp*Ru] fragment is η^5-coordinated by the cyclopentadiene ring of iron.[29] The reported Ru–Fe distances of

2.6688(7)/2.6743(7) Å are shorter compared to the one in **6** and are described as Ru–Fe single bonds.

The ^{1}H NMR as well as the $^{31}P\{^1H\}$ NMR spectrum (CD_2Cl_2) of a crystalline sample of **6** points to the presence of two conformers in solution which are formed in a ratio of 1:1.7. At room temperature, both conformers are involved in dynamic processes leading to signal broadening. This is most likely caused by the rotation of either one of the Cp''' ligands or the whole [Cp'''Fe$(CO)_2$] fragment. At lower temperatures, the rotation is slowed down resulting in sharp signals.‡ The $^{31}P\{^1H\}$ NMR spectrum shows an AMXY spin system for both isomers which resonate at similar chemical shifts so that they mainly overlap. The signals at δ = 501.1, 465.5, 144.1 and 126.0 ppm can be assigned to the main species while the signals at δ = 500.9, 457.0, 145.2 and 126.5 ppm correspond to the minor species. With chemical shifts and coupling constants (Table S5.7, ESI†) being almost identical, the structure of the two species must be very similar.‡ However, these findings compare well to [(Cp''Fe)(μ,$\eta^{5:2}$-P_4){Cp''Fe(CO)}][8] (δ = 567.2 and 169.1 ppm) and **IV**[28] (δ = 74.0 and 125.4 ppm) showing both an AA'XX' spin system for the *catena*-P_4 unit. The dirhodium complex **III**[11] (δ= 201.4 and 150.8 ppm) reveals an AA'NMXX' spin system (N and M correspond to Rh).

To obtain deeper insight into the electronic structure of **6**, DFT calculations at the BP86/def2-TZVP level were performed which show the absence of a direct Ru1–Fe1 bond. Instead, a multi-center bond with bond contributions of Ru1 = 40%, Fe1 = 25% and P1 = P4 = 17.5% is present. The Wiberg Bond Index of the Ru1–Fe1 bond of only 0.32 is in good agreement with the multi-center bond description. The corresponding localized molecular orbital, which contains 41% Ru, 24% Fe and 35% P atomic orbital contribution,

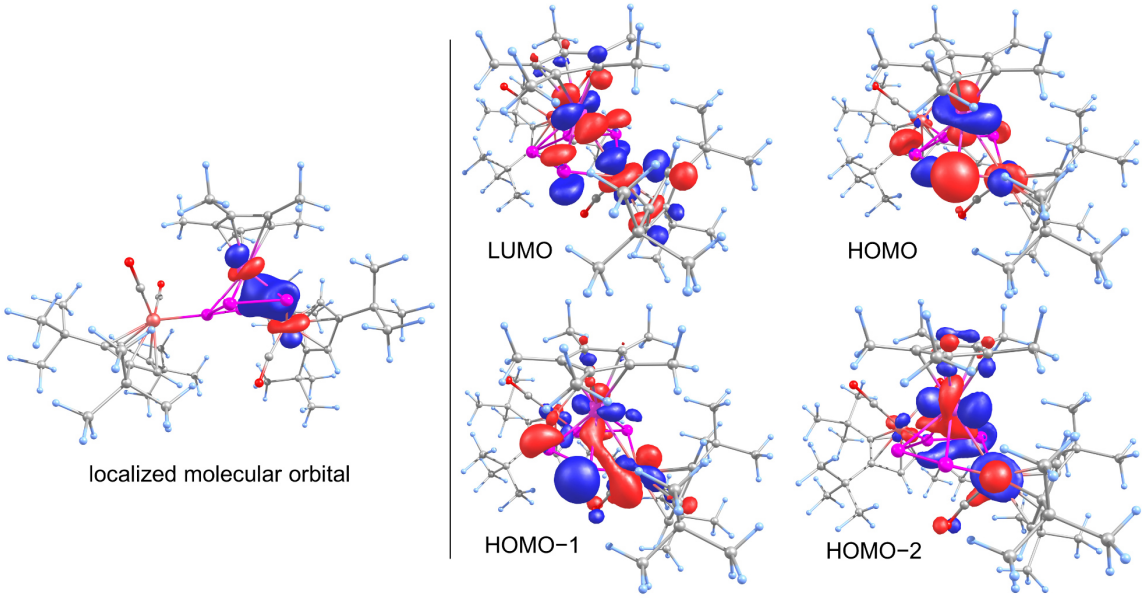

Figure 5.3. Left: The localized molecular orbital of **6** showing the interaction between Ru, Fe and P. Right: Frontier orbitals in **6** at the BP86/def2-TZVP level.

is depicted in Figure 5.3 (left). We could not locate a bond-critical point between Ru and Fe1 by the analysis of the topology of the electron density of **6** by means of the Atoms in Molecules (AIM) approach. However, a ring-critical point could be detected, situated in the plane spanned by Ru, Fe1, P1 and P4. The frontier orbitals in **6** are depicted on the right hand side in Figure 5.3. The highest occupied molecular orbital (HOMO) shows mainly the lone pairs of the phosphorus atoms while both HOMO−1 and HOMO−2 show mainly bonding interaction within the P_4Fe unit. The lowest unoccupied molecular orbital (LUMO) shows mainly nonbonding orbitals at the phosphorus as well as the metal atoms.

Furthermore, we were interested in why **5** transforms into **6**, while the transformation from **2** to the hypothetical complex $[\{Cp'''Fe(CO)_2\}\{Cp'''Fe(CO)\}(\mu_3,\eta^{4:2:1}\text{-}P_4)(CymRu)]^{2+}$ (**7**) is not observed under the same conditions. Therefore, we determined the natural charge distribution of the four complexes.‡ According to this, the $[CymRu]^{2+}$ fragments act as weak electron acceptors, while $[Cp^*Ru]^+$ act as strong electron acceptors. In contrast, the *cyclo*-P_4R_2 (R = $Cp'''Fe(CO)_2$) units in **2** and **5** act as strong electron donors. During the transformation from *cyclo*-P_4R_2 units to *catena*-P_4 units, this effect is even enhanced. Therefore, it is suggested that the further transformation is dependent on the nature of the ligands that are attached to the central Lewis acid.

The disfavored formation of **7** in comparison to **6** is also highlighted by the calculated reaction energies at the B3LYP level (solvation effects incorporated by the COSMO model). The calculations showed that the formation of **6** starting from **5** is endothermic by 95.87 kJ/mol. However, these calculations do not take into account the terms of entropy which should have a mayor impact due to the release of CO gas during this process. The formation of **7** starting from **2** would be endothermic by 150.87 kJ/mol which shows that, in principle, the formation of **6** in comparison to **7** would be energetically less disfavored.

5.3. Conclusion

In summary, we could show that the P_4 butterfly complex **1** can easily be activated by a vast variety of different d^6 metal-based Lewis acids, leading to the formation of **2**–**5** bearing *cyclo*-P_4R_2 units. However, by using $[Cp^*Ru(NCCH_3)_3][PF_6]$ in the presence of light **6** is formed. Complex **6** exhibits an irontetraphosphaene unit which is formed via CO elimination and the subsequent insertion of the iron fragment into a P–P bond. However, this second activation step is not observed for complexes **2**–**4** under the same reaction conditions. DFT calculations confirmed that the transformation is strongly dependent on the nature of the ligand at the Lewis acid. The formation of different complexes under mild conditions highlights the high diversity of binding modes of the P_4 unit in **1**.

5.4. Reference

‡ See ESI† for further information.

[1] C. Chow, M. Taoufik, E. A. Quadrelli, *Eur. J. Inorg. Chem.* **2011**, *2011*, 1349.
[2] a) D. W. Stephan, *Dalton Trans.* **2009**, 3129; b) G. C. Welch, R. R. S. Juan, J. D. Masuda, D. W. Stephan, *Science* **2006**, *314*, 1124.
[3] a) D. M. Ermert, L. J. Murray, *Dalton Trans.* **2016**, *45*, 14499; b) N. Hazari, *Chem. Soc. Rev.* **2010**, *39*, 4044.
[4] a) M. Behrens, *Angew. Chem. Int. Ed.* **2014**, *53*, 12022; b) V. P. Indrakanti, J. D. Kubicki, H. H. Schobert, *Energy & Environmental Science* **2009**, *2*, 745.
[5] a) M. Scheer, G. Balázs, A. Seitz, *Chem. Rev.* **2010**, *110*, 4236; b) N. A. Giffin, J. D. Masuda, *Coord. Chem. Rev.* **2011**, *255*, 1342.
[6] a) B. M. Cossairt, N. A. Piro, C. C. Cummins, *Chem. Rev.* **2010**, *110*, 4164; b) M. Caporali, L. Gonsalvi, A. Rossin, M. Peruzzini, *Chem. Rev.* **2010**, *110*, 4178.
[7] a) S. Heinl, A. Y. Timoshkin, J. Müller, M. Scheer, *Chem. Commun.* **2018**, *54*, 2244; b) M. Scheer, K. Schuster, U. Becker, *Phosphorus Sulfur Silicon Relat. Elem.* **1996**, *109*, 141.
[8] O. J. Scherer, G. Schwarz, G. Wolmershäuser, *Z. Anorg. Allg. Chem.* **1996**, *622*, 951.
[9] O. J. Scherer, T. Hilt, G. Wolmershäuser, *Organometallics* **1998**, *17*, 4110.
[10] S. Dürr, D. Ertler, U. Radius, *Inorg. Chem.* **2012**, *51*, 3904.
[11] O. J. Scherer, M. Swarowsky, H. Swarowsky, G. Wolmershäuser, *Angew. Chem. Int. Ed.* **1988**, *27*, 694.
[12] J. J. Weigand, M. Holthausen, R. Fröhlich, *Angew. Chem. Int. Ed.* **2009**, *48*, 295.
[13] O. J. Scherer, M. Swarowsky, G. Wolmershaeuser, *Organometallics* **1989**, *8*, 841.
[14] B. Zarzycki, F. M. Bickelhaupt, U. Radius, *Dalton Trans.* **2013**, *42*, 7468.
[15] O. J. Scherer, T. Dave, J. Braun, G. Wolmershäuser, *J. Organomet. Chem.* **1988**, *350*, C20-C24.
[16] M. Modl, S. Heinl, G. Balázs, F. Delgado Calvo, M. Caporali, G. Manca, M. Keilwerth, K. Meyer, M. Peruzzini, M. Scheer, *Chem. Eur. J.* **2019**, *25*, 6300.
[17] a) D. Yakhvarov, P. Barbaro, L. Gonsalvi, S. Mañas Carpio, S. Midollini, A. Orlandini, M. Peruzzini, O. Sinyashin, F. Zanobini, *Angew. Chem. Int. Ed.* **2006**, *45*, 4182; b) M. Di Vaira, M. P. Ehses, M. Peruzzini, P. Stoppioni, *Eur. J. Inorg. Chem.* **2000**, *2000*, 2193; c) A. P. Ginsberg, W. E. Lindsell, *J. Am. Chem. Soc.* **1971**, *93*, 2082.
[18] J. J. Schneider, D. Wolf, C. Janiak, O. Heinemann, J. Rust, C. Krüger, *Chem. Eur. J.* **1998**, *4*, 1982.
[19] C. Schwarzmaier, A. Y. Timoshkin, G. Balázs, M. Scheer, *Angew. Chem. Int. Ed.* **2014**, *53*, 9077.
[20] a) O. J. Scherer, T. Hilt, G. Wolmershäuser, *Angew. Chem. Int. Ed.* **2000**, *39*, 1425; b) M. Scheer, S. Deng, O. J. Scherer, M. Sierka, *Angew. Chem. Int. Ed.* **2005**, *44*, 3755.
[21] C. Schwarzmaier, S. Heinl, G. Balázs, M. Scheer, *Angew. Chem. Int. Ed.* **2015**, *54*, 13116.
[22] J. Müller, S. Heinl, C. Schwarzmaier, G. Balázs, M. Keilwerth, K. Meyer, M. Scheer, *Angew. Chem. Int. Ed.* **2017**, *56*, 7312.
[23] J. Müller, M. Scheer, *Chem. Eur. J.* **2021**, *27*, 3675.
[24] P. Pyykkö, M. Atsumi, *Chem. Eur. J.* **2009**, *15*, 186.
[25] F. Kraus, J. C. Aschenbrenner, N. Korber, *Angew. Chem. Int. Ed.* **2003**, *42*, 4030.
[26] a) A. Cavaillé, N. Saffon‐Merceron, N. Nebra, M. Fustier‐Boutignon, N. Mézailles, *Angew. Chem. Int. Ed.* **2018**, *57*, 1874; b) U. Chakraborty, J. Leitl, B. Muhldorf, M. Bodensteiner, S. Pelties, R. Wolf, *Dalton Trans.* **2018**, *47*, 3693; c) F. Dielmann, A. Timoshkin, M. Piesch, G. Balázs, M. Scheer, *Angew. Chem. Int. Ed.* **2017**, *56*, 1671; d) M. Piesch, S. Reichl, M. Seidl, G. Balázs, M. Scheer, *Angew. Chem. Int. Ed.* **2019**, *58*, 16563; e) O. J. Scherer, R. Winter, G. Wolmershäuser, *Z. Anorg. Allg. Chem.* **1993**, *619*, 827.
[27] S. Alvarez, *Dalton Trans.* **2013**, *42*, 8617.
[28] C. G. P. Ziegler, T. M. Maier, S. Pelties, C. Taube, F. Hennersdorf, A. W. Ehlers, J. J. Weigand, R. Wolf, *Chem. Sci.* **2019**, *10*, 1302.
[29] J. N. L. Dennett, S. A. R. Knox, K. M. Anderson, J. P. H. Charmant, A. G. Orpen, *Dalton Trans.* **2005**, 63.

5.5. Supporting Information

Synthesis and Characterization

General Remarks:

All manipulations were performed with rigorous exclusion of oxygen and moisture using Schlenk-type glassware on a dual manifold Schlenk line with Argon inert gas or glove box filled with N_2 or Ar containing a high-capacity recirculator (<0.1 ppm O_2). All solvents except were dried using a MB SPS-800 device of company MBRAUN, degassed and saturated with argon. Mass spectrometry was performed using a Waters Micromass LCT (ESI-MS) and a Jeol AccuTOF GCX (LIFDI-MS), respectively. Elemental analysis (CHN) was determined using a Vario micro cube. Infrared spectroscopy was performed using a Thermo Scientific Nicolet iS5. spectrometer.

$Tl[PF_6]$ (97%) was purchased by abcr and was used without further purification. Compound $[\{Cp'''Fe(CO)_2\}_2(\mu,\eta^{1:1}\text{-}P_4)]$[1] (**1**) and $[Cp^*Ru(NCCH_3)_3][PF_6]$[2] were synthesized according to literature known procedures.

Synthesis of $[\{Cp'''Fe(CO)_2\}_2(\mu_3,\eta^{4:1:1}\text{-}P_4)\{CymRu\}][PF_6]_2$ (2)

The reaction is best performed in the absence of light. Although the ^{31}P NMR spectra of the reaction mixtures (with light and without light) are comparable, crystallization works much better when light is excluded.

0.100 g of compound **1** (0.123 mmol, 1eq), 0.038 g of $[CymRuCl_2]_2$ (0.061 mmol, 0.5eq) and 0.129 g $Tl[PF_6]$ (0.368 mmol, 3eq) are suspended in 20 ml CH_2Cl_2. The mixture is stirred for 16 h at room temperature during which an off-white precipitate is formed. The suspension is filtered over diatomaceous earth to give a dark yellow solution. Crystals of **2** can be obtained by layering a CH_2Cl_2 solution under pentane.

Yield: 0.080 g (0,060 mmol, 49%)

Analytical data of **2**:

NMR (CD_2Cl_2, 298 K)	^1H: δ [ppm] = 1.33 (s,18, -($C_4\underline{H}_9$)), 1.35 (d, $^3J_{HH}$ = 6.93 Hz, 6H, $MeC_6H_4CH(C\underline{H}_3)_2$) 1.45 (s, 36H, -($C_4\underline{H}_9$)$_2$), 2.59 (s, 3H, $C\underline{H}_3C_6H_4{}^iPr$), 2.84 (sept, $^3J_{HH}$ = 6.90 Hz, 1H, $MeC_6H_4C\underline{H}(CH_3)_2$), 5.66 (m, 4H, $C_5\underline{H}_2{}^tBu_3$). 6.71 (m, 4H, $MeC_6\underline{H}_4{}^iPr$).
	$^{31}P\{^1H\}$: δ [ppm] = 148.9 (m, 2P), 102.9 (m, 2P), –143.7 (sept. 2P, $^1J_{PF}$ = 710 Hz).

	Coupling constants of the cation are summarized in Table S5.2.
IR (CH_2Cl_2)	$\tilde{\nu}$ [cm^{-1}] = 2037.4 (s), 1997.3 (vs)
Elemental analysis ($C_{48}H_{72}F_{12}Fe_2O_4P_6Ru \cdot (C_5H_{12})_{0.2}$)	Calculated: C 43.46, H 5.54 Found: C 43.38, H 5.24.
Mass spectrometry (ESI, CH_3CN)	m/z: 1208.2 (< 1%) [M +PF_6 – CO + $NCCH_3$]$^+$, 1195.2 (3%) [M + PF_6]$^+$, 705.1 (22%) [M – Cp'''Fe$(CO)_2$]$^+$, 525.1 (100%) [M]$^{2+}$, 399.2 (6%) [Cp'''Fe$(CO)(NCCH_3)_2$]$^+$, 386.2 (46%) [Cp'''Fe$(CO)_2(NCCH_3)$]$^+$, 373.1 (8%) [Cp'''Fe$(CO)_3$]$^+$, 358.2 (20%) [Cp'''Fe$(CO)(NCCH_3)$]$^+$, 345.1 (6%) [Cp'''Fe$(CO)_2$]$^+$, 330.2 (60%) [Cp'''Fe$(NCCH_3)$]$^+$, 317.2 (2%) [Cp'''Fe(CO)]$^+$, 289.2 (2%) [Cp'''Fe]$^+$, 144.8 [PF_6]$^-$.

Synthesis of [{Cp'''Fe$(CO)_2$}$_2$(μ_3,$\eta^{4:1:1}$-P_4)(Cp*Rh)][PF_6]$_2$ (3)

0.100 g of compound 1 (0.123 mmol, 1eq), 0.054 g of [Cp*$RhBr_2$]$_2$ (0.068 mmol, 0.55eq) and 0.129 mg Tl[PF_6] (0.368 mg, 3eq) are suspended in 10 ml of CH_2Cl_2 and stirred for 16 h at room temperature. The mixture is filtered over diatomaceous earth and the solvent of the filtrate is removed in vacuo to give **3** as a dark orange powder. Crystals of **3** are obtained by layering a CH_2Cl_2 solution under hexane.

Yield: 0.086g (0,064 mmol, 52%)

Analytical data of **3**:

NMR (CD_2Cl_2, 298 K)	^{1}H: δ [ppm] = 1.36 (s,18H, -($C_4\underline{H}_9$)), 1.48 (s, 36H, -($C_4\underline{H}_9$)$_2$), 2.46 (s, 15H, $C_5(C\underline{H}_3)_5$) 5.73 (m, 4H, $C_5\underline{H}_2{}^t$Bu$_3$). ^{31}P{^{1}H}: δ [ppm] = 129.8 (m, 2P), 121.1 (m, 2P), –143.7 (sept. 2P, $^1J_{PF}$ = 711 Hz). Coupling constants of the cation are summarized in Table S5.3.
IR (CH_2Cl_2)	$\tilde{\nu}$ [cm^{-1}] = 2004 (vs), 2042 (vs)
Elemental analysis ($C_{48}H_{73}F_{12}Fe_2O_4P_6Rh \cdot (CH_2Cl_2)_2$)	Calculated: C 39.71, H 5.13 Found: C 40.27, H 4.99.
Mass spectrometry (ESI, CH_3CN)	m/z: 1197.2 (5%) [M + PF_6]$^+$, 707.1 (100%) [M – Cp'''Fe$(CO)_2$]$^+$, 526.1 (51%) [M]$^{2+}$, 386.2 (86%) [Cp'''Fe$(CO)_2(NCCH_3)$]$^+$, 358.2 (11%) [Cp'''Fe$(CO)(NCCH_3)$]$^+$, 345.1 (7%) [Cp'''Fe$(CO)_2$]$^+$, 330.2 (23%) [Cp'''Fe$(NCCH_3)$]$^+$, 317.2 (1%) [Cp'''Fe(CO)]$^+$, 144.8 [PF_6]$^-$.

Analytical data of the side product:

NMR (CD_2Cl_2, 298 K)	$^{31}P\{^1H\}$: δ [ppm] = 201.7 (m, 2P), 157.7 (m, 1P), 125.7 (m, 1P,). Coupling constants are summarized in Table S5.4.

Synthesis of [{Cp'''Fe(CO)$_2$}$_2$(μ$_3$,η$^{4:1:1}$-P$_4$)(Cp*Ir)][PF$_6$]$_2$ (4)

0.100 g of compound **1** (0.123 mmol, 1eq), 0.049 g of $[Cp^*IrCl_2]_2$ (0.061 mmol, 0.5eq) and 0.129 g Tl[PF_6] (0.368 mmol, 3eq) are transferred to a Young-tube and suspended in 20 ml CH_3CN. The mixture is treated in the ultrasonic bath for 16 h during which an off-white precipitate is formed. After evaporating the solvent, the residue is washed several times with thf which was rejected afterwards. The remaining residue is taken up in CH_2Cl_2 and filtered over diatomaceous earth. Evaporation of the solvent gives analytically pure **4** as a dark yellow powder. Crystals of **4** can be obtained by layering a CH_2Cl_2 solution under hexane.

Yield: 0.093g (0,065 mmol, 53%)

Analytical data of **4**:

NMR (CD_3CN, 298 K)	^1H: δ [ppm] = 1.35 (s,18H, -($C_4\underline{H}_9$)), 1.46 (s, 36H, -($C_4\underline{H}_9$)$_2$), 2.64 (s, 15H, $C_5(C\underline{H}_3)_5$) 5.79 (m br, 4H, $C_5\underline{H}_2{}^tBu_3$). $^{31}P\{^1H\}$: δ [ppm] = 62.2 (m, 2P), 102.3 (m, 2P), –143.7 (sept. 2P, $^1J_{PF}$ = 706 Hz). Coupling constants of the cation are summarized in Table S5.5.
NMR (CD_2Cl_2, 298 K)	$^{31}P\{^1H\}$: δ [ppm] = 60.5 (m, 2P), 107.1 (m, 2P), –143.6 (sept. 2P, $^1J_{PF}$ = 706 Hz).
IR (CH_2Cl_2)	$\tilde{\nu}$ [cm^{-1}] = 2003 (vs), 2041 (vs)
Elemental analysis ($C_{48}H_{73}F_{12}Fe_2O_4P_6Ir\cdot(CH_2Cl_2)_{2.5}$)	Calculated: C 36.89, H 4.78 Found: C 37.23, H 4.54.
Mass spectrometry (ESI, CH_3CN)	m/z: 1287.3 (1%) $[M+PF_6]^+$,797.2 (22%) $[M – (Cp'''Fe(CO)_2)]^+$, 571.1 (100%) $[M]^{2+}$, 399.4 (15%) $[Cp'''Fe(CO)(NCCH_3)_2]^+$, 387.4 (21%) $[Cp'''Fe(CO)_2(NCCH_3)]^+$, 358.4 (14%) $[Cp'''Fe(CO)(NCCH_3)]^+$

Synthesis of [{Cp'''Fe(CO)$_2$}$_2$(μ$_3$,η$^{4:1:1}$-P$_4$)(Cp*Ru)][PF$_6$] (5)

In the absence of light are 0.200 g of compound **1** (0.246 mmol, 1eq) and 0.260 g of $[Cp^*Ru(NCCH_3)_3][PF_6]$ (0.516 mmol, 2.1eq) suspended in 15 ml of CH_2Cl_2 and stirred for 16 h at room temperature. The solvent is removed in vacuo and the residue is first washed

with hexane and then taken up in CH_2Cl_2 and filtered over diatomaceous earth. Drying the CH_2Cl_2 solution in vacuo gives **5** as a red powder.

Yield: 0.241 g (0,201 mmol, 82%)

Analytical data of **5**:

NMR (CD_2Cl_2, 298 K)	^{1}H: δ [ppm] = 1.34 (s br,18, -($C_4\underline{H}_9$)), 1.47 (s, 36H, -($C_4\underline{H}_9$)$_2$), 2.27(s, 15H, $C_5(C\underline{H}_3)_5$), 5.34 (m, br, 4H, $C_5\underline{H}_2{}^t Bu_3$). ^{31}P{^{1}H}: δ [ppm] = 51.6 (m, 2P), 82.0 (m, 2P), –143.7 (sept. 2P, $^1J_{PF}$ = 710 Hz). Coupling constants of the cation are summarized in Table S5.6.
IR (CH_2Cl_2)	$\tilde{\nu}$ [cm^{-1}] = 1990 (s), 2030 (s)
Elemental analysis ($C_{48}H_{73}F_6Fe_2O_4P_5Ru_1 \cdot (C_7H_8)_{0.66}$)	Calculated: C 50.32, H 6.28 Found: C 50.77, H 6.09.
Mass spectrometry (ESI, CH_3CN)	m/z: 1051.2 (100%) $[M]^+$, 1023.2 (10%) $[M – CO]^+$

Synthesis of [{Cp'''Fe(CO)$_2$}{Cp'''Fe(CO)}(μ$_3$,η$^{4:2:1}$-P$_4$)(Cp*Ru)][PF$_6$] (6)

0.200 g of compound **1** (0.246 mmol, 1eq) and 0.260 g of [Cp*Ru($NCCH_3$)$_3$][PF_6] (0.516 mmol, 2.1eq) are suspended in 15 ml of CH_2Cl_2 and stirred for 3 days at room temperature. The solvent is removed in vacuo and the residue is first washed with toluene and then taken up in ortho-difluorobenzene and filtered over diatomaceous earth. Drying the solution in vacuo gives a red powder. Crystals of **6** are obtained by layering a thf solution under hexane.

Yield: 0.063g (0,054 mmol, 22%)

Analytical data of **6**:

NMR (CD_2Cl_2, 298 K)	^{1}H: δ [ppm] = 1.37 (s, 9H, -($C_4\underline{H}_9$)), 1.46 (s, 9H, -($C_4\underline{H}_9$)), 1.49 (s, 9H, -($C_4\underline{H}_9$)), 1.5 (very broad, ω½ ≈ 80 Hz, 18H, -($C_4\underline{H}_9$)$_2$), 1.52 (s ,9H, -($C_4\underline{H}_9$)), 1.79 (s ,15H, -($C_5(C\underline{H}_3)_5$), 5.1 (very broad, ω½ ≈ 80 Hz, 2H, $C_5\underline{H}_2{}^t Bu_3$) 5.16 (m broad, 1H, $C_5\underline{H}_2{}^t Bu_3$), 5.20 (m broad, 1H, $C_5\underline{H}_2{}^t Bu_3$). ^{31}P{^{1}H}: two isomers present in solution Isomer 1: δ [ppm] = 126.0 (m, 1P), 144.1 (m, 1P), 465.5 (m. 1P), 501.1 (m, 1P). Isomer 2: δ [ppm] = 126.5 (m, 1P), 145.2 (m, 1P), 457.0 (m. 1P), 500.9 (m, 1P). Coupling constants of the cation are summarized in Table S5.7.

IR (CH_2Cl_2)	$\tilde{\nu}$ [cm^{-1}] = 1957 (m), 1985 (s), 2026 (s)
Elemental analysis ($C_{47}H_{73}F_6Fe_2O_3P_5Ru_1$)	Calculated: C 48.34, H 6.30 Found: C 45.18, H 5.77. The large deviation is probably caused by excess $[Cp^*Ru(solv)_x][PF_6]$, which adsorbs on crystals of **6**. Due to its similar solubility to **6**, it cannot be removed by washing.
Mass spectrometry (ESI, CH_3CN)	m/z: 1023.2 (100%) $[M]^+$

Crystallographic Details

General remarks:

Single crystal structure analyses were performed using either Rigaku (formerly Agilent Technologies) diffractometer GV50, TitanS2 diffractometer (**6**) or a Gemini Ultra diffractometer (Oxford diffraction) with an AtlasS2 detector (**2, 3, 4**). Frames integration and data reduction were performed with the CrysAlisPro[3] software package. All structures were solved ether by ShelXT[4] (**2, 3, 4**) or ShelXS[5] (**6**) using the software Olex2[6] and refined by full-matrix least-squares method against F^2 in anisotropic approximation using ShelXL[4]. Hydrogen atoms were refined in calculated positions using riding on pivot atom model. Further details are given in Table S5.1.

CCDC-2051733 (**2**), CCDC-2051734 (**3**), CCDC-2051735 (**4**), and CCDC-2051736 (**6**) contain the supplementary crystallographic data for this paper. These data can be obtained free of charge at www.ccdc.cam.ac.uk/conts/retrieving.html (or from the Cambridge Crystallographic Data Centre, 12 Union Road, Cambridge CB2 1EZ, UK; Fax: + 44-1223-336-033; e-mail: deposit@ccdc.cam.ac.uk).

Table S5.1. Crystallographic data and details of diffraction experiments for **2**, **3**, **4**, and **6**.

Compound	**2**	**3** · $2(CH_2Cl_2)$	**4** · $2(CH_2Cl_2)$	**6** · $0.7(C_4H_8O)$
Formula	$C_{48}H_{72}F_{12}Fe_2O_4P_6Ru$	$C_{50}H_{77}Cl_4F_{12}Fe_2O_4P_6Rh$	$C_{50}H_{77}Cl_4F_{12}Fe_2IrO_4P_6$	$C_{49.8}H_{78.6}F_6Fe_2O_{3.7}P_5Ru$
$D_{calc.}$/ g cm^{-3}	1.520	1.555	1.648	1.347
μ/mm^{-1}	0.986	9.179	2.890	7.558
Formula Weight	1339.64	1512.34	1601.63	1218.14
Color	clear dark yellow	clear orange	clear orange	dark red
Shape	plate	block	block	plate
Size/mm^3	0.46×0.31×0.25	0.17×0.13×0.09	0.38×0.25×0.12	0.32×0.16×0.11
T/K	123(1)	123(1)	123(1)	123.(1)
Crystal System	monoclinic	triclinic	triclinic	monoclinic
Space Group	$P2_1/n$	P-1	P-1	$P2_1/c$
a/Å	10.0919(2)	12.9624(4)	12.9537(2)	18.66252(20)
b/Å	14.4515(2)	14.8814(4)	14.8742(2)	16.39571(14)
c/Å	40.1739(6)	18.4164(4)	18.4134(2)	20.2876(3)
α/°	90	73.521(2)	73.4890(10)	90
β/°	92.7650(10)	72.266(3)	72.3460(10)	104.5480(11)
γ/°	90	80.180(2)	80.0700(10)	90
V/$Å^3$	5852.26(17)	3230.90(16)	3226.85(8)	6008.68(11)
Z	4	2	2	4

Z'	1	1	1	1
Wavelength/Å	0.71073	1.54184	0.71073	1.54184
Radiation type	MoK$_a$	Cu K$_a$	Mo K$_a$	Cu K$_a$
Θ_{min}/°	3.357	3.527	3.208	2.446
Θ_{max}/°	32.463	71.928	32.890	74.387
Measured Refl's.	79434	34376	124329	63495
Ind't Refl's	19438	12257	22599	12096
Refl's with I > 2(I)	16675	11123	20785	11464
R_{int}	0.0374	0.0322	0.0305	0.0421
Parameters	744	825	772	645
Restraints	297	54	92	0
Largest Peak	0.688	0.519	1.068	0.622
Deepest Hole	-0.874	-0.554	-0.862	-0.982
GooF	1.080	1.014	1.028	1.042
wR_2 (all data)	0.0924	0.0671	0.0519	0.0887
wR_2	0.0880	0.0648	0.0503	0.0873
R_1 (all data)	0.0481	0.0328	0.0267	0.0349
R_1	0.0386	0.0283	0.0222	0.0332

X–ray diffraction on Crystals of **2**

In the crystal structure of [{Cp'''Fe(CO)$_2$}$_2$(μ_3,$\eta^{4:1:1}$-P_4){CymRu}][PF_6]$_2$ (**2**) a methyl group of the cymene ligand as well as one PF_6 anion is disordered over two position and was refined to an occupancy of 56.459:43.541 and 65.893:34.107, respectively.

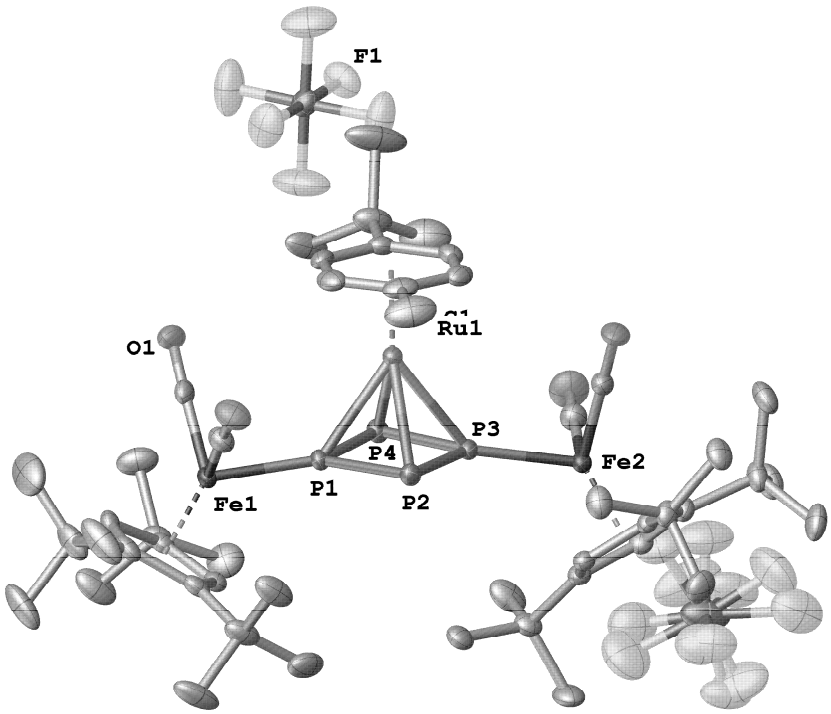

Figure S5.1. Molecular structure of **2** in the crystal. Hydrogen atoms are omitted for clarity. ADPs are drawn at 50% probability level. Selected bond length [Å] and angles [°] are: P1-P4 2.1410(7), P1-P2 2.1434(7), P4-P3 2.1481(7), P3-P2 2.1356(7), Fe1-P1 2.1800(5), Fe2-P3 2.1813(5), Ru1-$P_{4,cent.}$ 1.8890(2), Ru1-$C_{6,cent.}$ 1.7433(8), P4-P1-P2 97.34(3), P1-P4-P3 82.50(2), P2-P3-P4 97.37(3), P3-P2-P1 82.74(2).

X–ray diffraction on Crystals of **3**

In the crystal structure of [{Cp'''Fe(CO)$_2$}$_2$(μ_3,$\eta^{4:1:1}$-P_4){Cp*Rh}][PF_6]$_2$ · 2(CH_2Cl_2) (**3**) the two CH_2Cl_2 molecules as well as one PF_6 anion is disordered over two position and was refined to an occupancy of 70:30, 55:45 and 90:10, respectively.

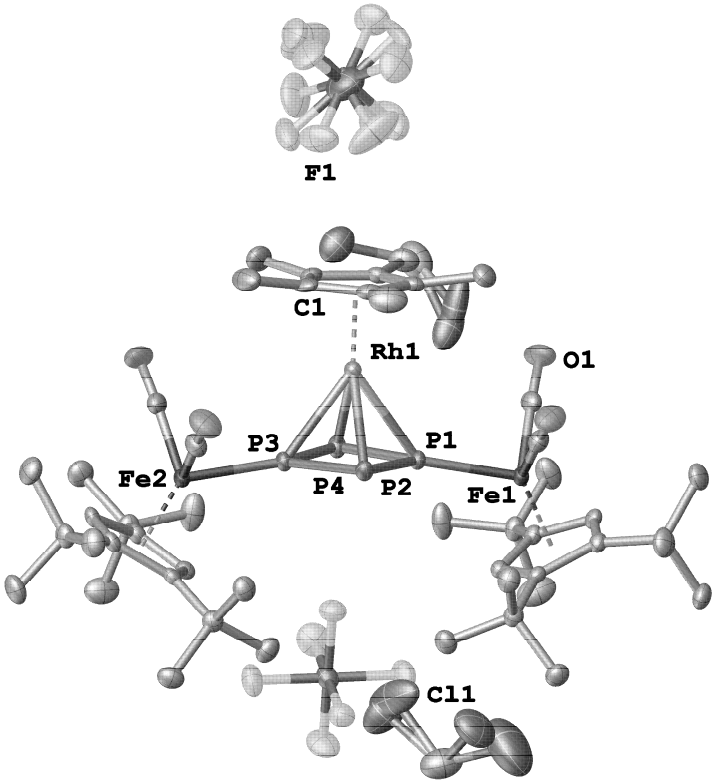

Figure S5.2. Molecular structure of **3** in the crystal. Hydrogen atoms are omitted for clarity. ADPs are drawn at 50% probability level. Selected bond length [Å] and angles [°] are: P1-P4 2.1456(8), P1-P2 2.1447(8), P4-P3 2.1459(8), P3-P2 2.1433(8), Fe1-P1 2.2100(6), Fe2-P3 2.2091(6), Rh1-$P_{4,cent.}$ 1.8938(3), Rh1-$Cp^*_{cent.}$ 1.8531(10), P4-P1-P2 97.34(3), P1-P4-P3 83.02(3), P2-P3-P4 96.91(3), P3-P2-P1 83.10(3).

X–ray diffraction on Crystals of **4**

In the crystal structure of [{Cp'''Fe(CO)$_2$}$_2$(μ_3,$\eta^{4:1:1}$-P_4){Cp*Ir}][PF_6]$_2$ · 2(CH_2Cl_2) (**4**) a chlorine atom of a CH_2Cl_2 molecule as well as the second CH_2Cl_2 molecule is disordered over two position and was refined to an occupancy of 60:40 and 70.563:29.437, respectively.

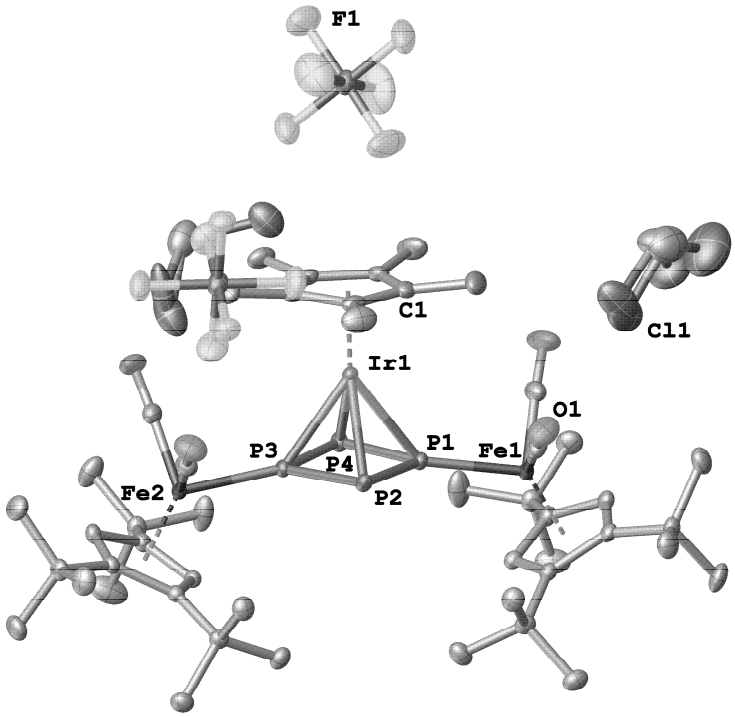

Figure S5.3. Molecular structure of **4** in the crystal. Hydrogen atoms are omitted for clarity. ADPs are drawn at 50% probability level. Selected bond length [Å] and angles [°] are: P1-P4 2.1488(6), P1-P2 2.1512(6), P4-P3 2.1501(6), P3-P2 2.1518(6), Fe1-P1 2.2073(4), Fe2-P3 2.2074(4), Ir1-$P_{4,cent.}$ 1.8915(2), Ir1-$Cp^*_{cent.}$ 1.8542(7), P4-P1-P2 96.82(2), P1-P4-P3 83.10(2), P2-P3-P4 96.76(2), P3-P2-P1 83.20(2).

X–ray diffraction on Crystals of **6**

In the crystal structure of $[\{Cp'''Fe(CO)_2\}\{Cp'''Fe(CO)\}(\mu_3,\eta^{4:2:1}\text{-}P_4)(Cp^*Ru)][PF_6] \cdot 0.7(C_4H_8O)$ (**6**) only one of the two enantiomers (Figure S5.4: 1S-2R-3R-4R-5S enantiomer, Figure S5.5: 1R-2S-3S-4S-5R enantiomer) is present in the asymmetric unit. The second enantiomer is obtained by symmetry generation. The position of thf molecule is occupied by 70%.

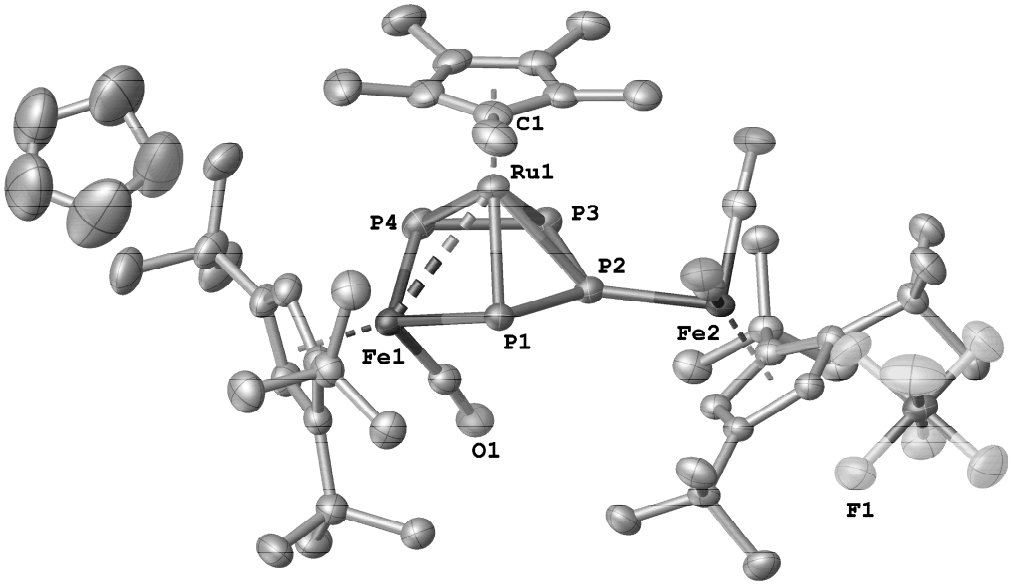

Figure S5.4. Molecular structure of the 1S-2R-3R-4R-5S enantiomer of **6** in the crystal. Hydrogen atoms are omitted for clarity. ADPs are drawn at 50% probability level. Selected bond length [Å] and angles [°] are: P1-P2 2.1360(8), P2-P3 2.1335(8), P3-P4 2.1446(8), Ru1-P1 2.3592(5), Ru1-P2 2.4454(5), Ru1-P3 2.4469(6), Ru1-P4 2.3513(6), Ru1···Fe1 2.9052(4), Fe1-P1 2.2539(6), Fe1-P4 2.2498(7), Fe2-P2 2.2413(6), Ru1-$Cp^*_{cent.}$ 1.9069(10), P4-Fe1-P1 99.44(2), P2-P1-Fe1 102.26(3), P3-P2-P1 111.67(3), P3-P4-Fe1 108.53(3).

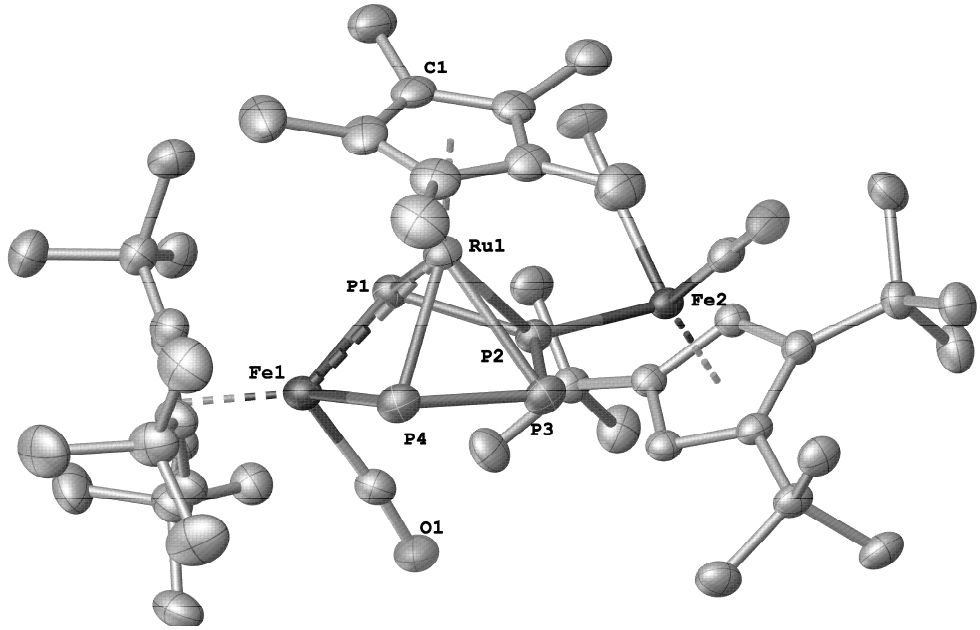

Figure S5.5. Molecular structure of the cationic part of the 1R-2S-3S-4S-5R enantiomer of **6** in the crystal. Hydrogen atoms are omitted for clarity. ADPs are drawn at 50% probability level.

^{1}H NMR and ^{31}P NMR Spectroscopy

General remarks:

^{1}H and ^{31}P NMR spectra were recorded on a Bruker Avance III HD 400 (^{1}H: 400.130 MHz, ^{31}P: 161.976 MHz) at 298 K. The chemical shifts are reported in ppm relative to external TMS (^{1}H) and H_3PO_4 (^{31}P). The ^{31}P NMR simulation was performed with the simulation tool of Bruker TopSpin (Version 4.0.8.).

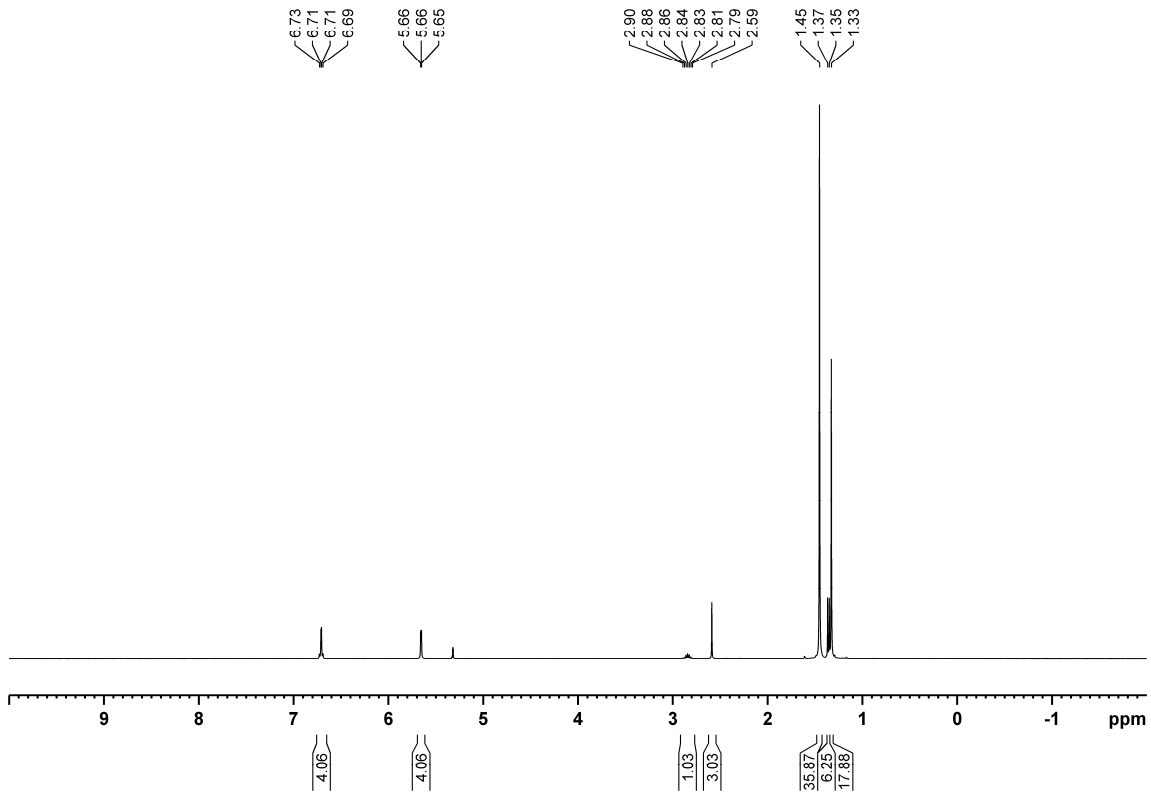

Figure S5.6. ^{1}H NMR spectrum of **2** in CD_2Cl_2.

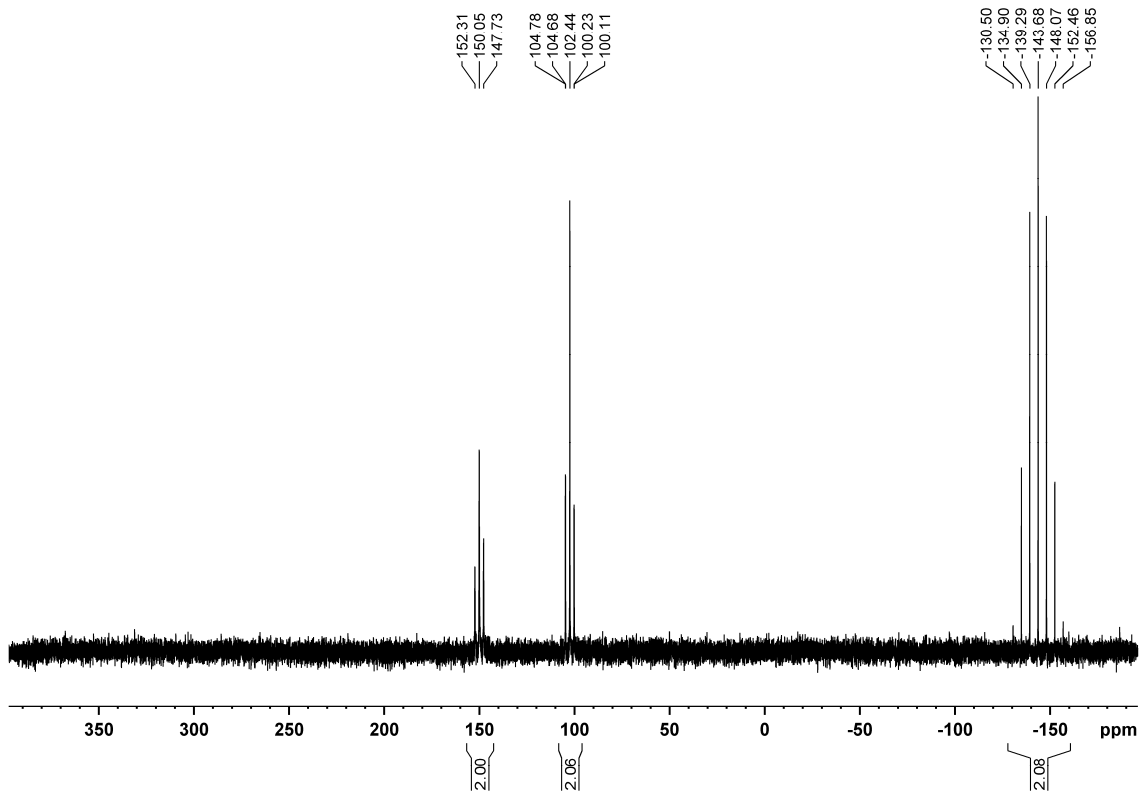

Figure S5.7. $^{31}P\{^{1}H\}$ NMR spectrum of **2** in CD_2Cl_2.

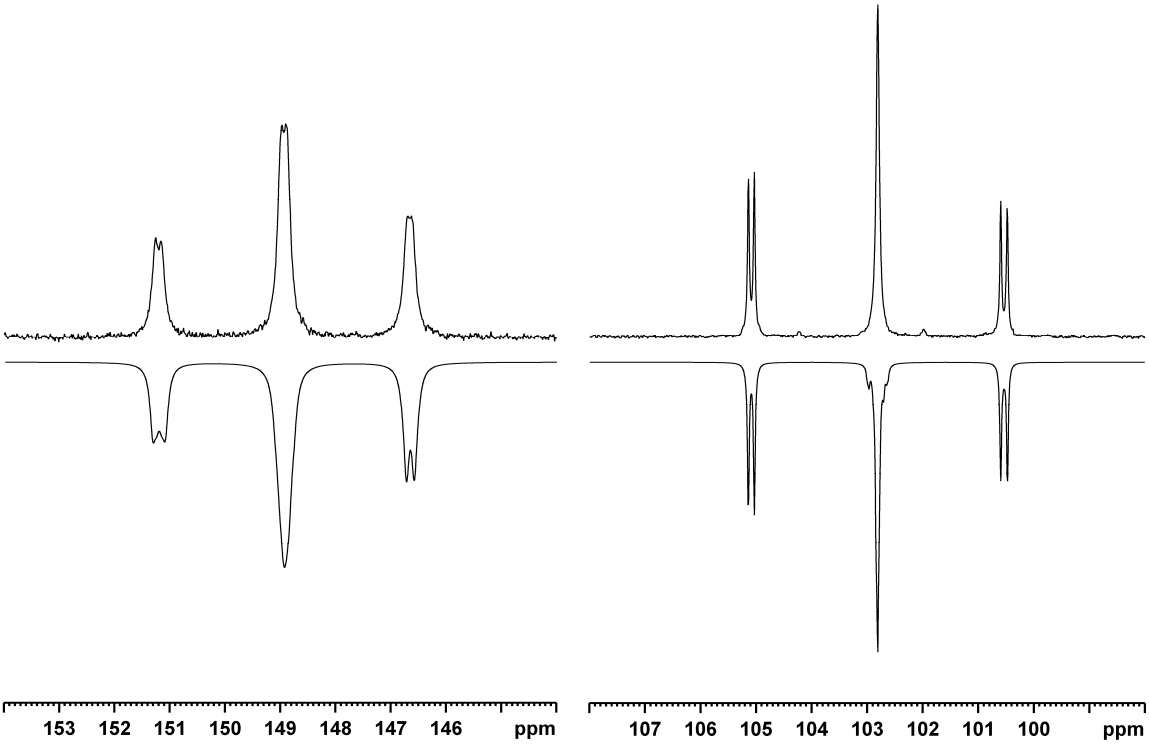

Figure S5.8. Simulated $^{31}P\{^1H\}$ NMR spectrum of **2** (AA'XX' spin system).

Table S5.2. Calculated coupling constants of the cation of **2** (AA'XX' spin system) with a R-factor of 1.66%.

Chemical shift [ppm]		Coupling constants [Hz]			
A	148.9	J_{AX}	377.3	$J_{AA'}$	13.8
A'	148.8	$J_{AX'}$	366.5	$J_{XX'}$	14.4
X	102.9	$J_{A'X}$	362.3		
X'	102.9	$J_{A'X'}$	369.2		

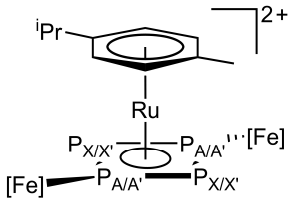

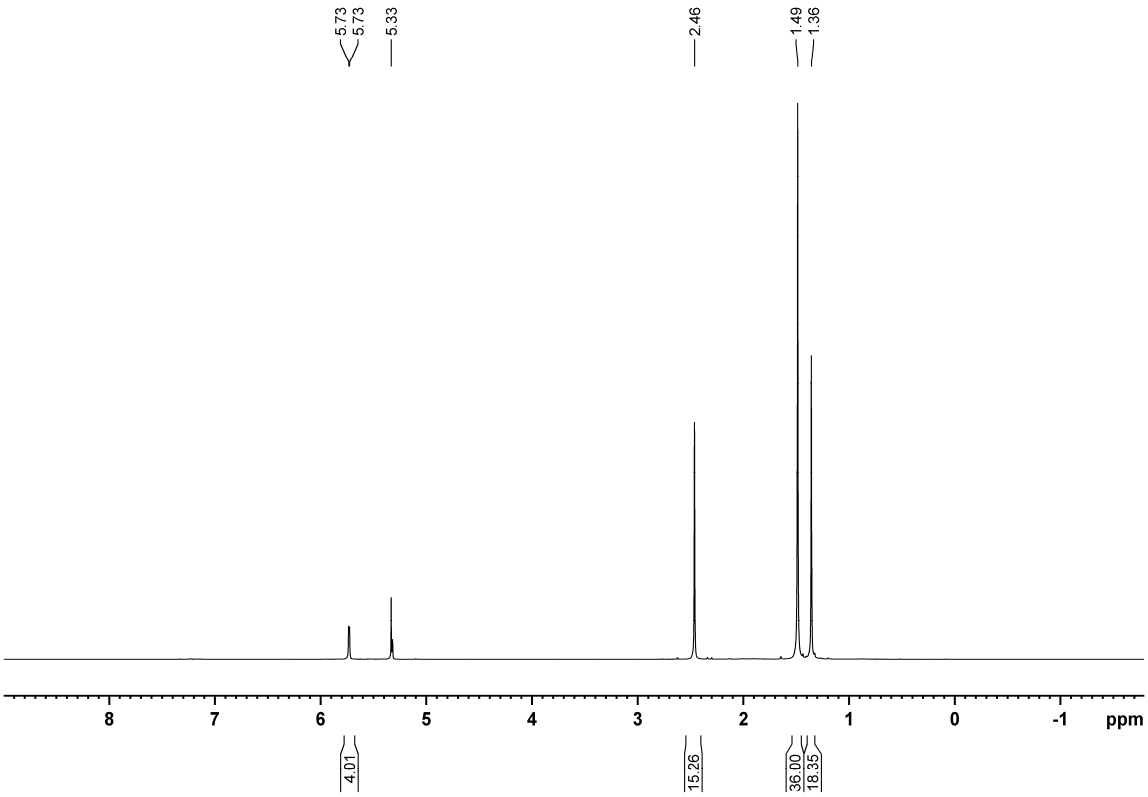

Figure S5.9. ^{1}H NMR spectrum of **3** in CD_2Cl_2.

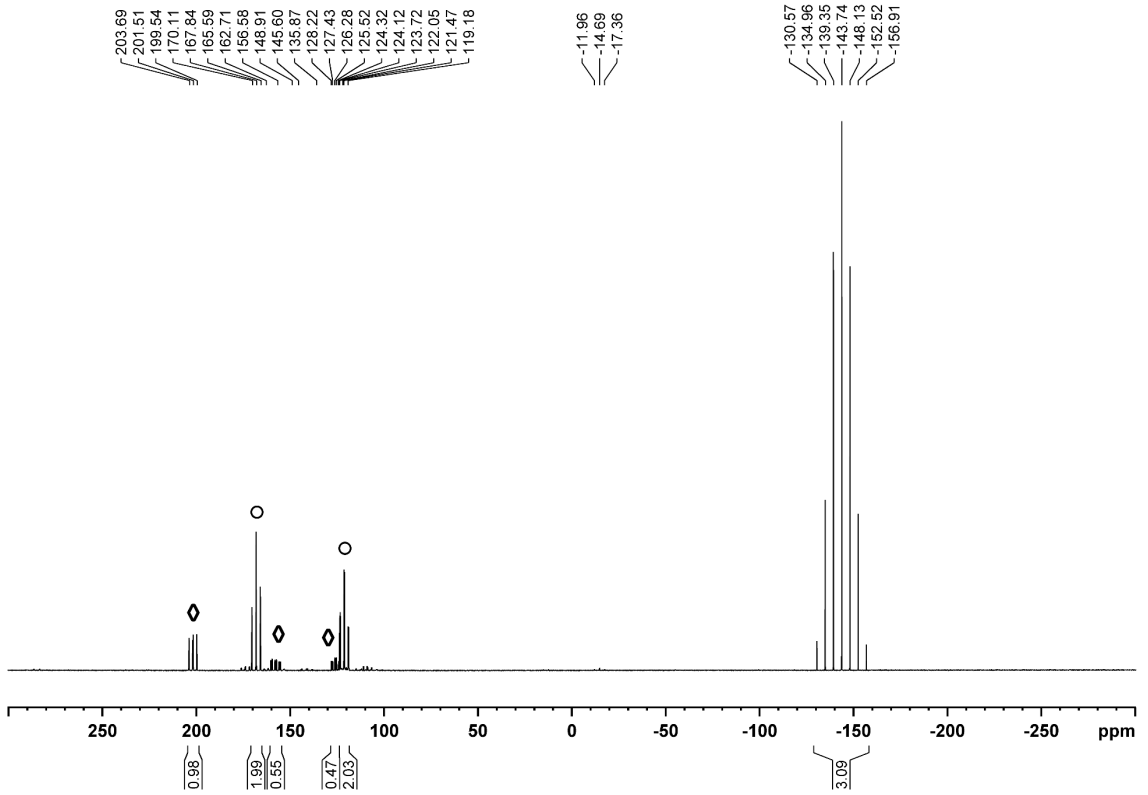

Figure S5.10. $^{31}P\{^{1}H\}$ NMR spectrum of the reaction solution of **3** in CD_2Cl_2. The signals marked with a circle (○) can be assigned to **3**, while the signals marked with a diamond (◊) indicate the formation of a side products with an AA'MNX spin system (see Figure S5.13, Table S5.4 and Scheme S5.1).

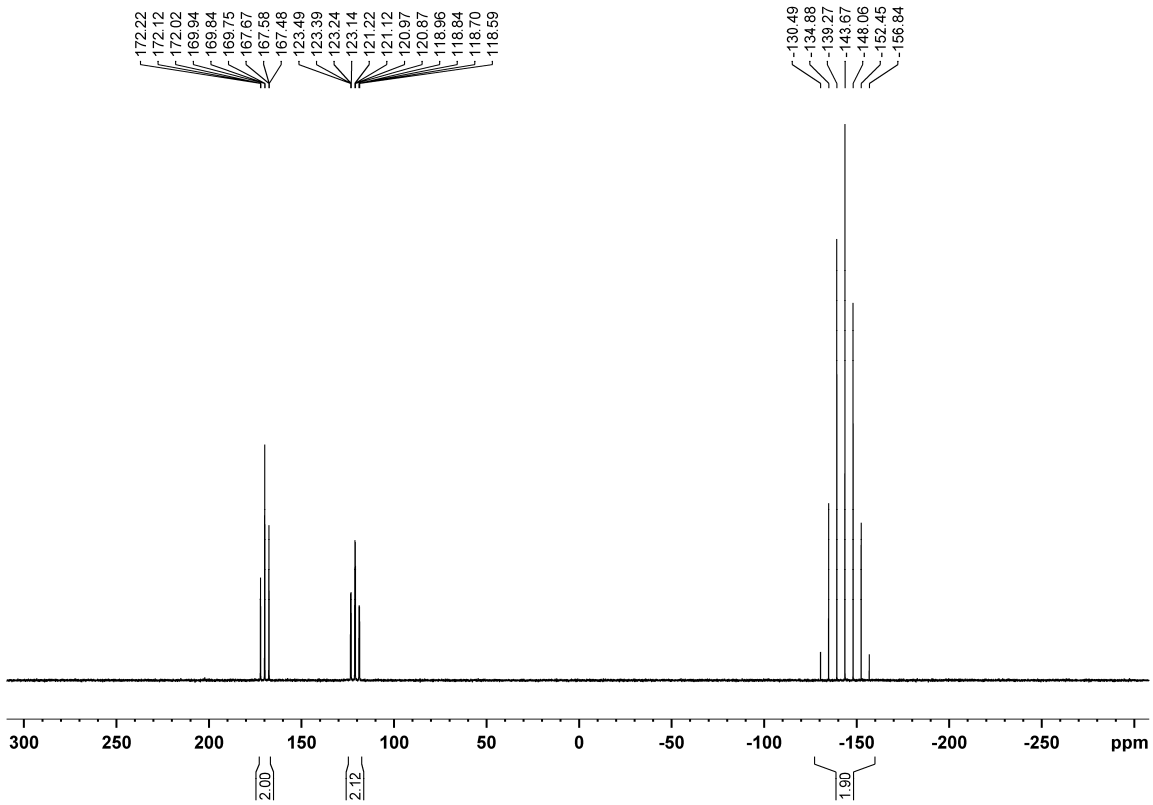

Figure S5.11. $^{31}P\{^{1}H\}$ NMR spectrum of **3** in CD_2Cl_2.

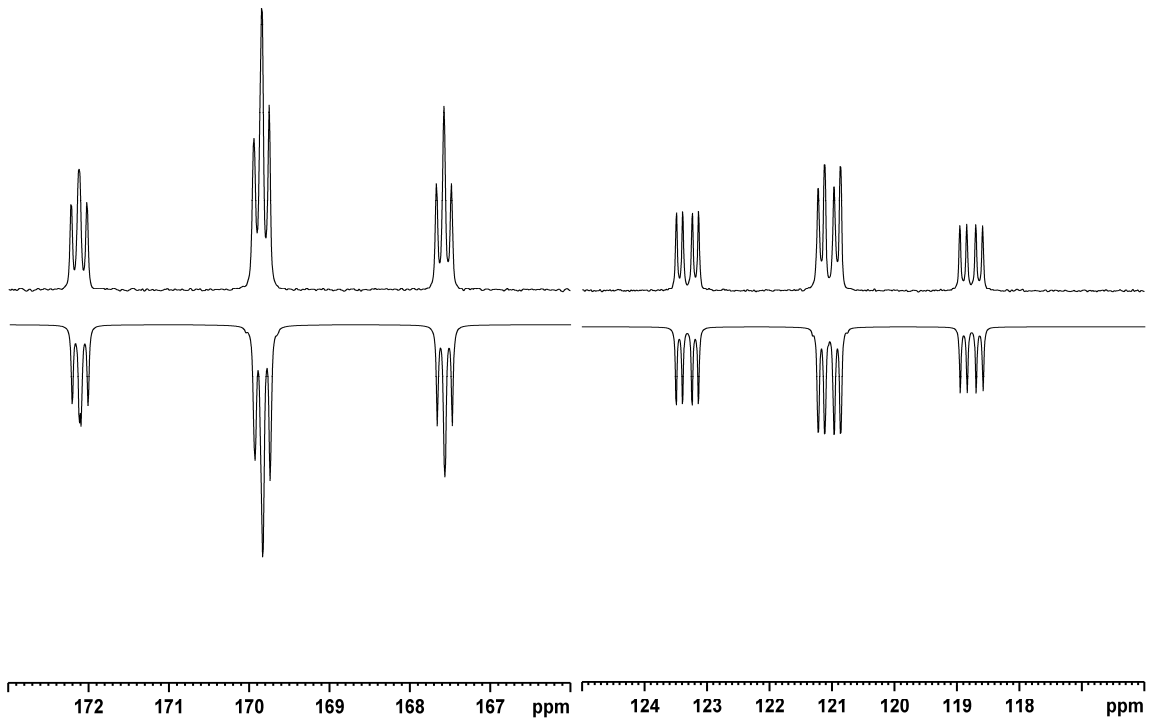

Figure S5.12. Simulated $^{31}P\{^{1}H\}$ NMR spectrum of **3** (AA'MM'X spin system, X corresponds to Rh).

Table S5.3. Calculated coupling constants of the cation of **3** (AA'MM'X spin system) with a R-factor of 1.15%.

Chemical shift [ppm]		Coupling constants [Hz]					
A	169.8	J_{AM}	372.7	$J_{AA'}$	1.9	J_{MX}	41.0
A'	169.8	$J_{AM'}$	364.4	$J_{MM'}$	15.3	$J_{M'X}$	41.4
M	121.1	$J_{A'M}$	365.1	J_{AX}	13.9		
M'	121.1	$J_{A'M'}$	370.8	$J_{A'X}$	13.7		

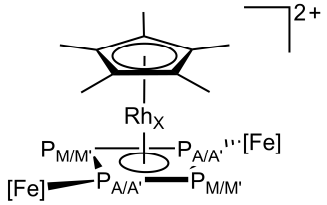

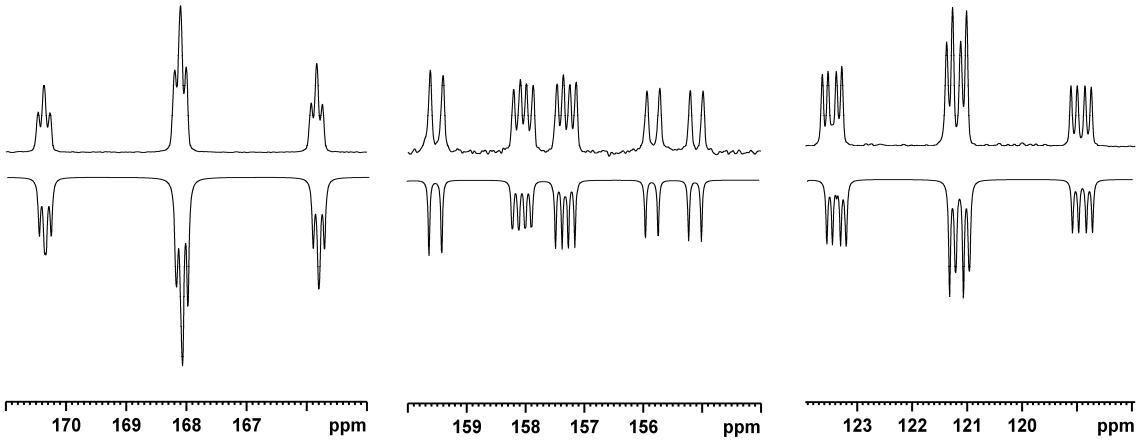

Figure S5.13. Simulated ^{31}P NMR spectrum of the side product with an AA'MNX spin system (X corresponds to Rh) of the synthesis of **3** (see Figure S5.10)

Table S5.4. Calculated coupling constants of the side product in the synthesis of **3** (AA'MNX spin system) with a R-factor of 3.67%.

Chemical shift [ppm]		Coupling constants [Hz]					
A	201.7	J_{AM}	359.4	J_{NM}	118.8	J_{MX}	35.1
A'	201.7	J_{AN}	315.9	$J_{AA'}$	12.8	J_{NX}	24.8
M	157.7	$J_{A'M}$	356.8	J_{AX}	15.7		
N	125.7	$J_{A'N}$	314.7	$J_{A'X}$	15.7		

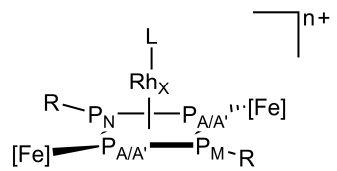

Scheme S5.1. Postulated structure of the byproduct based on the coupling constants obtained by the simulation. R and L are possible pattern for substitution.

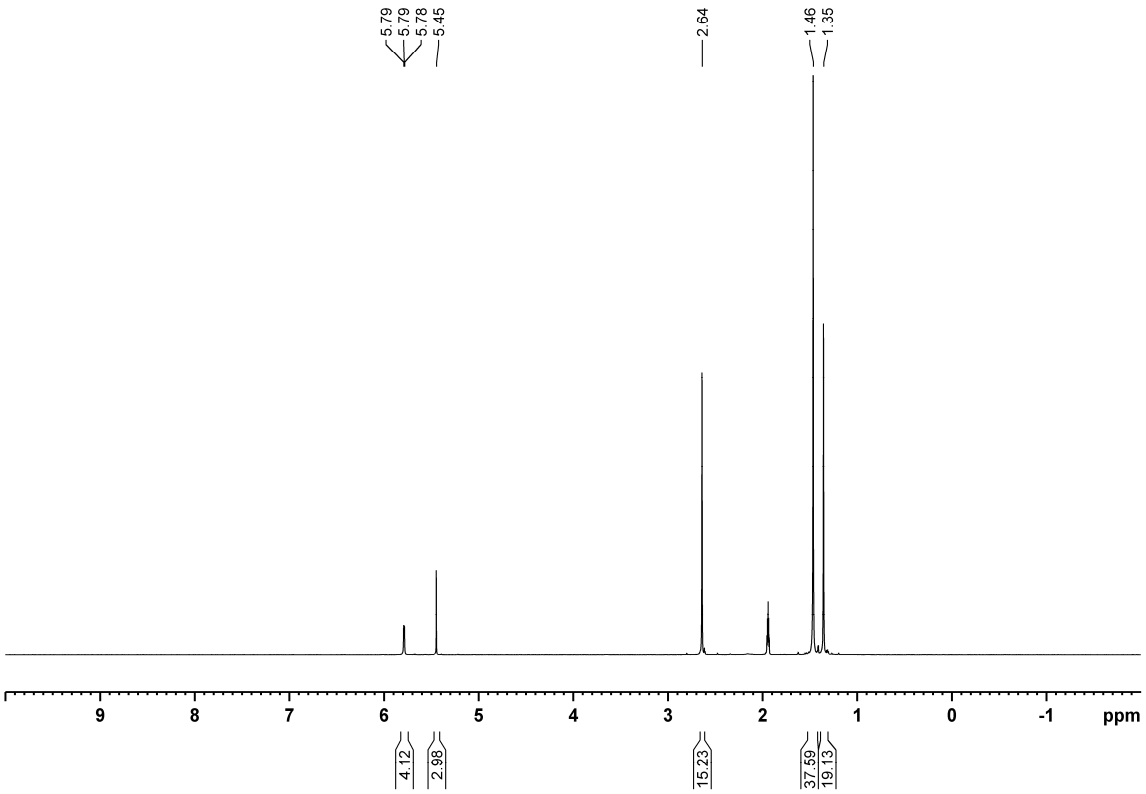

Figure S5.14. ^{1}H NMR spectrum of **4** in CD_3CN.

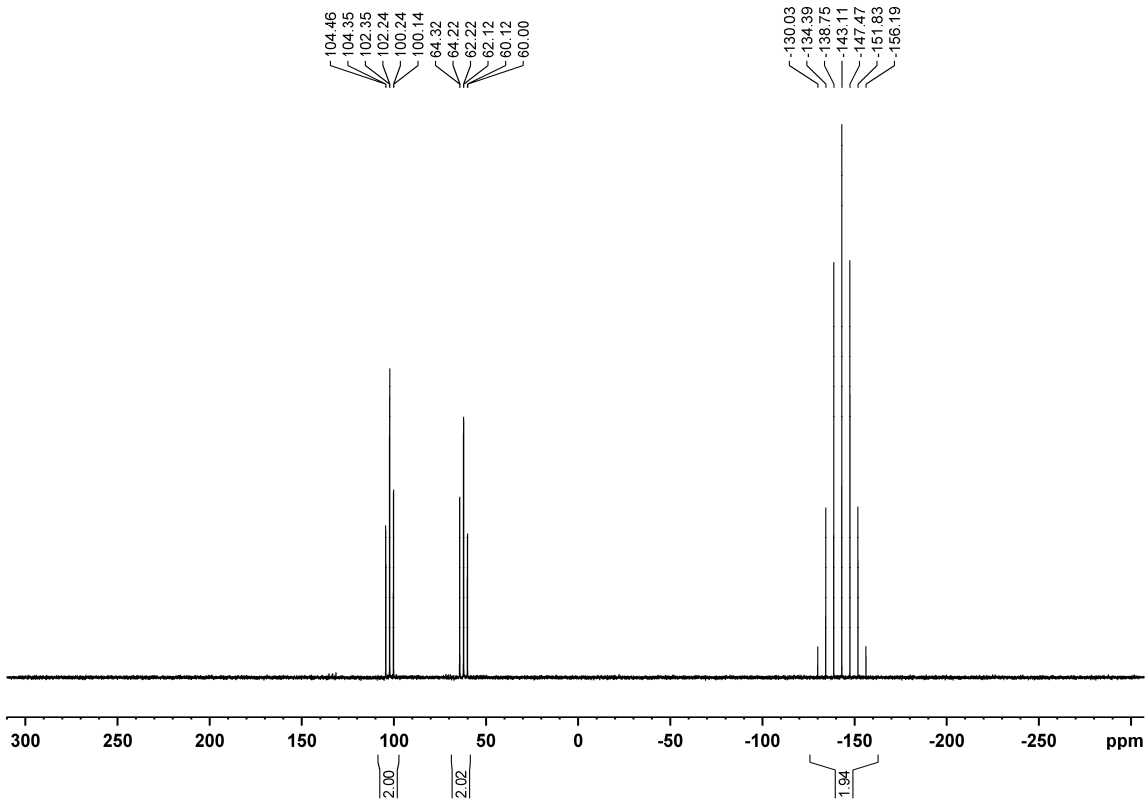

Figure S5.15. $^{31}P\{^{1}H\}$ NMR spectrum of **4** in CD_3CN.

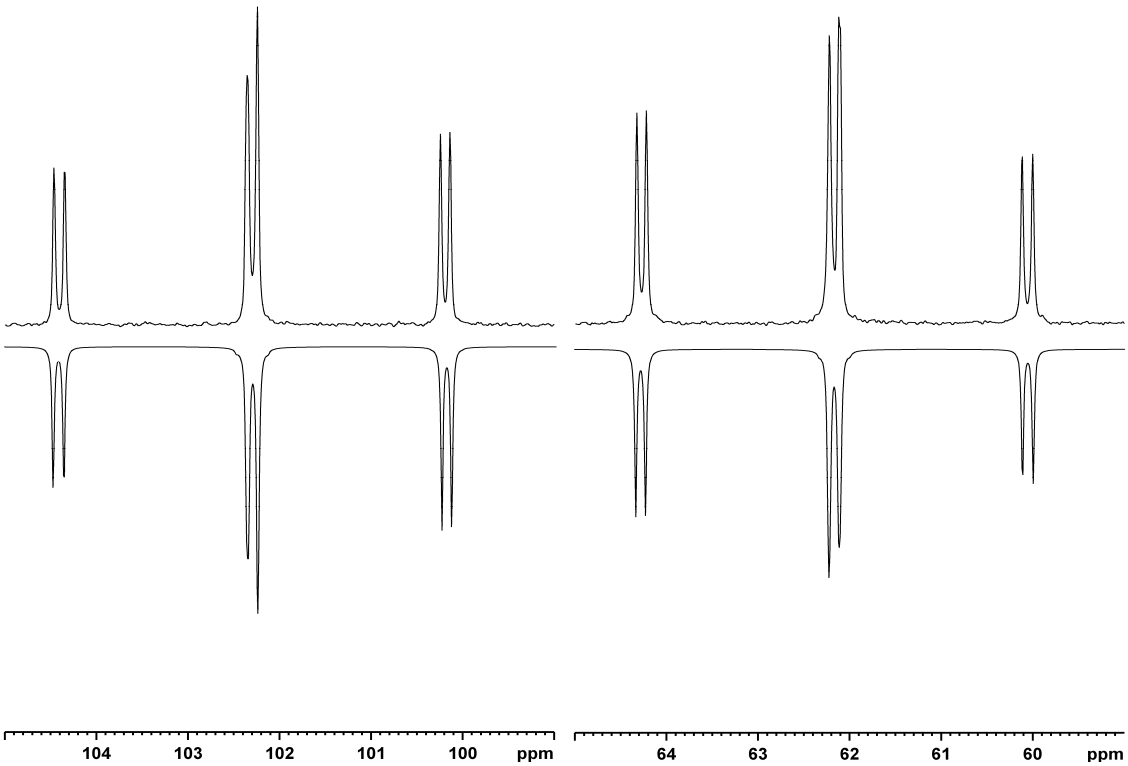

Figure S5.16. Simulated $^{31}P\{^1H\}$ NMR spectrum of **4** (AA'XX' spin system).

Table S5.5. Calculated coupling constants of the cation of **4** (AA'XX' spin system) with a R-factor of 1.08%.

Chemical shift [ppm]		Coupling constants [Hz]	
A	102.3	J_{AX}	338.1
A'	102.3	$J_{AX'}$	343.1
X	62.2	$J_{A'X}$	345.6
X'	26.2	$J_{A'X'}$	340.2
		$J_{AA'}$	17.9

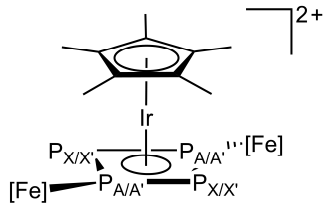

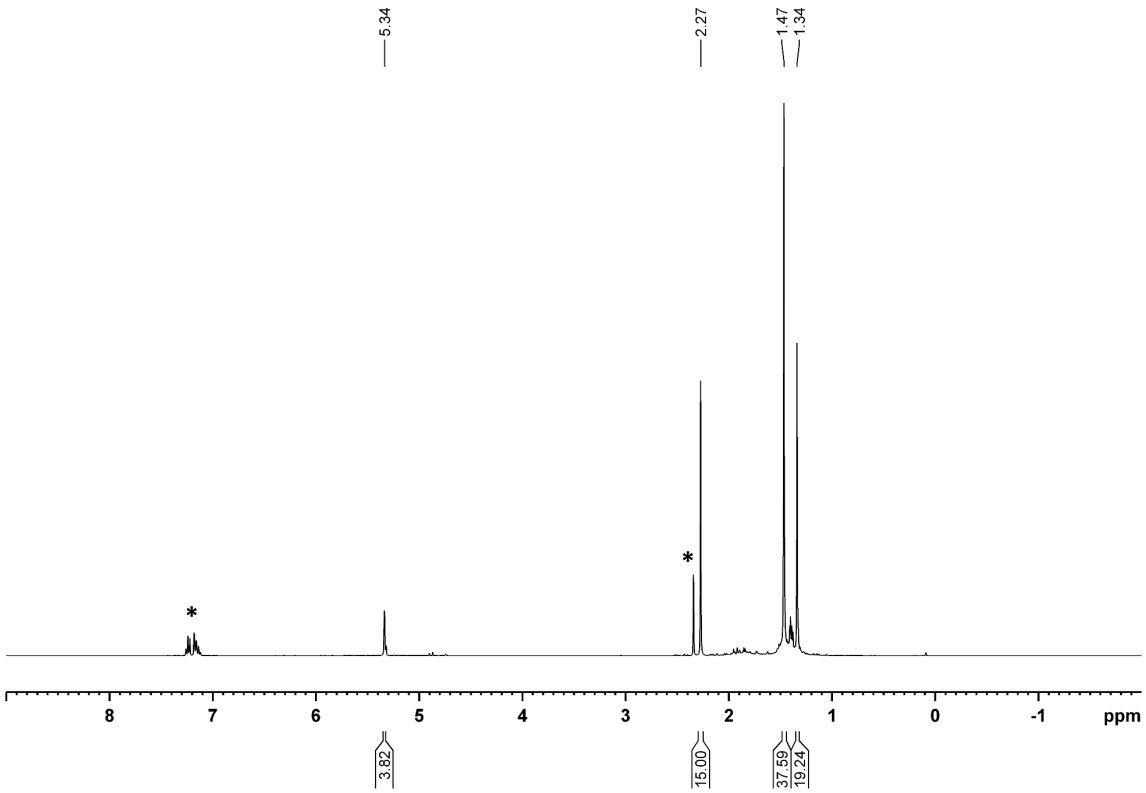

Figure S5.17. ^{1}H NMR spectrum of **5** in CD_2Cl_2. Signals marked with a star (*) are assigned to toluene.

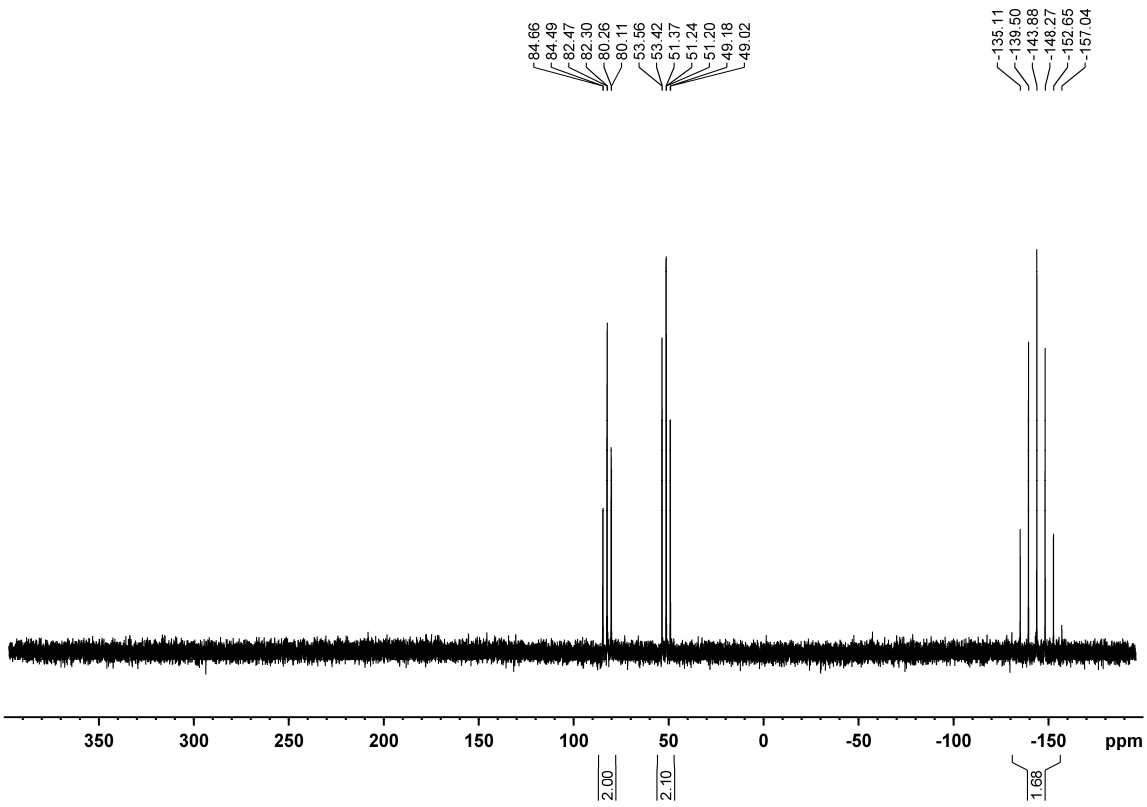

Figure S5.18. $^{31}P\{^{1}H\}$ NMR spectrum of **5** in CD_2Cl_2.

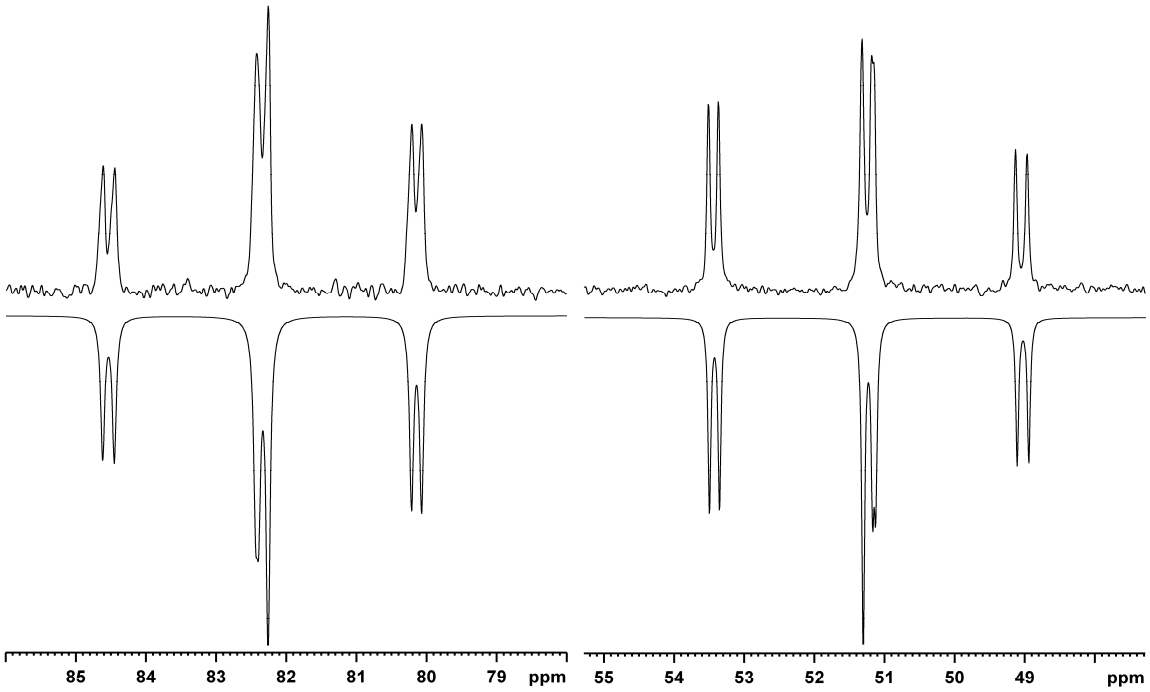

Figure S5.19. Simulated $^{31}P\{^1H\}$ NMR spectrum of **5** (AA'XX' spin system).

Table S5.6. Calculated coupling constants of the cation of **5** (AA'XX' spin system) with a R-factor of 2.74%.

Chemical shift [ppm]		Coupling constants [Hz]			
A	82.0	J_{AX}	352.6	$J_{AA'}$	25.9
X	82.0	$J_{AX'}$	361.5	$J_{XX'}$	31.4
X	51.7	$J_{A'X}$	359.4		
X'	51.7	$J_{A'X'}$	352.3		

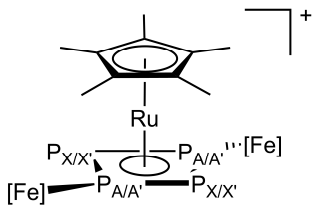

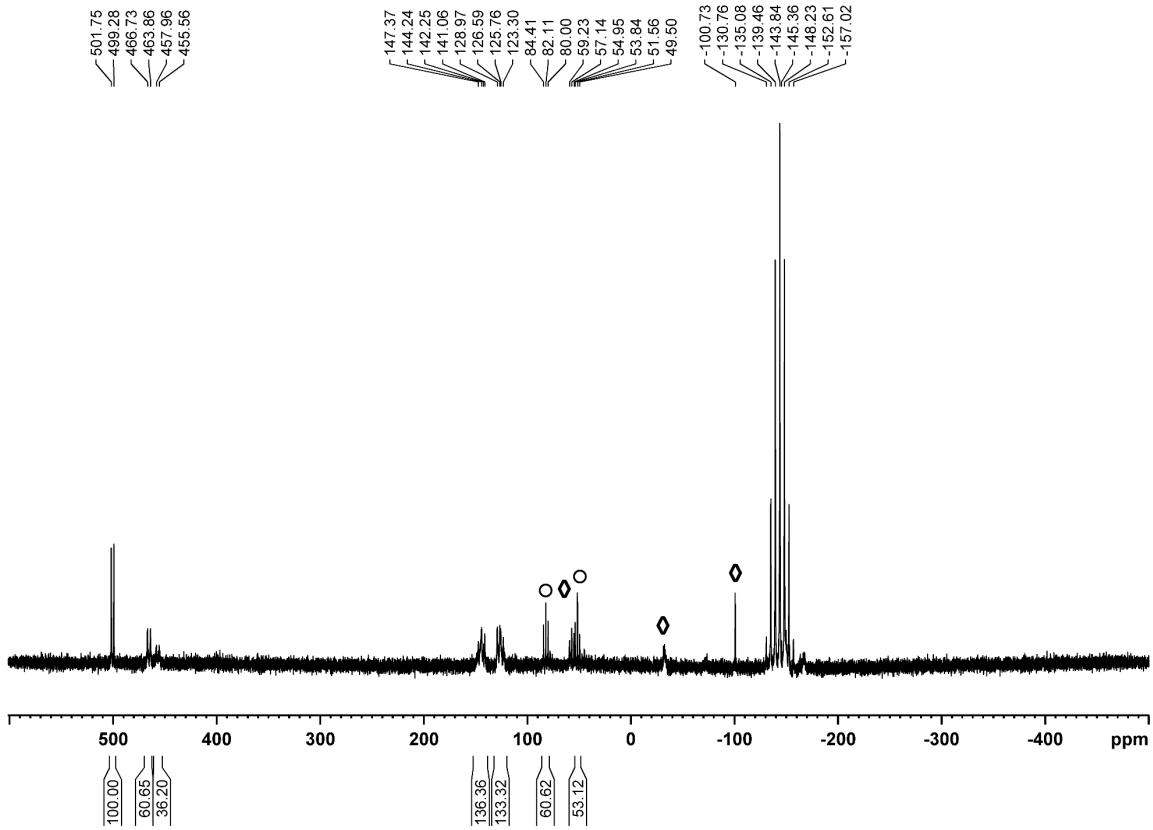

Figure S5.20. $^{31}P\{^1H\}$ NMR spectrum of the reaction mixture of **6** in CD_2Cl_2. The signals marked with the circle (○) can be assigned to **5**, while the signals marked with a diamond (◊) indicate the formation of side or degradation products.

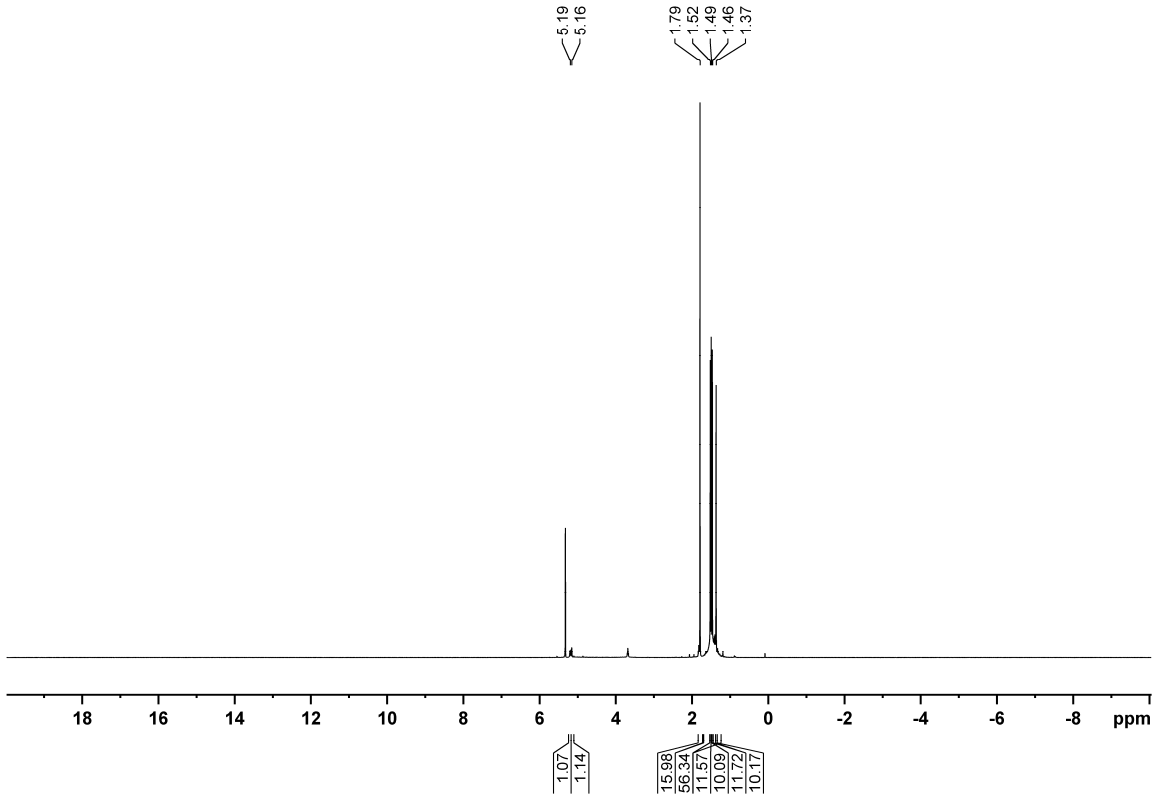

Figure S5.21. ^1H NMR spectrum of a crystalline sample of **6** in CD_2Cl_2. The aliphatic region (approx. δ = 1.3 – 1.7 ppm) shows four singlets with an integral of approx. 9 each. Additionally, a broad signal lays underneath the four singlets with an integral of 18 (56-(4*9)≈18).

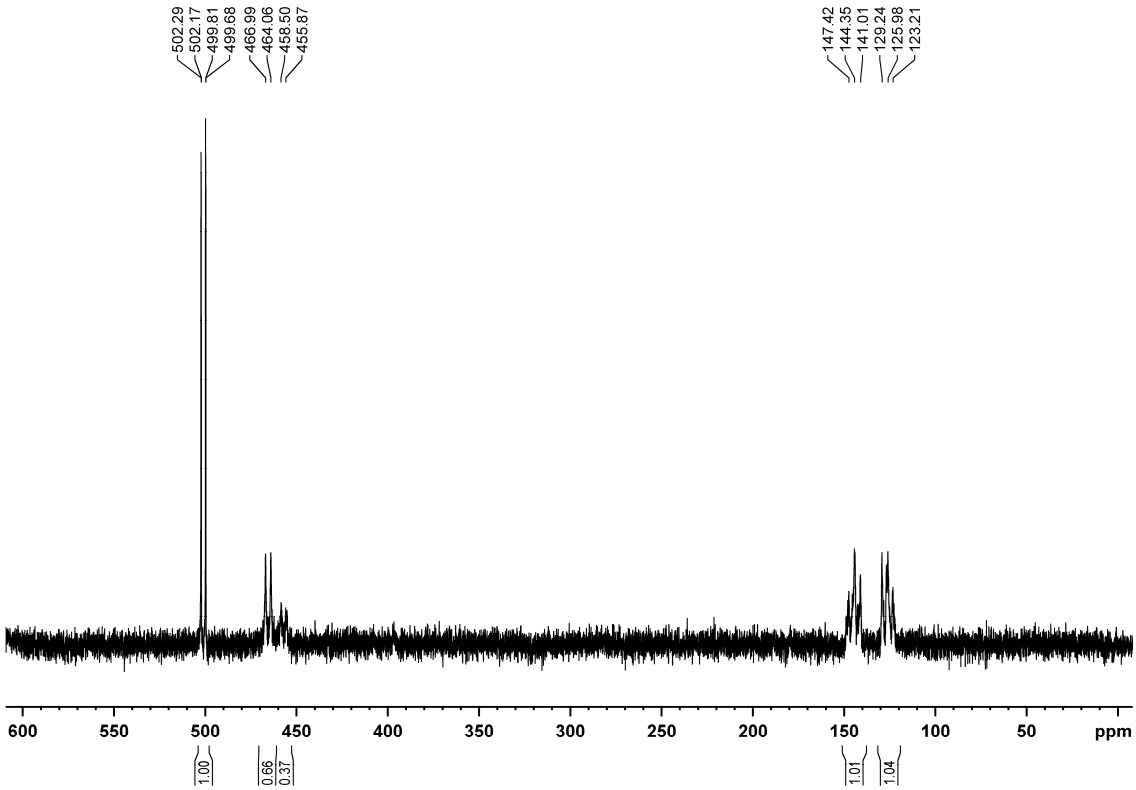

Figure S5.22. $^{31}P\{^{1}H\}$ NMR spectrum of a crystalline sample of **6** in CD_2Cl_2 that indicates the presence of two isomers in solution.

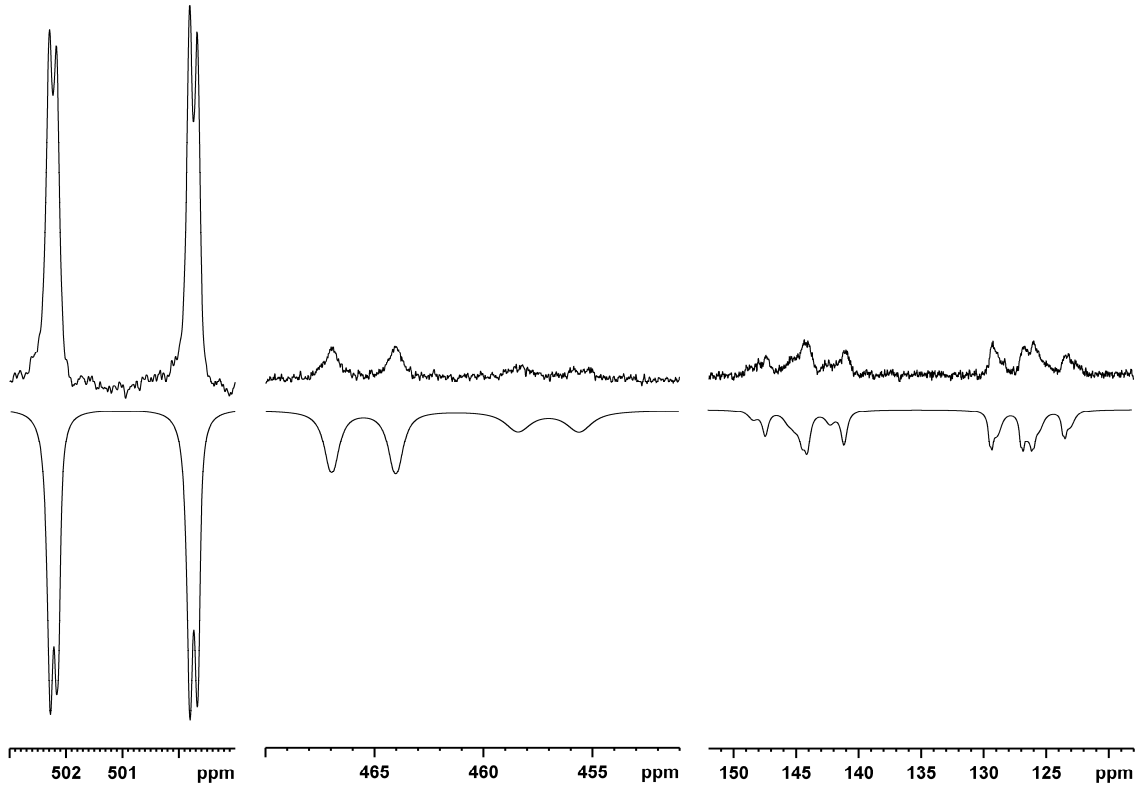

Figure S5.23. Simulated $^{31}P\{^{1}H\}$ NMR spectrum of **6** (AMXY spin system).

Table S5.7. Calculated coupling constants of the two isomers of **6** (AMXY spin system) with a R-factor of 1.76%. The two isomers were refined to a distribution of 63% to 37%.

Isomer 1						Isomer 2					
Chemical shift [ppm]		Coupling constants [Hz]				Chemical shift [ppm]		Coupling constants [Hz]			
A	501.1	J_{AY}	406.5	J_{AM}	3.2	A	500.9	J_{AY}	407.3	J_{AM}	6.8
M	465.5	J_{MX}	480.6	J_{AX}	–3.4	M	457.0	J_{MX}	458.0	J_{AX}	–8.6
X	144.1	J_{XY}	544.9	J_{MY}	26.7	X	145.2	J_{XY}	546.1	J_{MY}	30.1
Y	126.0					Y	126.5				

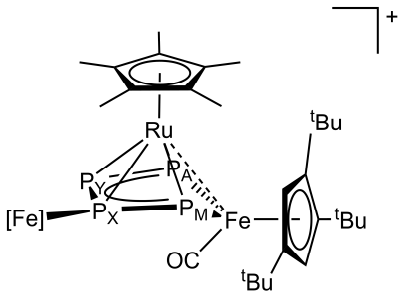

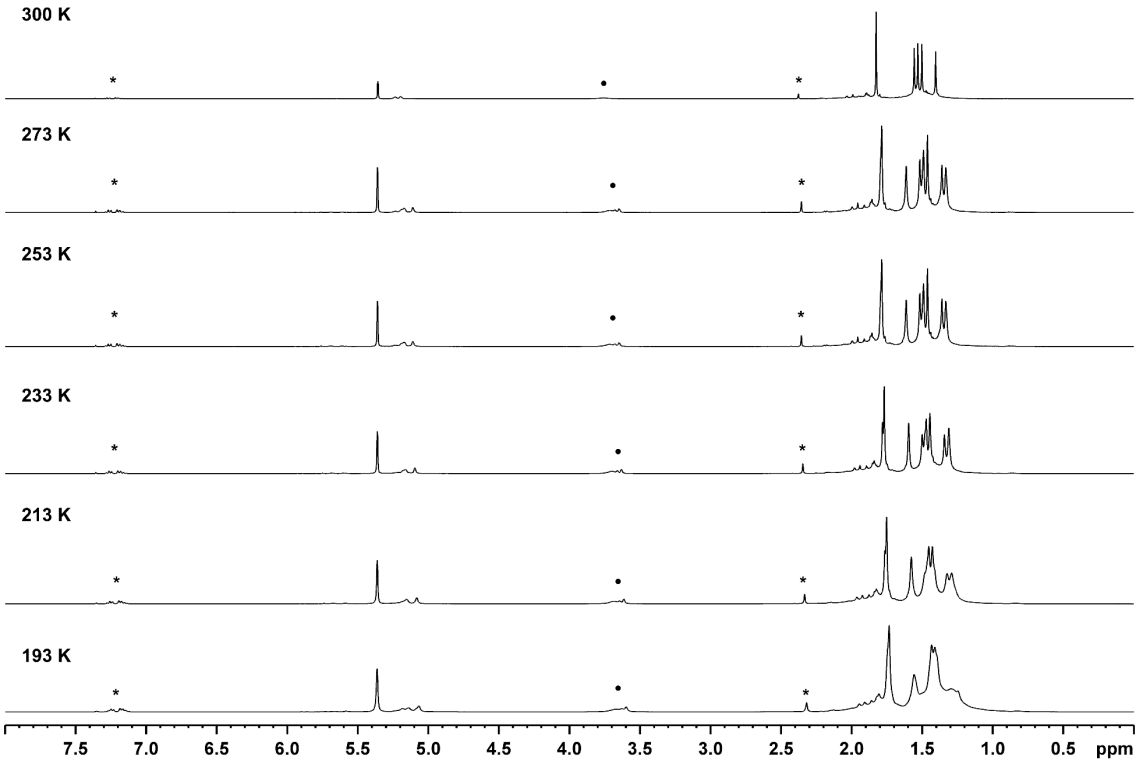

Figure S5.24. ^{1}H NMR spectra of a crystalline sample of **6** in CD_2Cl_2 at different temperatures. Signals marked with a star (*) are assigned to toluene, while the broad signals marked with a dot (•) are assigned to impurities of $[Cp^*Ru(thf)_x][PF_6]$.

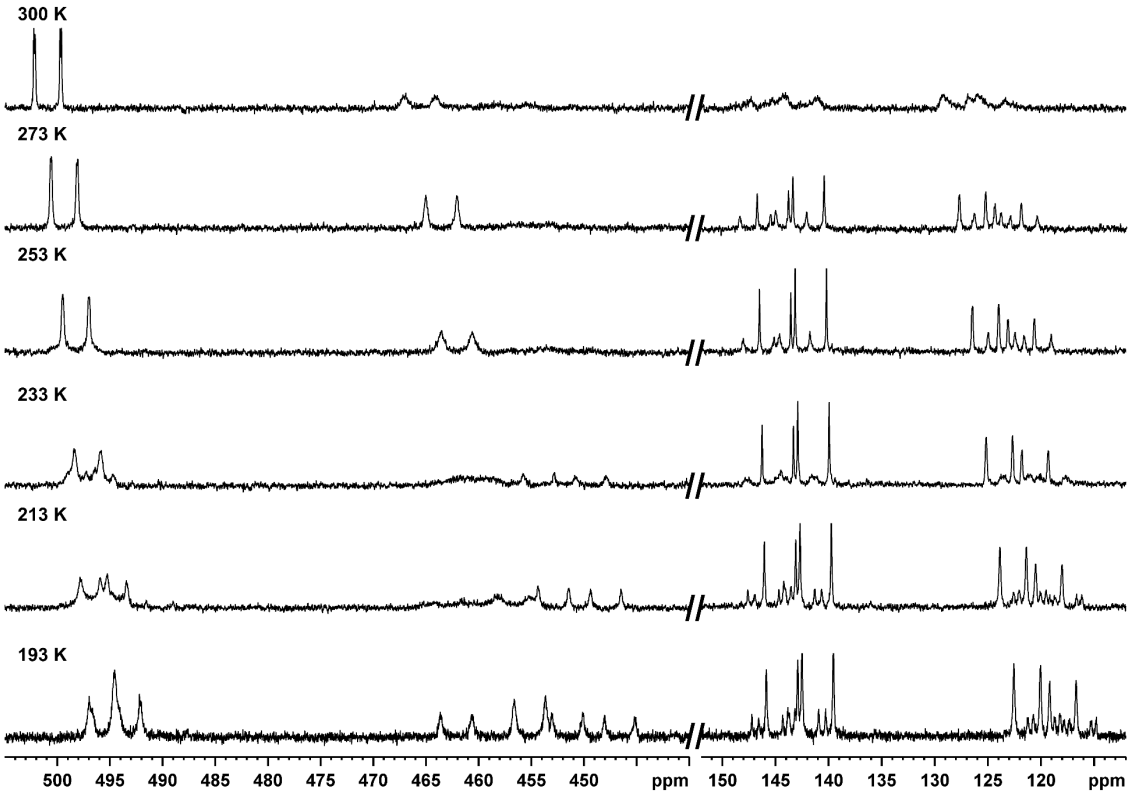

Figure S5.25. $^{31}P\{^1H\}$ NMR spectra of a crystalline sample of **6** in CD_2Cl_2 at different temperatures.

Computational Details

General remarks:

All calculations have been performed with the TURBOMOLE program package[7] at the RI[8,9]-BP86[10]/def2-TZVP[9,11] level of theory. To speed up the geometry optimization the Multipole Accelerated Resolution-of-the-Identity (MARI-J)[8,9,12] approximation has been used. For the reaction energies single point calculations at the B3LYP/def2-TZVP level have been performed in which the solvent effects have been incorporated via the COSMO method (acetonitrile ε = 35.688). The numbering of the atoms in the computational part differs from that of the main part.

Table S5.8. Partial charge of the fragments of **6**, **7**, **5** and **2**.

		Partial charge	Percentage [%]		Partial charge	Percentage [%]
Complex	**6**			**7**		
Iron fragment	Cp'''Fe2(CO)	0.08	8.00	Cp'''Fe2(CO)	0.33	16.39
Iron fragment	Cp'''Fe3$(CO)_2$	0.34	34.38	Cp'''Fe3$(CO)_2$	0.49	24.70
Ligand (Ru)	Cp*	0.29	28.74	Cym	0.64	32.17
Ruthenium	Ru1	-0.35	-35.00	Ru1	-0.40	-20.12
P_4 unit	P_4	0.64	63.88	P_4	0.94	46.86
Total charge		1.00	100.00		2.00	100.00
Complex	**5**			**2**		
Iron fragment	Cp'''Fe2$(CO)_2$	0.35	35.22	Cp'''Fe2$(CO)_2$	0.51	25.73
Iron fragment	Cp'''Fe3$(CO)_2$	0.34	34.30	Cp'''Fe3$(CO)_2$	0.52	25.76
Ligand (Ru)	Cp*	0.18	18.04	Cym	0.52	26.01
Ruthenium	Ru1	-0.37	-37.04	Ru1	-0.41	-20.26
P_4 unit	P_4	0.49	49.48	P_4	0.86	42.76
Total charge		1.00	100.00		2.00	100.00

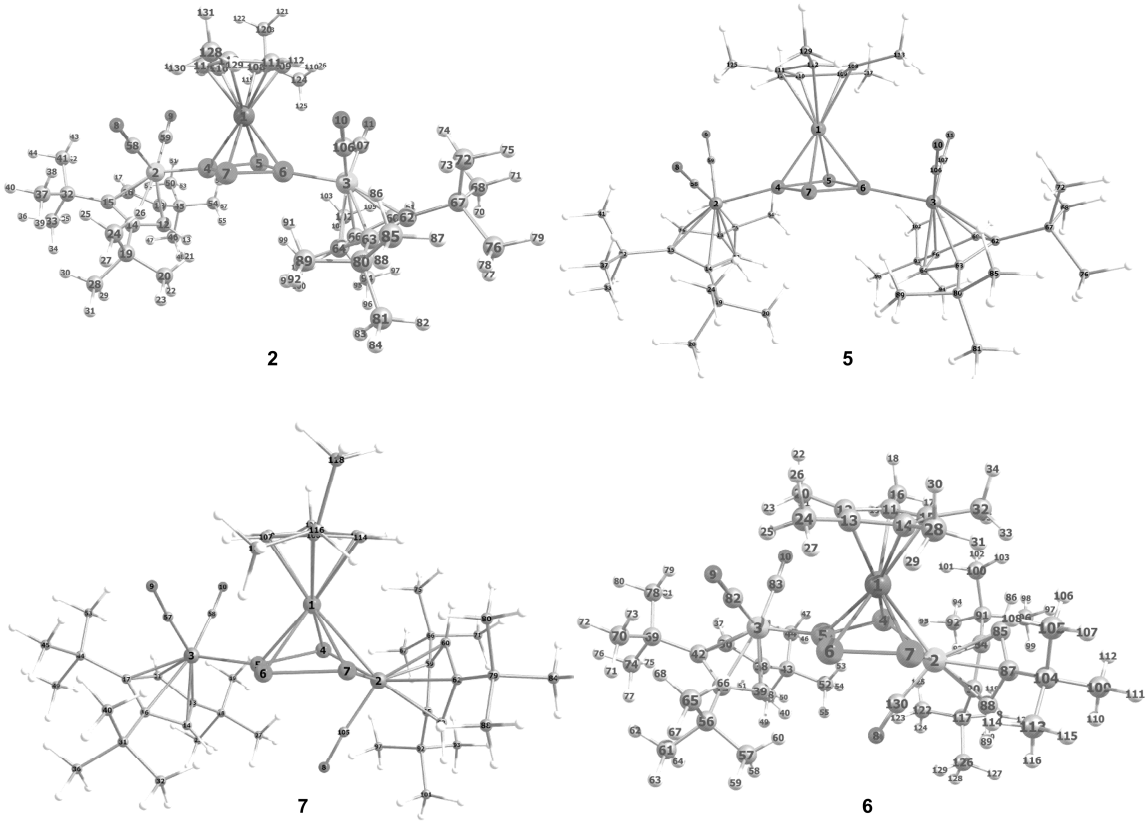

Figure S5.26. Optimized structure of $[\{Cp'''Fe(CO)_2\}_2(\mu_3,\eta^{4:1:1}\text{-}P_4)(CymRu)]^{2+}$ (**2**), $[\{Cp'''Fe(CO)_2\}_2(\mu_3,\eta^{4:1:1}\text{-}P_4)(Cp^*Ru)]^{+}$ (**5**) $[\{Cp'''Fe(CO)_2\}\{Cp'''Fe(CO)\}(\mu_3,\eta^{4:2:1}\text{-}P_4)(CymRu)]^{2+}$ (**7**) and $[\{Cp'''Fe(CO)_2\}\{Cp'''Fe(CO)\}(\mu_3,\eta^{4:2:1}\text{-}P_4)(Cp^*Ru)]^{+}$ (**6**) with the atom assignment.

Table S5.9. Calculated total energy of complexes **2**, **5**, **6**, **7** and CO.

	5	**6**	**2**	**7**	CO
BP86/def2-TZVP					
Tot. E [au]	-6163.618	-6050.2167	-6162.736	-6049.308	-113.365
Tot. E [kJ/mol]	-16182579.092	-15884843.558	-16180261.959	-15882457.721	-297640.623
B3LYP/def2-TZVP; COSMO (acetonitrile)					
Tot. E. [a.u.]	-6160.950	-6047.602	-6160.191	-6046.823	-113.311
Tot. E. [kJ/mol]	-16175573.423	-15877979.547	-16173582.450	-15875933.929	-297497.986
Tot E. + OC corr [au]	-6160.945	-6047.598	-6160.184	-6046.815	-113.311
Tot E. + OC corr [kJ/mol]	-16175561.872	-15877967.975	-16173562.440	-15875913.548	-297498.024

Table S5.10. Calculated reaction energies at the SP-COSMO-B3LYP level of the transformation of **5** to **6** and **2** to **7**.

Reaction	Reaction energy [kJ/mol]
$[\{Cp'''Fe(CO)_2\}_2(\mu_3,\eta^{4:1:1}\text{-}P_4)(Cp^*Ru)]^+$ ➔ $[\{Cp'''Fe(CO)_2\}\{Cp'''Fe(CO)\}(\mu_3,\eta^{4:2:1}\text{-}P_4)(Cp^*Ru)]^+ + CO$	95.87
$[\{Cp'''Fe(CO)_2\}_2(\mu_3,\eta^{4:1:1}\text{-}P_4)(CymRu)]^{2+}$ ➔ $[\{Cp'''Fe(CO)_2\}\{Cp'''Fe(CO)\}(\mu_3,\eta^{4:2:1}\text{-}P_4)(CymRu)]^{2+} + CO$	150.87

Table S5.11. Selected Wiberg bond indices for $[\{Cp'''Fe(CO)_2\}\{Cp'''Fe(CO)\}(\mu_3,\eta^{4:2:1}\text{-}P_4)(Cp^*Ru)]^+$ (6).

Fe2 - Ru1	0.317	P4 - Ru1	1.015	P5 - P4	0.974
P4 - Fe2	0.796	P5 - Ru1	0.604	P6 - P5	1.012
P5 - Fe3	0.970	P6 - Ru1	0.742	P7 - P6	1.127
P7 - Fe2	0.768	P7 - Ru1	1.082	P7 ··· P4	0.029

Reference:

[1] C. Schwarzmaier, A. Y. Timoshkin, G. Balázs, M. Scheer, *Angew. Chem. Int. Ed.* **2014**, *53*, 9077.
[2] F. Kleinbeck, G. J. Fettes, L. D. Fader, E. M. Carreira, *Chem. Eur. J.* **2012**, *18*, 3598.
[3] *CrysAlisPro Software System*, Agilent Technologies UK Ltd, Yarnton, Oxford, **2014**.
[4] G. Sheldrick, *Acta Cryst. A* **2015**, *71*, 3.
[5] G. M. Sheldrick, *Acta Cryst. A* **2015**, *71*, 3.
[6] O. V. Dolomanov, L. J. Bourhis, R. J. Gildea, J. A. K. Howard, H. Puschmann, *J. Appl. Crystallogr.* **2009**, *42*, 339.
[7] a) R. Ahlrichs, M. Bär, M. Häser, H. Horn, C. Kölmel, *Chem. Phys. Lett.* **1989**, *162*, 165; b) O. Treutler, R. Ahlrichs, *J. Chem. Phys.* **1995**, *102*, 346.
[8] K. Eichkorn, O. Treutler, H. Öhm, M. Häser, R. Ahlrichs, *Chem. Phys. Lett.* **1995**, *242*, 652.
[9] K. Eichkorn, F. Weigend, O. Treutler, R. Ahlrichs, *Theor. Chem. Acc.* **1997**, *97*, 119.
[10] a) P. A. M. Dirac, *Proceedings of the Royal Society of London. Series A* **1929**, *123*, 714; b) J. C. Slater, *Physical Review* **1951**, *81*, 385; c) S. H. Vosko, L. Wilk, M. Nusair, *Can. J. Phys.* **1980**, *58*, 1200; d) A. D. Becke, *Physical Review A* **1988**, *38*, 3098; e) J. P. Perdew, *Physical Review B* **1986**, *33*, 8822; f) J. P. Perdew, *Physical Review B* **1986**, *34*, 7406.
[11] A. Schäfer, C. Huber, R. Ahlrichs, *J. Chem. Phys.* **1994**, *100*, 5829.
[12] M. Sierka, A. Hogekamp, R. Ahlrichs, *J. Chem. Phys.* **2003**, *118*, 9136.

Preface

The following chapter has not been published until the submission of this thesis.

Authors

Julian Müller, Eugenia Peresypkina, Alexander V. Virovets, Michael Bodensteiner, Manfred Scheer.

Author contribution

The preparation of the manuscript was done by J. Müller. M. Scheer supervised the research and revised the manuscript. The synthesis and characterization (NMR, IR, EA, MS) of all compounds was done by J.Müller. The single crystal X-ray diffraction measurements and the structural refinement of compound **Br-R²**, **1a**, **2a$_{Na}$**, **2b$_{Na}$**, **2b$_{Tl}$**, **3a**, **6**, **8a** were done by J. Müller. M. Bodensteiner performed the single crystal X-ray diffraction measurement of compound **1b** and **3b**. The refinement of the structures of **1b** and **3b** was done by J. Müller. E. Peresypkina and A. V. Virovets performed the single crystal X-ray diffraction measurement and structural refinement of compound **4b**, **5**, **7**, **8b** and **9**. E. Peresypkina and A. V. Virovets provided a part of the discussion of **9**. The Section 'crystallographic details' in the Supporting Information was written by E. Peresypkina and A. V. Virovets.

Acknowledgements

This work was supported by the Deutsche Forschungsgemeinschaft (Sche 348/44-1). Parts of this research (projects I-20180967, I-20190914, I-20190225) were carried out at PETRA III at DESY, a member of the Helmholtz Association (HGF). A.V. and E.P. are grateful to Dr. Souane, Dr. L. Noohinejad and Dr. M. Tolkiehn for the help regarding the use of P11 and P24 beamlines.

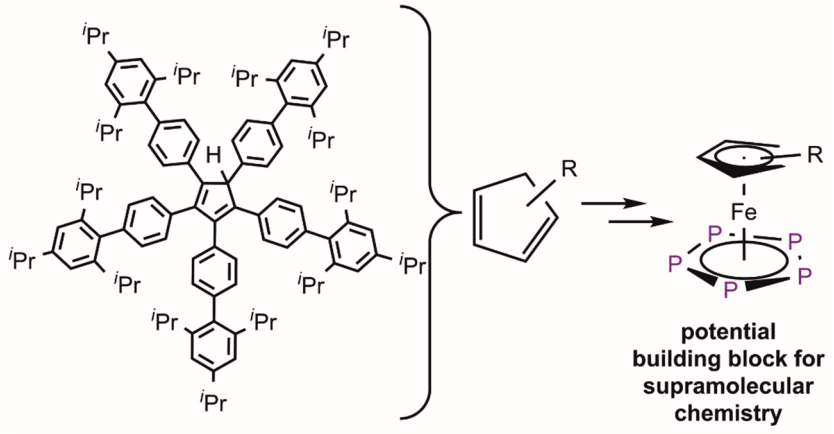
iPr
H
R
Fe
P
potential
building block for
supramolecular
chemistry

6. Total Synthesis of the Super Bulky [Cp^{XXL}Fe(η^5-P$_5$)] – A Potential Building Block for Supramolecular Aggregates

Abstract: *We report on the total synthesis of the new pentaphosphaferrocene derivative [Cp^{XXL}Fe(η^5-P$_5$)] (**6**), starting with the super bulky cyclopentadiene Cp^{XXL}H (**1b**) (Cp^{XXL} = C$_5$(2,4,6-triisopropyl-1,1'-biphenyl)$_5$). All intermediate products were isolated and fully characterized by spectroscopic methods as well as by single crystal X-ray diffraction. Additionally, the first result in supramolecular chemistry is obtained in the reaction of **6** with CuBr which yields in the novel supramolecular cluster with the general formula [{Cp^{XXL}Fe(η^4-P$_5$)}$_3$(Cu$_X$Br$_{X-3}$)(solv)$_y$] (**9**, solv = methanol or acetonitrile). Furthermore, the formation of remarkable stable cyclopentadienyl radicals could be observed which allowed their characterization by single crystal X-ray diffraction. The reaction of these cyclopentadienyl radicals with P$_4$ leads to formation of organo-substituted P$_4$ butterfly compounds.*

6.1. Introduction

Since the discovery of ferrocene ([(η^5-Cp)$_2$Fe]) in 1951,[1] cyclopentadienyl derivatives (Cp^R) have become one of the most important ligand groups in organometallic chemistry. In the last years, cyclopentadienyl complexes with all transition and main group metals, lanthanoids, and many actinoids have been synthesized. Thereby the Cp^R ligand exhibits mainly an η^5 binding mode and acts as a 6 π-electron donor. However, less frequently also an η^1, η^2, η^3, and η^4 binding mode is observed. The Cp^R–M bond is typically very stable, which is why Cp^R ligands are excellent spectator ligands and commonly used in catalysis.[2] In addition, the C$_5$H$_5$ unit can be easily functionalized, allowing the electronic and steric properties to be changed selectively.[3] Therefore, a vast variety of different Cp derivatives is known, and some examples are depicted in Scheme 6.1 (top). In recent years, there has been a trend towards ever larger Cp^R ligands. Due to their steric protection, the characterization of intermediates as well as complexes with new structural motives could be enabled. This is exemplified by the structure of [Cp$^R{}_2$Sn] which is strongly related to the size of the Cp^R ligand. The Cp$_{cent.}$–M–Cp$_{cent.}$ angle in [Cp$_2$Sn] is 143.7°/147.0°,[4] while this angle widens to 155° in [Cp*$_2$Sn][5] and finally increases to 180° in [Cp$^{Ph}{}_2$Sn][6] and [Cp$^{BIG}{}_2$Sn].[7] Another example is the kinetic stabilization of reactive 17 valence electron (VE) transition metal species in solution by large Cp^R ligands.[8]

The synthesis of [Cp*Fe(η^5-P$_5$)] in 1987 by the group of Scherer was another milestone in organometallic chemistry.[9] Compared to ferrocene, the pentaphosphaferrocene bears a *cyclo*-P$_5$ ligand which is isolobal to the Cp ligand.[10] While the oxidation of [(η^5-Cp)$_2$Fe] is mainly iron centered and the reduction leads to fragmentation, the oxidation of [Cp*Fe(η^5-P$_5$)] leads to the formation of the P,P coupled dimer [(Cp*Fe)$_2$(μ,η$^{4:4}$-P$_{10}$)]$^{2+}$.[11,12] In the dication, the P atoms, that connect the two P$_5$ units, are bend out of the former P$_5$ plane which results in an η^4 coordinated envelope structure. A similar dimeric species is observed by reduction, whereas the twofold reduction yields the monomeric dianion

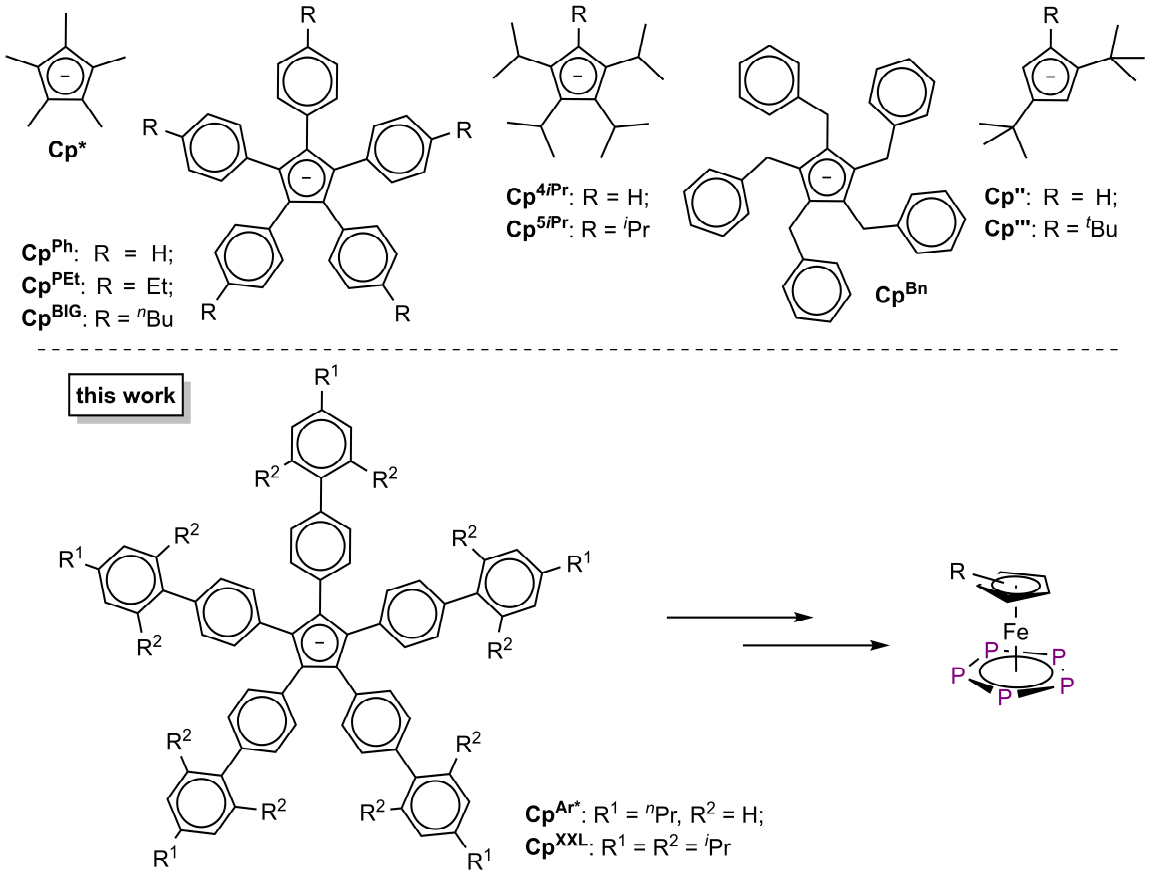

Scheme 6.1. Top: Selected examples of common Cp^R ligands as negatively charged 6 π-electron donors. Bottom: The Cp^{Ar*} and Cp^{XXL} ligand are presented in this work and were the starting point for the synthesis of super bulky pentaphosphaferrocenes.

[Cp*Fe(η^4-P$_5$)]$^{2-}$. Reactions of [Cp*Fe(η^5-P$_5$)] with ionic main group nucleophiles lead also to the formation of complexes with the P$_5$ unit in an envelope conformation.[13] Since each P atom in the *cyclo*-P$_5$ unit bears a lone pair, the pentaphosphaferrocenes show a rich coordination chemistry. The group of Scherer investigated the reactivity towards transition metal-based Lewis acids, where either an η^1 or an η^2 coordination of the *cyclo*-P$_5$ unit is observed.[14] Our group could show that reactions of [Cp*Fe(η^5-P$_5$)] with coinage metal salts lead to the formation of 1D and 2D polymers[15,16,17,18] or fullerene-like spherical aggregates.[16,19–24] A similar coordination behavior was observed for [Cp^{Bn}Fe(η^5-P$_5$)][15,25] and the larger pentaphosphaferrocene derivative [Cp^{BIG}Fe(η^5-P$_5$)].[26,27] However, more sterically demanding Cp^R ligands significantly influence the properties of the spherical aggregates. On the one hand, the solubility of the coordination compounds can be increased which allowed their characterization also in solution. On the other hand, the use of bulky pentaphosphaferrocene derivatives induces the formation of supramolecular aggregates with novel skeletal structures. When using [Cp*Fe(η^5-P$_5$)], the obtained supramolecules are either build up by 8,[23] 9,[18,23] 11,[28] 12,[19–24] or 13[29] pentaphosphaferrocene units. However, only the aggregates containing 12 pentaphosphaferrocene units exhibit fullerene-like structure. These fullerene-like supramolecules are derived from either 80 or 90-vertex scaffolds. However, if the sterical

demand of the Cp^R ligands is increased, the pentaphosphaferrocene units must be further apart, resulting in a rearrangement of the building blocks. In principle, the system can react in two different ways: On the one hand, the supramolecules can also be built up from 12 bulky pentaphosphaferrocene units to yield even larger fullerene-like aggregates. On the other hand, a smaller number of five-fold symmetrical building blocks can be used, leading to novel supramolecules with sizes that should be comparable to that of the 80-vertex ball based on [Cp*Fe(η^5-P$_5$)]. According to this concept, the use of the bulky building block [Cp^{BIG}Fe(η^5-P$_5$)] leads to the formation of [{Cp^{BIG}Fe(η^5-P$_5$)}$_{12}$Cu$_{70}$Br$_{83}$], which shows the topology of the unprecedented icosahedral C$_{140}$ fullerene.[26]

Based on the results in supramolecular chemistry, obtained first with [Cp*Fe(η^5-P$_5$)] and then with the sterically more demanding building block [Cp^{BIG}Fe(η^5-P$_5$)], we were encouraged to synthesize a pentaphosphaferrocene derivative with an even larger Cp^R ligand. The use of this super bulky building block in supramolecular chemistry should result in novel and possibly even larger supramolecular aggregates. Herein, we present the synthesis of the super bulky penta-arylated Cp^{Ar*} and Cp^{XXL} ligands and the total synthesis of the pentaphosphaferrocene derivative [Cp^{XXL}Fe(η^5-P$_5$)] (**6**; Scheme 6.1, bottom). As a proof of concept, **6** was reacted with CuBr which leads to a novel supramolecular aggregate with the general formula [{Cp^{XXL}Fe(η^4-P$_5$)}$_3$(Cu$_X$Br$_{X-3}$)(solv)$_y$] (**9**, solv = methanol or acetonitrile). Additionally, it could be shown that the new cyclopentadienyl derivatives form remarkably stable radicals which allowed their characterization by single crystal X-ray diffraction. Furthermore, to test their synthetic potential, the reactivity towards white phosphorus (P$_4$) is presented.

6.2. Results and Discussion

Preface

A general reaction pathway that is usually applied for the synthesis of pentaphosphaferrocene derivatives with bulky Cp ligands is depicted in Scheme 6.2 and starts with the corresponding cyclopentadiene derivative.[30] The following metalation is the starting point for the synthesis of [Cp^{R}Fe(CO)$_2$Br]. This Fe^{II} containing compound can be reduced to the Fe^I containing dimer [Cp^{R}Fe(CO)$_2$]$_2$. Finally, the co-thermolysis of the iron dimer with P$_4$ yields the desired pentaphosphaferrocene derivative.

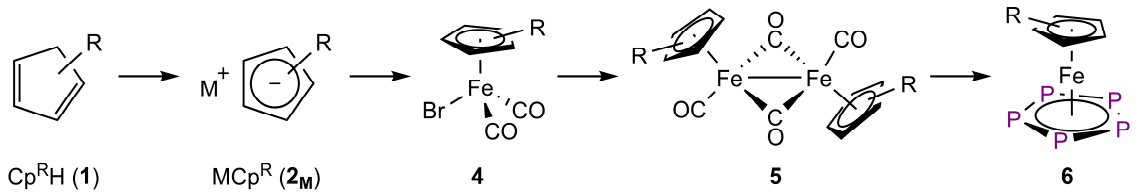

Scheme 6.2. General reaction steps for the synthesis of pentaphosphaferrocene.

Our investigation started with the synthesis of $Cp^{Ar*}H$ (**1a**; Scheme 6.1, bottom) which was then transferred into $NaCp^{Ar*}$ (**2a$_{Na}$**). However, the following synthesis of $[Cp^{Ar*}Fe(CO)_2Br]$ (**4a**) was a turning point, since regardless of the chosen reaction pathways, the formation of **4a** could not be observed spectroscopically. Despite several attempts, the only products that could be identified and isolated were the degradation products **1a** and the $Cp^{Ar*\bullet}$ radical (**3a**). The formation of $Cp^{Ph\bullet}$, and $Cp^{BIG\bullet}$ radicals in similar reactions as intermediates and side products has already been discussed in literature since they are easily recognized by their intense blue color.[30–32] However, the dark green radical **3a** seems to be remarkably stable since it is formed in large quantities and can be easily crystallized (vide infra). This high stability can be explained by the tremendous stabilization of the radical **3a** by delocalization over the central C_5 ring and ten adjacent phenyl groups. Moreover, this delocalization lowers the electron density in the central C_5 ring of the Cp^{Ar*} anion (**2a**) which is why the Cp^{Ar*} ligand is a very weak electron donating ligand. The combination of these two effects thus hinders the formation of the crucial complex **4a**, needed for the synthesis of the corresponding pentaphosphaferrocene derivative.

To reduce the amount of delocalization, the ligand design was changed to $Cp^{XXL}H$ (**1b**; Scheme 6.1, bottom). The substitution of all outer phenyl groups with ^{i}Pr groups in the *ortho* and *para*-position leads to a sterically induced rotation of the second ring plane by approx. 90°. Therefore, the outer ring planes should be electronically decoupled from the inner ones. Consequently, the $Cp^{XXL\bullet}$ radical (**3b**) is stabilized only by delocalization over the central C_5 ring and five phenyl groups, resulting in a decrease of the overall stability of **3b** to a level that is comparable to the $Cp^{Ph\bullet}$, $Cp^{PEt\bullet}$, and $Cp^{BIG\bullet}$ radicals. Additionally, a reduced delocalization should lead to a higher electron density in the central C_5 unit and in better electron donating properties which is needed to build up Cp^{XXL} containing iron complexes.

Synthesis of the Super Bulky Cyclopentadienyl Ligands and Radicals

The cyclopentadiene derivatives **1a** and **1b** are synthesized in moderate yields (53% for **1a** and 51% for **1b**) via a palladium catalyzed one-pot synthesis,[33] starting with $[Cp_2ZrCl_2]$ and 4-bromo-4'-propyl-1,1'-biphenyl (**Br-R^1**) or 4'-bromo-2,4,6-triisopropyl-1,1'-biphenyl (**Br-R^2**), respectively (Scheme 6.3).

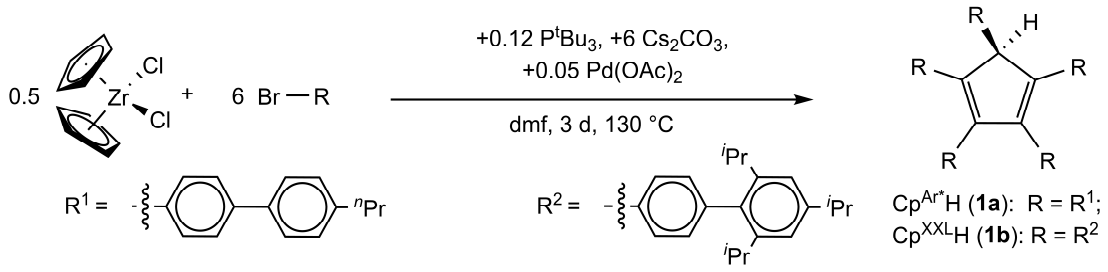

Scheme 6.3. Synthesis of the cyclopentadiene derivatives **1a** and **1b** via a palladium catalyzed one-pot synthesis.

The single crystal X-ray structure analysis confirmed the formation of penta-substituted cyclopentadiene derivatives (Figure 6.1). In both structures, one of the central C atoms is clearly sp^3 hybridized since the attached aryl substituent is bend out of the *cyclo*-C_5 plane.

The ^1H NMR spectra of **1a** (C_6D_6) and **1b** ($CDCl_3$) show the characteristic signal for the protonated C_5 ring at δ = 5.32 ppm (**1a**) and 5.27 ppm (**1b**). Furthermore, the additional bond to a hydrogen atom of one of the central C atoms leads to a splitting of the signals into three sets with an integral ratio of 1:2:2. As these signals superimpose, only two sets of signals with an integral ratio of 3:2 are observed.

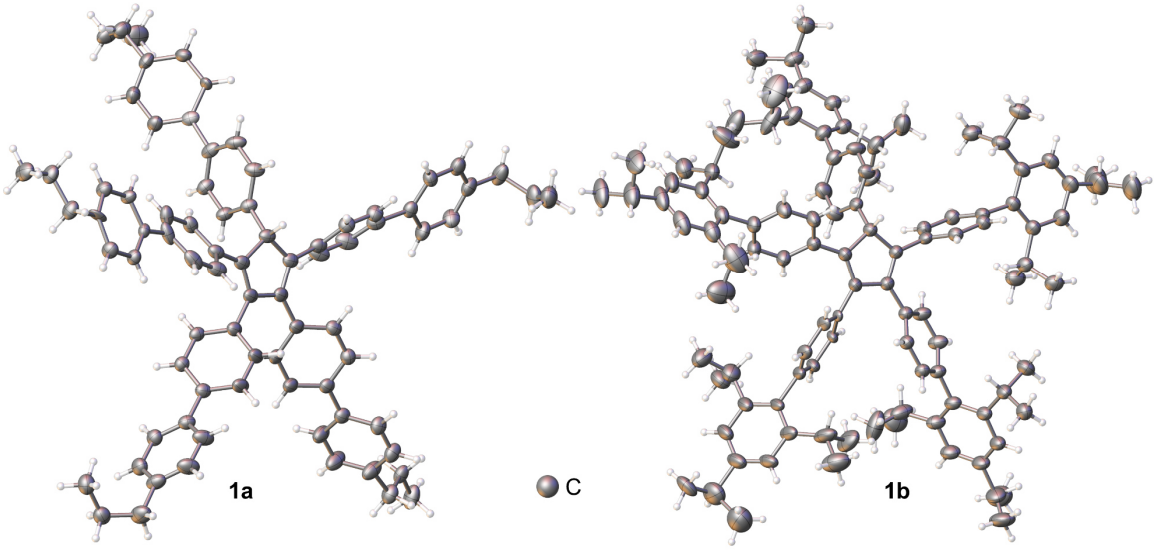

Figure 6.1. Molecular structure of **1a** (left) and **1b** in solid state. Solvent molecules are omitted for clarity and atom displacement parameters (ADPs) are shown at 50% probability level.

The following metalation of the cyclopentadiene is a crucial step in this chemistry. On the one hand, deprotonation provides the metalated Cp ligand, on the other hand it is also suitable as a purification step. The main problem in the one pot synthesis of **1a** and **1b** is column chromatographic work up. Since the reaction is performed on a multi-gram scale and many side products exhibit almost the same solubility as the product, the column chromatographic workup must be repeated several times to obtain **1a** or **1b** in analytically pure form. Therefore, generally the most practical method is the removal of by-products by filtration, followed by one-time column chromatographic workup and reaction of the resulting mixture with an alkali metal base. The formed salt can be washed with nonpolar solvents which typically allows the isolation of analytical pure MCp^R.

According to this procedure, $NaCp^{Ar*}$ (**2a$_{Na}$**) and $NaCp^{XXL}$ (**2b$_{Na}$**) were synthesized from the cyclopentadienes and $NaNH_2$ in thf (Scheme 6.4). While **2a$_{Na}$** can be isolated in good yields (79%), **2b$_{Na}$** is only obtained in small amounts and in low purity, since **2b$_{Na}$** is highly soluble in non-polar solvents like toluene, hexane, and pentane. The change to KCp^{XXL} (**2b$_K$**), which was synthesized from **1b** and KH, resulted in only a slight decrease of the solubility in nonpolar solvents. Finally, only the synthesis of $TlCp^{XXL}$ (**2b$_{Tl}$**) allowed the

isolation of a MCp^{XXL} salt in the desired purity and good yields (67%). The thallium salt **2b$_{Tl}$** is obtained as bright yellow powder from the reaction of **1b** and TlOEt in hexane.

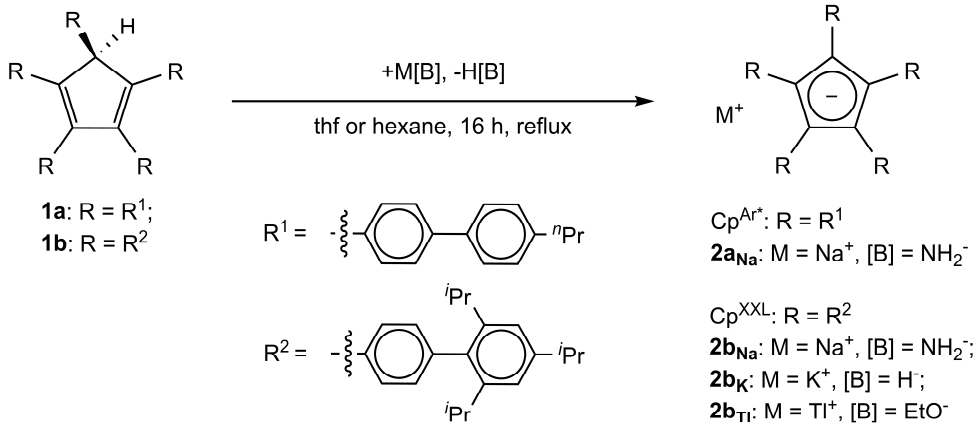

Scheme 6.4. Metalation of **1a** and **1b**.

Crystals suitable for single crystal X-ray analysis were obtained for **2a$_{Na}$** at −35°C from a thf/hexane solution, while crystals of **2b$_{Tl}$** were obtained by slow diffusion of a CH_2Cl_2 solution into hexane. Compound **2b$_{Na}$** could be crystallized under the same conditions as **2a$_{Na}$**, but the quality of the crystals was poor, so only the connectivity could be confirmed (see Figure S6.2). The molecular structures of **2a$_{Na}$** and **2b$_{Tl}$** in the solid state are depicted in Figure 6.2 and reveal that within the C_5 rings all C atoms are sp^2 hybridized and possess almost identical C–C bond lengths (1.414(3) Å – 1.429(2) Å in **2a$_{Na}$** and 1.411(5) Å – 1.435(5) Å in **2b$_{Tl}$**). The inner phenyl groups of the five aryl substituents are not co-planar to the central C_5 ring but are twisted by 39.86(6)° – 56.56(7)° in **2a$_{Na}$** and 46.96(19)° – 51.85(19)° in **2b$_{Tl}$**, which results in the typical propeller-like configuration.[34–36] The influence of the ^{i}Pr substituents at the Cp^{XXL} ligand can be determined from the twist angle of the inner and outer phenyl groups. While the twist angles in **2a$_{Na}$** vary from 20.99(6)° to 36.82(6)°, the twist angles in **2b$_{Tl}$** are clearly increased as they vary from 76.69(13)° to 88.70(19)°. However, the most remarkable feature when comparing the structures is that in **2a$_{Na}$** the Cp^{Ar*} anion is non-coordinated. Typically, either 1D coordination polymers or oligomers are observed in the solid state structures of [M(solvent)$_x$Cp^R] (M = Li, Na, K, Rb, Cs).[32,34,36,37,38] Only in the presence of strong donating ligands like crown ethers, the complete separation of the ions can be observed.[39] The fact that in **2a$_{Na}$** the sodium cation is only stabilized by six relatively weakly coordinating thf molecules and no cation-anion interaction is observed, highlights that Cp^{Ar*} is a very poor electron donating ligand. This is probably due to the extraordinary mesomeric stabilization of the cyclopentadienyl anion, caused by delocalization of the electron density over the C_5 ring and ten phenyl groups. Contrary to **2a$_{Na}$**, both **2b$_{Tl}$** and **2b$_{Na}$** (see SI for more information) have contact ion pairs in the solid state, indicating that the introduction of ^{i}Pr groups hampers delocalization. Due to the steric bulk of the ^{i}Pr substituents, the formation of a coordination polymer is hindered. Instead, dimers are present which are build up by metallocene anions [Cp$^{XXL}_2$M]$^-$ (M = Na,

Tl) and an external metal cation that coordinates the sandwich complex from one side (see Figure S6.2 and Figure S6.3). The formation of these neutral units is often found in structures of alkali metal compounds with bulky Cp-ligands.[34] While the external sodium cation in **2b$_{Na}$** is coordinatively saturated by thf molecules,[40] the external thallium cation in **2b$_{Tl}$** is not coordinated by any solvent molecules (**2b$_{Tl}$** was crystallized from a CH_2Cl_2/hexane mixture). However, the thallium cation exhibits intermolecular Tl–C distances of 3.322(7) Å – 3.656(9) Å (Tl–C$_{6,cent.}$ = 3.190(4) Å) to an adjacent triisopropyl-phenyl group (see Figure S6.4). These distances are in good agreement with thallium(I)arene compounds known in the literature and therefore indicate intermolecular stabilization of the external thallium cation.[41] The two identical Tl–Cp distances to the inner Tl atom are with 2.697(2) Å shorter than the distance of 2.796(2) Å to the external Tl atom. The bond lengths are comparable to the ones in polymeric TlCp* (2.71(1) Å)[42] and Tl(C_5Me_4H) (2.68 Å and 2.70 Å)[37] while they are significantly shorter than in TlCp (3.19(10) Å).[43] However, the Tl-Cp bond lengths in **2b$_{Tl}$** are much longer compared to those in TlCp^{Bn} (2.490 Å[44] and 2.494(4) Å[45]).

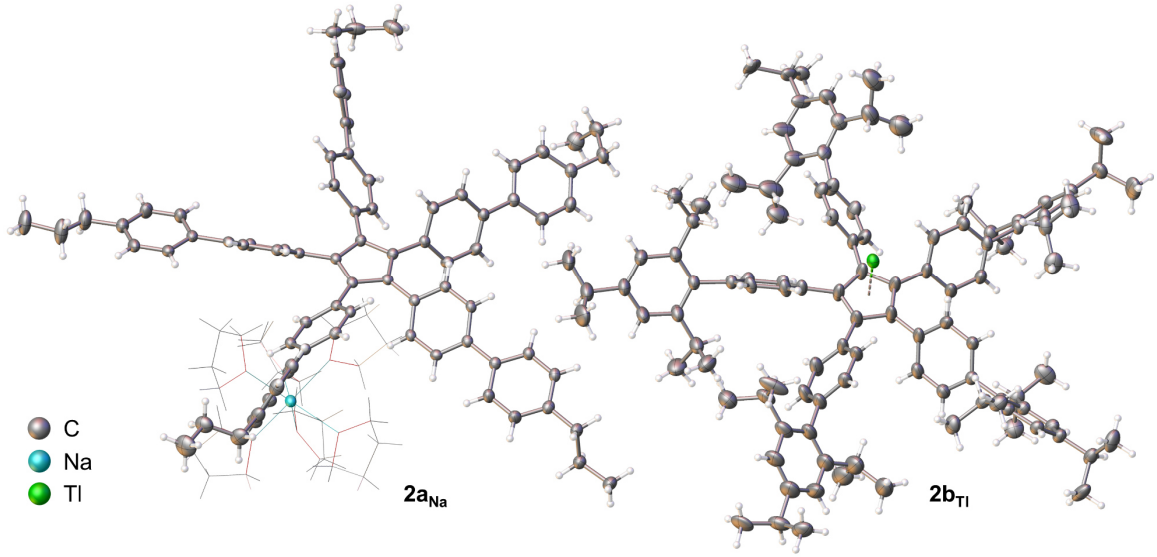

Figure 6.2. Molecular structure of **2a$_{Na}$** (left) and **2b$_{Tl}$** (right) in solid state. The thf molecules of the [Na(thf)$_6$]$^+$ cation are shown as a wire frame model and additional solvent molecules are omitted for clarity. For **2b$_{Tl}$** only half of Tl[Cp$^{XXL}_2$Tl] is shown which is present in solid state (see Figure S6.3). ADPs are shown at 50% probability level.

Due to the high radical stability, solutions of **2a$_{Na}$** always contain small amounts of **3a**, which is why no reliable ^{1}H NMR spectrum could be obtained. With the more stable **2b$_{Tl}$**, the formation of radicals in solution can be prevented if it is handled carefully. The ^{1}H NMR spectrum of **2b$_{Tl}$** in CD_2Cl_2 shows one sharp set of signals for the five magnetically equivalent substituents of the Cp^{XXL} ligand.

Although radicals are typically known for particularly high reactivity, the two cyclopentadienyl radicals **3a** and **3b** appear to be moderately stable. Therefore, the formation and properties of the new cyclopentadienyl radicals is further investigated. The

interest of chemists in cyclopentadienyl radicals started almost a century ago when Ziegler and Schnell observed the Cp^{Ph} radical the first time.[46] Since then, the exact structure of Cp^R-radicals has been widely discussed.[47,48] In the meantime, several derivatives have been synthesized and characterized spectroscopically[47,49,50,51] as well as by single crystal X-ray diffraction.[52–55] As mentioned before, the formation of Cp^{Ar*}• (**3a**) as well as Cp^{XXL}• (**3b**) can be observed, due to their intense green (**3a**) and blue (**3b**) colors, in many reactions as side or degradation products. To investigate these remarkably stable radicals in detail, we synthesized **3a** and **3b** via oxidation of the metalated cyclopentadienyl with CuBr (Scheme 6.5).[56]

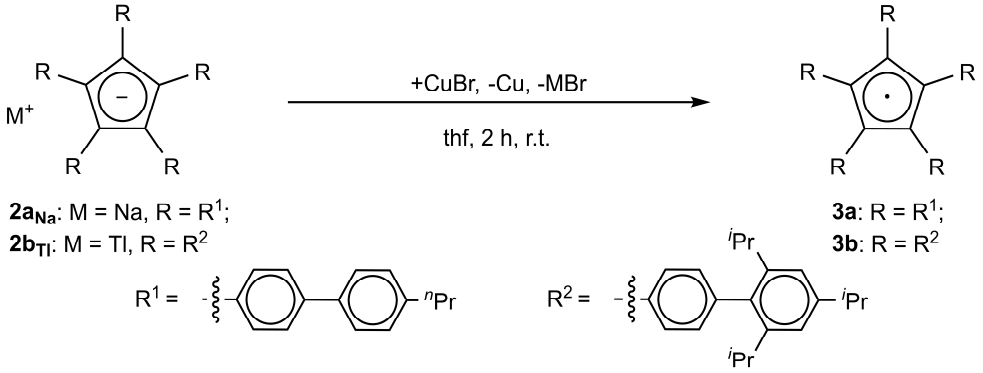

Scheme 6.5. Synthesis of **3a** and **3b** via oxidation with CuBr.[57] The amount of the radical formed in the reaction solution is difficult to determine by spectroscopic methods, so no exact data can be given.[58]

The synthesis of **3a** is completed within 2 h since the following filtration shows no residue of yellow **2a$_{Na}$**. However, the synthesis of **3b** is slower. Even after stirring for 24 h, traces of yellow **2b$_{Tl}$** are still present and can be removed by filtration. On the one hand, the slower reaction speed might be related to the stronger interaction between the thallium cation and the Cp^{XXL} anion, compared to the very weak interaction between Na$^+$ and the Cp^{Ar*} anion. On the other hand, **2b$_{Tl}$** is less soluble in thf than **2a$_{Na}$**, which could also slow down the reaction. Finally, the two radicals should exhibit different stabilities as it can already be roughly estimated from their colors. The group of Kurreck studied the Cp^{Ph}•, the Cp^{PMe}• (Cp^{PMe} = η^5-C$_5$(C$_6$H$_4$CH$_3$)$_5$) as well as the Cp^{BiPh}• (Cp^{BiPh} = η^5-C$_5$(C$_6$H$_4$C$_6$H$_5$)$_5$) radicals.[49] These radicals show absorption maxima at λ$_{max}$ = 585 nm (Cp^{Ph}•), 613 nm (Cp^{Ph*}•), and 677 nm (Cp^{BiPh}•) which is shifted to longer wavelengths with increasing substitution. A similar trend was observed in the calculated excitation energies for the first excited state. Compared to Cp^{Ph}• the excitation energy decreases with Cp^{PMe}• by 2.3 kcal/mol and with Cp^{BiPh}• by 6.7 kcal/mol. In the case of **3a** the absorption maximum is at λ$_{max}$ = 681 nm,[59] which shows that it is comparable to Cp^{BiPh}•. In comparison, the absorption maximum of **3b** at λ$_{max}$ = 620 nm is strongly redshifted. Therefore, the electronically structure of **3b** is comparable to the blue colored Cp^{Ph}•, Cp^{PMe}•, Cp^{PEt}• and Cp^{BIG}• radicals.[56,60] This feature highlights again that the new ligand design of Cp^{XXL} leads to an altered electronic structure compared to the Cp^{Ar*} ligand, while however the huge steric demand is maintained.

Radicals **3a** and **3b** each show a signal in the EPR spectrum, referring to g-factors of 2.004 (**3a** in toluene at 77 K) and 2.000 (**3b** in toluene at 77 K), respectively. The values are in good agreement with other cyclopentadienyl radicals.[51–53,55,56,60–62]

Both radicals can be crystallized by slow diffusion of a toluene solution into acetonitrile. Crystals of **3a** can be obtained as dark green blocks, while **3b** crystallizes as reddish blue blocks. In both cases the crystals are always polluted with the degradation products **1a** and **1b**, which are obtained as colorless crystals. Crystals of **3a** and **3b** must therefore always be separated manually, which is why the isolated yield of the analytically pure radicals is very low (8% (**3a**) and 2% (**3b**)).

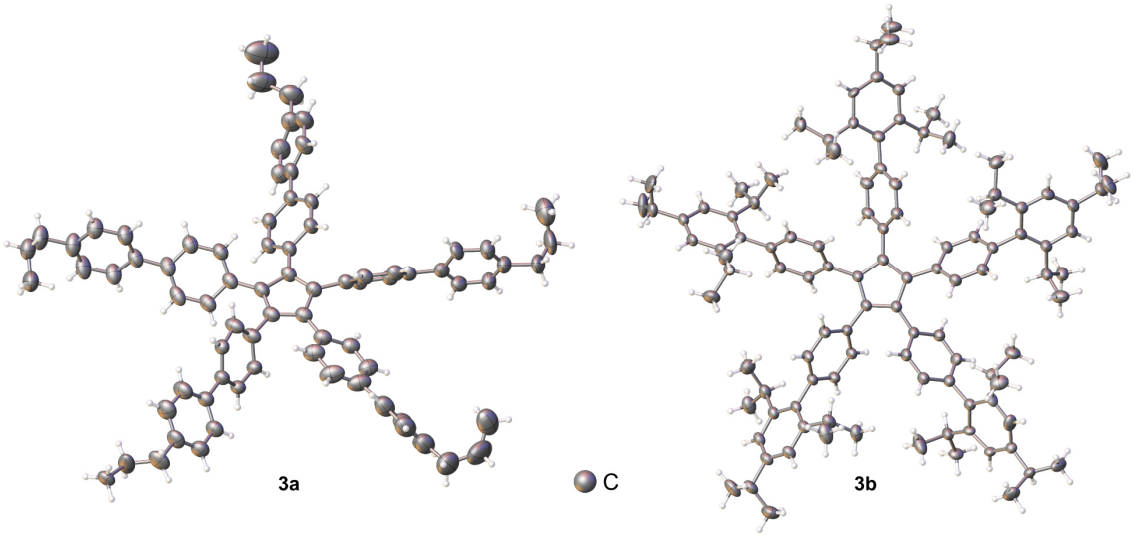

Figure 6.3. Molecular structure of **3a** (left) and **3b** (right) in solid state. ADPs are shown at 50% probability level.

The molecular structure of **3a** and **3b** in solid state is depicted in Figure 6.3. In both structures, all aryl substituents are in the C_5 plane, which shows that the C atoms of the C_5 rings are sp^2 hybridized. The C–C bond length in the C_5 ring are with 1.385(3) Å – 1.472(4) Å in **3a** and 1.4162(18) Å – 1.4374(17) Å in **3b** comparable to the ones in the corresponding anions as well as other structural characterized cyclopentadienyl radicals.[52–55,62] Remarkable is the packing of the radicals in solid state. Radical **3a** forms layers that are slightly shifted against each other (see Figure S6.5). Hereby, short intermolecular H···C contacts within these layers are observed, due to the propeller-like configuration of the aryl substituents. The H···C distances are shorter than the sum of the van der Waals radii for C and H (2.90 Å) and go down to 2.641(3)°Å which is in good agreement with already reported H···C contacts.[63,64] In the solid state structure of **3b**, dimeric units are present which are reminiscent of metallocene structures, where the formal position of the metal is not occupied (see Figure S6.6). In this dimeric units, the central C_5 rings are parallel to each other and are orientated in a staggered conformation while the $C_{5,cent.}$–$C_{5,cent.}$ distance is 4.7059(13) Å. The reason for the formation of dimeric

units in the solid state is most likely the stabilization of 18 intermolecular short H···C contact in the range of 2.7633(15) Å– 3.0690(15) Å between C_{Phenyl} and H_{Phenyl} and H_{Methyl}, respectively (see Figure S6.7).

Synthesis of Cyclopentadienyl Iron Carbonyl Complexes 4 and 5.

As mentioned before, the formation of [Cp^{Ar*}Fe(CO)$_2$Br] (**4a**) could not be observed, although two reaction pathways have been tested (Scheme 6.6). Pathway 1 is the common method to synthesize [Cp^{R}Fe(CO)$_2$Br] with sterically demanding Cp^R ligands to give the respective products in moderate to good yields, starting with the corresponding NaCp^R salt.[30,65,66] However, performing the same protocol starting with **2a$_{Na}$**, no reaction occurs and only the decomposition compounds **3a** and **1a** could be observed. In pathway 2, the Cp^{Ar*} anion is first oxidized to the dark yellow Cp^{Ar*}Br,[67] while the reduction with [Fe(CO)$_5$] gives dark green **3a** and [Fe(CO)$_x$Br] at room temperature.[31,68] Subsequent thermolysis should yield the desired complex. But even after several hours of heating, the color of the reaction mixture is still dark green. In addition, the formation of a metallic mirror is observed, which most likely results from the thermal decomposition of [Fe(CO)$_x$Br]. By subsequent IR spectroscopical investigations, the characteristic CO absorption bands for **4a** could not be detected. Summarizing the results of these two reaction pathways, it must be concluded that with the Cp^{Ar*} ligand, which on the one hand is a very poor electron donating ligand and on the other hand forms the extremely stable radical **3a**, the formation of **4a** is not possible. Therefore, we were not able to continue the synthesis of the Cp^{Ar*} containing pentaphosphaferrocene derivative. For this reason, we then focused only on the synthesis of the corresponding Cp^{XXL} complexes.

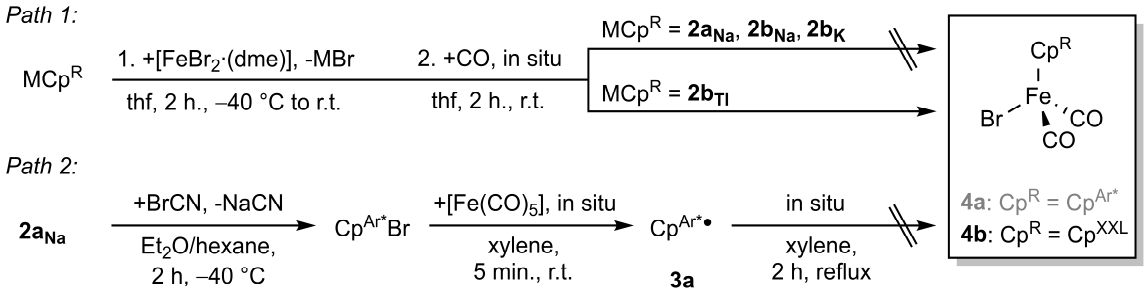

Scheme 6.6. Reaction pathway for the synthesis of **4b** (Path 1). The synthesis of **4a** was not successful regardless the chosen reaction pathway which is why it is greyed out.

Surprisingly, the use of both **2b$_{Na}$** and **2b$_K$** did not lead to formation of [Cp^{XXL}Fe(CO)$_2$Br] (**4b**) via reaction pathway 1. This indicates that although the introduction of the ^{i}Pr substituents has improved the electron-donating properties of the Cp^{XXL} ligand compared to Cp^{Ar*}, the Cp^{XXL} ligand is a weaker electron donor than the Cp^{Ph} or Cp^{BIG} ligand. More precisely, the Cp^{BIG} ligand should be a stronger electron donor than the Cp^{Ph} ligand, because of the +I effect of the ^{n}Bu groups. However, despite the unfavorable overlap due to the ^{i}Pr substituents, the outer triisopropylphenyl groups act as weak −M substituents,

thus reducing the electron density in the central C_5 ring in the Cp^{XXL} ligand. However, this disadvantage could be overcome by reacting [$FeBr_2$·(dme)] (dme = dimethoxyethane) with **2b$_{Tl}$** which leads finally to the formation of [$Cp^{XXL}Fe(CO)_2Br$] (**4b**) in quantitative yield of 98%. The reason for this is most likely an equilibrium between the free Cp^R ligand, a dissociated Br^-, and a $[FeBrL_x]^+$ (L = solvent molecules) moiety. By using **2b$_{Na}$** and **2b$_K$**, the dissociated bromide anions cannot be removed from the equilibrium, since NaBr and KBr are still slightly soluble in thf. However, by using **2b$_{Tl}$**, the bromide anions are removed from the equilibrium by precipitation of insoluble TlBr, leading to **4b**.

The formation of **4b** can best be verified by IR spectroscopy since a toluene solution shows two strong absorption bands in the range of CO stretching frequencies at $\tilde{\nu}$ = 1996 cm^{-1} and 2035 cm^{-1} that compare well to those of the Cp^{BIG} derivative ($\tilde{\nu}$ = 1991 cm^{-1} and 2032 cm^{-1}).[30] The ^1H NMR spectrum of **4b** in CD_2Cl_2 shows the typical set of signals. However, the signals are very broad which might be attributed to a partial decomposition of **4b** is solution. The reason for this might either be a dissociative disproportion reaction which generates small amounts of the radical **3b** or the spontaneous release of CO. The release of CO in solution at room temperature was already observed for the similar complexes [$Cp^RFe(CO)_2X$] (Cp^R = η^5-C_5H_5, η^5-$C_5H_4CO_2Me$; X = Cl, Br, I).[69]

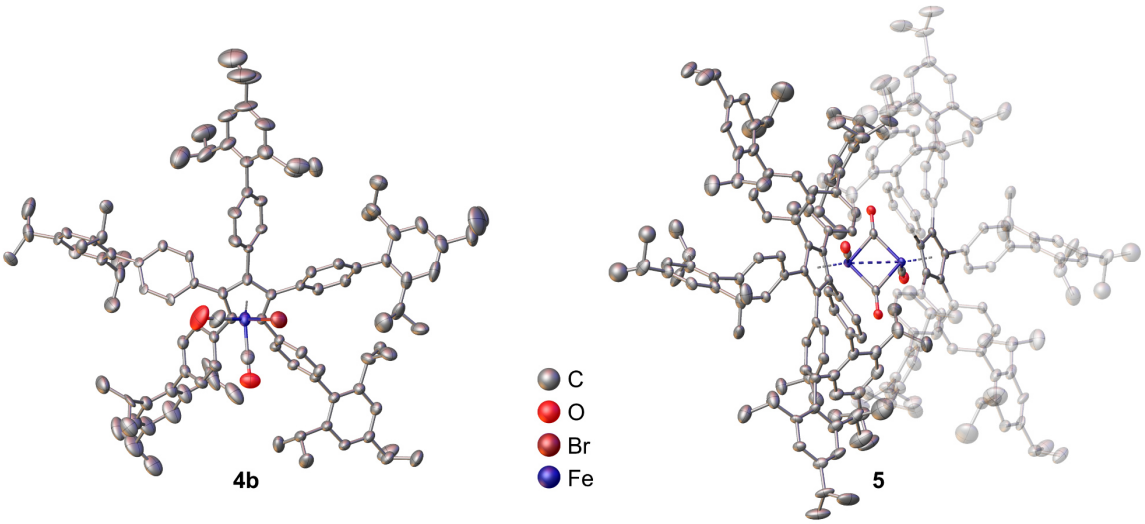

Figure 6.4. Molecular structure of **4b** (left) and **5** (right) in solid state. In the structure of **5**, the substituents of the second Cp^{XXL} ligand are translucent for clarity. Hydrogen atoms as well as solvent molecules are also omitted for clarity. ADPs are shown at 50% probability level.

The molecular structure of **4b** is depicted on the left at Figure 6.4 and is comparable to other [$Cp^RFe(CO)_2Br$] compounds. However, a closer comparison shows that **4b** exhibits the longest Fe–$Cp_{Cent.}$ distances in this group of complexes. Since the Fe–$Cp_{Cent.}$ distances increase in the order from Cp^R = η^5-C_5H_5 (1.710(2) Å),[70] η^5-$C_5H_4CO_2Me$ (1.714(3) Å),[69] η^5-$C_5Me_4(CF_3)$ (1.729(1) Å),[71] Cp^{Ph} (1.738(5) Å)[72] to Cp^{XXL} (1.746(3)/1.748(2) Å), this indicates that the distance is affected by both steric and electronic properties of the Cp^R ligands.

The reduction of **4b** with KC_8 leads to the formation of the iron dimer [Cp^{XXL}Fe(CO)$_2$]$_2$ (**5**) in moderate yields of 55% (Scheme 6.7). Since the starting material as well as the iron dimer exhibit similar solubility, KC_8 is typically used in a slight excess to produce small amounts of the ferrate K[Cp^{R}Fe(CO)$_2$].[30,65] Normally, washing the crude mixture with highly polar solvents like acetonitrile gives access to the analytically pure iron dimer. However, in the case of the corresponding Cp^{XXL} containing complexes, this procedure is not feasible since the ferrate salt is insoluble in highly polar solvents like acetonitrile. On the other hand, the starting material as well as the two products are at least slightly soluble in thf, pentane, or diethyl ether. A separation by column chromatography is also problematic since **5** partly decomposes on the column. Therefore, the only practical method for purification of **5** is crystallization. This gives **5** as dark green prisms and traces of the degradation product **1a** as colorless crystals which must be separated manually.

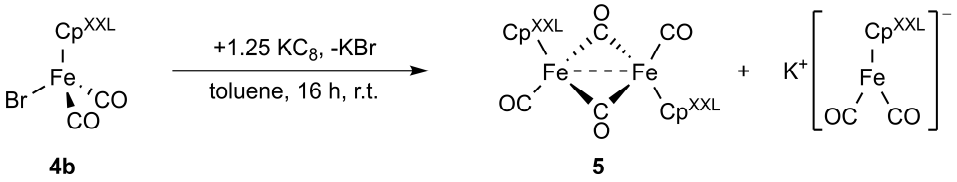

4b **5**

Scheme 6.7. Synthesis of **5** via the reduction of **4b** with KC_8.

The molecular structure of **5** reveals the formation of the dimeric iron complex with the expected *trans* orientation of the two Cp^{XXL} ligands (Figure 6.4, right). Due to the sterical influence of the Cp^{XXL}-ligands, the Fe–Fe distance is with 2.6083(5) Å one of the longest among dimeric iron carbonyl complexes.[64,65,69,73] However, surprisingly, the Fe–Fe distance is slightly shorter than the corresponding distance in the sterically less demanding Cp^{BIG} analogue (2.6180(3) Å) which might be related to the electronic structure of the Cp^{XXL} ligand.[30]

The ^{1}H NMR spectrum of **5** in thf-d$_8$ shows very broad signals for the Cp^{XXL} ligand in the expected region. This broadening might be attributed either to dynamic processes of the ligand, or to a monomer-dimer equilibrium in solution. The assumption of a monomer-dimer equilibrium is supported by the presence of four peaks in the region of the CO stretching frequencies in the IR spectrum. Here, the absorption bands in a toluene solution of **5** at $\tilde{\nu}$ = 1782 cm^{-1} and 1954 cm^{-1} can be assigned to the dimer, while the two weak absorption bands at $\tilde{\nu}$ = 1924 cm^{-1} and 1990 cm^{-1} can be assigned to the 17 VE monomer. These findings are in good agreement with other pentaaryl-substituted Cp derivatives.[30,74]

Synthesis and Characterization of the Pentaphosphaferrocene Derivative 6 and the P$_4$ Butterfly Compounds 7 and 8

Thermolytic treatment of the iron dimer **5** in the presence of P$_4$ leads to the formation of the pentaphosphaferrocene derivative [Cp^{XXL}Fe(η^5-P$_5$)] (**6**) in moderate yields of 25%

(Scheme 6.8, top).[75] However, stirring **5** in the presence of P_4 at room temperature yields quantitatively (according to IR spectroscopy of the reaction solution, isolated yield: 49%) in [{Cp^{XXL}Fe(CO)$_2$}$_2$(μ,η$^{1:1}$-P$_4$)] (**7**) that bears a tetraphospha-bicylo[1.1.0]butane unit (Scheme 6.8, bottom). The central P_4 unit of **7** is also commonly referred to as butterfly motif. Furthermore, complex **7** can be transformed into **6** if treated with additional P_4 under thermolytic conditions.

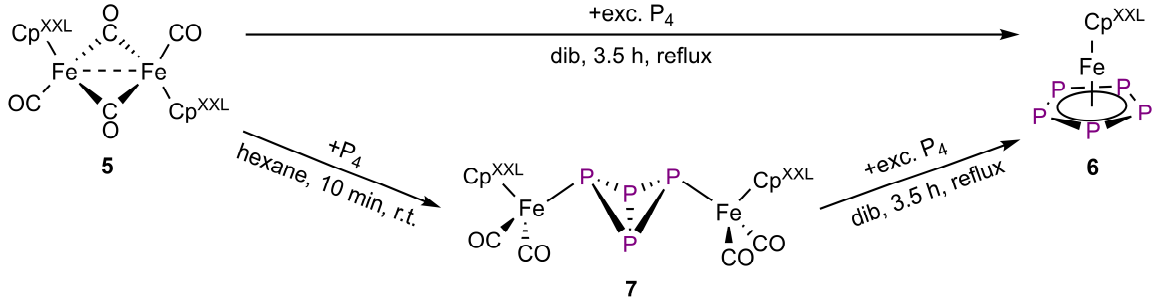

Scheme 6.8. Isolated reaction products of **5** with white phosphorus. dib = 1,2-diisopropylbenzene.

Complex **6** can be obtained after column chromatographic workup and elutes first as an intense green fraction. However, the column chromatographic workup is problematic since the band of **6** separates only poorly from a following red band. This is most likely caused by the ligand Cp^{XXL}, which stabilizes the different reaction products and strongly dominates their solubility. Therefore, the red fraction always contains traces of **6**. Despite several attempts, the exact molecular structure of the red byproduct could not be unambiguously clarified yet. However, we assume that the byproduct is [(Cp^{XXL}Fe)$_2$(μ,η$^{4:4}$-P$_4$)] since corresponding complexes with the Cp''' and Cp^{BIG} ligand are formed under the same conditions.[30,76]

Pentaphosphaferrocene **6** crystallizes as thin green needles by slow diffusion of a toluene solution into acetonitrile. The molecular structure of **6** is depicted in Figure 6.5 (left) and shows a staggered conformation with a P_5–C_5 twist angle of approx. 16°. The bond distances and angles are in the expected region and are comparable to previously reported pentaphosphaferrocene derivatives.[30,64,76,77] However, with the Cp^{XXL} ligand attached to the [FeP$_5$] fragment, **6** is the largest pentaphosphaferrocene derivative reported so far. This is demonstrated by an average $C_{5,cent.}$–$C_{outmost}$ distance (see Figure 6.5) of about 12 Å ([Cp^{BIG}Fe(η^5-P$_5$)] ≈ 9 Å, [Cp*Fe(η^5-P$_5$)] ≈ 3 Å).[26]

The ^{31}P{^{1}H} NMR spectrum of **6** in C_6D_6 shows a sharp singlet at δ = 174.6 ppm. Compound **6** has the strongest low-field shifted signal among the known pentaphosphaferrocene derivatives.[9,30,64,76,77] The ^{1}H NMR spectrum of **6** in C_6D_6 shows sharp signals for the 15 isopropyl groups at δ = 1.19 ppm (doublet), 1.25 ppm (doublet), 2.85 ppm (septet), and 2.96 ppm (septet) with an integral ratio of 60:30:5:10. However, the signals in the aromatic region split up into a multiplet at δ = 7.19 ppm, a singlet at δ = 7.22 ppm, and one very broad signal ($\omega_{½}$ ≈ 160 Hz) at δ = 7.48 ppm, where each signal

exhibits an integral of 10. The broad signal in the aromatic region may be caused by dynamic processes in solution that cannot be resolved on the NMR time scale.

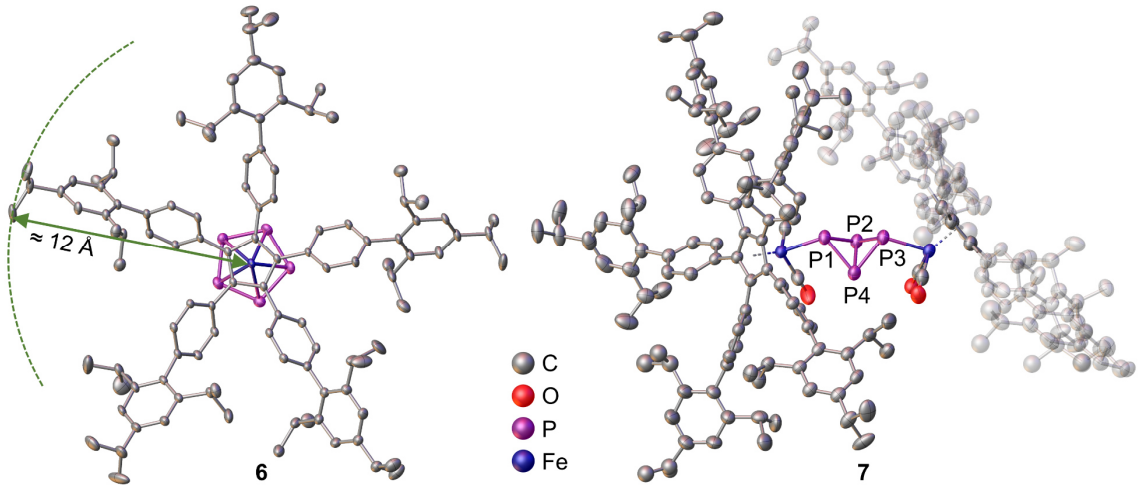

Figure 6.5. Molecular structure of **6** (left) in a top view and **7** (right) in solid state. The dotted line in the structure of **6** indicates the circular area that is roughly blocked by the Cp^{XXL} ligand with a radius of approx. 12 Å ($C_{5,cent.}$–$C_{outmost}$ distance). In the structure of **7**, the substituents of the second Cp^{XXL} ligand are translucent for clarity. Hydrogen atoms as well as solvent molecules are also omitted for clarity. ADPs are shown at 50% probability level.

The P_4 butterfly complex **7** can be crystallized as orange prisms by slow diffusion of a toluene solution into acetonitrile. The molecular structure of **7** shows a central P_4 butterfly unit that is stabilized by two [Cp^{XXL}Fe(CO)$_2$] fragments (Figure 6.5, right). The P–P bond distances between the "wing-tip" (P1 and P3) and the "bridge-head" (P2 and P4) phosphorus atoms vary from 2.21611(1) Å to 2.23343(1) Å and are in the range of P–P single bonds (2.20 Å – 2.25 Å). In contrast, the bond between the two "bridge-head" phosphorus atoms has with 2.18515(1) Å slightly double bond character. With a distance between the two "wing-tip" phosphorus atoms of 2.79551(1) Å, the P_4 unit is almost identical to that in [{Cp^{BIG}Fe(CO)$_2$}$_2$(μ,η$^{1:1}$-P$_4$)].[78] However, a comparison with the derivative containing Cp'", shows that stabilization by both a Cp^{BIG} and a Cp^{XXL} ligand leads to a slight P–P bond elongation, while the distance between the two "wing tip" phosphorus atoms is shortened by about 0.2 Å.[76] The Fe–P distances are with 2.31142(1) Å and 2.31709(1) Å slightly shorter than the corresponding distances in the Cp''' (2.348(2) Å and 2.3552(19) Å) and the Cp^{BIG} (2.3397(4) Å) stabilized derivatives.

The ^{1}H NMR spectrum of **7** shows the appropriate but slightly broadened set of signals for the two magnetically equivalent Cp^{XXL} ligands. The ^{31}P{^{1}H} NMR spectrum in C_6D_6 reveals two triplets (A_2X_2 spin system) at δ = −51.5 ppm and −315.5 ppm ($^1J_{PP}$ = 190 Hz) which is characteristic for P_4 butterfly moieties.[79] A comparison of the chemical shifts of the derivatives with a Cp'' (δ = −84.2 ppm and −325.5 ppm),[80] Cp''' (δ = −81.4 ppm and −324.5 ppm),[76] or Cp^{BIG} (δ = −53.9 ppm and −317.1 ppm)[78] ligand shows that the signals

are significantly low field shifted when the sterical bulk of the ligand increases or the electron donating properties of the ligand decreases.

The reaction of P_4 with the iron dimer **5**, which dissociates into reactive 17 VE radical monomers in solution, shows that P_4 reacts readily with radicals. Therefore, we also reacted the cyclopentadienyl radicals **3a** and **3b** with P_4 at room temperature (Scheme 6.9) which yield the organo-substituted P_4 butterfly complexes $Cp^R{}_2P_4$ (Cp^R = Cp^{Ar*} **8a**, Cp^{XXL} **8b**). The analogue compounds with Cp*, Cp''', Cp^{4iPr} , and Cp^{BIG} have also been reported by our group.[56,60] The reaction time for the formation of **8a** and **8b** is not equal. While the reaction of **8a** finishes within 2 h and results in a brown reaction solution, the reaction solution of **8b** is still dark blue after stirring for 24 h. Surprisingly, the $^{31}P\{^1H\}$ NMR spectrum of the crude mixture of **8b** in C_6D_6 did not show any signals, besides the singlet at δ = −520.5 ppm which is assigned to P_4. On the other hand, the $^{31}P\{^1H\}$ NMR spectrum of the crude mixture of **8a** in C_6D_6 shows two triplets at δ = −302.3 ppm and δ = −174.3 ppm (A_2X_2 spin system, $^1J_{PP}$ = 193 Hz) for the P_4 butterfly moiety, which is in good agreement to other organo-substituted P_4 butterfly compounds.[56,81] However, by layering the crude toluene reaction solutions with acetonitrile, three kinds of crystals can be obtained in both cases. On the one hand, colorless crystals of **1a** or **1b** as well as crystals of **3a** (dark green) or **3b** (reddish blue) are formed. On the other hand, small amounts of bright yellow crystals of **8a** and **8b** can be isolated in moderate yields (14% for **8a** and 25% for **8b**) which must be separated manually.

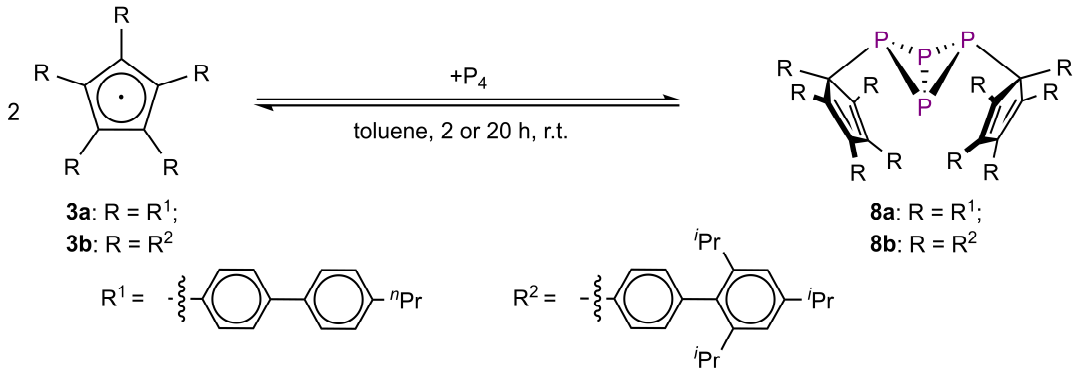

Scheme 6.9. Synthesis of organo-substituted P_4 butterfly compounds **8a** and **8b**.

The $^{31}P\{^1H\}$ NMR spectrum of crystalline **8b** in C_6D_6 show the expected two triplets at δ = −312.7 ppm and δ = −183.1 ppm (A_2X_2 spin system, $^1J_{PP}$ = 193 Hz). However, the $^{31}P\{^1H\}$ NMR spectra of crystalline samples of **8a** and **8b** contain always traces of P_4. This finding indicates that in solution **8a** and **8b** are in equilibrium with P_4 and the respective radical. The same behavior was also observed for $Cp^{BIG}{}_2P_4$.[60] However, the decomposition of $Cp^{BIG}{}_2P_4$ is slower, as only 35% of the butterfly compound decomposed into P_4 and the corresponding $Cp^{BIG\bullet}$ radicals within 72 h. Since **8b** cannot be detected in the reaction mixture (probably due to its low concentration) and is only formed in larger quantities during crystallization, the equilibrium in solution of **8b** is strongly shifted towards the side

of the starting materials. However, as compound **8a** is already present in the reaction solution, **8a** exhibits a higher stability in solution than **8b**. Therefore, it can be deducted that the decomposition of $Cp^{BIG}{}_2P_4$, **8a**, and **8b** is probably caused mainly by steric effects as this would explain the trend of stability in solution of $Cp^{BIG}{}_2P_4$ > **8a** > **8b**. The surprisingly low stability of **8b** is most likely caused by steric repulsion of the *i*Pr groups of the two Cp^{XXL} units, as these are in spatial proximity (vide infra). Due to the partly decomposition of **8a** and **8b** into the corresponding radicals, no reliable ^{1}H NMR spectrum could be recorded.

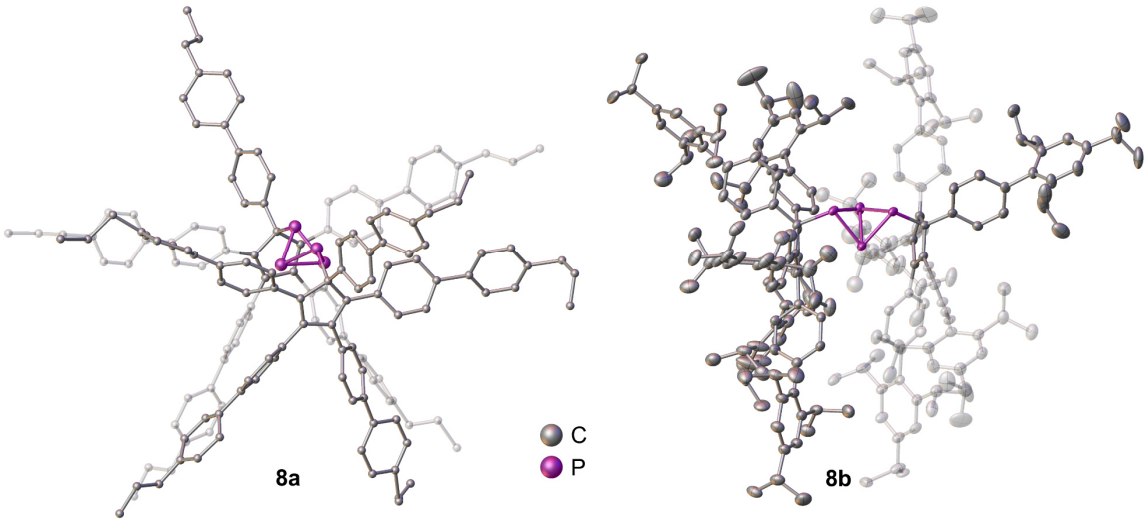

Figure 6.6. Molecular structure of **8a** (left) and **8b** (right) in solid state. Four aryl substituents, that are in the C_5 plane, of one of the Cp^R units are translucent for clarity. Hydrogen atoms as well as solvent molecules are also omitted for clarity. **8a** is shown in the "balls and sticks" model. ADPs of **8b** are shown at 50% probability level.

The molecular structures of **8a** and **8b** in the solid state are depicted in Figure 6.6. Unfortunately, the crystals of **8a** were of deficient quality which is why the structure could not be refined in anisotropic approximation and therefore, its structure is not discussed in detail. In both cases the structures show clearly that the carbon atom bound to the phosphorus atom is sp^3 hybridized, since the aryl substituents are bend out of the C_5 ring plane. Furthermore, the C–C bond distribution within the C_5 units of **8b** indicates the presence of butadiene systems. The P–P bond lengths of **8b** vary from 2.1801(10) Å to 2.2121(8) Å, while the P–C bond distances are in the range of 1.933(3) Å to 1.972(2) Å. Compared to $Cp^R{}_2P_4$ (Cp^R = Cp*, Cp‴, Cp^{4iPr}, Cp^{BIG}) the P–P bond distances are in the same range.[56] However, the P–C bond distances show a trend to a bond elongation by increasing sterical demand of the Cp^R unit, with the longest distance being found in **8b**. Noteworthy is that in **8a** the Cp^{Ar*} units are almost in an eclipsed conformation while in **8b** the Cp^{XXL} units show a staggered one. The different conformation of the Cp^{XXL} units in **8b** is most likely induced by the additional bulk of the *i*Pr groups as this leads to stronger repulsion. This finding might also be the reason for the surprisingly low stability of **8b** in solution.

The use of 6 as building block in supramolecular chemistry.

Based on the previous results, the novel super bulky pentaphosphaferrocene derivative **6** was tested as building block in supramolecular chemistry. The reaction of **6** with an excess of CuBr leads to a color change from green to reddish brown. By layering the CH_2Cl_2 reaction mixture with methanol, small amounts of black crystals of a novel supramolecule with the general formula of $[\{Cp^{XXL}Fe(\eta^4\text{-}P_5)\}_3(Cu_XBr_{X-3})(solv)_y]$ (**9**, solv = methanol or acetonitrile) can be obtained. Unfortunately, the exact formula of the product could not be determined within the scope of this work, as the crystals were seriously twinned and poorly scattering. For this reason, the crystal structure determination was performed at a synchrotron at 6 K. Compound **9** crystallizes in the trigonal space group *R*3*c* as a racemic twin with two crystallographically independent molecules (**9a** and **9b**) in the unit cell, each occupying positions on the 3-fold axis. Both co-crystallized supramolecules contain three units of **6**, surrounded by a core of disordered Cu and Br atoms. Preliminary refinement shows that each molecule has a slightly different composition and molecular structure. These differences can explain the fact that compound **9** (or rather a co-crystal or solid solution) crystallizes with two unique crystallographic positions. Supramolecule **9a** is localized at the coordinates with the center ($^1/_3$, $^2/_3$, z) while **9b** possesses the center (0, 0, z). Due to the more severely disordered scaffold of **9b**, it can only be defined as charge balanced neutral moiety in the current state of structure refinement. However, the search for final non-contradictory combination of atomic positions and occupancies of the heavy atoms is still underway. The other molecule has the formula of $[\{Cp^{XXL}Fe(\eta^4\text{-}P_5)\}_3Cu_{15.5}Br_{12.5}(solv)_x]$ (**9a**; solv = methanol or acetonitrile) and is depicted in Figure 6.7. In both **9a** and **9b**, the P_5 ligands exhibit an envelope conformation which is why the presence of $[Cp^{XXL}Fe(\eta^4\text{-}P_5)]^-$ units is suggested (vide infra).[12] However, in both molecules the copper coordination is similar, but occupation factors are different and the Cp^{XXL} ligands are disordered over two positions.

The envelope structure of the P_5 ligands results from one P atom being bent out of the former P_5 ring. Therefore, the P_5 unit is only η^4 coordinated, by the iron atom. In **9a**, the three P–P bond lengths which connect the four P atoms that are coordinated by the iron atom vary from 2.1345(39) Å to 2.1475(37) Å and indicate a butadiene-like arrangement. The P–P bonds to the P atom bend out of plane have more single bond character which is indicated by longer bond length of 2.1814(41) Å and 2.1921(40) Å. Similar, but slightly shorter P–P bond length are found in $[K(dme)_2K(dme)][(Cp^*Fe)(\mu,\eta^{4:4}\text{-}P_{10})]$ which is formally build up by two P–P bonded $[Cp^*Fe(\eta^4\text{-}P_5)]^-$ units.[12] The P–P bond elongation in **9a** is most likely induced by the additional coordination to Cu atoms which leads to formation of a supramolecular aggregate. However, the reason for the formation of $[Cp^{XXL}Fe(\eta^4\text{-}P_5)]^-$ is still unclear.

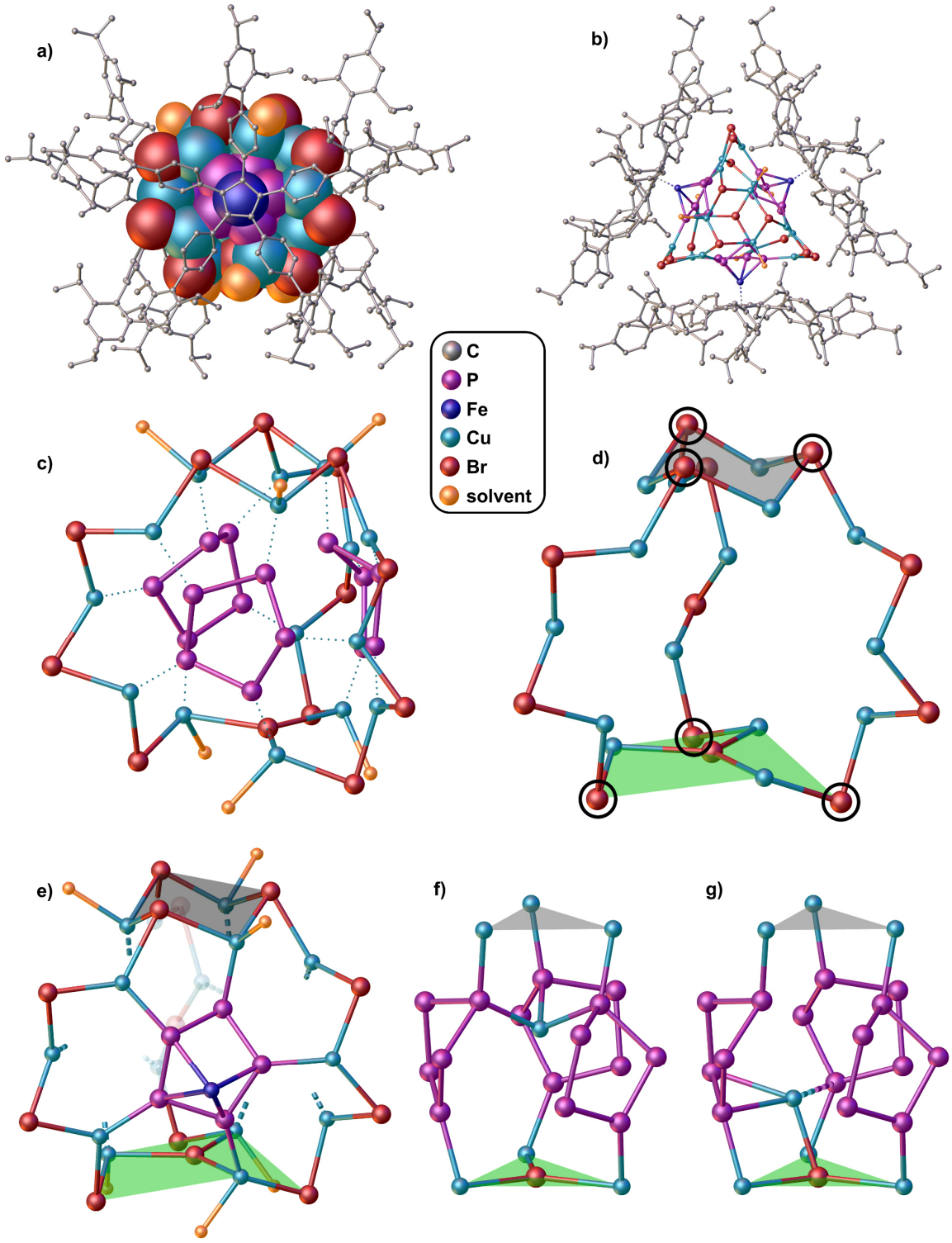

Figure 6.7. Molecular anatomy of [{Cp^{XXL}Fe(η^4-P$_5$)}$_3$Cu$_{15.5}$Br$_{12.5}$(solv)$_x$] (**9a**, solv = methanol or acetonitrile). a) Entire supramolecule as a space-filling model, except for the Cp^{XXL} ligands. H atoms and minor parts of disorder are omitted for clarity. b) Top view of **9a** as a ball-and-stick model, showing the trigonal prismatic shape. c) Idealized central P$_{15}$Cu$_{17}$Br$_{13}$ scaffold, showing the Cu–P bonds as dotted lines. d) Outer Cu$_{15}$Br$_{13}$ scaffold, with the marked "top body" (gray highlighted Cu$_3$Br$_3$ ring) and "bottom body" (green highlighted Br(CuBr)$_3$ unit). The corners of the distorted trigonal prism are defined by the six bromide atoms marked with black circles. e) Framing of the envelope-shaped P$_5$ units by the outer scaffold. Only one P$_5$ unit is shown and the third Cu$_3$Br$_2$ strand is translucent for clarity. f) Position 1 of a Cu atom in the center. g) Position 2 of a Cu atom in the center. The "top" and "bottom body" are indicated by the corresponding Cu atoms.

When considering all 17 Cu and 13 Br positions, the idealized structure of **9a** can be described as a slightly distorted trigonal prism (Figure 6.7). The faces of the prism are defined by the three [Cp^{XXL}Fe(η^4-P$_5$)]$^-$ units, with the Cu and Br positions occupied on average by only 15.5 Cu and 12.5 Br atoms, respectively, to maintain charge balance. In the idealized structure, the P_5 units are held together by an outer frame of 15 Cu and 13 Br atoms that build up the bodies as well as the edges. The "top body" (gray plane in Figure 6.7 d)) is built up by a Cu_3Br_3 ring in chair conformation, while the "bottom body" (green plane in Figure 6.7 d)) consists out of a $Br(CuBr)_3$ unit. The corners of the two trigonal bodies are defined by six Br atoms (marked with black circles in Figure 6.7 d)). The edges of the prism are built up by three strands of Cu_3Br_2 chains which connect the six bromide atoms positioned at the corners. Each of three P_5 units is framed into the scaffold by coordinating five Cu atoms of the outer scaffold (Figure 6.7 e)). This leads to a trigonal coordination geometry for all Cu atoms in the strands since all coordinate to two bromide and one phosphorus atom. However, the Cu atoms that are part of the bodies are tetrahedrally coordinated by two bromide atoms, one phosphorus atom and an additional solvent molecule (acetonitrile or methanol; Figure 6.7 e)). The folded P_5 units are all similarly orientated since all P atoms bend out of plane, coordinate a Cu atom of the "top body". Due to the presence of negatively charged [Cp^{XXL}Fe(η^4-P$_5$)]$^-$ units, the Cu–P bond distances (2.1725(33) Å to 2.2160(131) Å) are significantly shorter than in other supramolecular aggregates, obtained with neutral pentaphosphaferrocenes.[19,20] In the center of the cluster, two positions can be occupied by one Cu atom. At $^1/_6$ of the molecules, both positions are vacant, while in $^1/_2$ of the molecules, position 1 (Figure 6.7 f)) and in $^1/_3$ of the molecules, position 2 (Figure 6.7 g)) is occupied. The Cu atom at position 1 is coordinated by the three P atoms bent out of the P_5 plane, resulting in a trigonal pyramidal geometry. However, the Cu atom at position 2 is only coordinated by one P_5 unit and the central Br atom of the $Br(CuBr)_3$ unit of the "bottom body" plane. The corresponding P_5 unit coordinates the Cu atom in an η^2 fashion which is leads to longer Cu–P distances of 2.4580(44) Å and 2.4639(45) Å. However, an additional Cu–P distance of 2.8764(45) Å indicates a weak interaction with a second P_5 unit via an η^1 coordination.

Due to the low yield (≈ 1%), **9** could not be investigated by other analytical methods which would also give insight into the exact composition of **9**.

6.3. Conclusion

In conclusion we present the total synthesis of the novel pentaphosphaferrocene [Cp^{XXL}Fe(η^5-P$_5$)] (**6**), where each intermediate product could be fully characterized. The concept behind synthesizing a super bulky pentaphosphaferrocene is to introduce **6** as a building block into supramolecular chemistry. Hereby, the steric repulsion of the attached super bulky, penta-arylated Cp^{XXL} ligand should lead to new supramolecular aggregates.

As a proof of concept, **6** was reacted with CuBr which leads to the formation of the unprecedented supramolecule [{$Cp^{XXL}Fe(\eta^4\text{-}P_5)$}$_3$$Cu_{15.5}Br_{12.5}(solv)_x$] (**9a**; solv = methanol or acetonitrile) with a trigonal prismatic scaffold. At the beginning of the synthesis of the novel pentaphosphaferrocene, two new, super bulky cyclopentadienyl derivatives $Cp^{Ar*}H$ (**1a**) and $Cp^{XXL}H$ (**1b**) were synthesized. Despite both Cp^R ligands exhibit similar steric bulk, their electronic properties are very different. In the Cp^{Ar*} anion (**2a**) as well as the Cp^{Ar*}• radical (**3a**) the electron density is distributed of the central C_5 ring as well as ten phenyl groups. This results in weak electron-donating properties, the formation of the remarkably stable radical **3a** and is probable the reason why no iron complexes with the Cp^{Ar*} ligand were accessible. By the introduction of ^{i}Pr substituents in the *ortho* and *para* position of the outer phenyl group, the delocalization of the electron density could be reduced in the Cp^{XXL} ligand. This yields in better electron donating properties of the Cp^{XXL} anion (**2b**), a slightly lower stability of the Cp^{XXL}• radical (**3b**) and allowed finally the synthesis of Cp^{XXL} containing iron complexes. Due to the high stability of **3a** and **3b**, both radicals could be characterized by single crystal X-ray diffraction. Finally, the reaction of **3a** and **3b** with P_4 yields the organo-substituted P_4 butterfly compounds $Cp^{Ar*}_2P_4$ (**8a**) and $Cp^{XXL}_2P_4$ (**8b**), respectively. Based on this preliminary work, further studies will be conducted on the use of **6** as a super bulky building block in supramolecular chemistry.

6.4. Reference

[1] T. J. Kealy, P. L. Pauson, *Nat. Chem.* **1951**, *168*, 1039.

[2] a) J. A. Gladysz, *Chem. Rev.* **2000**, *100*, 1167; b) J. B. Aberg, J. Nyhlén, B. Martín-Matute, T. Privalov, J.-E. Bäckvall, *J. Am. Chem. Soc.* **2009**, *131*, 9500; c) J. Nyhlén, T. Privalov, J.-E. Bäckvall, *Chem. Eur. J.* **2009**, *15*, 5220; d) S.-B. Ko, B. Baburaj, M.-J. Kim, J. Park, *J. Org. Chem.* **2007**, *72*, 6860; e) B. Martín-Matute, J. B. Aberg, M. Edin, J.-E. Bäckvall, *Chem. Eur. J.* **2007**, *13*, 6063; f) B. Martín-Matute, M. Edin, K. Bogár, F. B. Kaynak, J.-E. Bäckvall, *J. Am. Chem. Soc.* **2005**, *127*, 8817; g) J. H. Choi, Y. K. Choi, Y. H. Kim, E. S. Park, E. J. Kim, M.-J. Kim, J. Park, *J. Org. Chem.* **2004**, *69*, 1972; h) B. Martín-Matute, M. Edin, K. Bogár, J.-E. Bäckvall, *Angew. Chem. Int. Ed.* **2004**, *43*, 6535; i) I. D. Hills, G. C. Fu, *Angew. Chem. Int. Ed.* **2003**, *42*, 3921; j) A. H. Mermerian, G. C. Fu, *J. Am. Chem. Soc.* **2003**, *125*, 4050; k) J. H. Choi, Y. H. Kim, S. H. Nam, S. T. Shin, M.-J. Kim, J. Park, *Angew. Chem. Int. Ed.* **2002**, *41*, 2373; l) K. Kaleta, A. Hildebrandt, F. Strehler, P. Arndt, H. Jiao, A. Spannenberg, H. Lang, U. Rosenthal, *Angew. Chem. Int. Ed.* **2011**, *50*, 11248.

[3] a) L. D. Field, C. M. Lindall, A. F. Masters, G. K. B. Clentsmith, *Coord. Chem. Rev.* **2011**, *255*, 1733; b) A. Frei, *Chem. Eur. J.* **2019**, *25*; c) C. Janiak, H. Schumann, *Adv. Organoment. Chem.* **1991**, *33*, 291.

[4] J. L. Atwood, W. E. Hunter, A. H. Cowley, R. A. Jones, C. A. Stewart, *J. Chem. Soc. Chem. Comm.* **1981**, 925.

[5] P. Jutzi, F. Kohl, P. Hofmann, C. Krüger, Y.-H. Tsay, *Chem. Ber.* **1980**, *113*, 757.

[6] M. J. Heeg, R. H. Herber, C. Janiak, J. J. Zuckerman, H. Schumann, W. F. Manders, *J. Organomet. Chem.* **1988**, *346*, 321.

[7] S. Harder, D. Naglav, P. Schwerdtfeger, I. Nowik, R. H. Herber, *Inorg. Chem.* **2014**, *53*, 2188.

[8] a) T. J. Jaeger, M. C. Baird, *Organometallics* **1988**, *7*, 2074; b) W. C. Watkins, T. Jaeger, C. E. Kidd, S. Fortier, M. C. Baird, G. Kiss, G. C. Roper, C. D. Hoff, *J. Am. Chem. Soc.* **1992**, *114*, 907; c) R. J. Hoobler, M. A. Hutton, M. M. Dillard, M. P. Castellani, A. L. Rheingold, A. L. Rieger, P. H. Rieger, T. C. Richards, W. E. Geiger, *Organometallics* **1993**, *12*, 116.

[9] O. J. Scherer, T. Brück, *Angew. Chem.* **1987**, *99*, 59.

[10] a) F. G. A. Stone, *Angew. Chem. Int. Ed.* **1984**, *23*, 89; b) R. Hoffmann, *Angew. Chem. Int. Ed.* **1982**, *21*, 711; c) M. Baudler, S. Akpapoglou, D. Ouzounis, F. Wasgestian, B. Meinigke, H. Budzikiewicz, H. Münster, *Angew. Chem.* **1988**, *100*, 288; d) H. Grützmacher, *Z. Anorg. Allg. Chem.* **2012**, *638*, 1877.

[11] R. F. Winter, W. E. Geiger, *Organometallics* **1999**, *18*, 1827.

[12] M. V. Butovskiy, G. Balázs, M. Bodensteiner, E. V. Peresypkina, A. V. Virovets, J. Sutter, M. Scheer, *Angew. Chem. Int. Ed.* **2013**, *52*, 2972.

[13] E. Mädl, M. V. Butovskii, G. Balázs, E. V. Peresypkina, A. V. Virovets, M. Seidl, M. Scheer, *Angew. Chem. Int. Ed.* **2014**, *53*, 7643.
[14] a) O. J. Scherer, T. Brück, G. Wolmershäuser, *Chem. Ber.* **1989**, *122*, 2049; b) M. Detzel, T. Mohr, O. J. Scherer, G. Wolmershäuser, *Angew. Chem. Int. Ed.* **1994**, *33*, 1110; c) O. J. Scherer, S. Weigel, G. Wolmershäuser, *Chem. Eur. J.* **1998**, *4*, 1910.
[15] C. Heindl, E. Peresypkina, A. V. Virovets, I. S. Bushmarinov, M. G. Medvedev, B. Krämer, B. Dittrich, M. Scheer, *Angew. Chem. Int. Ed.* **2017**, *56*, 13237.
[16] M. Scheer, *Dalton Trans.* **2008**, 4372.
[17] a) M. Scheer, L. J. Gregoriades, A. V. Virovets, W. Kunz, R. Neueder, I. Krossing, *Angew. Chem. Int. Ed.* **2006**, *45*, 5689; b) F. Dielmann, A. Schindler, S. Scheuermayer, J. Bai, R. Merkle, M. Zabel, A. V. Virovets, E. V. Peresypkina, G. Brunklaus, H. Eckert, M. Scheer, *Chem. Eur. J.* **2012**, *18*, 1168.
[18] C. Schwarzmaier, A. Schindler, C. Heindl, S. Scheuermayer, E. V. Peresypkina, A. V. Virovets, M. Neumeier, R. Gschwind, M. Scheer, *Angew. Chem. Int. Ed.* **2013**, *52*, 10896.
[19] J. Bai, A. V. Virovets, M. Scheer, *Science* **2003**, *300*, 781.
[20] M. Scheer, J. Bai, B. P. Johnson, R. Merkle, A. V. Virovets, C. E. Anson, *Eur. J. Inorg. Chem.* **2005**, 4023.
[21] M. Scheer, A. Schindler, C. Gröger, A. V. Virovets, E. V. Peresypkina, *Angew. Chem. Int. Ed.* **2009**, *48*, 5046.
[22] M. Scheer, A. Schindler, J. Bai, B. P. Johnson, R. Merkle, R. Winter, A. V. Virovets, E. V. Peresypkina, V. A. Blatov, M. Sierka, H. Eckert, *Chem. Eur. J.* **2010**, *16*, 2092.
[23] E. Peresypkina, C. Heindl, A. Virovets, H. Brake, E. Mädl, M. Scheer, *Chem. Eur. J.* **2018**, *24*, 2503.
[24] E. V. Peresypkina, C. Heindl, A. Schindler, M. Bodensteiner, A. V. Virovets, M. Scheer, *Z. Kristallogr. Cryst. Mater.* **2014**, *229*, 735.
[25] a) F. Dielmann, M. Fleischmann, C. Heindl, E. V. Peresypkina, A. V. Virovets, R. M. Gschwind, M. Scheer, *Chem. Eur. J.* **2015**, *21*, 6208; b) C. Heindl, E. V. Peresypkina, A. V. Virovets, W. Kremer, M. Scheer, *J. Am. Chem. Soc.* **2015**, *137*, 10938; c) F. Dielmann, C. Heindl, F. Hastreiter, E. V. Peresypkina, A. V. Virovets, R. M. Gschwind, M. Scheer, *Angew. Chem. Int. Ed.* **2014**, *53*, 13605.
[26] S. Heinl, E. Peresypkina, J. Sutter, M. Scheer, *Angew. Chem. Int. Ed.* **2015**, *54*, 13431.
[27] C. Heindl, S. Heinl, D. Lüdeker, G. Brunklaus, W. Kremer, M. Scheer, *Inorganica Chim. Acta* **2014**, *422*, 218.
[28] H. Brake, E. Peresypkina, C. Heindl, A. V. Virovets, W. Kremer, M. Scheer, *Chem. Sci.* **2019**, *10*, 2940.
[29] M. Scheer, A. Schindler, R. Merkle, B. P. Johnson, M. Linseis, R. Winter, C. E. Anson, A. V. Virovets, *J. Am. Chem. Soc.* **2007**, *129*, 13386.
[30] S. Heinl, G. Balázs, M. Scheer, *Phosphorus Sulfur Silicon Relat. Elem.* **2014**, *189*, 924.
[31] J.-Y. Thépot, C. Lapinte, *J. Organomet. Chem.* **2002**, *656*, 146.
[32] G. R. Giesbrecht, J. C. Gordon, D. L. Clark, B. L. Scott, *Dalton Trans.* **2003**, 2658.
[33] G. Dyker, J. Heiermann, M. Miura, J.-I. Inoh, S. Pivsa-Art, T. Satoh, M. Nomura, *Chem. Eur. J.* **2000**, *6*, 3426.
[34] Y. Schulte, C. Stienen, C. Wölper, S. Schulz, *Organometallics* **2019**, *38*, 2381.
[35] Y. Schulte, H. Weinert, C. Wölper, S. Schulz, *Organometallics* **2020**, *39*, 206.
[36] S. Harder, C. Ruspic, *J. Organomet. Chem.* **2009**, *694*, 1180.
[37] Herbert Schumann, Homa Kucht, Andreas Kucht, Frank H. Görlitz, Andreas Dietrich, *Z. Naturforsch. B* **1992**, *47*, 1241.
[38] a) S. Harder, *Coord. Chem. Rev.* **1998**, *176*, 17; b) S. Harder, *Coord. Chem. Rev.* **2000**, *199*, 331.
[39] H. Chen, P. Jutzi, W. Leffers, M. M. Olmstead, P. P. Power, *Organometallics* **1991**, *10*, 1282.
[40] The exact amount of thf cannot be clarified unambiguously since the obtained X-ray data is of insufficient quality.
[41] C. Janiak, *Coord. Chem. Rev.* **1997**, *163*, 107.
[42] H. Werner, H. Otto, H. J. Kraus, *J. Organomet. Chem.* **1986**, *315*, C57-C60.
[43] E. Frason, F. Menegus, C. Panttoni, *Nature* **1963**, *199*, 1087.
[44] H. Schumann, C. Janiak, J. Pickardt, U. Börner, *Angew. Chem. Int. Ed.* **1987**, *26*, 789.
[45] H. Schumann, C. Janiak, M. A. Khan, J. J. Zuckerman, *J. Organomet. Chem.* **1988**, *354*, 7.
[46] K. Ziegler, B. Schnell, *Justus Liebigs Ann. Chem.* **1925**, *445*, 266.
[47] G. R. Liebling, H. M. McConnell, *The Journal of Chemical Physics* **1965**, *42*, 3931.
[48] a) J. C. Rienstra-Kiracofe, D. E. Graham, H. F. Schaefer, *Mol. Phys.* **1998**, *94*, 767; b) M. Bearpark, M. Robb, N. Yamamoto, *Spectrochim. Acta A* **1999**, *55*, 639; c) J. H. Kiefer, R. S. Tranter, H. Wang, A. F. Wagner, *Int. J. Chem. Kinet.* **2001**, *33*, 834; d) B. E. Applegate, T. A. Miller, T. A. Barckholtz, *J. Chem. Phys.* **2001**, *114*, 4855; e) R. L. Lord, S. E. Wheeler, H. F. Schaefer, *J. Phys. Chem. A* **2005**, *109*, 10084; f) T. Sato, K. Tokunaga, K. Tanaka, *J. Chem. Phys.* **2006**, *124*, 24314; g) X. Zhou, D. A. Hrovat, W. T. Borden, *J. Am. Chem. Soc.* **2007**, *129*, 10785; h) L. Andjelkovic, M. Peric, M. Zlatar, M. Gruden-Pavlovic, *J. Serb. Chem. Soc.* **2015**, *80*, 877; i) D. Leicht, M. Kaufmann, G. Schwaab, M. Havenith, *J. Chem. Phys.* **2016**, *145*, 74304.
[49] W. Broser, P. Siegle, H. Kurreck, *Chem. Ber.* **1968**, *101*, 69.
[50] a) K. Möbius, H. van Willigen, A. H. Maki, *Mol. Phys.* **1971**, *20*, 289; b) L. Yu, J. M. Williamson, T. A. Miller, *Chem. Phys. Lett.* **1989**, *162*, 431; c) L. Yu, J. Williamson, S. C. Foster, T. A. Miller, *J. Chem. Phys.* **1992**, *97*, 5273; d) N. Jux, K. Holczer, Y. Rubin, *Angew. Chem.* **1996**, *108*, 2116.
[51] T. Chen, H. H. Günthard, *Chem. Phys.* **1985**, *97*, 187.

[52] P. R. Nimax, F. Zoller, T. Blockhaus, T. Küblböck, D. Fattakhova-Rohlfing, K. Sünkel, *New J. Chem.* **2020**, *44*, 72.
[53] H. Sitzmann, R. Boese, *Angew. Chem.* **1991**, *103*, 1027.
[54] C. Janiak, R. Weimann, F. Görlitz, *Organometallics* **1997**, *16*, 4933.
[55] T. Kitagawa, K. Ogawa, K. Komatsu, *J. Am. Chem. Soc.* **2004**, *126*, 9930.
[56] S. Heinl, S. Reisinger, C. Schwarzmaier, M. Bodensteiner, M. Scheer, *Angew. Chem. Int. Ed.* **2014**, *53*, 7639.
[57] In principle, the synthesis of **3b** should also be possible starting from $\mathbf{2b_{Na}}$ or $\mathbf{2b_{K}}$. Due to their low purity, however, the synthesis was only carried out with $\mathbf{2b_{Tl}}$.
[58] The reaction is assumed to be quantitative.
[59] The value is probably affected by an error. See SI for further information.
[60] S. Heinl, G. Balázs, A. Stauber, M. Scheer, *Angew. Chem. Int. Ed.* **2016**, *55*, 15524.
[61] T. Kubo, Y. Katada, A. Shimizu, Y. Hirao, K. Sato, T. Takui, M. Uruichi, K. Yakushi, R. C. Haddon, *J. Am. Chem. Soc.* **2011**, *133*, 14240.
[62] H. Sitzmann, H. Bock, R. Boese, T. Dezember, Z. Havlas, W. Kaim, M. Moscherosch, L. Zanathy, *J. Am. Chem. Soc.* **1993**, *115*, 12003.
[63] C. Ruspic, J. R. Moss, M. Schürmann, S. Harder, *Angew. Chem. Int. Ed.* **2008**, *47*, 2121.
[64] F. Dielmann, R. Merkle, S. Heinl, M. Scheer, *Z. Naturforsch. B* **2009**, 3.
[65] H. Sitzmann, T. Dezember, W. Kaim, F. Baumann, D. Stalke, J. Kärcher, E. Dormann, H. Winter, C. Wachter, M. Kelemen, *Angew. Chem. Int. Ed.* **1996**, *35*, 2872.
[66] M. Wallasch, G. Wolmershäuser, H. Sitzmann, *Angew. Chem. Int. Ed.* **2005**, *44*, 2597.
[67] P. Jutzi, K.-H. Schwartzen, A. Mix, *Chem. Ber.* **1990**, *123*, 837.
[68] S. McVey, P. L. Pauson, *J. Chem. Soc.* **1965**, 4312.
[69] D. Scapens, H. Adams, T. R. Johnson, B. E. Mann, P. Sawle, R. Aqil, T. Perrior, R. Motterlini, *Dalton Trans.* **2007**, 4962.
[70] Y. V. Torubaev, I. V. Skabitskiy, P. Rusina, A. A. Pasynskii, D. K. Rai, A. Singh, *CrystEngComm* **2018**, *20*, 2258.
[71] J. M. O'Connor, K. K. Baldridge, S. Cope, R. L. Holland, *Polyhedron* **2019**, *157*, 406.
[72] L. D. Field, T. W. Hambley, C. M. Lindall, A. F. Masters, *Polyhedron* **1989**, *8*, 2425.
[73] a) M. Scheer, K. Schuster, U. Becker, A. Krug, H. Hartung, *J. Organomet. Chem.* **1993**, *460*, 105; b) R. G. Teller, J. M. Williams, *Inorg. Chem.* **1980**, *19*, 2770; c) R. F. Bryan, P. T. Greene, *J. Chem. Soc. A* **1970**, 3064; d) R. F. Bryan, P. T. Greene, M. J. Newlands, D. S. Field, *J. Chem. Soc. A* **1970**, 3068.
[74] a) I. Kuksis, M. C. Baird, *Organometallics* **1996**, *15*, 4755; b) I. Kuksis, M. C. Baird, *Organometallics* **1994**, *13*, 1551.
[75] For the co-thermolysis of **5** with P_4, also the mixture of **5** and **1a** can be used since chromatographic workup is needed for purification.
[76] O. J. Scherer, T. Hilt, G. Wolmershäuser, *Organometallics* **1998**, *17*, 4110.
[77] O. J. Scherer, T. Brück, G. Wolmershäuser, *Chem. Ber.* **1988**, *121*, 935.
[78] S. Heinl, M. Scheer, *Chem. Sci.* **2014**, *5*, 3221.
[79] a) O. J. Scherer, M. Swarowsky, H. Swarowsky, G. Wolmershäuser, *Angew. Chem. Int. Ed.* **1988**, *27*, 694; b) C. Schwarzmaier, A. Y. Timoshkin, G. Balázs, M. Scheer, *Angew. Chem. Int. Ed.* **2014**, *53*, 9077; c) S. Pelties, D. Herrmann, B. de Bruin, F. Hartl, R. Wolf, *Chem. Commun.* **2014**, *50*, 7014; d) J. W. Dube, C. M. E. Graham, C. L. B. Macdonald, Z. D. Brown, P. P. Power, P. J. Ragogna, *Chem. Eur. J.* **2014**, *20*, 6739.
[80] O. J. Scherer, G. Schwarz, G. Wolmershäuser, *Z. Anorg. Allg. Chem.* **1996**, *622*, 951.
[81] a) A. R. Fox, R. J. Wright, E. Rivard, P. P. Power, *Angew. Chem.* **2005**, *117*, 7907; b) E. Fluck, R. Riedel, H.-D. Hausen, G. Heckmann, *Z. Anorg. Allg. Chem.* **1987**, *551*, 85; c) R. Riedel, H.-D. Hausen, E. Fluck, *Angew. Chem. Int. Ed.* **1985**, *24*, 1056.

6.5. Supporting Information

Synthesis and Characterization

General Remarks:

All manipulations were performed with rigorous exclusion of oxygen and moisture using Schlenk-type glassware on a dual manifold Schlenk line with Argon inert gas or glove box filled with N2 containing a high-capacity recirculator (<0.1 ppm O2). Solvents were dried using a MB SPS-800 device of company MBRAUN, degassed and saturated with argon. Mass spectrometry was performed using an Agilent Q-TOF 6540 UHD (ESI-MS) and a JEOL AccuTOF GCX (LIFDI-MS, EI-MS, FD-MS), respectively. Elemental analysis (CHN) was determined using a Vario micro cube and Vario EL III instrument. Infrared spectroscopy was performed using a Bruker ALPHA Platinum-ATR-Spectrometer or a VARIAN FTS-800 FT-IR spectrometer. Diatomaceous earth was routinely stored at 110 °C prior to use, then dried in vacuo with the aid of a heat gun. Silica gel 60 used for the column chromatography was heated under vacuo (3 d, 10^{-6} mbar, 230 °C) prior to use.

TlOEt was purchased by Sigma-Aldrich. 1-Bromo-2,4,6-triisopropylbenzene, 1-Iodo-4-bromobenzene and [$NiCl_2(PPh_3)_2$] was purchased by fluorochem. $Pd(OAc)_2$, Cs_2CO_3, P^tBu_3, 4-bromo-4'-propyl-1,1'-biphenyl (**Br-R^1**), and [Cp_2ZrCl_2] were purchased by ABCR and was used without further purification.

Synthesis of 4'-bromo-2,4,6-triisopropyl-1,1'-biphenyl (Br-R^2)

12.027 g magnesium powder (494.86 mmol, 2.1eq) is heated in vacuo for 2 hours. Then 700 ml thf and a spatula tip of iodine is added. The suspension is stirred for 16 h at room temperature. 50.22 ml of 1-Bromo-2,4,6-triisopropylbenzene (235.65 mmol, 1eq) is degassed, dissolved in 300 ml thf, and slowly added via the reflux condenser to the suspension. The reaction mixture is heated to reflux for 10 days. The resulting brownish suspension is cooled to room temperature and filtered over diatomaceous earth. The resulting brown solution is slowly added to 100.00 g 1-Iodo-4-bromobenzene (353.47 mmol, 1.5eq) and 15.42 g [$NiCl_2(PPh_3)_2$] (23.56 mmol, 0.1eq) suspended in 300 ml thf. During addition, the reaction mixture turns deep red and grows warm to about 45 °C. The mixture is heated to reflux for 3.5 days to give a brown suspension, then cooled to room temperature. The reaction is quenched with 500 ml HCl (0.1 mol/l) and stirred for 16 h at room temperature. From now on no protection gas is needed.

The phases are separated, and the aqueous phases is extracted three times with each 300 ml hexane and then three times with each 50 ml dichloromethane. All organic phases are merged, and the solvent is removed in vacuo. The crude product is purified by column

chromatography (dry-load, silica gel, hexane, l = 30 cm, d = 6.5 cm) to give a mixture of starting material and product. Subsequent sublimation of the starting material (80 °C, 1 · 10^{-6} bar) gives pure **Br-R^2**.

Crystals suitable for single crystal diffraction can be obtained by layering a CH_2Cl_2 solution of **Br-R^2** under acetone.

Yield: 42.93 g (119.47 mmol, 51% (related to 1-Bromo-2,4,6-triisopropylbenzene))

Analytical data of **Br-R^2**:

NMR (CD_2Cl_2, 298 K) 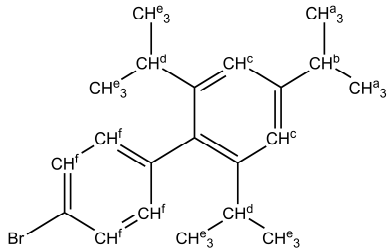	^{1}H: δ [ppm] = 1.09 (d, 12H, $^3J_{HH}$ = 6.88 Hz, CH(C<u>H</u>$^e_3$)$_2$), 1.31 (d, 6H, $^3J_{HH}$ = 6.93 Hz, CH(C<u>H</u>$^a_3$)$_2$), 2.60 (sept, $^3J_{HH}$ = 6.88 Hz, 2H, C<u>H</u>^{d}(CH$_3$)$_2$), 2.96 (sept, $^3J_{HH}$ = 6.93 Hz, 1H, C<u>H</u>^{b}(CH$_3$)$_2$), 7.09 (m, 4H, C<u>H</u>^{f}), 7.56 (m, 2H, C<u>H</u>^{c}).
Elemental analysis ($C_{21}H_{27}Br\cdot(C_7H_8)_{0.5}$)	Calculated: C 72.58, H 7.71 Found: C 72.59, H 7.95
Mass spectrometry (EI, toluene)	m/z: 358.1 (52%) $[M]^{+\bullet}$, 343.1 (30%) $[M - CH_3]^{+\bullet}$, 315.1 (14%) $[M - C_3H_7]^{+\bullet}$, 264.2 (94%) $[M - CH_3 - Br]^{+\bullet}$, 221.1 (100%) $[M - CH_3 - Br - C_3H_7]^{+\bullet}$,

Synthesis of Cp^{Ar*}H (1a)

The synthesis is based on a literature known procedure, but slightly modified.[1]

0.339 g $Pd(OAc)_2$ (1.514 mmol, 0.1eq), 59.201 g Cs_2CO_3 (181.699 mmol, 12eq), 0.735 g P^{t}Bu$_3$ (3.634 mmol, 0.24eq), 4.426 g [Cp_2ZrCl_2] (15.142 mmol, 1eq) and 50.0 g 4-Bromo-4'-n-propylbiphenyl (181.699 mmol, 12eq) are suspended in a mixture of 500 ml dmf and stirred for 3 days at 130 °C. The mixture is cooled to room temperature and then slowly quenched with 69.577 g p-toluenesulfonic acid monohydrate (363.399 mmol, 24eq). Gas evolution can be observed during addition. From now on no protection gas is needed. Then 400 ml CH_2Cl_2 are added, and the mixture is stirred for 16 h.

The reaction mixture filtered over silica gel (l = 10 cm, d = 5 cm) and washed with CH_2Cl_2. The filtrate is dried in vacuo to give a brown powder. The powder is transferred to a large frit and washed several times with hexane and then with acetone, discarding the hexane and acetone solutions. The solid remaining on the frit is dissolved in toluene and filtered, giving a yellow solution of crude **1a**. Analytically pure **1a** can be obtained by recrystallization from a hot toluene/hexane mixture.

Crystals suitable for single crystal diffraction can be obtained by layering a toluene solution of **1a** under acetonitrile.

Yield: 16.60 g (16.00 mmol, 53% (related to [Cp_2ZrCl_2]))

Analytical data of **1a**:

NMR (C_6D_6, 298 K)	[ppm] = 0.82 (t, 9H, $^3J_{HH}$ = 7.28 Hz, $-CH_2CH_2C\underline{H}_3$), 0.84 (t, 6H, $^3J_{HH}$ = 7.28 Hz, $-C\underline{H}_2CH_2CH_3$), 1.50 (m, 10H, $-CH_2C\underline{H}_2CH_3$), 2.40 (t, 6H, $^3J_{HH}$ = 6.61 Hz, $-C\underline{H}_2CH_2CH_3$), 2.41 (t, 4H, $^3J_{HH}$ = 6.61 Hz, $-C\underline{H}_2CH_2CH_3$), 5.32 (s, 1H, $C_5Ar_5\underline{H}$), 7.00 (m, 10H, $C_6\underline{H}_4$) 7.42 (m, 30H, $C_6\underline{H}_4$)
Elemental analysis ($C_{80}H_{76}$)	Calculated: C 92.62, H 7.38 Found: C 92.52, H 7.26
Mass spectrometry (FD, toluene)	m/z: 1036.6 (100 %) $[M]^{+\bullet}$

Synthesis of $Cp^{XXL}H$ (1b)

The synthesis is based on a literature known procedure, but slightly modified.[1]

0.260 g $Pd(OAc)_2$ (1.160 mmol, 0.1eq), 45.335 g Cs_2CO_3 (139.140 mmol, 12eq), 0.563 g P^tBu_3 (2.783 mmol, 0.24eq), 3.389 g [Cp_2ZrCl_2] (11.595 mmol, 1eq) and 50.0 g **Br-R²** (139.140 mmol, 12eq) are suspended in a mixture of 500 ml dmf and 200 ml toluene and stirred for 3 days at 130 °C. The mixture is cooled to room temperature and then slowly quenched with 52.933 g p-toluenesulfonic acid monohydrate (276.280 mmol, 24eq). Gas evolution can be observed during addition. From now on no protection gas is needed. Then 200 ml H_2O are added, and the mixture is stirred for 16 h.

The two phases are separated, and the aqueous phase is extracted five times with 300 ml pentane each. All organic phases are merged, and the solvent is removed in vacuo. Column chromatography (silica gel, hexane/toluene = 5/1; l = 30 cm; d = 6.5 cm) was used for purification. However, the obtained yellow/brownish solid is not completely pure (75 % according to ^{1}H NMR).

m (yellow/brownish solid): 21.45 g (according to ^{1}H NMR only 75 % pure)
m (**1b**) = 16.09 g (11.03 mmol, 48% (related to [Cp_2ZrCl_2]))

An analytically pure sample of **1b** can be obtained by the hydrolysis of a CH_2Cl_2 solution of $\mathbf{2b_{Tl}}$ with an aqueous solution of $NaHCO_3$. The phases are separated, and the aqueous phase is extracted with pentane. The organic phases are merged, and the solvent is removed in vacuo. The residue is taken up in CH_2Cl_2 and layered under acetone to give **1b** as colorless needles.

Analytical data of **1b**:

NMR ($CDCl_3$, 298 K)	^1H: δ [ppm] = 1.04 (m, 60H, $CH(C\underline{H}_3)_2$), 1.30 (m, 30H, $CH(C\underline{H}_3)_2$), 2.64 (m, 10H, $C\underline{H}(CH_3)_2$), 2.93 (sept, $^3J_{HH}$ = 6.9 Hz, 5H, $C\underline{H}(CH_3)_2$), 5.27 (s, 1H, $C_5Ar_5\underline{H}$), 6.90 (m, 4H, C<u>H</u>), 7.03 (m, 14H, C<u>H</u>), 7.12 (m, 6H, C<u>H</u>), 7.21 (m, 4H, C<u>H</u>), 7.43 (m, 2H, C<u>H</u>).
Elemental analysis ($C_{110}H_{136}$)	Calculated: C 90.60, H 9.40 Found: C 90.53, H 9.40
Mass spectrometry (LIFDI, toluene)	m/z: 1458.1 (100 %) $[M]^{+\bullet}$

Synthesis of $NaCp^{Ar*}$ ($2a_{Na}$)

0.789 g $NaNH_2$ (20.226 mmol, 1.32eq) is suspended in 100 ml thf. 15.886g **1a** (15.312 mmol, 1eq) is dissolved in 100 ml thf and slowly added to the $NaNH_2$ suspension. The suspension is heated for 16 h to reflux to give a dark yellow suspension. The mixture is cooled to room temperature and the mixture is filtered over diatomaceous earth. The obtained filtrate is evaporated to dryness, giving crude **$2a_{Na}$** as a brownish yellow powder. The powder is dissolved in acetonitrile and filtered over diatomaceous earth. The obtained filtrate is evaporated to dryness. The powder is taken up in thf and a concentrated solution is stored at −35 C°, to give analytically pure **$2a_{Na}$** as multicrystalline dark yellow solid.

Crystals suitable for single crystal diffraction can be obtained by storing a concentrated thf/hexane mixture at −35 C°.

Yield: 12.888 g (12.165 mmol, 79%)

Analytical data of **$2a_{Na}$**:

NMR (thf-d_8, 298 K)	Due to the high sensitivity of solutions of **$2a_{Na}$**, always traces of **3a** are present which is why no reliable ^1H NMR spectrum could be obtained (Figure S6.11).
Elemental analysis ($NaC_{80}H_{75}\cdot(C_4H_8O)_3$)	Calculated: C 86.61, H 7.82 Found: C 86.33, H 7.02
Mass spectrometry (ESI, H_3CCN)	m/z: 1035.8 $[Cp^{Ar*}]^-$

Synthesis of $TlCp^{XXL}$ ($2b_{Tl}$)

5.600 g **1b** (3.840 mmol, 1eq) is dissolved in 100 ml hexane. 0.30 ml TlOEt (1.054 g, 4.224 mmol, 1.1eq) is suspended in 10 ml hexane and slowly added to the **1b** solution. The suspension is heated for 20 h to reflux to give an orange suspension. The mixture is cooled to room temperature and the solution is decanted off to leave a bright yellow powder behind. This powder is washed three times with each 50 ml hexane. Then the powder is

dissolved in thf and filtered over diatomaceous earth to give a bright yellow solution. Evaporation of the solvent gives pure **$2b_{Tl}$** as bright yellow powder.

Crystals suitable for single crystal diffraction can be obtained by layering a CH_2Cl_2 solution of **$2b_{Tl}$** under hexane.

Yield: 4.280 g (2.576 mmol, 67%)

Analytical data of **$2b_{Tl}$**:

NMR (CD_2Cl_2, 298 K)	^{1}H: δ [ppm] = 1.02 (br d, $^3J_{HH}$ = 6.8 Hz, 60H, CH(C<u>H</u>$_3$)$_2$), 1.27 (d, $^3J_{HH}$ = 6.9 Hz, 30H, CH(C<u>H</u>$_3$)$_2$), 2.72 (sept, $^3J_{HH}$ = 6.8 Hz, 10H, C<u>H</u>(CH$_3$)$_2$), 2.92 (sept, $^3J_{HH}$ = 6.9 Hz, 5H, C<u>H</u>(CH$_3$)$_2$), 6.87 (m, 10H, C<u>H</u>), 7.02 (s, 10H, C<u>H</u>), 7.13 (m, 10H, C<u>H</u>).
Elemental analysis ($TlC_{110}H_{135}$)	Calculated: C 79.51, H 8.19 Found: C 79.55, H 8.23
Mass spectrometry (ESI, H_3CCN/CH_2Cl_2)	m/z: 1457.1 $[Cp^{XXL}]^-$

Synthesis of $Cp^{Ar^*\bullet}$ (3a)

The synthesis is based on a literature known procedure.[2]

0.150 g **$2a_{Na}$** (0.1416 mmol, 1eq) and 0.0223 g CuBr (0.1557 mmol, 1.1eq) are suspended in thf 25 ml and stirred at room temperature for 2 h to give a dark reaction mixture. Then the solvent is removed, the residue is taken up in toluene and filtered over diatomaceous earth to give a dark green solution. Layering a toluene solution under acetonitrile gives dark green crystals of **3a** and colorless crystals of **1a**.

The crystals must be separated manually, that is why the isolated yield is so low.

Yield of **3a**: 0.0117 g (0.0113 mmol, 8%)

Analytical data of **3a**

EPR (toluene, 77 K)	2.004 g
UV-Vis (benzene)	$\lambda_{max,Vis}$ [nm]: 681

Synthesis of $Cp^{XXL\bullet}$ (3b)

The synthesis is based on a literature known procedure.[2]

0.5000 g **$2b_{Tl}$** (0.3009 mmol, 1eq) and 0.0475 g CuBr (0.3310 mmol ,1.1eq) are suspended in thf 50 ml and stirred at room temperature for 24 h to give a dark turquoise/black reaction mixture. Then the solvent is removed, the residue is taken up in pentane and filtered over diatomaceous earth to give a dark blue solution. Layering a

toluene solution under acetonitrile gives dark reddish blue crystals of **3b** and colorless crystals of **1b**.

The crystals must be separated manually, that is why the isolated yield is so low.

Yield of **3b**: 0.0068 g (0.0047 mmol, 2%)

Analytical data of **3b**

EPR (toluene, 77 K)	2.000
UV-Vis (benzene)	$\lambda_{max,Vis}$ [nm]: 620 ε [$l \cdot mol^{-1} \cdot cm^{-1}$]: 2.87
Mass spectrometry (LIFDI, toluene)	m/z: 1458.0 (100%) $[Cp^{XXL}H]^{+\bullet}$

Attempts to synthesize [$Cp^{Ar*}Fe(CO)_2Br$] (3b)

Despite several attempts **3b** could not be obtained, although two reaction pathways have been tested.

Pathway 1:

0.6349 g [$FeBr_2$·dme] (2.0765 mmol, 1.1eq) is suspended in 100 ml thf and cooled to –40 °C. 2.000 g **$2a_{Na}$** (1.8877 mmol, 1eq) is dissolved in 100 ml thf and slowly dropped to the cold suspension. The mixture is stirred for 2.5 h during which it is warmed to room temperature. Bubbling CO gas through the reaction mixture for 2 h result in a dark green suspension. The mixture is stirred for another 16 h under CO atmosphere. The solvent is then removed, the residue is taken up in toluene and filtered off via diatomaceous earth. The subsequent IR spectroscopic investigation showed no signals for CO groups in the typical range.

Pathway 2:

0.5000 g **$2a_{Na}$** (0.4719 mmol, 1eq) is suspended in 100 ml toluene and cooled to −40 C°. In a second flask, 0.0500 g BrCN (0.4719 mmol, 1eq) is added to 20 ml Et_2O. The BrCN solution is added to the suspension of **$2a_{Na}$** to give a dark yellow mixture. The mixture is stirred for 2 h at −40 C° before it is allowed to reach room temperature. The solvent is then removed, the residue is taken up in xylene and filtered off via diatomaceous earth.

Then, 0.20 ml [$Fe(CO)_5$] (1.4803 mmol, 0.2900 g, 3.1eq) is added to the filtrate which leads to a color change from dark yellow to dark green within minutes. The mixture is heated for 2 h at reflux to give a dark greenish brown mixture. The solvent is then removed, the residue is taken up in toluene and filtered off via diatomaceous earth. The subsequent IR spectroscopic investigation showed no signals for CO groups in the expected region.

Synthesis of [$Cp^{XXL}Fe(CO)_2Br$] (4b)

The procedure is carried out in the absence of light.

2.2082 g [$FeBr_2$·dme] (7.2216 mmol, 1.5eq) is suspended in 100 ml thf and cooled to –40 °C. 8.000 g **$2b_{Tl}$** (4.8144 mmol, 1eq) is dissolved in 300 ml thf and slowly dropped to the cold suspension. The mixture is stirred for 2 h during which it is warmed to room temperature. Bubbling CO gas through the reaction mixture for 2 h result in the formation of a milky brown suspension. The solvent is then removed, the residue is taken up in hexane and filtered off via diatomaceous earth. Evaporation of the solvent gives **4b** as red brown powder.

Crystals suitable for X-ray analysis can be obtained by layering a CH_2Cl_2 solution of **4b** under acetonitrile.

Yield: 7.815 g (4.739 mmol, 98%)

Analytical data of **4b**:

NMR (CD_2Cl_2, 298 K)	^{1}H: δ [ppm] = 1.04 (br, 60H, $CH(C\underline{H}_3)_2$), 1.28 (br, 30H, $CH(C\underline{H}_3)_2$), 2.72 (br, 10H, $C\underline{H}(CH_3)_2$), 2.92 (br, 5H, $C\underline{H}(CH_3)_2$), 7.03 (br, 20H, C<u>H</u>), 7.33 (br, 10H, C<u>H</u>).
IR (toluene)	$\tilde{\nu}$ [cm^{-1}] = 1996 (vs), 2035 (vs)
IR (hexane)	$\tilde{\nu}$ [cm^{-1}] = 1999 (vs), 2037 (vs)
Elemental analysis	Calculated: C 77.50, H 7.90
($C_{112}H_{135}FeO_2Br\cdot(CH_2Cl_2)_{1.25}$)	Found: C 77.47, H 7.97
Mass spectrometry (LIFDI, toluene)	m/z: 1457.1 (100%) [Cp^{XXL}]$^{+\bullet}$

Synthesis of [$Cp^{XXL}Fe(CO)_2]_2$ (5)

The procedure is carried out in the absence of light.

0.4919 g KC_8 (3.6385 mmol, 1.2eq) is suspended in 50 ml toluene. 5.000 g **4b** (3.0321 mmol, 1eq) is dissolved in 300 ml toluene and added to the KC_8 suspension and stirred for 20 h at room temperature. Filtration over diatomaceous earth and subsequent evaporation gives a dark green powder. The powder is washed with acetone until the acetone solution is colorless. Drying the remaining dark green powder gives pure **5**.

Crystals suitable for X-ray analysis can be obtained by layering a toluene solution of **5** under acetonitrile.

Yield: 2.636 g (0.840 mmol, 55 %)

Analytical data of **5**:

NMR (thf-d_8, 298 K)	^{1}H: δ [ppm] = 0.98 (s br, 60H, CH(C<u>H</u>$_3$)$_2$), 1.23 (s br, 15H, CH(C<u>H</u>$_3$)$_2$), 1.24 (s br, 15H, CH(C<u>H</u>$_3$)$_2$), 2.66 (m br, 10H, C<u>H</u>(CH$_3$)$_2$), 2.87 (m br, 5H, C<u>H</u>(CH$_3$)$_2$), 7.03 (s br, 10H, C<u>H</u>), 7.09 (m br, 20H, C<u>H</u>).
IR (toluene)	Dimer: $\tilde{\nu}$ [cm^{-1}] = 1782 (s), 1954 (s). Monomer: $\tilde{\nu}$ [cm^{-1}] = 1924(w), 1990 (w).
IR (hexane)	Dimer: $\tilde{\nu}$ [cm^{-1}] = 1783 (s), 1955 (s). Monomer: $\tilde{\nu}$ [cm^{-1}] = 1929 (w), 1993 (w).
IR (pentane)	Dimer: $\tilde{\nu}$ [cm^{-1}] = 1783 (s), 1956 (s). Monomer: $\tilde{\nu}$ [cm^{-1}] = 1930 (w), 1994 (w).
Elemental analysis ($C_{224}H_{270}Fe_2O_4\cdot(C_6H_4Cl_2)_{1.33}$)	Calculated: C 83.32, H 8.28 Found: C 83.57, H 8.32
Mass spectrometry (LIFDI, toluene)	m/z: 1457.1 (100%) $[Cp^{XXL}H]^{+\bullet}$, 1548.0 (12%) $[Cp^{XXL} + C_7H_8 - H]^{+\bullet}$, 1605.00 (6%) $[Cp^{XXL}Fe(C_7H_8)]^{+\bullet}$,

Synthesis of [$Cp^{XXL}Fe(\eta^5\text{-}P_5)$] (6)

0.5000 g **5** (0.1593 mmol, 1eq) and 0.1974 g P_4 (1,5933 mmol, 10eq) are suspended in 125 ml diisoproplybenzene and heated to reflux for 3.5 h. The mixture is cooled to room temperature and the solvent is removed in vacuo to give a brownish/black residue. This is taken up in hexane and filtered over diatomaceous earth. The solvent is removed, and the filtrate is purified by column chromatography (silica gel, hexane/toluene = 10/1; l = 35 cm; d = 3.5 cm). The first green fraction is **6**.

Crystals suitable for X-ray analysis can be obtained for both complexes by layering a toluene solution under acetonitrile to give to **6** as green needles.

Yield: 0.131 g (0.0785 mmol, 25 %)

Analytical data of [$Cp^{XXL}Fe(\eta^5\text{-}P_5)$]:

NMR (C_6D_6, 298 K)	^{1}H: δ [ppm] = 1.19 (d, $^3J_{HH}$ = 6.86 Hz, 60H, CH(C<u>H</u>$_3$)$_2$), 1.25 (d, $^3J_{HH}$ = 6.92 Hz, 30H, CH(C<u>H</u>$_3$)$_2$), 2.85 (sept, $^3J_{HH}$ = 6.92 Hz, 5H, C<u>H</u>(CH$_3$)$_2$), 2.96 (sept, $^3J_{HH}$ = 6.86 Hz, 10H, C<u>H</u>(CH$_3$)$_2$), 7.19 (m, 10H, C<u>H</u>), 7.22 (s, 10H, C<u>H</u>), 7.48 (br, $\omega_{½}$ ≈ 160 Hz, 10H, C<u>H</u>). ^{31}P{^{1}H}: δ [ppm] = 174.6 (s, 5P, <u>P</u>$_5$).
Elemental analysis ($C_{110}H_{135}FeP_5$)	Calculated: C 79.21, H 8.16 Found: C 79.11, H 8.17

Mass spectrometry (LIFDI, toluene)	m/z: 1668.0 (100%) $[M]^{+\bullet}$

Synthesis of $[\{Cp^{XXL}Fe(CO)_2\}_2(\mu,\eta^{1:1}\text{-}P_4)]$ (7)

The procedure is carried out in the absence of light.

0.5000 g **5** (0.1593 mmol, 1eq) and 0.0217 g P_4 (0.1753 mmol, 1.1eq) are suspended in 20 ml hexane and stirred at room temperature for 15 min. After 1 minute the reaction mixture turns into a clear bright red/orange solution. Then the solution was concentrated and stored at −35 °C to give **7** as red/orange powder.

Crystals suitable for X-ray analysis can be obtained by layering a toluene solution of **7** under acetonitrile as orange prisms.

Yield: 0.252 g (0.0773 mmol, 49 %)

Analytical data of **7**:

NMR (CD_2Cl_2, 298 K)	^{1}H: δ [ppm] = 0.99 (br, 120H, CH($C\underline{H}_3$)$_2$), 1.25 (br, 60H, CH($C\underline{H}_3$)$_2$), 2.62 (br, 20H, C$\underline{H}$(CH_3)$_2$), 2.89 (br, 10H, C$\underline{H}$(CH_3)$_2$), 6.95 (br m, 20H, C$\underline{H}$), 6.99 (br s, 20H, C$\underline{H}$), 7.22 (br m, 20H, C$\underline{H}$). ^{31}P{^{1}H}: δ [ppm] = –313.7 (t, $^1J_{PP}$ = 189 Hz, 2P, bridge-head P), –48.5 (t, $^1J_{PP}$ = 189 Hz, 2P, wing-tip P).
NMR (C_6D_6, 298 K)	^{31}P{^{1}H}: δ [ppm] = –315.5 (t, $^1J_{PP}$ = 189 Hz, 2P, bridge-head P), –51.5 (t, $^1J_{PP}$ = 189 Hz, 2P, wing-tip P).
IR (hexane)	$\tilde{\nu}$ [cm^{-1}] = 1962 (vs,), 1998 (m). 2006 (s)
Elemental analysis ($C_{224}H_{270}Fe_2O_4P_4\cdot(Et_2O)$)	Calculated: C 82.08, H 8.46 Found: C 82.04, H 8.54
Mass spectrometry (LIFDI, toluene)	m/z: 1458.0 (100%) $[Cp^{XXL}H]^{+\bullet}$, 1605.0 (18%) $[Cp^{XXL}Fe(C_7H_8)]^{+\bullet}$

Synthesis of $Cp^{Ar^*}{}_2P_4$ (8a)

The synthesis is based on a literature known procedure.[2] The synthesis is performed in the absence of light.

A freshly prepared solution of 0.1957 g **3a** (0.1888 mmol, 2eq) in 20 ml thf is added to 0.0129 g P_4 (0.1038 mmol, 1.1eq) and stirred for 2 h at room temperature. The dark yellow solution is evaporated to dryness and taken up in toluene. Layering the toluene solution under acetonitrile gives a mixture of **8a** as yellow plates and **1a** as colorless blocks.

Yield: 0.0290 g (0.0132 mmol, 14%)

Analytical data of **8a**:

NMR (C_6D_6, 298 K)	No reliable ^{1}H NMR spectrum of **8a** could be obtained due to traces of radical **3a** that are always present in the reaction mixture. Furthermore, are crystals of **8a** always polluted with **1a**. $^{31}P\{^1H\}$: δ [ppm] = −174.3 (t, $^1J_{PP}$ = 193 Hz, 2P, wing-tip P), –302.3 (t, $^1J_{PP}$ = 193 Hz, 2P, bridge-head P).

Synthesis of $Cp^{XXL}_2P_4$ (8b)

The synthesis is based on a literature known procedure.[2] The synthesis is performed in the absence of light.

A freshly prepared solution of 0.1754 g **3b** (1.1204 mmol, 2eq) in 20 ml thf is added to 0.0224 g P_4 (1.805 mmol, 3eq) and stirred for 20 h at room temperature. The still deeply blue reaction solution is evaporated to dryness and taken up in toluene. Layering the toluene solution under acetonitrile gives a mixture of **8b** as yellow plates and **1b** as colorless blocks.

Yield: 0.0460 g (0.0151 mmol, 25%)

Analytical data of **8b**:

NMR (C_6D_6, 298 K)	No reliable ^{1}H NMR spectrum of **8b** could be obtained due to traces of radical **3b** that are always present in the reaction mixture. Furthermore, are crystals of **8b** always polluted with **1b**. $^{31}P\{^1H\}$: δ [ppm] = −183.1 (t, $^1J_{PP}$ = 193 Hz, 2P, wing-tip P), –312.7 (t, $^1J_{PP}$ = 193 Hz, 2P, bridge-head P).

Synthesis of [{$Cp^{XXL}Fe(\eta^4\text{-}P_5)$}$_3$($Cu_XBr_{X-3}$)(solv)$_y$] (9, solv = methanol or acetonitrile)

0.0100 g [$Cp^{XXL}Fe(\eta^5\text{-}P_5)$] (0.0060 mmol, 1eq) and 0.0103 g CuBr (0.0719 mmol, 12eq) are suspended in 5 ml acetonitrile and stirred for 15 minutes. After that, the solvent is removed, and the green residue is dissolved in 10 ml of CH_2Cl_2 leading to a dark orange solution. The mixture is stirred at room temperature for 3 days and is then filtered over diatomaceous earth. Layering the CH_2Cl_2 solution under methanol gives small amounts of **9** as black prisms.

Yield: >0.001 mg (>1%)

The only analytical data that could be obtained for **9** is the molecular structure in solid state (vide infra). Further characterization was not possible, due to the low yield.

Crystallographic Details

General remarks:

Crystals were taken from a Schlenk tube under a stream of argon and immediately covered with mineral oil to prevent decomposition and a loss of solvent. The quickly chosen single crystals covered by a protective layer of the oil were directly placed on a magnetic base and into a stream of cold nitrogen with a pre-centered goniometer head with a CryoMount® and attached to the goniometer of a diffractometer.

Single crystal structure analyses were performed using a Rigaku (formerly Agilent Technologies) SuperNova diffractometer, equipped either with Titan^{S2} CCD detector (**Br-R^2, 2b$_{Na}$, 2b$_{Tl}$, 3a, 4b, 6**) or SuperNova, Single source at offset, Atlas diffractometer (**2a$_{Na}$**) or a Gemini Ultra diffractometer (Oxford Diffraction) with an Atlas^{S2} detector (**1a**) or dual-wave XtaLAB Synergy R diffractometer, equipped with HyPix-Arc hybrid pixel detector (**1b, 3b**).

To collect diffraction data for **5** and **9** at the DESY PETRA III synchrotron, the crystals were carefully selected, mounted on a magnetic holder, checked for quality, and placed into a Dewar vessel with liquid nitrogen using standard cryo-crystallography tools. The X-ray diffraction study of **9** faced many challenges, as the crystals were systematically twinned and weakly scattering. Using standard procedures, the series of crystals **5** and **9** were placed into a special Dewar vessel filled with liquid nitrogen among other crystals in the P11 hutch. A robotic mounting/demounting was used for further manipulations. The data for **5** were collected at 7(2) K at P11 beamline (DESY PETRA III synchrotron)[3] on a 1-axis goniostat using 360°-rotation around φ with using 18 keV synchrotron radiation (λ = 0.6888 Å, 12% transmission) and shutterless data acquisition with 60 ms per 0.1° scan registered with DECTRIS PILATUS 6M photon counting detector. Crystal of **9** was measured at 6(2) K with shutterless data acquisition (30% transmission) with 40 ms per 0.1° scan.

The data for **8b** were collected at 14(2) K at P24 (DESY PETRA III synchrotron)[4] using Huber 3-cycle diffractometer equipped with MAR165 CCD detector and an open-flow He LT system. The crystals were chosen under argon and handled using mineral oil as described above. Data collection was performed by 360° ϕ-rotation with 0.2° scan width and exposure 1 s per frame at a wavelength λ = 0.56076 Å (22.11 keV).

Data reduction and absorption correction for all experiments was performed with CrysAlis software.[5] The structures were solved by direct methods with *SHELXS* or *SHELXT*[6] and were refined by full-matrix least-squares method against F^2 in anisotropic approximation using multiprocessor variable memory versions of *SHELXL*.[6] All non-hydrogen atoms with

occupancies higher than 0.5 were refined in anisotropic approximation, while the hydrogen atoms were refined riding on pivot atoms.

Further details are given in Table S6.1, Table S6.2, Table S6.3, and Table S6.4.

Table S6.1. Crystallographic data and details of diffraction experiments for **Br-R²**, **1a**, **1b** and **2a$_{Na}$**.

Compound	**Br-R²**	**1a**	**1b** · 1.18(C_7H_8)	**2a$_{Na}$** · 8(C_4H_8O)
Formula	$C_{21}H_{27}Br$	$C_{80}H_{76}$	$C_{118.26}H_{145.44}$	$C_{112}H_{139}NaO_8$
$D_{calc.}$/ g cm^{-3}	1.270	1.152	1.038	1.164
μ/mm^{-1}	2.917	0.484	0.428	0.589
Formula Weight	359.33	1037.40	1566.90	1636.21
Color	clear colorless	clear colorless	light brown	clear yellowish brown
Shape	block	needle	block	block
Size/mm^3	0.36×0.27×0.18	1.23×0.09×0.05	0.52×0.28×0.18	0.32×0.11×0.09
T/K	123.00(10)	124(2)	100.00(10)	123.01(10)
Crystal System	monoclinic	monoclinic	triclinic	monoclinic
Space Group	$P2_1/c$	$P2_1/c$	$P\bar{1}$	$P2_1/c$
a/Å	9.8190(2)	18.3118(7)	12.79990(10)	13.66214(14)
b/Å	10.9050(2)	32.9962(12)	18.21710(10)	19.1315(2)
c/Å	17.5642(3)	9.9972(4)	22.5485(2)	35.8560(4)
α/°	90	90	103.1560(10)	90
β/°	91.869(2)	97.950(4)	92.0040(10)	95.2393(10)
γ/°	90	90	100.6780(10)	90
V/Å^3	1879.71(6)	5982.5(4)	5014.77(7)	9332.79(18)
Z	4	4	2	4
Z'	1	1	1	1
Wavelength/Å	1.54184	1.54184	1.54184	1.54184
Radiation type	Cu Kα	Cu Kα	Cu Kα	Cu Kα
Θ_{min}/°	4.506	3.622	2.019	3.386
Θ_{max}/°	74.176	67.013	75.450	74.165
Measured Refl's.	10557	39323	124779	66729
Ind't Refl's	3673	10494	19927	18212
Refl's with I > 2(I)	3448	6845	16020	15520
R_{int}	0.0365	0.0750	0.0305	0.0354
Parameters	205	1014	1729	1113
Restraints	0	330	1742	0
Largest Peak	0.595	0.344	0.761	0.628
Deepest Hole	-0.623	-0.288	-0.320	-0.401
GooF	1.035	1.013	1.050	1.070
wR_2 (all data)	0.0983	0.1539	0.2171	0.1662
wR_2	0.0958	0.1286	0.2055	0.1594
R_1 (all data)	0.0386	0.0972	0.0804	0.0706
R_1	0.0366	0.0568	0.0689	0.0611

Table S6.2. Crystallographic data and details of diffraction experiments for **2b$_{Na}$**, **2b$_{Tl}$**, **3a** and **3b**.

Compound	**2b$_{Na}$** · 0.5(C_4H_8O)[a)]	**2b$_{Tl}$** · 0.3(CH_2Cl_2)	**3a**	**3b**
Formula	$C_{111.76}H_{137.85}NaO_{0.5}$	$C_{110.3}H_{135.6}Cl_{0.6}Tl$	$C_{80}H_{75}$	$C_{110}H_{135}$
$D_{calc.}$/ g cm^{-3}	0.823	1.075	1.159	1.015
μ/mm^{-1}	0.375	3.422	0.487	0.418
Formula Weight	1512.11	1687.02	1036.40	1457.17
Color	pale green	clear yellow	clear dark green	dark green
Shape	block	block	block	needle
Size/mm^3	0.19×0.17×0.11	0.18×0.13×0.10	0.49×0.11×0.09	0.16×0.13×0.07
T/K	123.0(2)	89.8(5)	89.9(5)	100.01(16)
Crystal System	monoclinic	triclinic	monoclinic	monoclinic
Space Group	$P2_1/n$	$P\bar{1}$	$P2_1/c$	$P2_1/n$
a/Å	14.6812(6)	14.5609(3)	10.2603(2)	14.48780(10)
b/Å	28.9269(10)	20.3372(3)	40.6728(7)	24.32730(10)
c/Å	28.7524(12)	20.5087(4)	28.7113(5)	27.93300(10)
α/°	90	117.540(2)	90	90

β/°	91.861(4)	94.040(2)	97.322(2)	104.38
γ/°	90	100.520(2)	90	90
V/Å^3	12204.2(8)	5210.30(19)	11884.0(4)	9536.60(8)
Z	4	2	8	4
Z'	1	1	2	1
Wavelength/Å	1.54184	1.54184	1.54184	1.54184
Radiation type	Cu K$_\alpha$	Cu K$_\alpha$	Cu K$_\alpha$	Cu K$_\alpha$
Θ_{min}/°	3.076	3.517	3.289	2.442
Θ_{max}/°	65.181	74.252	74.301	75.320
Measured Refl's.	45409	51644	53125	252669
Ind't Refl's	19813	20214	22772	19640
Refl's with I > 2(I)	10710	16584	16518	16577
R_{int}	0.0459	0.0461	0.0395	0.0264
Parameters	1570	1322	2172	1289
Restraints	1202	432	2561	540
Largest Peak	0.756	1.311	0.701	0.305
Deepest Hole	-0.249	-1.164	-0.413	-0.251
GooF	1.256	1.024	1.041	1.034
wR_2 (all data)	0.3903	0.1198	0.2679	0.1517
wR_2	0.3400	0.1112	0.2429	0.1452
R_1 (all data)	0.1593	0.0573	0.1069	0.0594
R_1	0.1215	0.0448	0.0689	0.0515

a) preliminary data, chemical formula is incorrect

Table S6.3. Crystallographic data and details of diffraction experiments for **4b**, **5**, **6** and **7**.

Compound	**4b** · 3(CH_2Cl_2) · 2(C_2H_3N)	**5** · 5.1(C_7H_8) · 0.7(C_2H_3N)	**6** · 1(C_7H_8)	**7** · 2.88(C_7H_8) · 1.7(C_2H_3N)
Formula	$C_{231}H_{282}Br_2Cl_6Fe_2N_2O_4$	$C_{261.1}H_{312.2}N_{0.7}O_4Fe_2$	$C_{117}H_{143}FeP_5$	$C_{247.56}H_{298.14}N_{1.7}O_4P_4Fe_2$
$D_{calc.}$/ g cm^{-3}	1.132	1.091	1.115	1.054
μ/mm^{-1}	2.617	1.464	2.214	0.116
Formula Weight	3634.79	3636.00	1760.01	3597.10
Color	clear dark red	green, brown	clear green	orange
Shape	block	elongated prism	needle	prism
Size/mm^3	0.43×0.27×0.20	0.41×0.12×0.09	0.31×0.08×0.04	0.2×0.1×0.1
T/K	122.96(11)	89.9(4)	122.98(10)	14(2)
Crystal System	monoclinic	triclinic	orthorhombic	monoclinic
Space Group	$P2_1/c$	$P\bar{1}$	$Pbca$	$P2_1/c$
a/Å	26.2647(3)	14.6992(4)	35.1370(3)	16.98776(8)
b/Å	23.7225(2)	19.9180(5)	15.1438(2)	21.53745(13)
c/Å	34.5585(3)	20.0332(5)	39.4008(6)	61.9901(3)
α/°	90	75.107(2)	90	90
β/°	97.8090(10)	87.830(2)	90	92.3799(5)
γ/°	90	77.506(2)	90	90
V/Å^3	21332.5(4)	5533.1(3)	20965.5(5)	22660.9(2)
Z	4	1	8	4
Z'	1	0.5	1	1
Wavelength/Å	1.54184	1.54178	1.54184	0.56076
Radiation type	Cu K$_\alpha$	Cu K$_\alpha$	Cu K$_\alpha$	synchrotron
Θ_{min}/°	3.277	3.671	3.370	2.771
Θ_{max}/°	74.118	74.266	74.003	20.232
Measured Refl's.	101072	40331	64472	290740
Ind't Refl's	41284	21553	20402	42696
Refl's with I > 2(I)	33815	17470	17346	28150
R_{int}	0.0355	0.0255	0.0387	0.0590
Parameters	3056	1686	1229	2666
Restraints	1331	60	108	12
Largest Peak	5.450	0.445	0.568	1.100
Deepest Hole	-1.744	-0.467	-0.319	-0.421
GooF	1.933	1.058	1.016	1.044
wR_2 (all data)	0.4318	0.1461	0.1405	0.2545
wR_2	0.4147	0.1415	0.1334	0.2449
R_1 (all data)	0.1617	0.0602	0.0614	0.1029
R_1	0.1492	0.0511	0.0514	0.0801

Table S6.4. Crystallographic data and details of diffraction experiments for **8a**, **8b**, and **9**.

Compound	**8a** · 3(C_4H_8O)[a]	**8b** · 2.95(C_7H_8) · 2.75(C_2H_3N)	**9**[a]
Formula	$C_{172}H_{171}O_3P_4$	$C_{246.15}H_{301.85}N_{2.75}P_4$	$C_{291.67}H_{419}Br_{11.75}Cl_{2.92}Cu_{14.33}Fe_3N_{5.33}P_{15}$
$D_{calc.}$/ g cm^{-3}	1.022	1.029	> 1.113
μ/mm^{-1}	0.868	0.080	>2.00
Formula Weight	2261.79	3422.92	>6585.14
Color	yellow	yellow	black
Shape	plate	prism	prism
Size/mm^3	0.29×0.25×0.12	0.40×0.30×0.30	0.20×0.15×0.15
T/K	123.0(2)	7(2)	6.1
Crystal System	triclinic	triclinic	trigonal
Space Group	$P\bar{1}$	$P\bar{1}$	$R3c$
a/Å	17.6046(10)	22.99535(18)	38.75571(17)
b/Å	20.9917(19)	25.3652(2)	38.75571(17)
c/Å	22.0631(13)	39.6432(4)	90.6531(5)
α/°	68.082(7)	100.5687(8)	90
β/°	86.679(5)	96.6481(8)	90
γ/°	76.422(6)	100.3355(7)	120
V/Å^3	7348.7(10)	22096.2(4)	117919.2(9)
Z	2	4	6
Z'	1	2	2
Wavelength/Å	1.54184	0.6888	0.6888
Radiation type	Cu K_α	synchrotron	synchrotron
Θ_{min}/°	2.331	1.503	1.571
Θ_{max}/°	74.569	25.499	24.835
Measured Refl's.	46003	259107	211118
Ind't Refl's	28261	84834	49515
Refl's with I > 2(I)	10565	56932	40863
R_{int}	0.2306	0.0310	0.0417
Parameters	1428	5257	2522
Restraints	135	43	1
Largest Peak	1.383	1.402	2.472
Deepest Hole	-1.149	-0.647	-0.776
GooF	1.239	1.064	1.065
wR_2 (all data)	0.5346	0.2445	0.2329
wR_2	0.4528	0.2330	0.2162
R_1 (all data)	0.2954	0.0977	0.0927
R_1	0.2004	0.0760	0.0805
Flack parameter	–	–	0.953(9)

a) preliminary data, chemical formula is incorrect

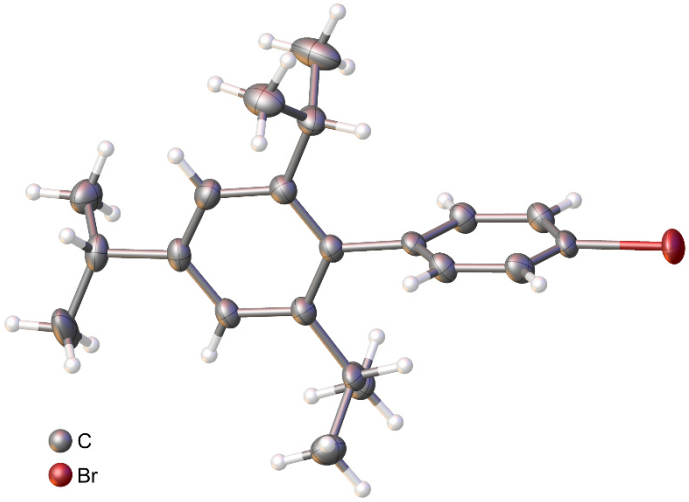

Figure S6.1. Molecular structure of **Br-R²** in the crystal. ADPs are shown at 50% probability level.

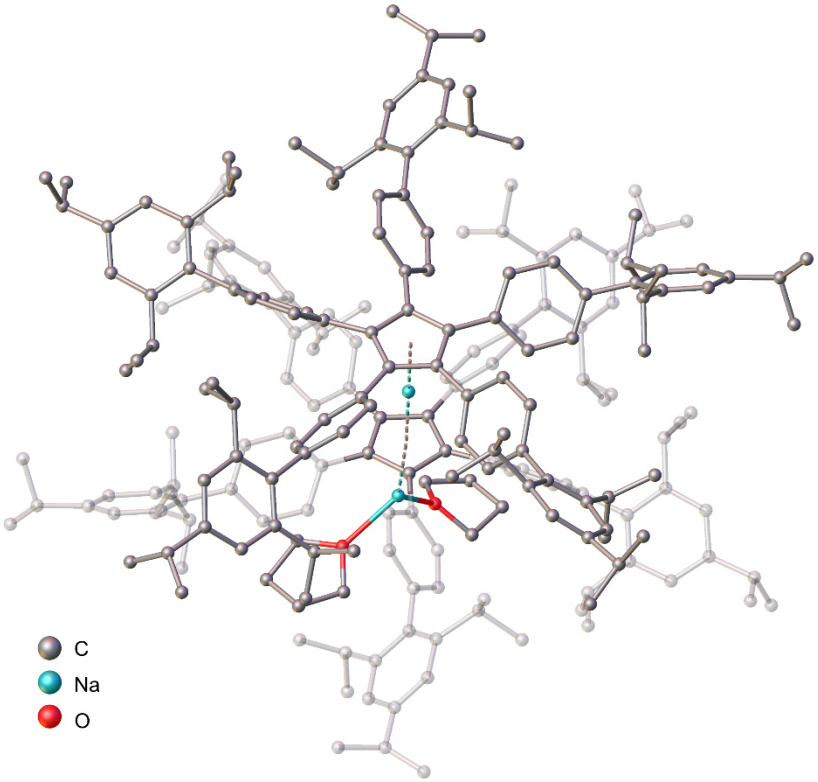

Figure S6.2. Model of the molecular structure of **2b$_{Na}$** in the crystal, showing the presence of the dimer [Na(thf)$_x$][Cp^{XXL}_2Na] in solid state. The positions of the two thf molecules are not fully occupied. The exact amount could not be determined due to poor crystal quality. H atoms are omitted and the substituents of the lower Cp^{XXL} unit are translucent for clarity.

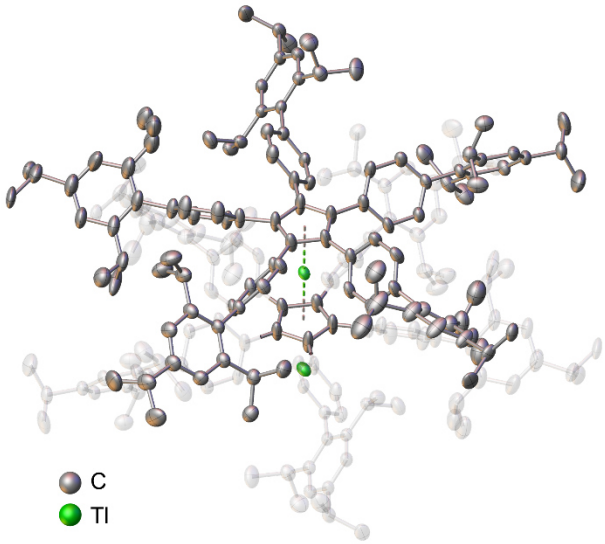

Figure S6.3. Molecular structure of **$2b_{Tl}$** in the crystal, showing the presence of the dimer $Tl[Cp^{XXL}{}_2Tl]$ in solid state. H atoms are omitted and the substituents of the lower Cp^{XXL} unit are translucent for clarity.

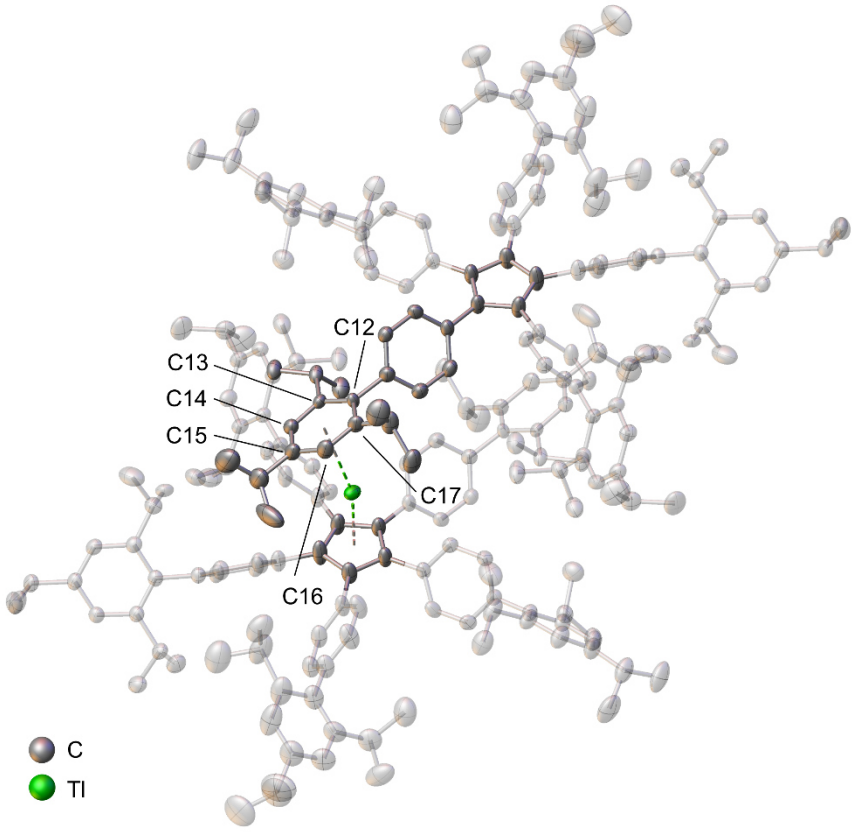

Figure S6.4. Molecular structure of **$2b_{Tl}$** in the crystal, showing the intermolecular stabilization of the external thallium cation by coordinating to an adjacent triisopropylphenyl group. Selected bond lengths [Å]: Tl-C12 3.584(8), Tl-C13 3.454(7), Tl-C14 3.322(7), Tl-C15 3.362(9), Tl-C16 3.506(10), Tl-C17 3.656(9), $Tl\text{-}C_{6,centr.}$ 3.190(4), $Tl\text{-}C_{5,centr.}$ 2.796(2).

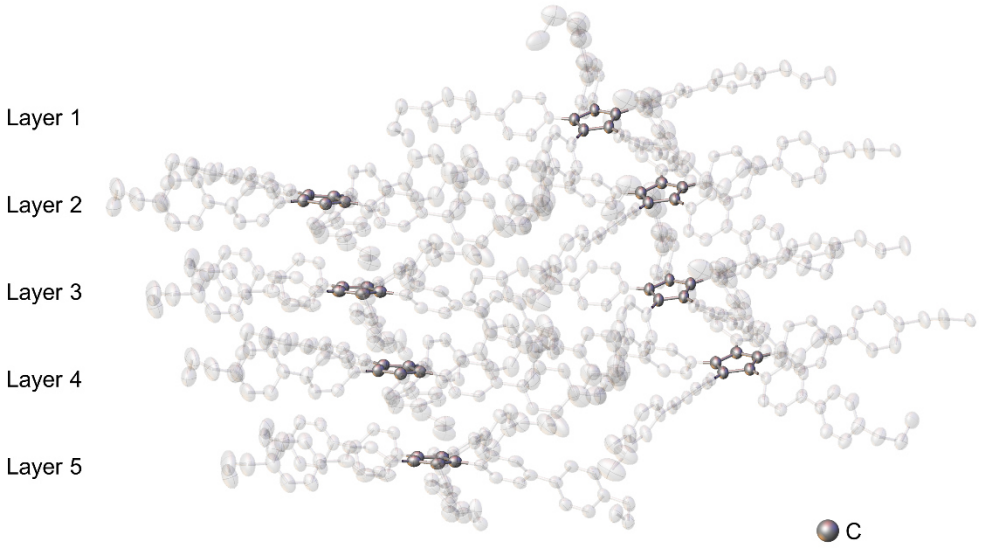

Figure S6.5. Section of the packing of **3a** in solid state. H atoms are omitted and the substituents of the C_5 rings are translucent for clarity.

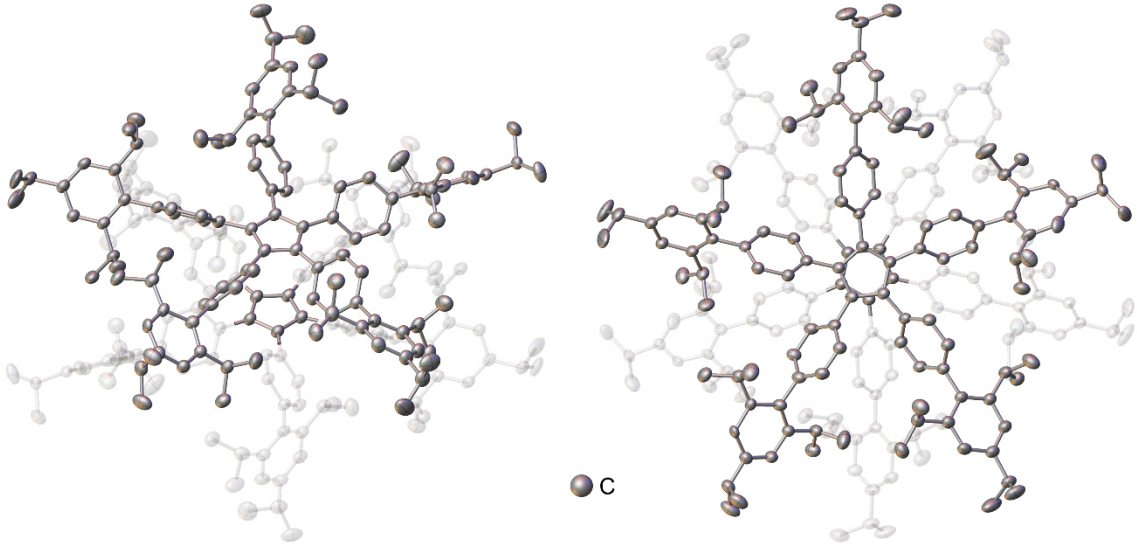

Figure S6.6. Packing of **3b** in solid state, showing the presence of dimeric units in solid state and are shown in a side (left) and top view (right). H atoms are omitted and the substituents of the lower unit of **3b** are translucent for clarity.

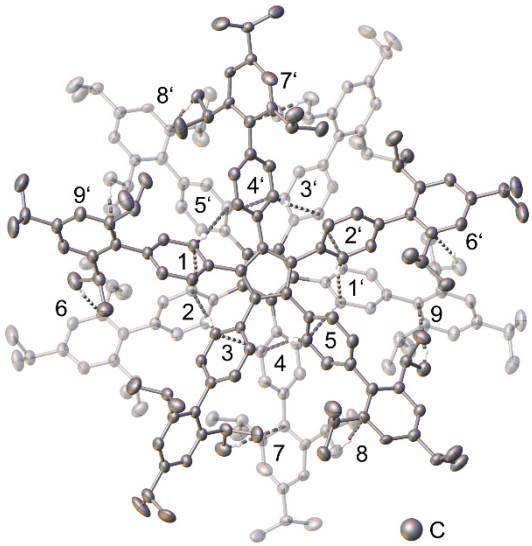

Figure S6.7. Molecular structure of **3b** in the crystal, showing the stabilization of the dimeric unit by short intermolecular H···C contacts. Only the involved H atoms are shown and the substituents of the lower unit of **3b** are translucent for clarity. Bond lengths [Å]: 1/1’ 2.7964(14), 2/2’ 2.8636(14), 3/3’ 3.0691(15), 4/4’ 2.7632(15), 5/5’ 2.8978(14), 6/6’ 2.8784(14), 7/7’ 2.9252(14), 8/8’ 2.770(5), 9/9’ 3.0380(13).

^{1}H NMR and ^{31}P NMR Spectroscopy

General remarks:

^{1}H and ^{31}P NMR spectra were recorded on a Bruker Avance III HD 400 (^{1}H: 400.130 MHz, ^{31}P: 161.976 MHz) at 298 K. The chemical shifts are reported in ppm relative to external TMS (^{1}H) and H_3PO_4 (^{31}P).

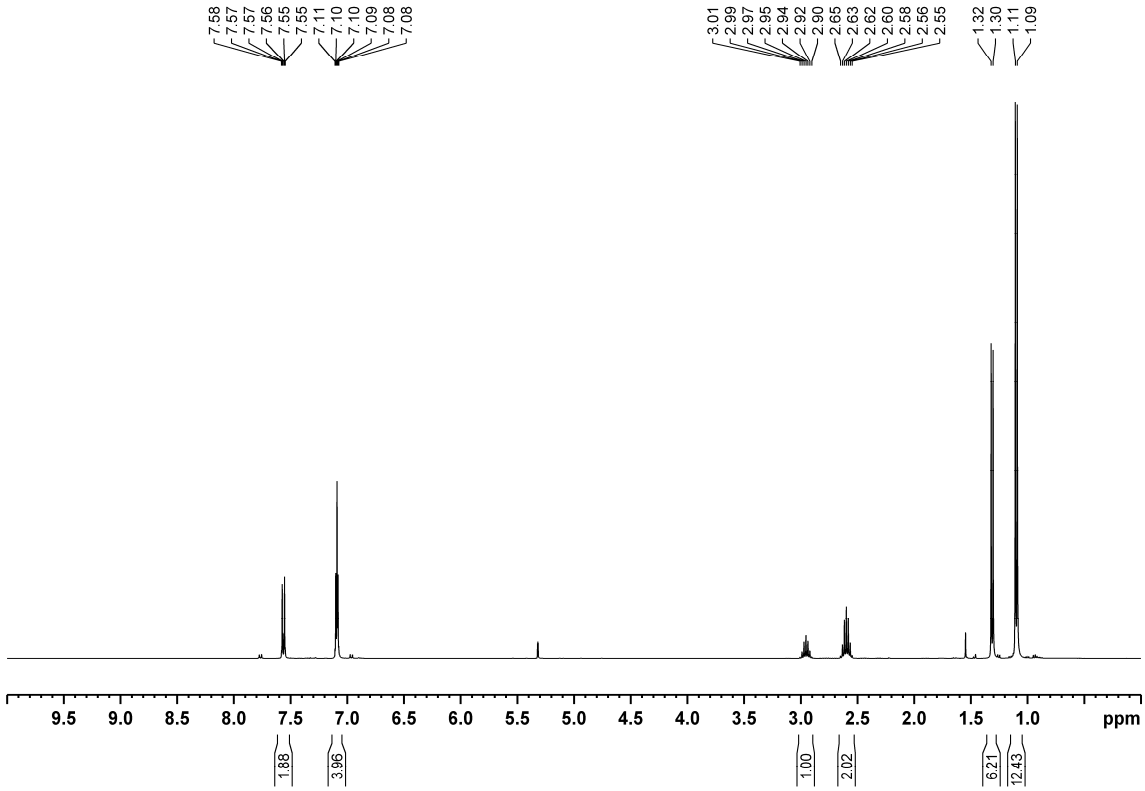

Figure S6.8. ^{1}H NMR spectrum of **Br-R^2** in CD_2Cl_2.

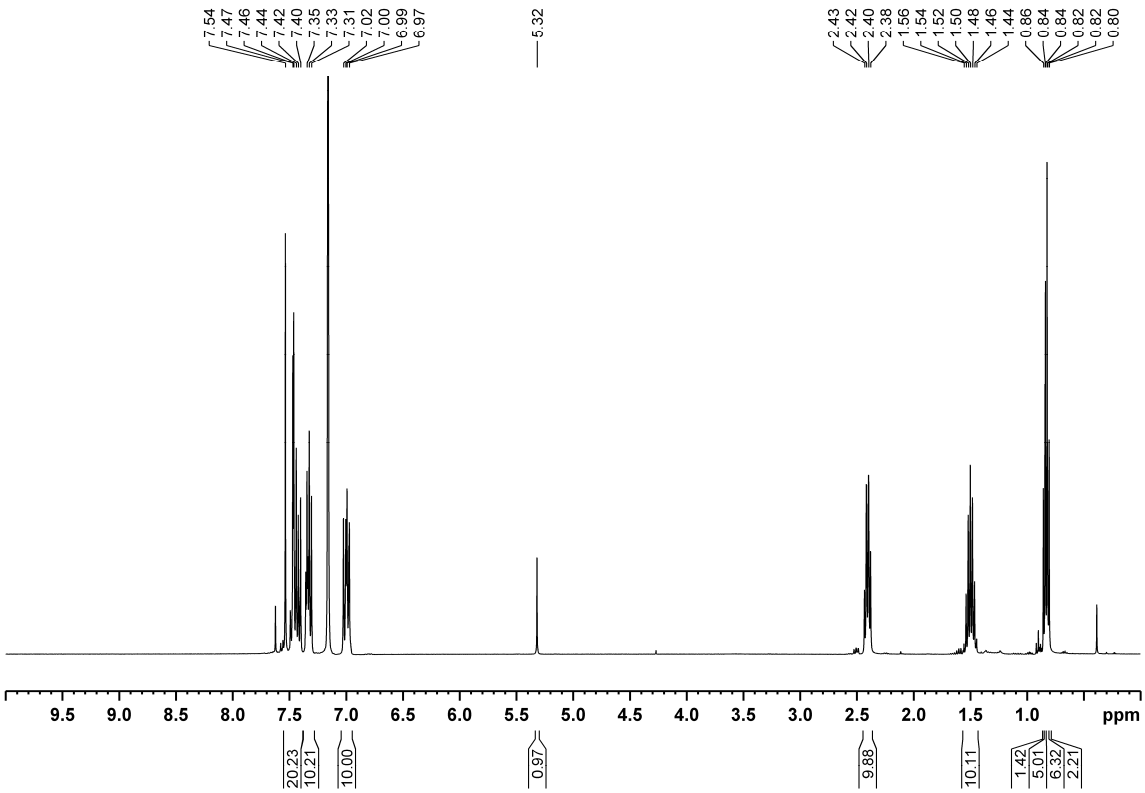

Figure S6.9. ^{1}H NMR spectrum of **1a** in C_6D_6.

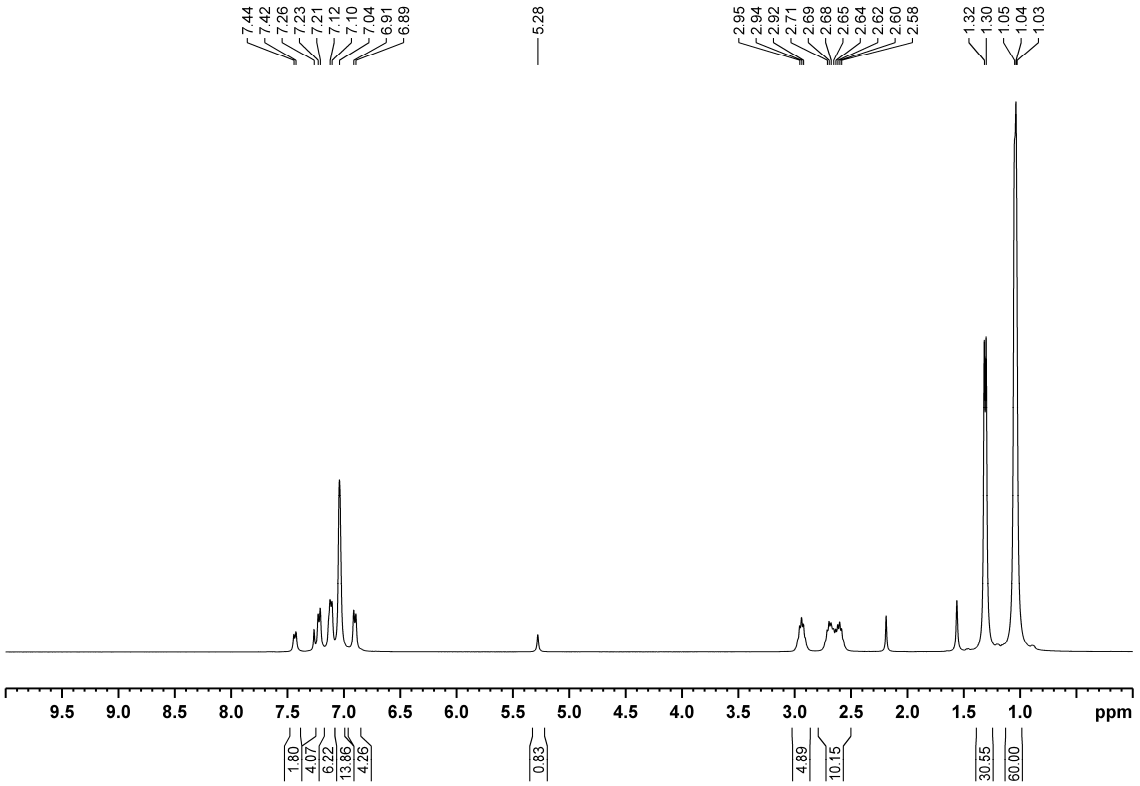

Figure S6.10. ^{1}H NMR spectrum of **1b** in $CDCl_3$.

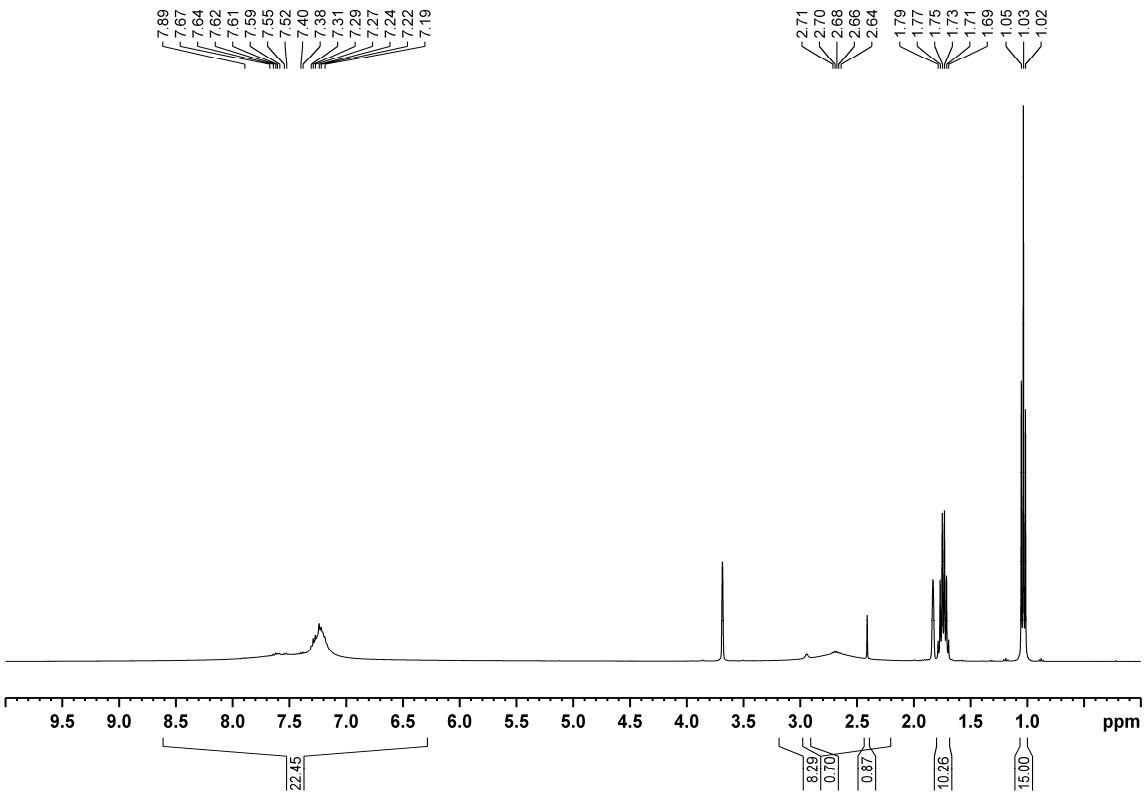

Figure S6.11. ^{1}H NMR spectrum of a mixture of **$2a_{Na}$** and **3a** in thf-d_8.

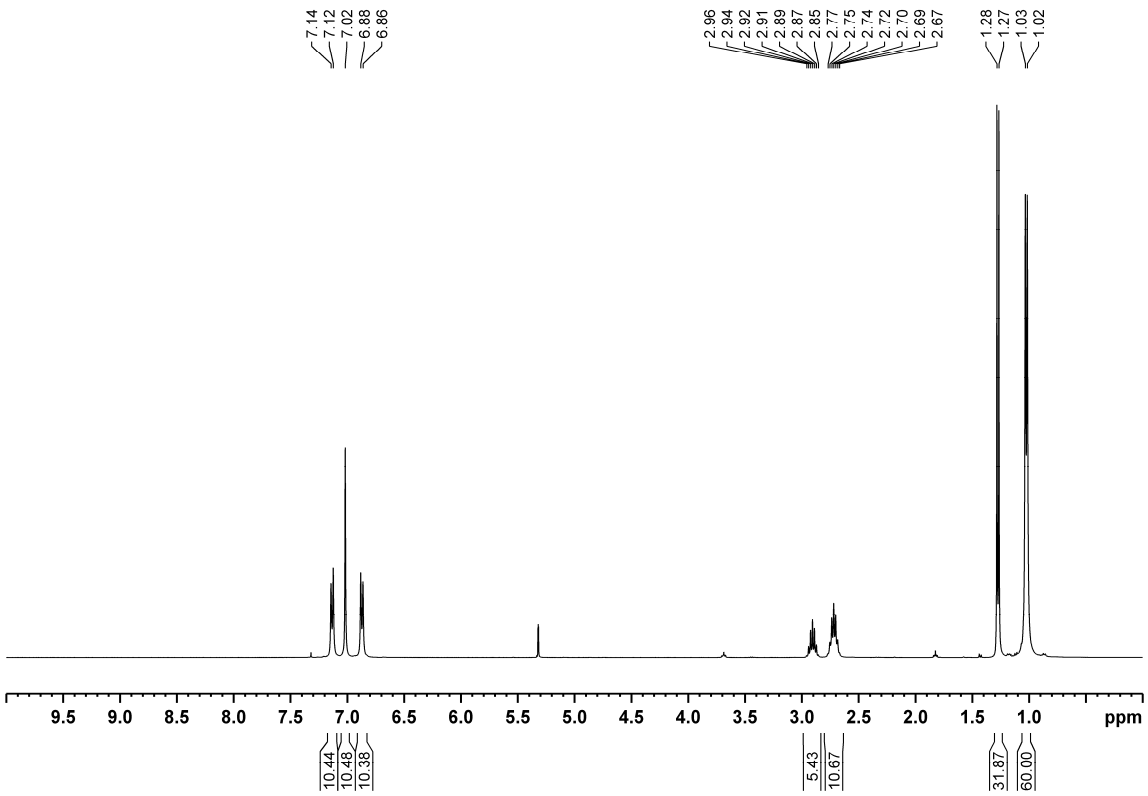

Figure S6.12. ^{1}H NMR spectrum of **2b$_{TI}$** in CD_2Cl_2.

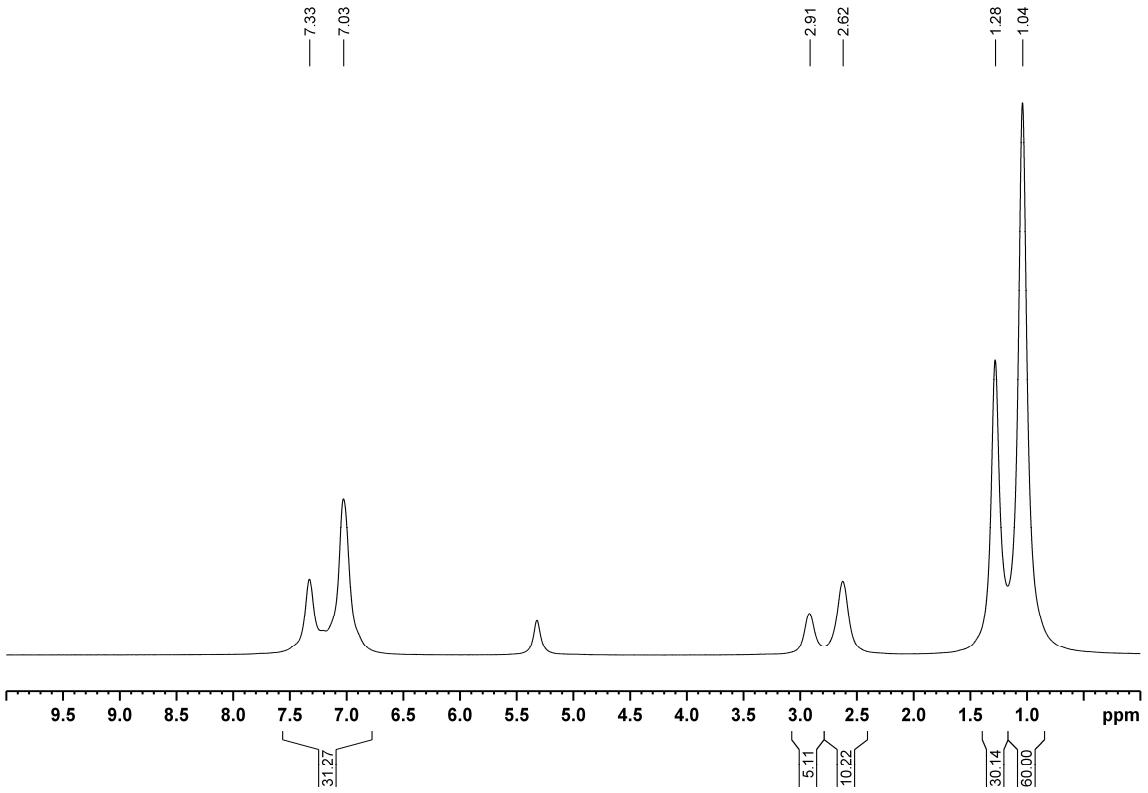

Figure S6.13. ^{1}H NMR spectrum of **4b** in CD_2Cl_2.

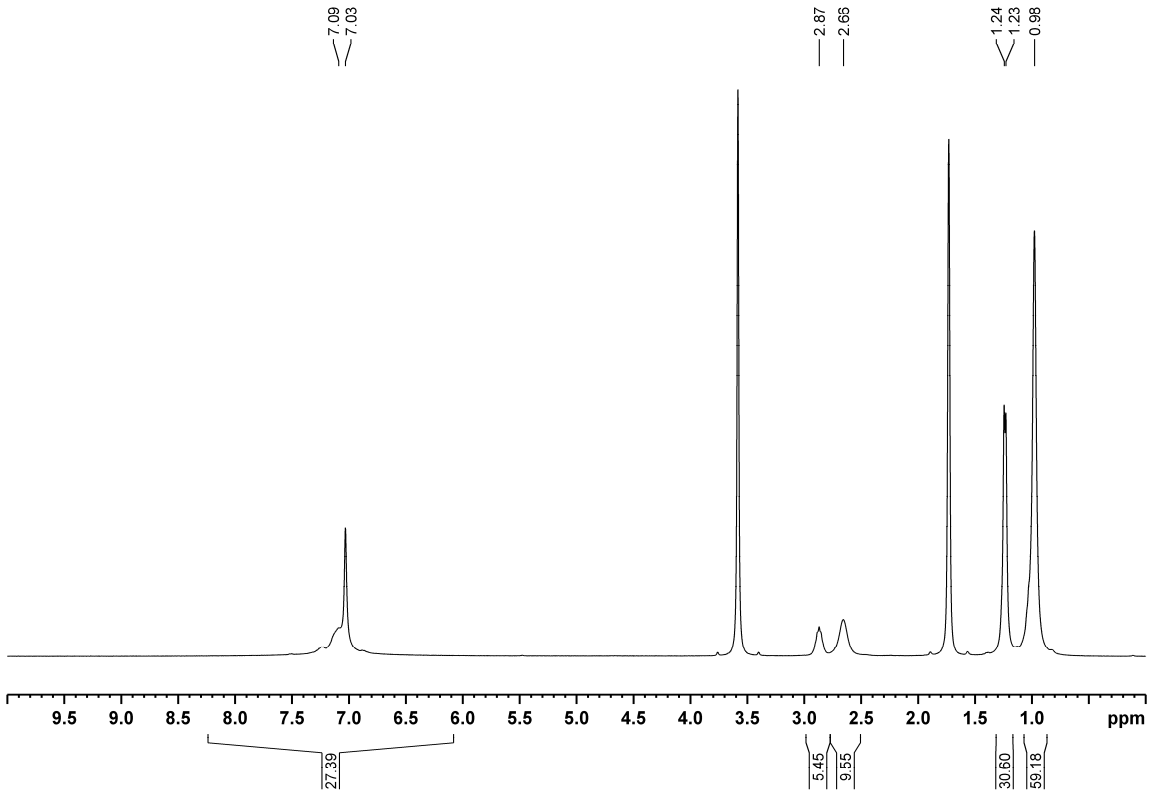

Figure S6.14. ^{1}H NMR spectrum of **5** in thf-d$_8$.

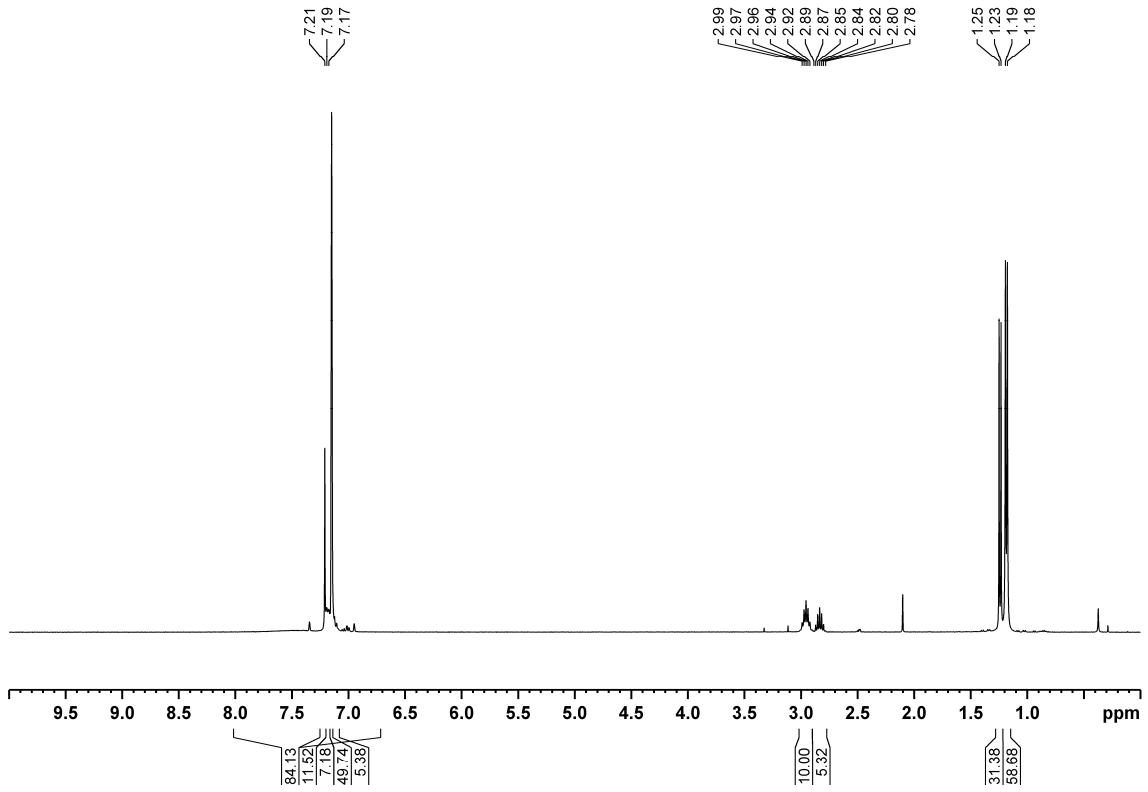

Figure S6.15. ^{1}H NMR spectrum of **6** in C$_6$D$_6$.

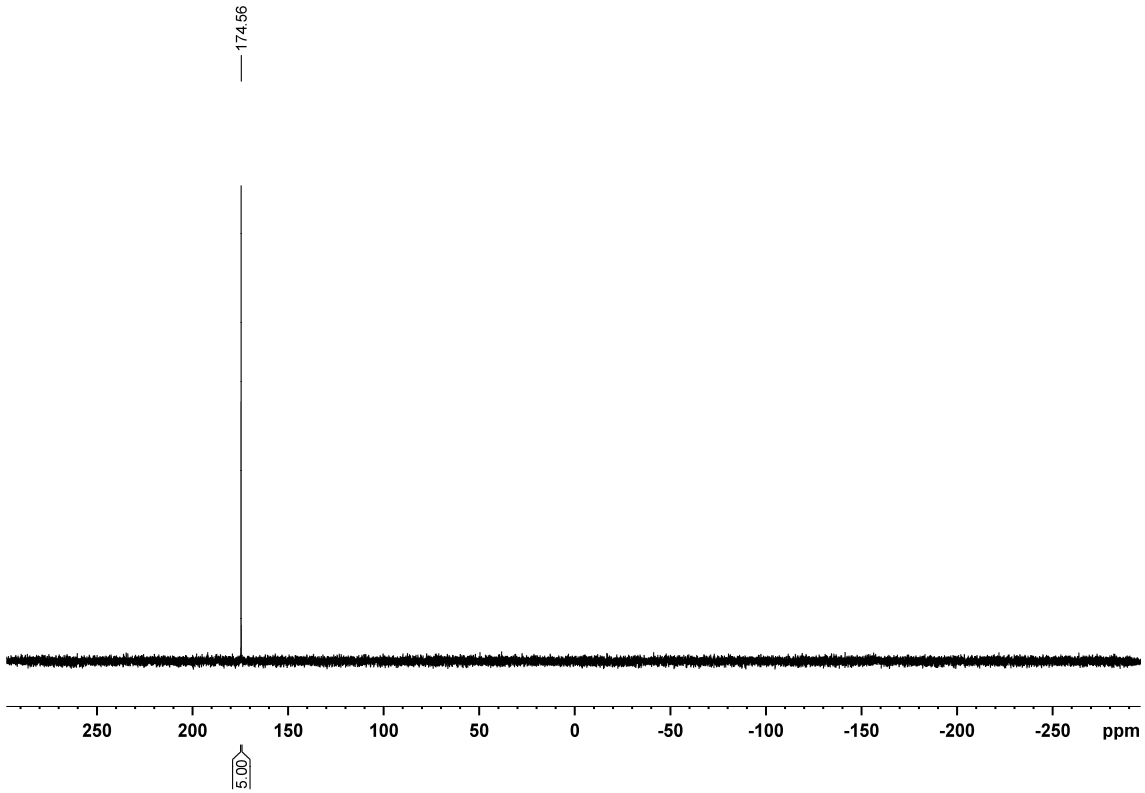

Figure S6.16. $^{31}P\{^1H\}$ NMR spectrum of **6** in C_6D_6.

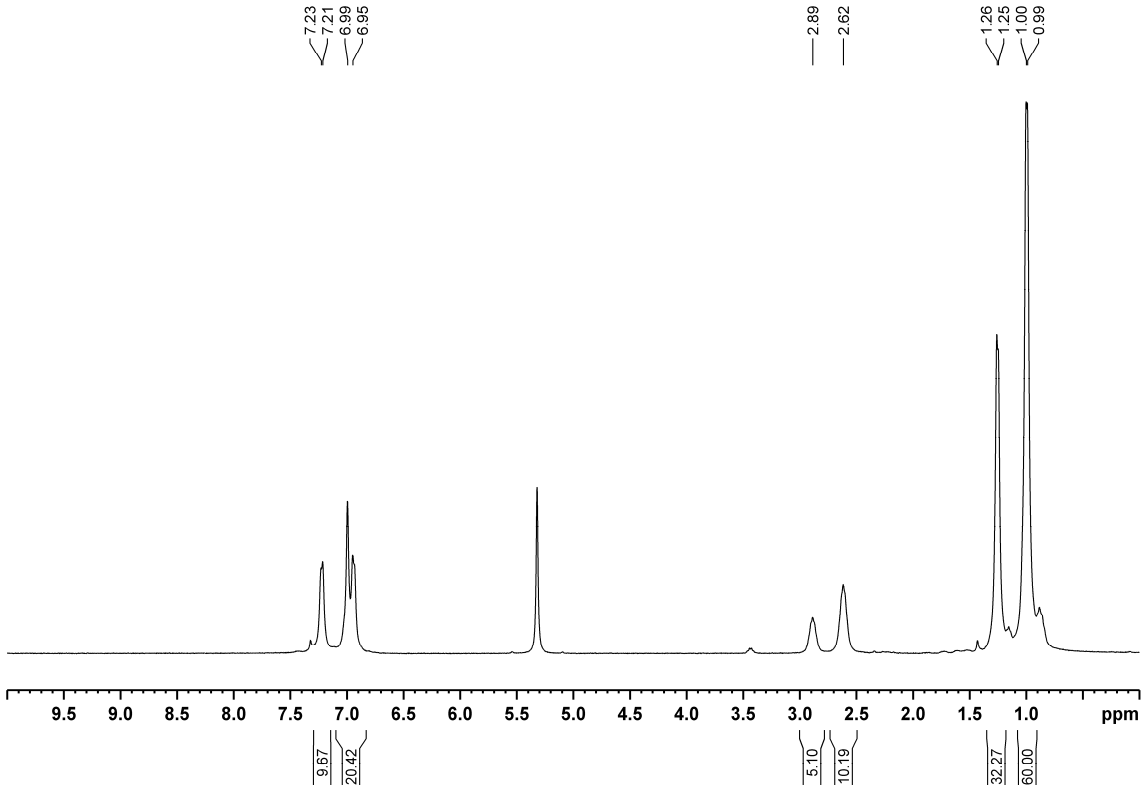

Figure S6.17. ^1H NMR spectrum of **7** in CD_2Cl_2.

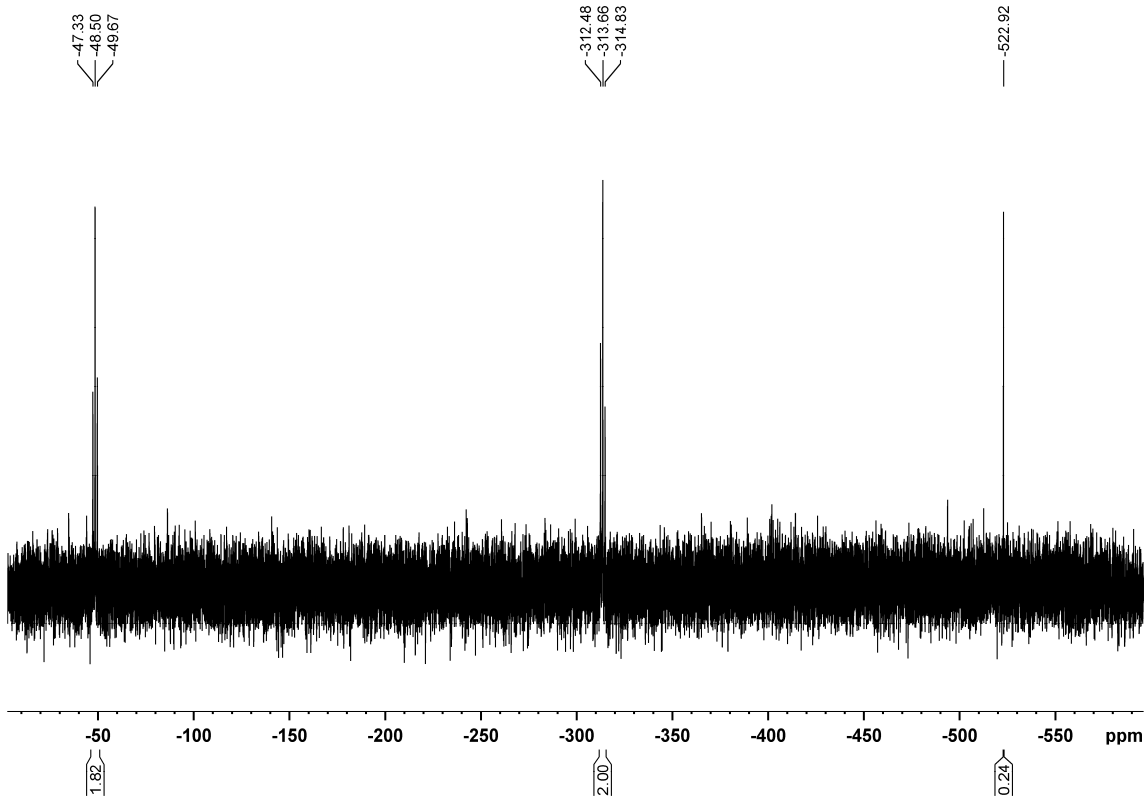

Figure S6.18. $^{31}P\{^1H\}$ NMR spectrum of **7** in CD_2Cl_2. The signal at −523 ppm can be assigned to P_4.

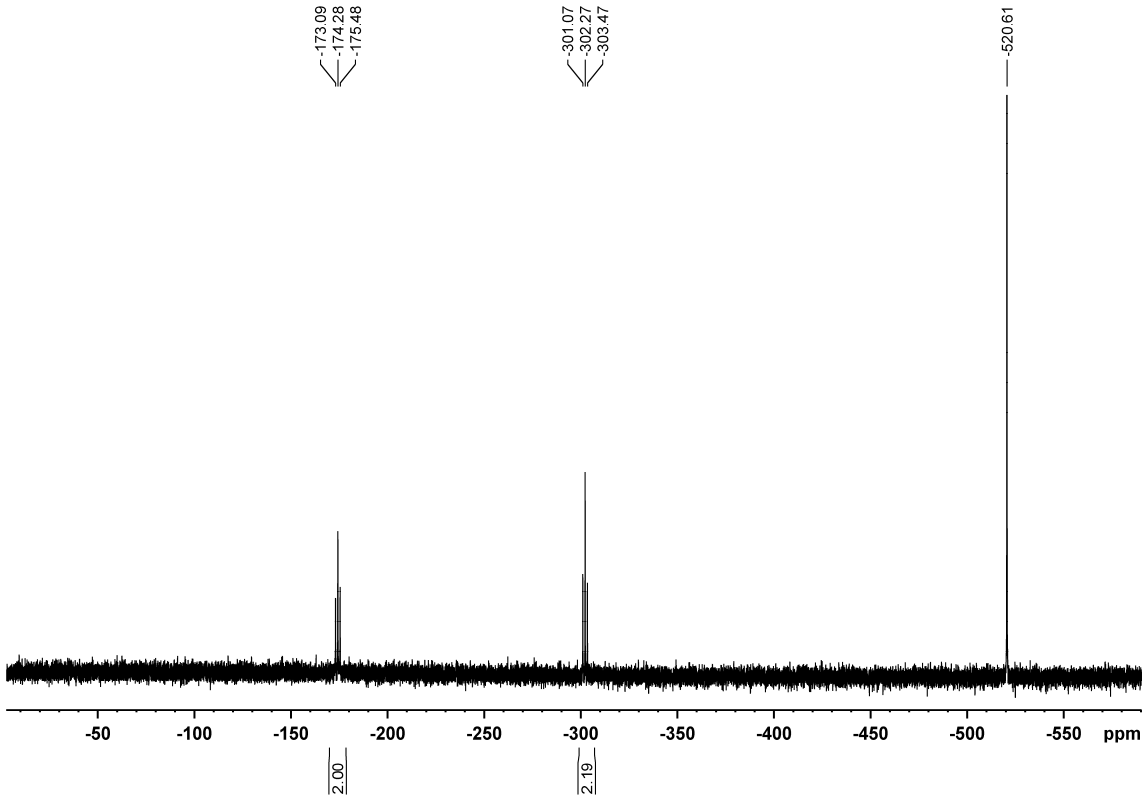

Figure S6.19. $^{31}P\{^1H\}$ NMR spectrum of **8a** in C_6D_6. The signal at −520 ppm can be assigned to P_4.

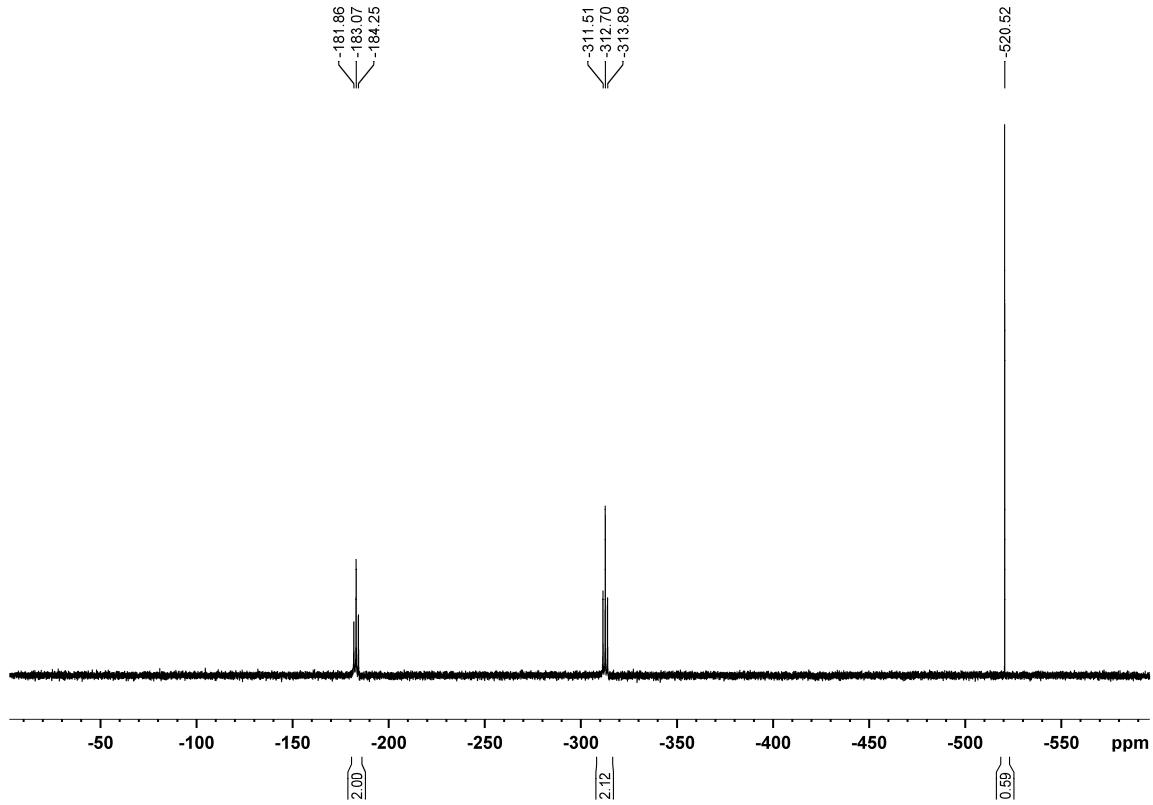

Figure S6.20. $^{31}P\{^1H\}$ NMR spectrum of **8b** in C_6D_6. The signal at −521 ppm can be assigned to P_4.

UV-Vis Spectroscopy

General remarks:

The measurements were carried out with a Varian Cary 50 spectrometer in a cuvette (d = 1 cm)

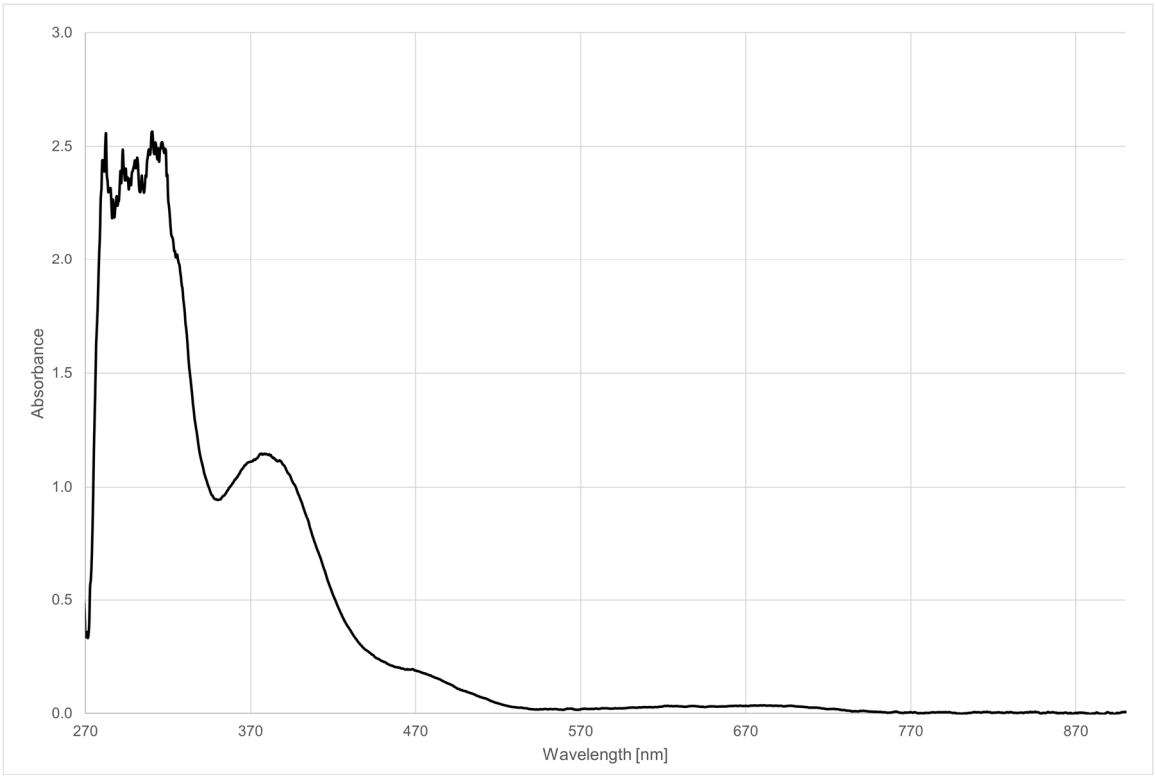

Figure S6.21. UV-Vis spectrum of a mixture of **1a** and **3a** in C_6H_6. Due to the sensitivity of **3a**, its concentration is very low.

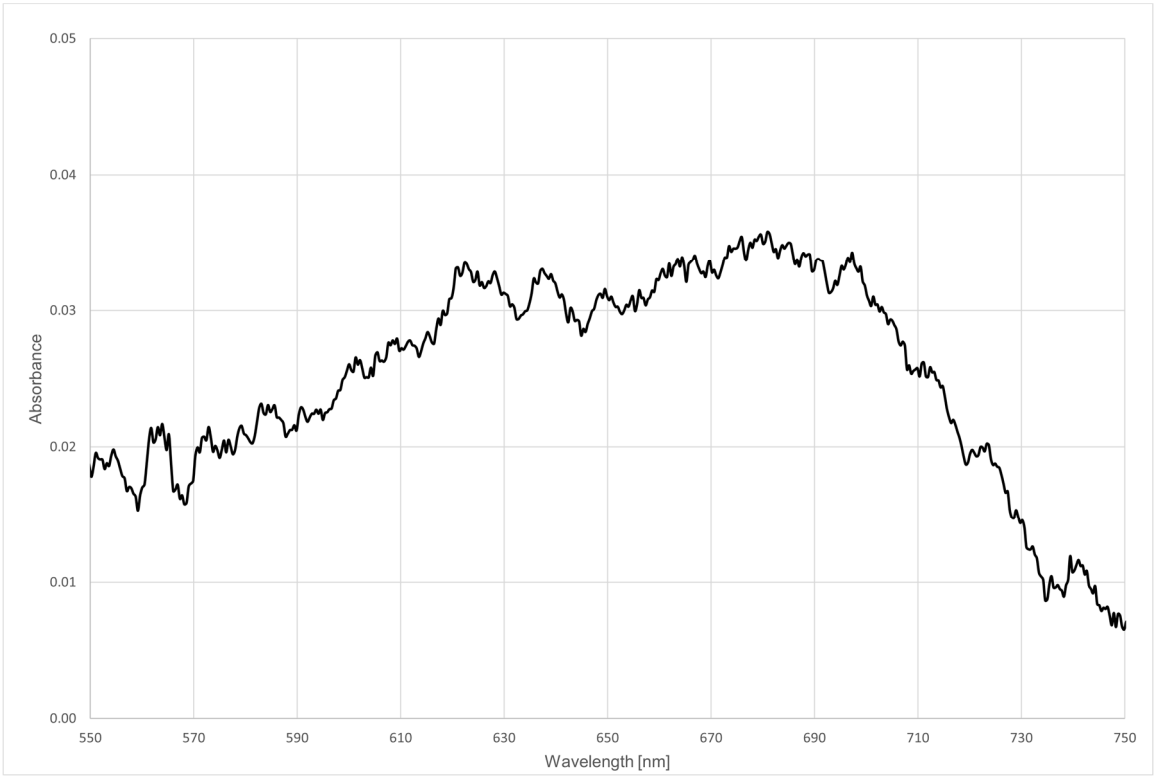

Figure S6.22. Magnification of the absorption maximum (λ_{max} = 681 nm) in the visible light range of **3a** in C_6H_6.

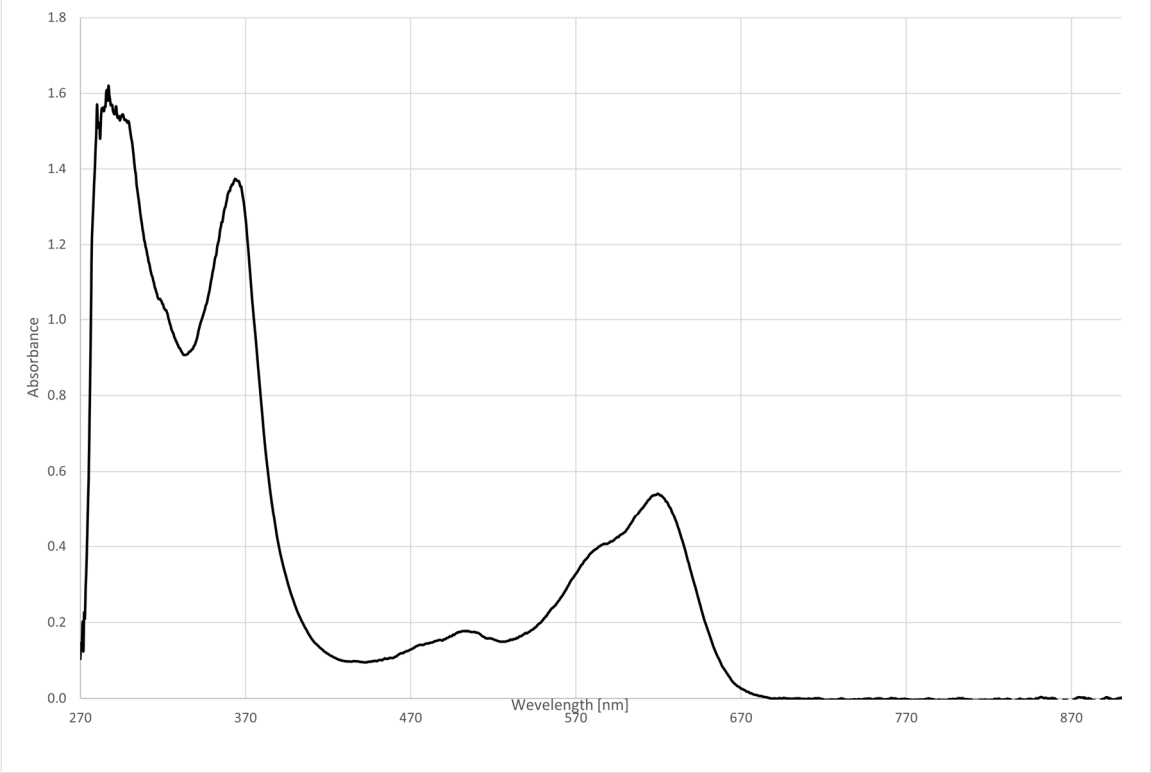

Figure S6.23. UV-Vis spectrum of **3b** in C_6H_6.

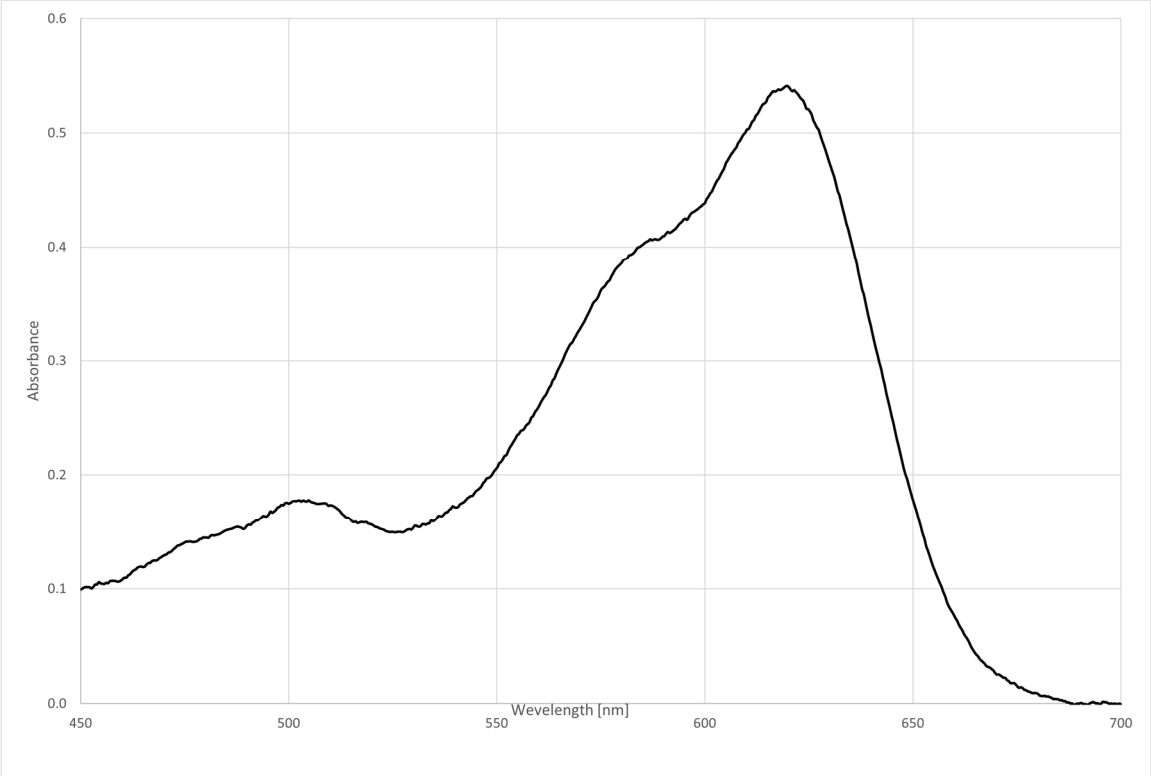

Figure S6.24. Magnification of the absorption maximum (λ_{max} = 620 nm) in the visible light range of **3b** in C_6H_6.

EPR Spectroscopy

General remarks:

The X-Band EPR measurements were carried out with a MiniScope MS400 device with a frequency of 9.44 GHz and a rectangular resonator TE102 of the company Magnettech GmbH.

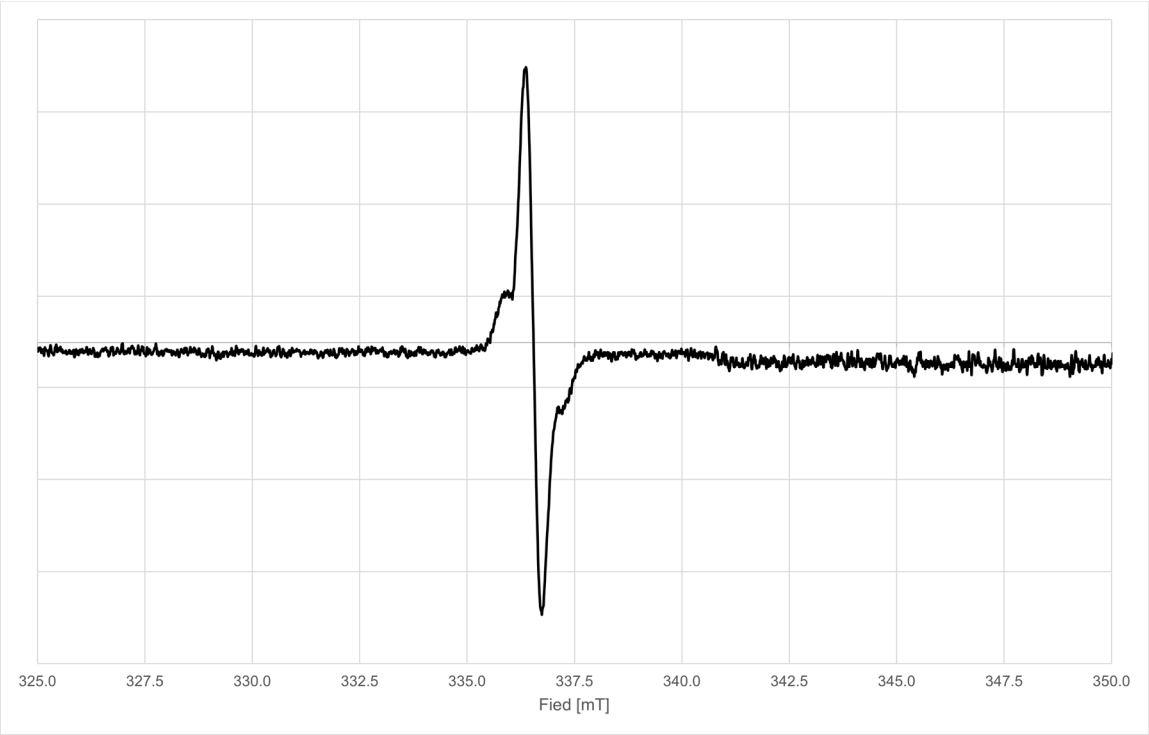

Figure S6.25. EPR spectrum of **3a** in toluene at 77 K.

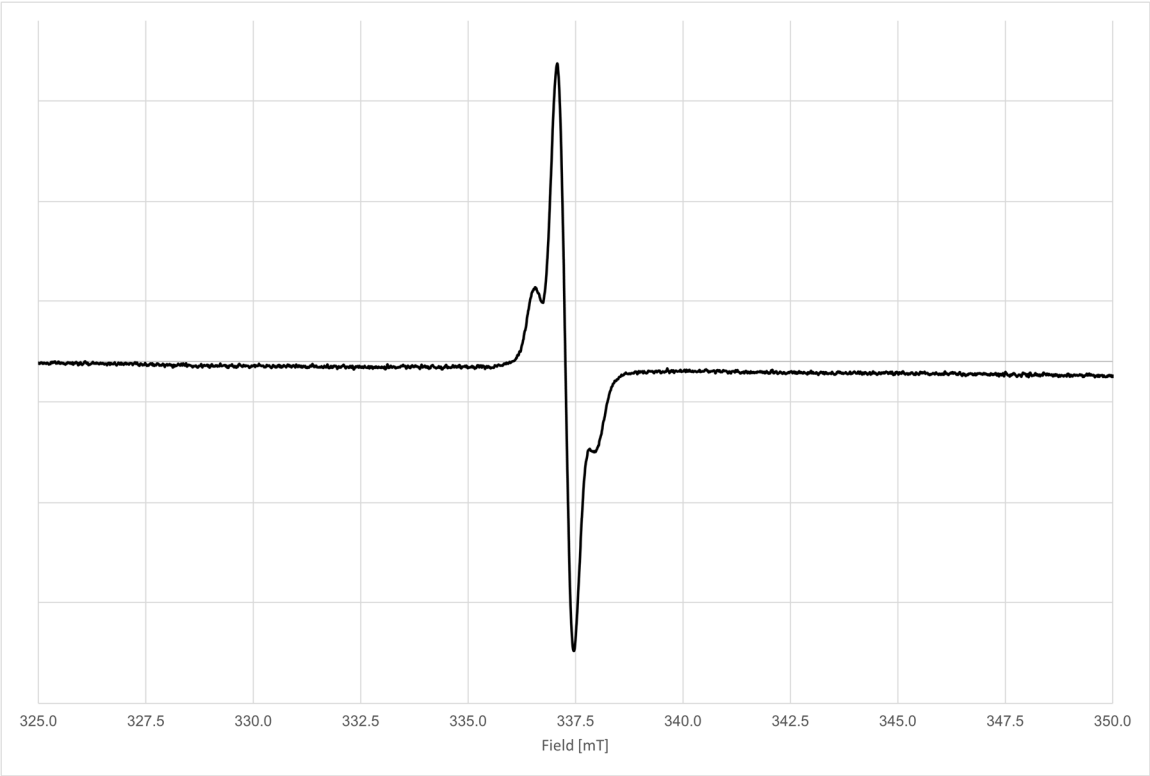

Figure S6.26. EPR spectrum of **3b** in toluene at 77 K.

Reference:

[1] G. Dyker, J. Heiermann, M. Miura, J.-I. Inoh, S. Pivsa-Art, T. Satoh, M. Nomura, *Chem. Eur. J.* **2000**, *6*, 3426.
[2] S. Heinl, S. Reisinger, C. Schwarzmaier, M. Bodensteiner, M. Scheer, *Angew. Chem. Int. Ed.* **2014**, *53*, 7639.
[3] A. Burkhardt, T. Pakendorf, B. Reime, J. Meyer, P. Fischer, N. Stübe, S. Panneerselvam, O. Lorbeer, K. Stachnik, M. Warmer et al., *Eur. Phys. J. Plus* **2016**, *131*.
[4] *Beamline P24, DESY PETRA III synchrotron,* can be found under https://photon-science.desy.de/facilities/petra_iii/beamlines/p24_chemical_crystallography/eh2/index_eng.html.
[5] *CrysAlisPro Software System*, Agilent Technologies UK Ltd, Yarnton, Oxford, **2014**.
[6] G. Sheldrick, *Acta Cryst. A* **2015**, *71*, 3.

7. Conclusion

This work gives an insight into the synthesis and reactivity of iron based polyphosphorus ligand complexes. The stabilization of these novel complexes is mainly provided by either bulky alkyl or super bulky pentaaryl substituted cyclopentadienyl ligands.

The first part of this thesis deals with the investigation of the reactivity and coordination behavior of the P_4 butterfly complex $[Cp'''Fe(CO)_2\}_2(\mu,\eta^{1:1}\text{-}P_4)]$ (**1**) towards late transition metal-based Lewis acids (Fe, Co, Ni, Zn, Ru, Rh, Ir). Depending on the nature of the Lewis acids the P_4 butterfly scaffold can either be preserved or a rearrangement can be induced. The exact reaction conditions are investigated in this thesis.

In the second part, the synthesis of complexes containing the super bulky Cp^{XXL} ligand are presented (Figure 7.1). The results are compared with the similar Cp^{Ar*} ligand which was synthesized during my master thesis. Both Cp^R ligands form remarkably stable radicals if not handled carefully. The formation of the Cp^R ligands is the initial step for the synthesis of a super bulky pentaphosphaferrocene derivative. The potential of $[Cp^{XXL}Fe(\eta^5\text{-}P_5)]$ (**2**) as a building block in supramolecular chemistry was demonstrated by the reaction with CuBr.

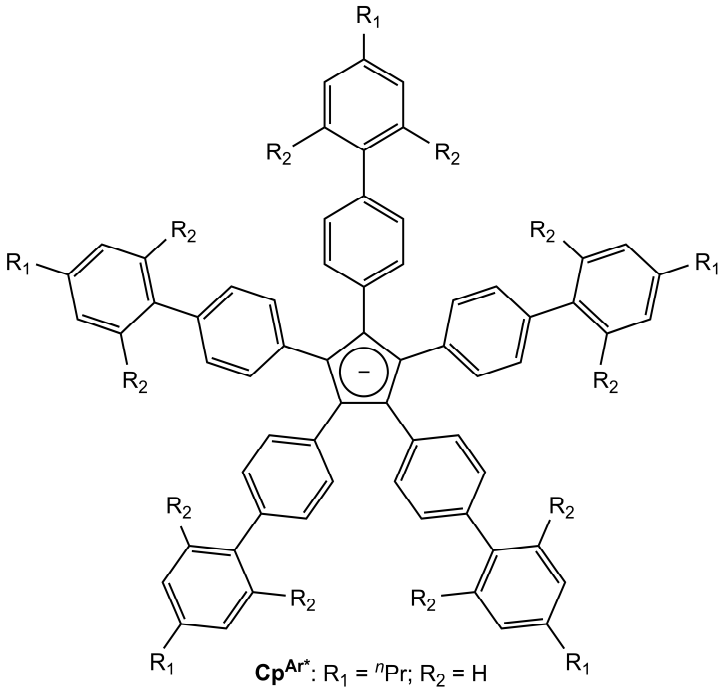

Figure 7.1. Structure of the super bulky Cp^{Ar*} and Cp^{XXL} ligands, shown as negatively charged 6π donors.

7.1. Reactivity of the P_4 Butterfly Complex towards Divalent Transition Metal Bromides

The P_4 butterfly complex $[Cp'''Fe(CO)_2\}_2(\mu,\eta^{1:1}\text{-}P_4)]$ (**1**) shows a versatile reactivity. On the one hand, it can react with the electrophiles PhC≡CPh or P≡C^{t}Bu to give triphospholyl and tetraphospholyl containing iron complexes under thermolytic conditions. However, **1** can also act as bidentate ligand towards Lewis acids. The obtained complexes are comparable to the analogue chelating complexes of dppm (dppm = $Ph_2PCH_2PPh_2$). Therefore, **1** can be described as an inorganic derivative of dppm. Until now, however, the coordination behavior of **1** to act as bidentate ligand could only be shown in reactions with coinage metal compounds as well as with $[FeBr_2\cdot(dme)]$ (dme = dimethoxyethane). In order to expand the scope of Lewis acids, **1** was reacted with the divalent metal bromide salts of Co, Ni, and Zn (Scheme 7.1).

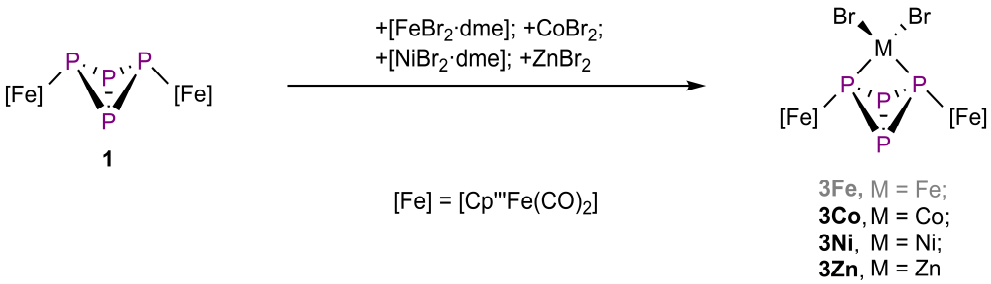

Scheme 7.1. Coordination compounds of **1**, obtained by the reactions with $[FeBr_2\cdot(dme)]$, $CoBr_2$, $[NiBr_2\cdot(dme)]$, and $ZnBr_2$, respectively. Due to the importance for this work, complex **3Fe** is added in this scheme although it was synthesized by Christoph Schwarzmaier.[1]

The reaction of **1** with $CoBr_2$, $[NiBr_2\cdot(dme)]$, or $ZnBr_2$ yield in the coordination compounds $[Cp'''Fe(CO)_2\}_2(\mu_3,\eta^{2:1:1}\text{-}P_4)(MBr_2)]$ (**3Co**: M = Co; **3Ni**: M = Ni, **3Zn**: M = Zn). In all these complexes the P_4 butterfly motif is unchanged and the central Lewis acids are coordinated via the two "wing-tip" phosphorus atoms. The same behavior was observed in $[Cp'''Fe(CO)_2\}_2(\mu_3,\eta^{2:1:1}\text{-}P_4)(FeBr_2)]$ (**3Fe**) which was synthesized by Christoph Schwarzmaier.[1] The NMR spectra of **3Co** and **3Ni** indicate that both complexes are paramagnetic while **3Zn** is diamagnetic. Furthermore, show the $^{31}P\{^1H\}$ NMR spectra of the reaction solution of **3Ni** and **3Zn** additional signals of diamagnetic side products that are formed in small amounts. According to simulations of the NMR spectra, it could be deduced that the two by-products no longer exhibit P_4 butterfly motifs. Despite several attempts, the exact structure of the side products could not be clarified yet.

According to these results, the description of **1** as an inorganic derivative of dppm is correct since the obtained complexes exhibit very small bite angles. However, the formation of side products that bear no longer a P_4 butterfly motif, indicates that this description is only valid under certain conditions. Compared to the ligand dppm, **1** seems to be electronically more flexible.

7.2. Coordination Behavior of the P_4 Butterfly Complex – the Conditions of Rearrangement

In her PhD thesis, Miriam Eberl was able to show that the butterfly complex **1** does not always behave as a spectator ligand, but also tends to rearrange itself.[2] This was demonstrated in the reaction of **1** with $[Co_2(CO)_8]$ and CuI, respectively. Similar observations were made in this dissertation on the reactivity of **1** towards labile ligated Lewis acids (Scheme 7.2).

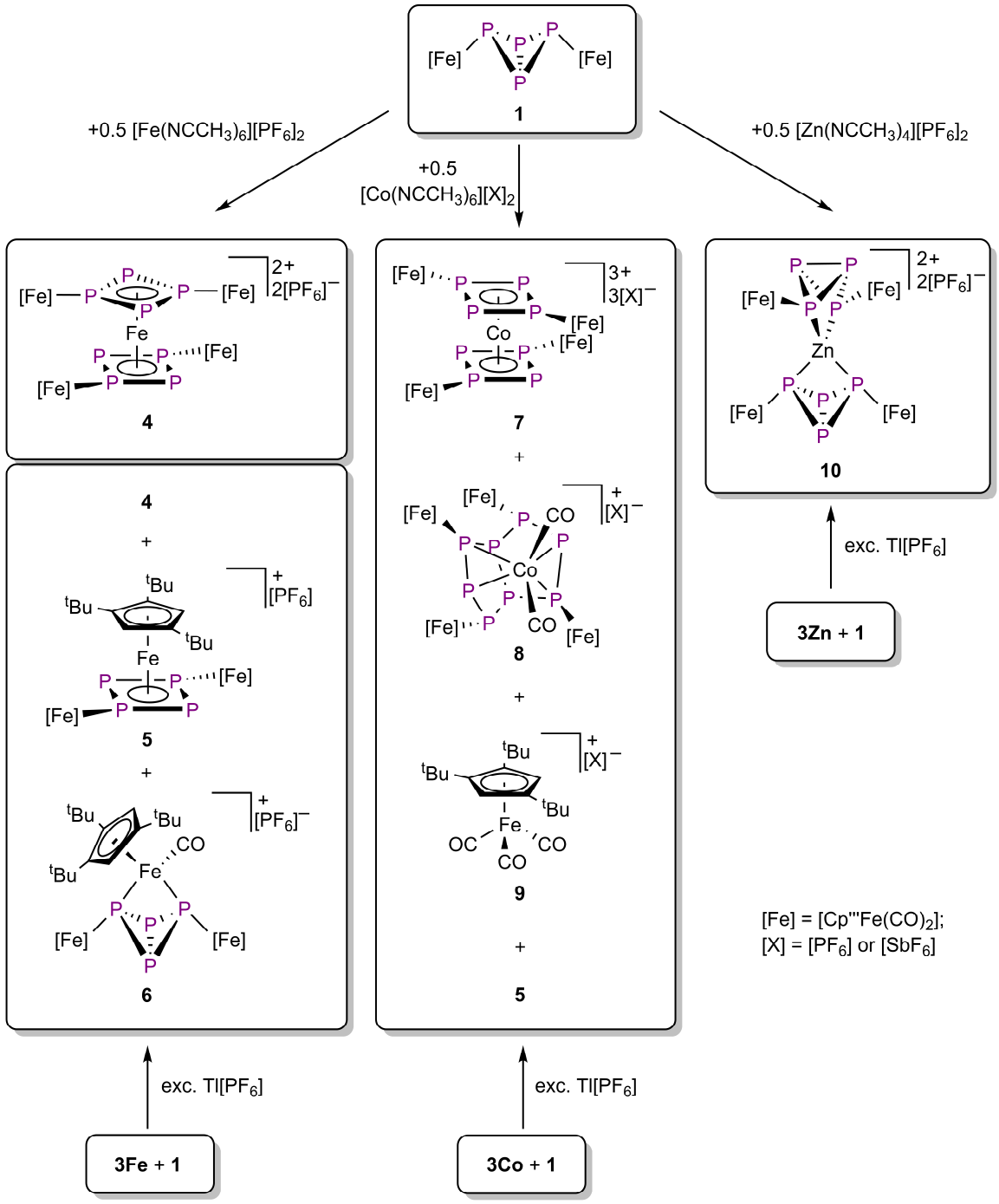

Scheme 7.2. Summary of the coordination compounds obtained from **1** with labile ligate Lewis acids.

Surprisingly, the reaction of **1** with $[Fe(NCCH_3)_6][PF_6]_2$ leads to the quantitative formation of $[\{(Cp'''Fe(CO)_2)_2(\mu_3,\eta^{4:1:1}\text{-}P_4)\}_2Fe][PF_6]_2$ (**4**), an unprecedented octaphosphorus iron sandwich complex. Obviously, an isomerization of the P_4 butterfly scaffold (4 σ-electron donor) to a *cyclo*-P_4R_2 (R = Cp'''Fe(CO)$_2$; 6 π-electron donor) unit has taken place during coordination (Scheme 7.3). The P–P bond lengths in the *cyclo*-P_4 units are in the range between a P–P single and a P=P double bond which indicates an aromatic character of the *cyclo*-P_4 units. By Mößbauer spectroscopy the central iron atom of **4** could be determined as iron(II) which shows that no redox processes are involved in the formation of **4**.

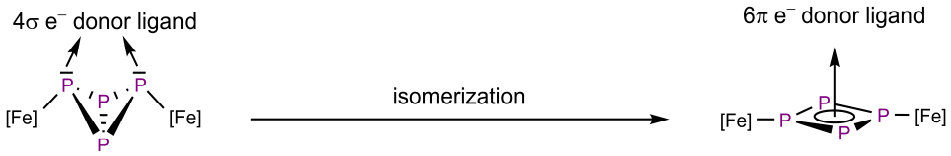

Scheme 7.3. Schematic representation of the isomerization of **1**.

Furthermore, it could be shown that **3Fe** can serve as precursor for the sandwich complex **4**. Therefore, **3Fe** was treated with one equivalent of **1** and an excess of $Tl[PF_6]$ in an ultrasonic bath which yields in **4**. In this process, however, a partial decomposition of **1** is induced and leads, inter alia, to the formation of the side products $[\{Cp'''Fe(CO)_2\}_2(\mu_3,\eta^{4:1:1}\text{-}P_4)(Cp'''Fe)][PF_6]$ (**5**) and $[\{Cp'''Fe(CO)_2\}_2(\mu_3,\eta^{2:1:1}\text{-}P_4)\{Cp'''Fe(CO)\}][PF_6]$ (**6**). While **5** bears also an aromatic *cyclo*-P_4R_2 ligand, the scaffold in **6** is preserved. The formation of **5** could also be obtained in a selective and quantitative approach (vide infra).

The same isomerization of the P_4 unit is observed in the reaction of **1** with $[Co(NCCH_3)_6][SbF_6]_2$ which leads to the formation of the sandwich complex $[\{(Cp'''Fe(CO)_2)_2(\mu_3,\eta^{4:1:1}\text{-}P_4)\}_2Co][SbF_6]_3$ (**7**). However, the main difference in the formation of the octaphosphorus sandwich complexes is that redox processes are involved in the formation of **7** since Co^{II} is oxidized to Co^{III}. Unfortunately, the exact oxidizing agent of this reaction could not be determined without any doubts. However, the redox processes induce a non-selective decomposition which results in the formation of the by-products $[\{Cp'''Fe(CO)_2\}_4(\mu_5,\eta^{4:1:1:1:1}\text{-}P_8)\{Co(CO)_2\}][SbF_6]$ (**8**), $[Cp'''Fe(CO)_3][SbF_6]$ (**9**), and **5**, among others. Complex **8** features a rare octaphosphabicyclo[3.3.0]octan unit which is most likely formed by a dimerization of **1** in the presence of $[Co(CO)_2]$. The same reaction outcome was observed when **3Co** was used as a precursor (Scheme 7.2).

The treatment of **1** with $[Ni(NCCH_3)_6][SbF_6]_2$ leads also to a non-selective decomposition of **1**, which might also be induced by redox processes. Unfortunately, only the formation of the nickel-free complexes **5** and **9** could be confirmed.

Reacting **1** with $[Zn(NCCH_3)_4][PF_6]_2$ yields quantitatively the spiro-complex $[\{(Cp'''Fe(CO)_2)_2(\mu_3,\eta^{2:1:1}\text{-}P_4)\}_2Zn][PF_6]_2$ (**10**). In contrast to the reactions with $[M(NCCH_3)_6]^{2+}$ (M = Fe, Co), the P_4 butterfly scaffolds are preserved when **10** is formed.

This finding can be explained by the d^{10} configuration of the Zn^{II} atom which enables the formation of a stable 18 valence electron complex by preservation of the P_4 butterfly scaffold (4 σ-electron donor). The synthesis of **10** starting from **3Zn** is quantitative and selective, as no decomposition can be observed.

The oxidation from Co^{II} to Co^{III} associated with the formation of **7** indicates that the isomerization occurs preferentially in the presence of d^6 metals. In order to get more insight into the isomerization of **1**, it was reacted with Lewis acids of d^6 metals. Due to the poor availability of metal complexes in which a d^6 metal is stabilized exclusively by labile ligands, the corresponding half-sandwich complexes were used (Scheme 7.4).

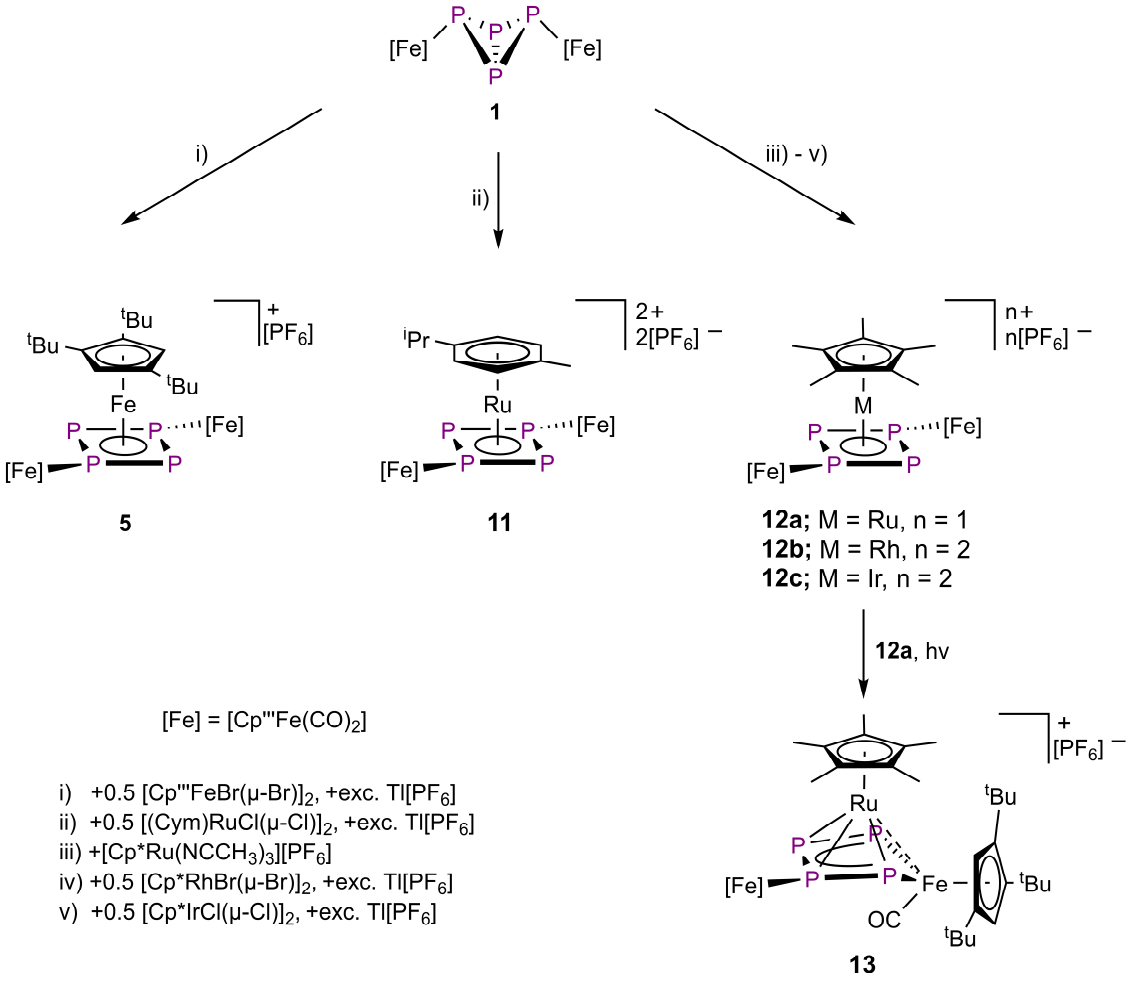

Scheme 7.4. Summary of the coordination compounds obtained from **1** with half sandwich complexes.

A suitable method to generate solvent stabilized half-sandwich complexes in situ is the abstraction of halides with an excess of $Tl[PF_6]$. The formation of these half-sandwich complexes in the presence of **1** gives access to complexes **5**, $[\{Cp'''Fe(CO)_2\}_2(\mu_3,\eta^{4:1:1}\text{-}P_4)\{(Cym)Ru\}][PF_6]_2$ (**11**, Cym = *para*-cymene) and $[\{Cp'''Fe(CO)_2\}_2(\mu_3,\eta^{4:1:1}\text{-}P_4)(Cp^*M)][PF_6]_2$ (**12b**, M = Rh; **12c**, M = Ir) in good yields, while $[\{Cp'''Fe(CO)_2\}_2(\mu_3,\eta^{4:1:1}\text{-}P_4)(Cp^*Ru)][PF_6]$ (**12a**) could be synthesized by reacting **1** with $[Cp^*Ru(NCCH_3)_6][PF_6]$. In all cases, the coordination of a half-sandwich complex of a d^6 metal results in an

isomerization of the P_4 butterfly scaffold to an aromatic *cyclo*-P_4 unit. Surprisingly, **12a** is the only complex from this group of complexes (**5**, **11**, and **12**) that rearranges itself when exposed to sunlight. The activation by sunlight induces an elimination of a carbonyl group that leads to the formation of [{Cp'''Fe(CO)$_2$}{Cp'''Fe(CO)}(μ_3,$\eta^{4:2:1}$-P_4)(Cp*Ru)][PF_6] (**13**). Complex **13** can be described as the twofold activated P_4 butterfly complex **1** and features a butadiene-like P_4 chain that chelates the [Cp'''Fe(CO)] fragment to form a five membered metallacycle. The [Cp*Ru] fragment is not only coordinated by the *catena*-P_4 unit, but additionally stabilized by a multicenter bond between Ru, Fe and the two P atoms, which was verified by DFT calculations. Furthermore, shows **13** dynamic behavior in solution which leads to two sets of signals in the $^{31}P\{^1H\}$ NMR spectrum. The fact that only **12a** is further activated by sunlight, is investigated by comparing the activation of **12a** with the hypothetical activation of **11** based on DFT calculations. It could be shown that the hypothetical activation of **11** is energetically disfavored compared to the activation of **12a** which is most likely due to different charge distributions, resulting from the different ligands attached to the Ru centers (neutral Cym versus anionic Cp*).

As a conclusion, it could be shown that the P_4 butterfly scaffold of complex **1** is electronically very flexible when it comes to the coordination of Lewis acids. On the one hand, **1** can act as a 4 σ-electron donating bidentate ligand to form complexes, comparable to dppm (Chapter 7.2). On the other hand, the P_4 butterfly scaffold of complex **1** can be isomerized to a 6 π-electron donating aromatic *cyclo*-P_4R_2 unit, giving excess to unique sandwich complexes. However, to induce the isomerization, the Lewis acids must meet certain criteria. 1) According to this work, the isomerization only occurs in the presence of d^6 metal centers, which is highlighted by the oxidation from Co^{II} to Co^{III} to form the octaphosphorus cobalt sandwich complex **7**. 2) The isomerization depends strongly on the type of ligand bound to the Lewis acid. This is particularly illustrated by the different reaction outcomes obtained by the coordination of different Fe^{II} containing species (**3Fe** versus **4** or **5**). However, it was not possible to determine the decisive factors of the ligands for isomerization. But the isomerization is most likely strongly connected to ligand field splitting as well as the overall Lewis acidity of the coordinated fragment, as the Br ligands induce a low ligand field splitting and $FeBr_2$ is a weak Lewis acid (results in **3Fe**) while the Cp''' ligand induces a high ligand field splitting and the [Cp'''Fe]$^+$ fragment is a strong Lewis acid (results in **5**). Additionally, if the right conditions are met, the exposure to sunlight can even induce a second activation of the P_4 butterfly unit. However, the general scope of reactants as well as the reaction conditions is rather limited since **1** tends to decompose under harsh reaction conditions.

7.3. Synthesis of Super Bulky Cp^R Ligands

In the last years, in organometallic chemistry a trend toward even bulkier Cp ligands has become apparent. In our group the bulky Cp^{BIG} and Cp^{PEt} ligands are already well established. Due to their sterical demand, several novel P_n ligand complexes could be stabilized. Therefore, the question arose whether an even larger Cp ligand could be applied in organometallic chemistry. For this purpose, the Cp^{Ar*} and Cp^{XXL} ligand have been synthesized (Scheme 7.5).

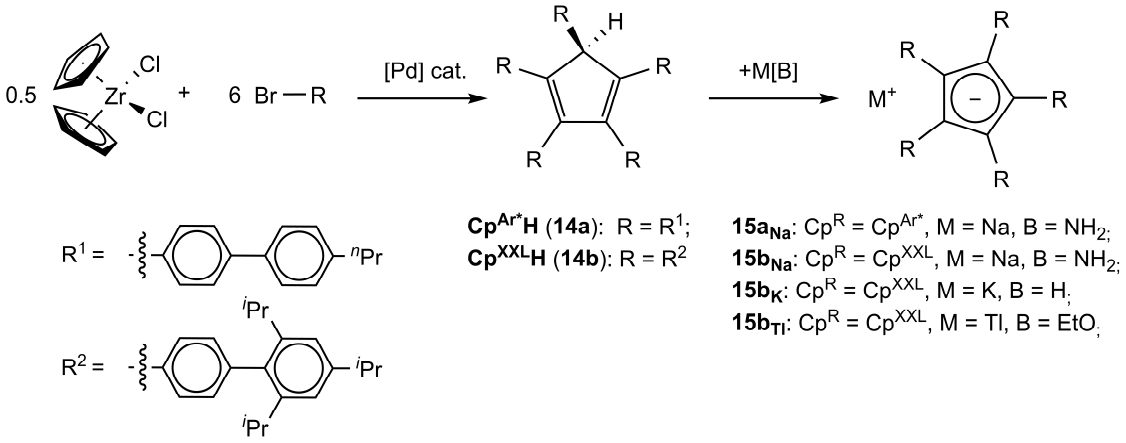

Scheme 7.5. Synthesis of the super bulky $Cp^{Ar*}H$ (**14a**) and $Cp^{XXL}H$ (**14b**) derivatives. The following metalation provides the starting material for the synthesis of metal complexes as well as the corresponding radicals.

The cyclopentadienyl derivatives $Cp^{Ar*}H$ (**14a**) and $Cp^{XXL}H$ (**14b**) have been synthesized via a palladium catalyzed one-pot reaction. In the reaction with the metal bases $NaNH_2$, KH, or TlOEt the metalated Cp ligands $NaCp^{Ar*}$ (**15a$_{Na}$**), $NaCp^{XXL}$ (**15b$_{Na}$**), KCp^{XXL} (**15b$_K$**) and $TlCp^{XXL}$ (**15b$_{Tl}$**) could be obtained, respectively. Although the Cp^{Ar*} and Cp^{XXL} ligands are comparable in their sterical bulk, they differ dramatically in their solubility as well as in their ability to donate electrons. Due to the high solubility of the Cp^{XXL} derivative, only **15b$_{Tl}$** could be isolated in an analytically pure form. A comparison of the structures of **15a** and **15b** shows that the Cp^{Ar*} ligand is a very poor electron donating ligand since the ions are completely separated in the solid state structure of **15a$_{Na}$**. The reason for this behavior is that the electrons in the Cp^{Ar*} ligand are delocalized over the C_5 ring and ten phenyl groups. In the case of the Cp^{XXL} ligand, the introduction of several ^{i}Pr substituents leads to a sterical induced rotation of the outer phenyl plane. Therefore, the area of delocalization is reduced which results in a higher electron density in the central C_5 ring and better electron donating properties.

7.4. Formation of Remarkably Stable Cp^R Radicals and Their Reactivity Towards P_4

The interest in Cp radicals started almost a century ago. Since then, the structure of Cp based radicals is investigated intensively. Until now, only a handful of stable Cp radicals

have been reported. In general, radicals are of particular interest as they are used for small molecule activation. Therefore, the formation of the Cp radicals, as well as their reactivity towards P_4 is investigated (Scheme 7.6).

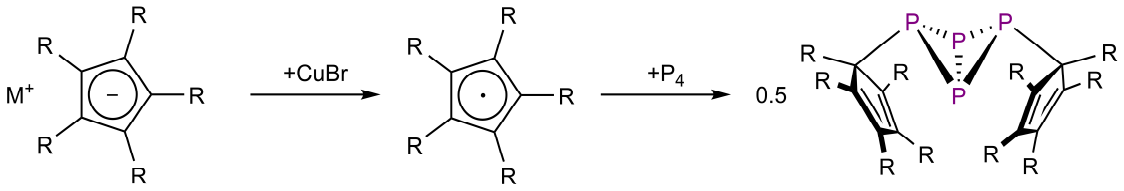

15a$_{Na}$: $Cp^R = Cp^{Ar*}$, M = Na; **15b$_{Tl}$**: $Cp^R = Cp^{XXL}$, M = Tl

16a: $Cp^R = Cp^{Ar*}$; **16b**: $Cp^R = Cp^{XXL}$

17a: $Cp^R = Cp^{Ar*}$; **17b**: $Cp^R = Cp^{XXL}$

Scheme 7.6. Formation of the Cp^{Ar*} radical (**16a**) and Cp^{XXL} radical (**16b**) and their reactivity towards P_4.

If not handled carefully, both cyclopentadienyl anions are easily oxidized to the Cp^{Ar*} radical (**16a**) or Cp^{XXL} radical (**16b**), respectively. Due to the extraordinary delocalization of the electron density, the radicals are remarkably stable. Therefore, **15a$_{Na}$** and **15b$_{Tl}$** were oxidized with CuBr which allowed the crystallization and characterization of **16a** and **16b** by single crystal X-ray diffraction.

Furthermore, the radicals are reacted with white phosphorus which leads via a P–P cleavage to the formation of the P_4 butterfly compounds $Cp^{Ar*}{}_2P_4$ (**17a**) and $Cp^{XXL}{}_2P_4$ (**17b**). Due to the increased sterical bulk of the additional ^{i}Pr substituents at the Cp^{XXL} units, **17b** exhibits only low stability in solution as it decomposes into **16b** and P_4.

7.5. Synthesis of a Super Bulky Pentaphosphaferrocene Derivative and Its Application as Building Block in Supramolecular Chemistry

Our group could show that pentaphosphaferrocenes are suitable building blocks in supramolecular chemistry. In self-assembly reactions with coinage metal salts, spherical aggregates with fullerene-like topology could be obtained. By using the larger building block $[Cp^{BIG}Fe(\eta^5\text{-}P_5)]$ instead of $[Cp^*Fe(\eta^5\text{-}P_5)]$, the size of the aggregates could be increased. Therefore, it was considered that by using an even larger Cp ligand, the size of the aggregates could be further increased. The different reaction steps for the synthesis of the super bulky pentaphosphaferrocene derivative $[Cp^{XXL}Fe(\eta^5\text{-}P_5)]$ (**2**) are summarized in (Scheme 7.7).

The first attempts to synthesize the intermediate complexes $[Cp^RFe(CO)_2Br]$ (**18a**, $Cp^R = Cp^{Ar*}$; **18b**, $Cp^R = Cp^{XXL}$) turned out to be more difficult than expected. Although the applied reaction pathway allowed the formation of analog complexes with sterically demanding Cp^R ligands like Cp^{BIG} or Cp^{PEt}, the desired complex could not be obtained starting from **15a$_{Na}$**, **15b$_{Na}$**, and **15b$_K$**, respectively. The difficulties in the synthesis of complexes with the

Cp^{Ar*} ligand are most likely caused by the poor electron donating properties due to the extraordinary delocalization of the electron density. Unfortunately, the synthesis of the Cp^{Ar*} containing complex **18a** could not be achieved, even though an alternative reaction pathway was tested. Even though, the Cp^{XXL} ligand exhibits better electron donating properties, the formation of **18b** was hampered. Only by starting from $\mathbf{15b_{Tl}}$, the crucial intermediate product **18b** could be obtained. The driving force for the formation of **18b** by staring from$\mathbf{15b_{Tl}}$ is most likely the elimination of poorly soluble TlBr.

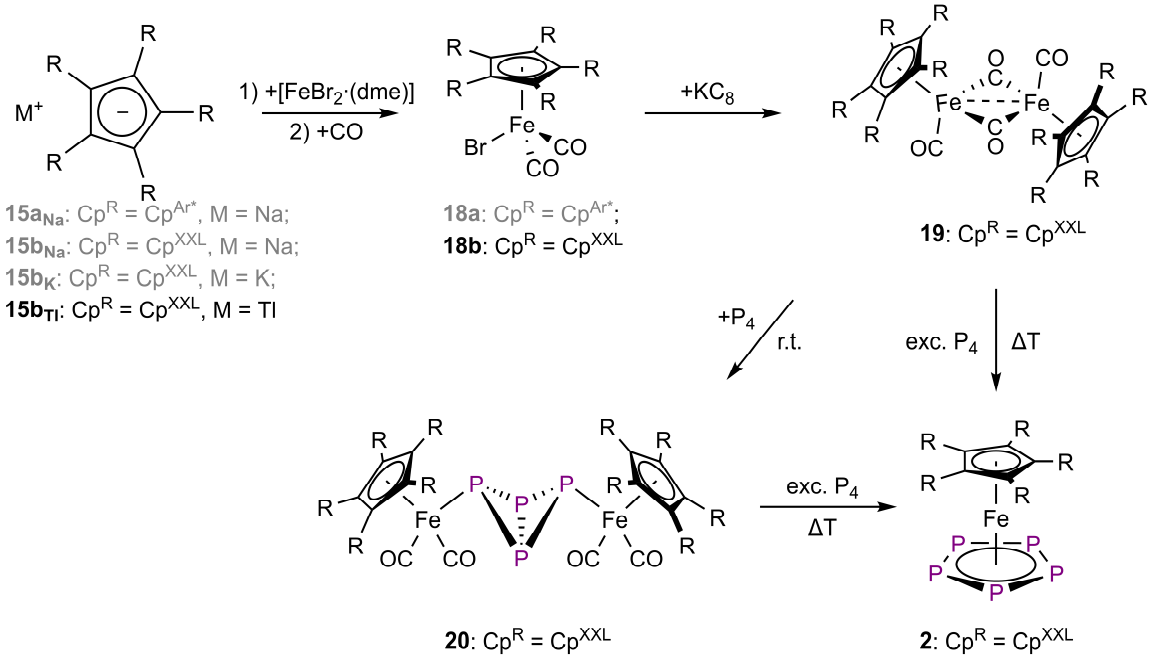

Scheme 7.7. Synthesis of the pentaphosphaferrocene derivative $[Cp^{XXL}Fe(\eta^5\text{-}P_5)]$ (**2**). The initial step for this synthesis is the formation of $[Cp^RFe(CO)_2Br]$ (**18a**, $Cp^R = Cp^{Ar*}$; **18b**, $Cp^R = Cp^{XXL}$). Unfortunately, the complexes could not be obtained starting with $\mathbf{15a_{Na}}$, $\mathbf{15b_{Na}}$ and $\mathbf{15b_K}$, which is why they are greyed out. Complex **18a** could not be obtained at all, which is why in the following only the Cp^{XXL} derivatives are presented.

Starting from **18b** the dimeric complex $[Cp^{XXL}Fe(CO)_2]_2$ (**19**) could be obtained via reduction with KC_8. The solid state structure of **19** reveals a remarkably long Fe–Fe bond. Furthermore, exhibits **19** a monomer-dimer equilibrium in solution, which was observed by IR spectroscopy. Due to the partly dissociation into reactive 17 valence electron species, **19** reacts at room temperature with P_4 selectively to the P_4 butterfly complex $[\{Cp^{XXL}Fe(CO)_2\}_2(\mu,\eta^{1:1}\text{-}P_4)]$ (**20**). Either complex **19** or **20** can be used as starting material for the synthesis of the pentaphosphaferrocene derivative **2** via a cothermolysis with an excess of P_4 in high boiling solvents. Due to the attached Cp^{XXL} ligand, **2** is the largest pentaphosphaferrocene derivative reported so far.

The suitability of **2** as building block in supramolecular chemistry is highlighted via the reaction of **2** with an excess of CuBr. The use of the super bulky pentaphosphaferrocene leads to the formation of a novel supramolecular cluster with the general formula $[(Cp^{XXL}FeP_5)_3(Cu_XBr_{X-3})(solv)_y]$ (**21**, solv = methanol or acetonitrile). Due to the intrinsic poor quality of crystals of Cp^{XXL} containing compounds, the exact formula of the

supramolecule could not be determined within the scope of this thesis. However, **21** crystallized with two crystallographically unique molecules (**21a** and **21b**) of similar, but different composition and molecular structure. Due to server disorder of **21b**, only the formula of **21a** could be determined as $[(Cp^{XXL}FeP_5)_3Cu_{15.5}Br_{12.5}(solv)_x]$ (**21a**; solv = methanol or acetonitrile; Figure 7.2) which exhibits a distorted trigonal prismatic shape. In both, **21a** and **21b**, all P_5 units exhibit envelope conformation which is why the presence of $[Cp^{XXL}Fe(\eta^4\text{-}P_5)]^-$ units is suggested. The reason for the formation of $[Cp^{XXL}Fe(\eta^4\text{-}P_5)]^-$ units is still unclear.

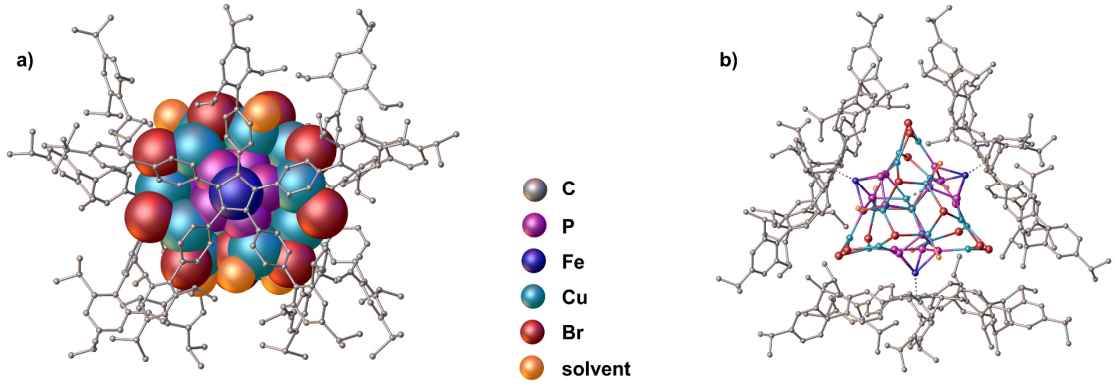

Figure 7.2. Idealized molecular anatomy of $[(Cp^{XXL}FeP_5)_3Cu_{15.5}Br_{12.5}(solv)_x]$ (**21a**) in solid state. a) Inorganic scaffold of the supramolecule as a space-filling model. The Cp^{XXL} ligands are shown as a ball-and-sick model and H atoms are omitted for clarity. b) Top view on the entire supramolecule as a ball-and-sick model.

7.6. Reference

[1] C. Schwarzmaier, *Ph.D. Thesis*, University of Regensburg, Regensburg, **2012**.
[2] M. Eberl, *Ph.D. thesis*, University of Regensburg, Regensburg, **2011**.

8. Appendix

8.1. Thematic List of Abbreviations

NMR Spectroscopy

NMR	Nuclear Magnetic Resonance
δ	chemical shift
ppm	part per million
Hz	Hertz, s^{-1}
J	coupling constant, Hz
s	singlet
d	doublet
t	triplet
q	quartet
m	multiplet
br	broad
$\omega_{½}$	half width at full maximum, Hz
VT	variable temperature
TMS	Tetramethylsilane, $Si(CH_3)_4$

Solvents

thf	tetrahydrofuran, C_4H_8O
tol	toluene, C_7H_8
dib	1,3-diisopropylbenzene, $C_{12}H_{18}$
dme	1,2-dimethoxyethane, $C_4H_{10}O_2$
CH_2Cl_2	dichloromethane
CH_3CN	acetonitrile
o-dfb	1,2-difluorbenzene, $C_6H_4F_2$
dmf	N,N-dimethylformamide, C_3H_7NO

Mass Spectrometry

MS	mass spectrometry
$[M]^+$	molecular ion peak
m/z	mass to charge ratio
LIFDI	liquid injection field desorption ionization
FD	field desorption
ESI	electro spray ionization
EI	electron impact

Ligands and substituents

Ar	aromatic substituent
R	organic substituent
Me	Methyl, $-CH_3$
Et ,	Ethyl, $-C_2H_5$
^{i}Pr	*iso*-Propyl, $-C_3H_7$
^{t}*Bu*	*tert*-Butyl, $-C_4H_9$
^{n}*Bu*	*n*-Butyl, $-C_4H_9$
Ph	Phenyl, $-C_6H_5$
Cp	cyclopentadienyl, η^5-C_5H_5
Cp^R	cyclopentadienyl derivative
Cp*	η^5-C_5Me_5
Cp^{4iPr}	η^5-$C_5{}^{i}Pr_4H$
Cp''	1,3-di-*tert*-butylcyclopentadienyl, η_5-$C_5H_3{}^{t}Bu_2$
Cp'''	1,2,4-tris-*tert*-butylcyclopentadienyl, η_5-$C_5H_2{}^{t}Bu_3$
Cp^{Ph}	pentakis-phenylcyclopentadienyl, η_5-$C_5(C_6H_5)_5$
Cp^{PEt}	pentakis-4-ethylphenylcyclopentadienyl, η^5-$C_5(4\text{-}EtC_6H_4)_5$
Cp^{BIG}	pentakis-4-*n*-butylphenylcyclopentadienyl, η^5-$C_5(4\text{-}{}^{n}BuC_6H_4)_5$
Cp^{Ar*}	η^5-C_5(4-*n*-propyl-1,1'-biphenyl)$_5$
Cp^{XXL}	η^5-C_5(2,4,6-triisopropyl-1,1'-biphenyl)$_5$

Evans Method

μ_{eff}	effective magnetic moment
μ_B	Bohr magneton

Mössbauer Spectroscopy

δ	isomer shift, $mm \cdot s^{-1}$
ΔE_q	quadrupole splitting, $mm \cdot s^{-1}$

IR Spectroscopy

IR	infrared spectroscopy
$\tilde{\nu}$	wavenumber, cm^{-1}
s	strong
w	weak
br	broad

Other

Å	Angstrom, 1 Å = $1 \cdot 10^{-10}$ m
T	temperature
K	Kelvin
°C	Degree Celsius
c	concentration, $mol \cdot L^{-1}$
d	distance, Å
r.t.	room temperature
M	metal
L	ligand
1D	one dimensional
2D	two dimensional
3D	three dimensional
DFT	density functional theory
VE	valence electrons
ADPs	atom displacement parameters

8.2. Acknowledgements

Finally, I would like to thank…

- Prof. Dr. Manfred Scheer for providing the interesting research topic and supervision. Additionally, for providing extraordinary and excellent working conditions and the freedom to pursue my own ideas in the lab.
- Dr. Gábor Balázs for always having time to discuss chemical or even non-chemical problems and to provide helpful, professional advice. Thanks for proofreading and several DFT calculations.
- Dr. Michael Seidl for proofreading, checking many of my structures and answering countless crystallographic questions.
- Dr. Eugenia Peresypkina and Dr. Alexander V. Virovets for their great help with almost all of the X-ray structural analyses of my Cp^{Ar*} and Cp^{XXL} compounds.
- Prof. Dr. Karsten Meyer and Martin Keilwerth for the Mößbauer experiments.
- the staff of the Central Analytical Services of the University of Regensburg: X-ray, MS, EA and NMR department. Especially, to Anette Schramm and Georgine Stühler for the countless NMR measurements and to Dr. Michael Bodensteiner for the help with various crystallographic problems.
- the staff of the glass blowing, electronics and mechanics facilities of the University of Regensburg for their valuable work.
- my former lab supervisors Dr. Sebastian Heinl, Dr. Fabian Spitzer and Dr. Moritz Modl for their help during my master thesis, encouraging discussions about filtration and several emotional moments (e.g. sad piano).
- my present and former lab colleges Martin Weber, Dominik Venus and Maria Haimerl for a great lab atmosphere and tolerating my experimental music. Special thanks to Maria for her inexhaustible supply of sweets.
- the inner circle of the "Spieleabend": Michi, Reini, Nicolò and Schotti for the many great evenings which have awakened my interest in board games.
- all present and former members of the Scheer group for the pleasant working atmosphere and an unforgettable time: Anna, Andi, Andrea, Bijan, Barbara B., Barbara K., Boi (for all the deep talk in the beer kitchen), Christoph, Claudi, Claudia, Dani, David, Dominik, Eric, Eva, Fabi, Felix L, Felix R. (for the athletic counterbalance at several parties), Gábor, Helena (for the mutual support in the last months), Hias, Jana, Jens, Julian L, Karin, Kevin, Küken, Lara, Lena, Liese, Lisa, Luis, Lukas, Maria, Martin W, Martin P., Martina, Matthias H., Mehdi, Michi, Mina, Moartl, Mo, Moni, Nase, Olli, Pavel, Petra, Rebecca, Reini, Robert, Rudi, Sabrina, Schotti, Sebi, Stephan, Thach, Tobi, Vroni, Walter, Wast, Wurzl.
- the members of the Bauer group: Alexander, Jonathan, Nicolò, Noel, Tanja, Tobi.

- Anna and Nicolò, who always had time for a coffee break and provided me with excellent espresso.
- my former roommate and fellow student Vally for having a good time.
- especially my family for their enduring support und always being there.
- above all Jessi. Thank you for everything!! You know what I mean 😉.